

Utah State University

DigitalCommons@USU

All Graduate Theses and Dissertations

Graduate Studies

5-2014

Quantum Mechanical Study of Weak Molecular Interactions

Upendra Adhikari
Utah State University

Follow this and additional works at: <https://digitalcommons.usu.edu/etd>



Part of the [Biochemistry Commons](#)

Recommended Citation

Adhikari, Upendra, "Quantum Mechanical Study of Weak Molecular Interactions" (2014). *All Graduate Theses and Dissertations*. 2184.

<https://digitalcommons.usu.edu/etd/2184>

This Dissertation is brought to you for free and open access by the Graduate Studies at DigitalCommons@USU. It has been accepted for inclusion in All Graduate Theses and Dissertations by an authorized administrator of DigitalCommons@USU. For more information, please contact digitalcommons@usu.edu.



QUANTUM MECHANICAL STUDY OF WEAK MOLECULAR INTERACTIONS

by

Upendra Adhikari

A dissertation submitted in partial fulfillment
of the requirements for the degree

of

DOCTOR OF PHILOSOPHY

in

Chemistry

Approved:

Steve Scheiner
Major Professor

Tapas Kar
Co-Advisor

David Farrelly
Committee Member

Alexander I. Boldyrev
Committee Member

Bradley S. Davidson
Committee Member

T. C. Shen
Committee Member

Mark R. McLellan
Vice President for Research and
Dean of the School of Graduate Studies

UTAH STATE UNIVERSITY
Logan, Utah

2014

Copyright © Upendra Adhikari 2014

All Rights Reserved

ABSTRACT

Quantum Mechanical Study of Weak Molecular Interactions

by

Upendra Adhikari, Doctor of Philosophy

Utah State University, 2014

Major Professor: Dr. Steve Scheiner
Co-Advisor: Dr. Tapas Kar
Department: Chemistry and Biochemistry

Noncovalent interactions have a long history and have received huge attention since their discovery almost a century ago. The prevalence of noncovalent interactions can be seen in the formation of simple dimers to structural and functional modification of large biomolecules. Even though plenty of experimental and theoretical studies are performed to understand various noncovalent interactions, the nature and variety of those interactions are still subject of study. And still they are receiving tremendous attention due to their significant role in the stability and conformation of biomolecules, catalysis of organic and inorganic reactions, crystal packing and material design. This dissertation explores various new sorts of noncovalent interactions, compares them with existing ones, and extensively studies the relevance of noncovalent interactions to various biological systems of interest by applying quantum mechanical tools. A new sort of noncovalent interaction has been identified where two electronegative atoms interact directly with each other with no intervening hydrogen or halogen atoms. These

interactions are found to be surprisingly strong, even stronger than regular OH...O and NH...O hydrogen bonds in some cases, and are stabilized by the charge transfer from electron donor to electron acceptor. The major portion of this dissertation deals with the rigorous investigation of new sorts of interactions like P...N, S...N, Cl...N and several other charge transfer types of interactions with side by side comparison with hydrogen and halogen bonds. Similarly, a new carbonyl-carbonyl stacking geometry in peptide-peptide interactions is explored. These stacking geometries are energetically close to stronger NH...O hydrogen bonds, and get some assistance from CH...O hydrogen bonds. Carbon is considered one of the potent H-bond donors, albeit weaker, due to its ubiquitous presence in biomolecules. So, another portion of this dissertation is focused on the study of neutral and charged CH hydrogen bonds simulating various interpeptide interactions and enzyme catalysis. And the last part of this dissertation deals with the putative H-bonds that might be present in tip functionalized carbon nanotubes.

(414 pages)

PUBLIC ABSTRACT

Quantum Mechanical Study of Weak Molecular Interactions

Upendra Adhikari, Doctor of Philosophy

Molecular interactions play key role in the existence of biomolecules like proteins and nucleic acids, and various materials. Molecular interactions are weak forces that hold different molecules or different fragments of the same molecule together, and are often referred to as noncovalent interactions. Due to the complexity in biomolecules, these interactions are still poorly understood. This dissertation presents results from quantum mechanical simulations of various types of noncovalent interactions, which are extremely important for the structure and functions of biomolecules and materials.

A new sort of noncovalent interaction is identified. This new sort of interaction originates from a direct interaction between two electronegative atoms. This interaction is represented as $BA\cdots D$, where A and D are electronegative atoms, and B is some substituent. In most cases, this new sort of interaction is found to be more stable than regular hydrogen bonds. These new interactions are found to have some potential to allow the development of materials with unusual physical properties.

This dissertation also explores the role of supposedly weaker CH hydrogen bonds on the configuration of peptide-peptide interactions, secondary structure of proteins, and mechanism of methyl transfer reaction in enzymes. Similarly, putative hydrogen bonding at the tips of functionalized carbon nanotubes is studied, which reveals the absence of OH and COOH groups together at the tips of carbon nanotubes.

ACKNOWLEDGMENTS

I would like to express my sincere gratitude to my advisor, Professor Steve Scheiner, for his continuous support, proper guidance and exceptional mentoring. I am indebted to him for his encouragement, inspiration and helping me grow as a better student, researcher and as a better person. I am also grateful to my co-advisor, Dr. Tapas Kar, for his invaluable support, cooperation and motivation.

I would like to thank my supervisory committee members, Dr. Bradley S. Davidson, Dr. David Farrelly, Dr. Alexander I. Boldyrev and Dr. T. C. Shen, for their priceless time and valuable suggestions.

I would like to thank all my colleagues, friends, and Nepali community in Logan for their wonderful companionship and support during my graduate study. Especially, I am grateful to Shuangkou Chen, Jared Moss, Binod Nepal, Jaya Shrestha, Vincent Nziko, Prakash Joshi, Sanjib Shrestha, Ram Neupane, and Jay Bhattarai.

Next, I want to thank the Department of Chemistry and Biochemistry, Utah State University for providing me the opportunity to pursue my scientific career. Computer, storage and other resources from the Division of Research Computing in the Office of Research and Graduate Studies at Utah State University are gratefully acknowledged. Similarly, I am grateful to the Office of Research and Graduate Studies, Utah State University for granting me the Dissertation Fellowship which eased my dissertation writing.

Most importantly, I would like to thank my parents for their continuous support, love and care throughout my life, without whom I would never get this achievement.

Similarly, my thanks go to my siblings, Ishowar Adhikari, Rammaya Thapa and Krishna Kumari Khatri, and all of my relatives for their love and support. Especially, I would like to thank my wife, Sarita. Her support, love, patience and encouragement were crucial for this achievement. I am grateful to my son, Aarush, for giving countless happiness and endless joy in my life.

Upendra Adhikari

CONTENTS

	Page
ABSTRACT.....	iii
PUBLIC ABSTRACT	v
ACKNOWLEDGMENTS	vi
LIST OF TABLES	xiii
LIST OF FIGURES	xvi
LIST OF ABBREVIATIONS.....	xxii
CHAPTER	
1. INTRODUCTION	1
References.....	12
2. THE S··N NONCOVALENT INTERACTION: COMPARISON WITH HYDROGEN AND HALOGEN BONDS.....	19
Abstract.....	19
2-1. Introduction	19
2-2. Computational Methods	21
2-3. Results	21
2-4. Conclusions	25
References.....	27
3. ABILITIES OF DIFFERENT ELECTRON DONORS (D) TO ENGAGE IN A P··D NONCOVALENT INTERACTION	34
Abstract.....	34
3-1. Introduction	34
3-2. Computational Methods	38
3-3. Results	39
3-3.1. Donors Containing Electronegative Atoms	39
3-3.2. Carbon-Containing Electron Donors	43
3-3.3. Secondary Minima	47

	3-4. Discussion and Conclusions	50
	References.....	56
4.	COMPARISON OF P···D (D=P,N) WITH OTHER NONCOVALENT BONDS IN MOLECULAR AGGREGATES	72
	Abstract	72
	4-1. Introduction	72
	4-2. Computational Methods	76
	4-3. Results	77
	4-3.1. (PH ₃) ₃	78
	4-3.2. PH ₃ tetramer	82
	4-3.3. NH ₃ -PH ₃ -PH ₃	84
	4-3.4. FPH ₂ -PH ₃ -PH ₃	87
	4-4. Discussion.....	91
	References.....	94
5.	SENSITIVITY OF PNICOGEN, CHALCOGEN, HALOGEN AND H- BONDS TO ANGULAR DISTORTIONS	105
	Abstract	105
	5-1. Introduction	105
	5-2. Computational Methods	107
	5-3. Results	109
	References.....	114
6.	SUBSTITUENT EFFECTS ON CL···N, S···N, AND P···N NONCOVALENT BONDS.....	122
	Abstract.....	122
	6-1. Introduction	122
	6-2. Computational Methods	126
	6-3. Results	127
	6-3.1. Analysis of Binding Energetics.....	130
	6-3.2. Source of Behavior of NO ₂ Substituent	134
	6-3.3. Alternate Minima	136
	6-3.4. Test of Various DFT Functionals.....	141
	6-4. Summary.....	144
	References.....	147

7.	EFFECTS OF CARBON CHAIN SUBSTITUENTS ON THE P...N NONCOVALENT BOND.....	162
	Abstract.....	162
	7-1. Introduction.....	162
	7-2. Computational Methods.....	164
	7-3. Results.....	165
	References.....	169
8.	CONTRIBUTIONS OF VARIOUS NONCOVALENT BONDS TO THE INTERACTION BETWEEN AN AMIDE AND S-CONTAINING MOLECULES.....	175
	Abstract.....	175
	8-1. Introduction.....	175
	8-2. Computational Methods.....	178
	8-3. Results.....	178
	8-3.1. CH ₃ SH.....	178
	8-3.2. CH ₃ SCH ₃	181
	8-3.3. CH ₃ SSCH ₃	183
	8-4. Discussion.....	185
	8-5. Conclusions.....	191
	References.....	192
9.	PREFERRED CONFIGURATIONS OF PEPTIDE-PEPTIDE INTERACTIONS.....	202
	Abstract.....	202
	9-1. Introduction.....	202
	9-2. Computational Methods.....	207
	9-3. Results.....	207
	9-3.1. Sensitivity to Basis Set Superposition Error.....	212
	9-3.2. Influence of C=O Dipole-Dipole Attractions.....	214
	9-4. Conclusions and Discussion.....	216
	References.....	221
10.	FIRST STEPS IN GROWTH OF A POLYPEPTIDE TOWARD β -SHEET STRUCTURE.....	231
	Abstract.....	231

10-1. Introduction	232
10-2. Computational Methods	235
10-3. Results	235
10-3.1. Individual Rotational Profiles	238
10-3.2 Explanation	241
10-4. Discussion.....	244
References.....	248
11. MAGNITUDE AND MECHANISM OF CHARGE ENHANCEMENT OF CH ₂ -O HYDROGEN BONDS	264
Abstract.....	264
11-1. Introduction	265
11-2. Computational Methods	269
11-3. Results	270
11-3.1. Solvent Effects	271
11-3.2. Distance from Center of Charge	273
11-3.3. Nature of Interaction	276
11-3.4. Other Geometries of H-bonds	280
11-4. Summary and Discussion	283
References.....	286
12. DO PHENOLIC AND CARBOXYLIC GROUPS COEXIST AT THE TIPS OF OXIDIZED SINGLE-WALL CARBON NANOTUBES (O-SWNTs)?.....	306
Abstract.....	306
12-1. Introduction	306
12-2. Models and Method of Calculations.....	310
12-3. Results and Discussion	312
12-3.1. SWNT-COOH.....	312
12-3.2. SWNT-OH	314
12-3.3. SWNT-COOH-OH.....	315
12-3.4. Charge distribution:.....	319
12-4. COOH and OH at the surface	320
12-5. Vibrational spectra of SWNT-COOH-OH	321
12-6. Conclusions	327
References.....	328

13. SUMMARY	345
References.....	351
APPENDIX.....	354
CURRICULUM VITAE	389

LIST OF TABLES

Table	Page
2-1. Energetic (kcal/mol), geometric and electronic aspects of XS···N complexes in Figure 2-1.....	31
2-2. Energetic (kcal/mol), geometric and electronic aspects of HS···N complexes in Figure 2-2.....	31
3-1. Energetic, geometric, and electronic aspects of FP···D complexes, all with FH ₂ P as electron acceptor.	65
3-2. SAPT decompositions (kcal/mol) of the complexation energies of the FP···D complexes, all with FH ₂ P as partner molecule.....	65
3-3. Energetic, geometric, and electronic aspects of FP···D complexes, for carbon-containing donors, all with FH ₂ P as partner molecule.	66
3-4. SAPT decompositions (kcal/mol) of the complexation energies of the FP···D complexes, all with FH ₂ P as partner molecule.....	66
3-5. FP···D binding energies (kcal/mol) with FH ₂ P compared with H-bonds formed with FH and HOH.	67
4-1. Intermolecular R(P··P) distances, Å, and NBO E(2), kcal/mol, for trimers illustrated in Fig 1. ^a	99
4-2. Intermolecular R(P··P) distances, Å, and NBO E(2), kcal/mol, for tetramers illustrated in Fig 2. ^a	99
4-3. Intermolecular R(P··N) and R(P··P) distances, Å, and NBO E(2), kcal/mol for trimers illustrated in Fig 3. ^a	100
4-4. Intermolecular R(P··P) and R(F··P) distances, Å, and NBO E(2), kcal/mol for trimers illustrated in Fig 4. ^a	100
5-1. Measures of sensitivity of interaction energy to angular distortion for complexes pairing various electron acceptors with NH ₃	118
5-2. Harmonic vibrational frequencies (cm ⁻¹) associated with intermolecular nonlinear distortions.....	119

5-3.	Changes incurred by various SAPT components of the total interaction energy (kcal/mol) as a result of 30° angular distortion for complexes pairing various electron acceptors with NH ₃	119
6-1.	Energetic (kcal/mol), geometric, and electronic aspects of BHS···NH ₃ complexes.	154
6-2.	Energetic (kcal/mol), geometric, and electronic aspects of BCl···NH ₃ complexes.	154
6-3.	SAPT components, kcal/mol, of interaction energies for BHS···NH ₃ complexes.	155
6-4.	SAPT components, kcal/mol, of interaction energies for BCl···NH ₃ complexes.	155
6-5.	Counterpoise corrected interaction energies (ΔE, kcal/mol) computed by MP2 and various DFT methods, for FSH/NH ₃ heterodimer, all with aug-cc-pVDZ basis set. Second column indicates primary molecular interactions present in each structure.	156
6-6.	Counterpoise corrected interaction energies (ΔE, kcal/mol) computed by MP2 and various DFT methods, for NH ₂ SH/NH ₃ heterodimer, all with aug-cc-pVDZ basis set. Second column indicates primary molecular interactions present in each structure.	156
7-1.	Energetic, geometric, and electronic aspects of RPH ₂ ···NH ₃ complexes.	172
7-2.	Energetic, geometric, and electronic aspects of FC ₃ H ₆ -PH ₂ ···NH ₃ complexes.	172
7-3.	Energetic, geometric, and electronic aspects of C ₄ H ₅ (F)-PH ₂ ···NH ₃ complexes.	173
7-4.	Energetic, geometric, and electronic aspects of fluorophenyl complexes.	173
8-1.	Total interaction energy ΔE and NBO second-order perturbation energy E(2) of its primary component interactions in complexes of NMA with CH ₃ SH. Energies in kcal/mol.	197
8-2.	Total interaction energy ΔE and NBO second-order perturbation energy E(2) of its primary component interactions in complexes of NMA with CH ₃ SCH ₃ . Energies in kcal/mol.	197

8-3.	Total interaction energy ΔE and NBO second-order perturbation energy $E(2)$ of its primary component interactions in complexes of NMA with CH_3SSCH_3 . Energies in kcal/mol.	198
8-4.	H-Bond energies (kcal/mol) of S-containing molecules coupled with NMA.	198
9-1.	Geometric and energetic (kcal/mol) aspects of $\text{NH}\cdots\text{O}$ H-bonded dimers.	227
9-2.	Geometric and energetic (kcal/mol) aspects of stacked dimers.	227
9-3.	SAPT contributions (kcal/mol) to total interaction energies of NMA dimers.	227
9-4.	Geometric and energetic aspects of $\text{NH}\cdots\text{O}$ dimers obtained without inclusion of counterpoise corrections in optimization algorithm.	228
11-1.	Binding energies (kcal/mol) of complexes with NMA computed at two levels of theory.	299
11-2.	$R(\text{H}\cdots\text{O})$ distances (\AA) in complexes of NMA with terminal methyl groups, at M06-2X/6-31+G** level.	299
11-3.	NBO values of $E(2)$ (kcal/mol) for complexes involving terminal methyl groups, at M06-2X/6-31+G** level.	299
11-4.	SAPT decomposition of total binding energies (kcal/mol) of S and N complexes with NMA as H-bond acceptor.	300
11-5.	Changes in NMR chemical shielding (σ , ppm) of protons caused by complexation with NMA at M06-2X/6-31+G** level.	300
12-1.	Vibrational frequencies (ν , in cm^{-1}), intensity (I , in km/mol , in parenthesis), bond distances (R , in \AA) of SWNT-COOH^a and SWNT-OH^b	337
12-2.	Relative energies (E_{rel} , in kcal/mol), relative enthalpy (H_{rel} , in kcal/mol), vibrational frequencies (ν , in cm^{-1}), intensity (I , in km/mol ; in parenthesis) of (n,n)- COOH-OH^a	338
12-3.	Relative energies (E^{rel} , in kcal/mol), relative enthalpy (H^{rel} , in kcal/mol), vibrational frequencies (ν , in cm^{-1}), intensity (I , in km/mol , in parenthesis) of (m,0)- COOH-OH^a	339

LIST OF FIGURES

Figure	Page
2-1. Optimized structures of XS \cdots N complexes for X= a) F, b) Cl, and c) Br. Counterpoise-corrected interaction energies in kcal/mol, distances in Å, and angles in degs.	31
2-2. Optimized geometries of HS \cdots N complexes. Counterpoise-corrected interaction energies in kcal/mol, distances in Å, and angles in degs.	32
2-3. Optimized geometries of SH \cdots N complexes. Counterpoise-corrected interaction energies in kcal/mol, distances in Å, and angles in degs.	32
2-4. Optimized geometries of a) NH \cdots F, b) SCl \cdots N, and c) SBr \cdots N complexes. Counterpoise-corrected interaction energies in kcal/mol, distances in Å, and angles in degs.	32
2-5. Electrostatic potentials of the isolated monomers of XSH and NH ₃ . Contour shown corresponds to ± 0.01 au, with blue/red indicating positive/negative sign of the potential.	33
3-1. Optimized geometries of complexes pairing FH ₂ P with various electron donor molecules. Distances in Å, and angles in degs. Counterpoise-corrected binding energy reported as blue number.	67
3-2. Density shifts occurring in the indicated FH ₂ P \cdots D complexes upon formation of each complex. Blue regions indicate density increase, red a decrease. Contours are shown at the 0.001 au level.	68
3-3. Electrostatic potentials of isolated monomers, oriented as they are within the optimized complexes with FH ₂ P. Blue and red regions indicate positive and negative potentials, respectively; contours at the ± 0.02 au level.	69
3-4. Optimized geometries of complexes pairing FH ₂ P with each of several unsaturated C-containing molecules. Distances in Å, and angles in degs. Blue X represents center of indicated C-C bond. Counterpoise-corrected binding energy reported as blue number.	69
3-5. Density shifts occurring in the indicated FH ₂ P \cdots D structures upon formation of each complex. Blue regions indicate density increase, red a decrease. Contours are shown at the 0.001 au level.	70

3-6.	Electrostatic potentials of isolated monomers, oriented as they are within the optimized complexes with FH ₂ P. Blue and red regions indicate positive and negative potentials, respectively; contours at the ±0.02 au level.....	70
3-7.	Interaction energies of each of the complexes formed by HF, H ₂ O, and FH ₂ P with various electron donors. Broken lines refer to H-bonds and solid to P···D.....	71
4-1.	Optimized geometries of the eight minima on the surface of the PH ₃ trimer. Binding energies are reported as the large blue numbers, followed by the same quantity including zero point vibrations. Broken lines indicate HP···P bonds, dispersion- dominated interactions are denoted by blue hatched lines. Small red numbers indicate the NBO value of E(2), in kcal/mol, for each charge transfer; values displayed when in excess of 0.5. Distances in Å, angles in degs.	101
4-2.	Optimized geometries of nine minima on the surface of the PH ₃ tetramer with binding energies in excess of 4 kcal/mol. Binding energies are indicated by the large blue numbers, followed by the same quantity including zero point vibrations. Broken lines indicate HP···P bonds, dispersion-dominated interactions are denoted by blue hatched lines. Small red numbers indicate the NBO value of E(2), in kcal/mol, for each charge transfer; values displayed when in excess of 0.5. Distances in Å, angles in degs.....	102
4-3.	Optimized geometries of the twelve minima on the surface of the NH ₃ -PH ₃ -PH ₃ mixed heterotrimer. Binding energies are denoted by the large blue numbers, followed by the same quantity including zero point vibrations. Broken lines indicate HA···D bonds where A,D=P,N and dispersion bonds are denoted by blue hatched lines. Small red numbers indicate the NBO value of E(2), in kcal/mol, for each charge transfer; values displayed when in excess of 0.5. Distances in Å, angles in degs.	103
4-4.	Optimized geometries of twelve minima on the surface of the FH ₂ P-PH ₃ -PH ₃ mixed heterotrimer. Binding energies are denoted by large blue numbers, followed by the same quantity including zero point vibrations. Small red numbers indicate the NBO value of E(2), in kcal/mol, for each charge transfer; values displayed when in excess of 0.5. Distances in Å, angles in degs.....	104
5-1.	Optimized geometries of various complexes, all involving NH ₃ as electron donor.	120

5-2.	Rise in energy that accompanies angular distortion in the complex of each indicated electron acceptor with NH ₃ . Curves represent parabola that are fit to the data points shown. H-bonding systems denoted by broken curves.	120
5-3.	Rise in the SAPT exchange repulsion energy that accompanies angular distortion in the dimer of each indicated electron acceptor with NH ₃ . H-bonding systems denoted by broken curves.....	121
5-4.	Electron densities of (a) FPH ₂ , (b) FSH, (c) FCl, (d) FH, (e) HOH, all at the 0.0001 au contour. Blue dashed lines represent alignment adopted by NH ₃ electron donor in optimized dimer geometry.....	121
6-1.	Optimized geometries of the BHS···NH ₃ complexes for B = a) CH ₃ , b) NH ₂ , c) CF ₃ , d) OH, e) Cl, f) NO ₂ , and g) F. Distances in Å and angles in degrees. Counterpoise-corrected binding energies ΔE (kcal/mol) in blue.....	157
6-2.	Optimized geometries of the BCl···NH ₃ complexes for B = a) CH ₃ , b) NH ₂ , c) CF ₃ , d) OH, e) Cl, f) NO ₂ , and g) F. Distances in Å and angles in degrees. Counterpoise-corrected binding energies ΔE (kcal/mol) in blue.....	158
6-3.	Binding energies of the BA···NH ₃ complexes for various B substituents. Electron acceptor atoms are as indicated Cl, S, and P.	159
6-4.	Electrostatic components of the BA···NH ₃ complexes for various B substituents. Electron acceptor atoms are as indicated Cl, S, and P.	159
6-5.	Induction energies of the BA···NH ₃ complexes for various B substituents. Electron acceptor atoms are as indicated Cl, S, and P.	160
6-6.	Density shifts occurring in the indicated BA···NH ₃ complexes upon formation of each complex. Blue regions indicate density increase, red a decrease. Contours are shown at the 0.0005 au level.	160
6-7.	Electrostatic potentials around several of the electron acceptor molecules. Blue regions indicate positive potential, negative by red. Contours are shown at the 0.02 au level. Numbers refer to SAPT ES components (kcal/mol) of the interaction of each monomer with NH ₃	161
7-1.	Optimized RH ₂ P···NH ₃ complexes with various carbon chains taken as R group.	174

8-1.	Optimized geometries of various minima on the potential energy surface of the CH ₃ SH/NMA heterodimer. Large blue numbers represent binding energies, in kcal/mol. Distances in Å and angles in degrees.	199
8-2.	Optimized geometries of various minima on the potential energy surface of the CH ₃ SCH ₃ /NMA heterodimer. Large blue numbers represent binding energies, in kcal/mol. Distances in Å and angles in degrees.	200
8-3.	Optimized geometries of various minima on the potential energy surface of the CH ₃ SSCH ₃ /NMA heterodimer. Large blue numbers represent binding energies, in kcal/mol. Distances in Å and angles in degrees.	201
9-1.	Geometrical dispositions of two NMA molecules in fully optimized dimers, with counterpoise corrections included in the optimization algorithm. Binding energies reported as large blue numbers; distances in Å and angles in degs. Two views are presented of dimer c so as to view both CH··O H-bonds.	228
9-2.	Electrostatic potentials of two NMA subunits in each of three different dimers. Blue regions correspond to positive potential, negative to red. Contour illustrated is 0.08 au.	229
9-3.	Shifts of electron density occurring in three NMA dimers. Purple regions denote added density, losses are shown in yellow. Contour illustrated is 0.0008 au. H-bonds are indicated by broken red line.	229
9-4.	Geometrical dispositions of two NMA molecules in fully optimized dimers, with counterpoise corrections not included in the optimization algorithm. Binding energies, corrected for basis set superposition error, reported as large blue numbers; distances in Å and angles in degs.	230
10-1.	Structures of molecule I, with lower peptide group turned so as to present its CO group toward the upper in a, and its NH group turned in this direction in b. Important atoms are labeled, as are the dihedral angles discussed in the text.	259
10-2.	Energy as a function of dihedral angle ψ for the simple dipeptide (broken curve) and full molecule I (solid curve). Red and blue colors indicate respectively whether the lower peptide is oriented with CO or NH group pointing up toward the upper dipeptide. Zero of energy is taken as the lowest value in the profile of each.	260
10-3.	Structures of minima on the potential energy surface of the dipeptide segment NH ₂ COCH ₂ NHCOCH ₃ , indicating internal H-bond.	260

- 10-4. Energy as a function of dihedral angle ψ for a) simple dipeptide and b) full molecule I with lower peptide held with CO group up facing the dipeptide. The interaction energy computed for the upper and lower units, in the absence of intervening phenyl and other groups, is shown in c. The sum of the latter interaction energy in c and the intrinsic energy of the dipeptide in a is depicted in d. For a, b, and d, the value of zero is assigned to the lowest energy; quantities shown in c represent absolute values.261
- 10-5. Energy as a function of dihedral angle ψ for a) simple dipeptide and b) full molecule I with lower peptide held with NH group up facing the dipeptide. c shows the interaction energy between the upper and lower units, in the absence of intervening phenyl and other groups, and d represents the sum of c and a.262
- 10-6. Structures of selected geometries of molecule I. Selected interatomic distances are in Å.263
- 11-1. Optimized geometries (MP2/aug-cc-pVDZ) of a) S(Me)₂, b) S(Me)₃⁺, c) N(Me)₃, and d) N(Me)₄⁺ complexes with NMA as H bond acceptor. Blue numbers represent counterpoise-corrected binding energies in kcal/mol. Distances in Å and angles in degrees.....301
- 11-2. Binding energies plotted against Onsager function (Fo) for S(Me)₂, S(Me)₃⁺, N(Me)₃ and N(Me)₄⁺ complexes with NMA as proton acceptor, as MP2/aug-cc-pVDZ level. Yellow and blue colors indicate S and N donors, respectively, solid curves for cationic and dotted for neutral complexes. Red line represents neutral water dimer.301
- 11-3. Optimized geometries (M06-2X/6-31+G**) for S⁺ and N⁺ complexes with elongated alkyl groups; NMA as proton acceptor. Blue numbers indicate counterpoise-corrected binding energies in kcal/mol. Distances in Å and angles in degrees.302
- 11-4. Variation of binding energy with increase in alkyl chain length of R₃S⁺ (yellow) and R₄N⁺ (blue) complexes with NMA. Solid lines represent trifurcated CH•••O H bonding with one CH of each of three terminal CH₃ groups; dotted lines indicate O interacting with the three CH₂ groups closest to central S or N atom.302
- 11-5. Electrostatic potential maps for alkyl-substituted S⁺ and N⁺ monomers. Contours range from 0.20 - 0.25 au. Blue and red colors indicate most and least positive regions, respectively, on the van der Waals atomic surface.303

11-6.	Electron density shifts arising from formation of each complex: proton donor is listed, and NMA is proton acceptor in all cases. Blue regions indicate density increase, and red a density loss. Contours are shown at the 0.0005 au level.	304
11-7.	Variation of binding energy for cationic complexes with increase in alkyl chain length. Broken curves were generated when all three CH donors arise from the same terminal methyl group; a single CH••O H-bond is characterized by solid curves. N donors are indicated by blue, and S by yellow.	305
12-1.	Optimized structures (top and side-view) of (n,n)-COOH and (m,0)-COOH. Distances in Å and angles in degree.	339
12-2.	Optimized structures of (n,n)-COOH and (m,0)-OH. Distances in Å and angles in degree.	340
12-3.	Optimized structures of (4,4)-COOH-OH. Distances in Å and angles in degree.	340
12-4.	Optimized structures of (m,0)-COOH-OH, m = 8, 9, 10. Distances in Å and angles in degree.	341
12-5.	M06-2X optimized structures of (8,0)-COOH-OH and (4,4)-COOH-OH where both functional groups are at the surface. Distances in Å and angles in degree. 6-31G* basis functions are used for all C and H atoms, and 6-31+G* is used for all oxygen atoms.	341
12-6.	Variation of C=O (left) and ph-OH (right) frequencies of SWNTs-COOH-OH with diameter of SWNTs.	342
12-7.	Variation of intensity of C=O mode (left) and Ph-OH (right) of SWNTs-COOH-OH with diameter of tubes.	342
12-8.	Structure of salicylic acid and different isomers obtained from B3LYP/6-31G*(O+). Bond distances are in Å, and angles are in degree.	343
12-9.	Optimized structures of (5,5)-COOH-OH. Distances in Å and angles in degree.	343
12-10.	Optimized structures of (6,6)-COOH-OH. Distances in Å and angles in degree.	344

LIST OF ABBREVIATIONS

Abbreviation	Definition
MP2	Second Order Moller-Plesset Perturbation Theory
NBO	Natural Bond Orbital
SAPT	Symmetry Adapted Perturbation Theory
EX	Exchange Repulsion
ES	Electrostatic
IND	Induction
DISP	Dispersion
EXIND	Exchange Repulsion Induction
EXDISP	Exchange Repulsion Dispersion
GIAO	Gauge Independent Atomic Orbital
CPCM	Conductor Polarized Continuum Model
NMA	N-Methyl Acetamide
CCSD(T)	Coupled Cluster Single Double (Triple)
DFT	Density Functional Theory

CHAPTER 1

INTRODUCTION

Noncovalent interactions are weak interactions formed between two different species or between different fragments of the same species. Although noncovalent interactions are much weaker than covalent bonds formed by mutual sharing of electrons, they play extremely important role in the existence of biomolecules and various materials.¹⁻⁸ Covalent bonds result in the formation of molecules whereas noncovalent interactions result in the formation of molecular clusters.

After the formulation of definition of covalent bond by Lewis⁹ nearly a century ago, a clear theoretical and experimental process of covalent bond forming and breaking is established. But, due to the existence of a plethora of ways noncovalent interactions might be formed, a unified theory of noncovalent interactions still does not exist and several classifications are being used. A noncovalent interaction ranges from weak van der Waals forces, which arise due to London dispersions, to strong hydrogen bonds. Due to this reason, researches are being focused on exploring and unifying the wide variety of noncovalent interactions that has direct implications on both biological and material science. Noncovalent interactions are involved in a wide range of chemical processes, and are crucial in supramolecular chemistry, organization of various biomolecules, crystal engineering, drug design, and catalysis.^{3,10-14}

Of the several types of noncovalent interactions, hydrogen bond (H-bond) is the most important and rigorously studied noncovalent interactions over the years.¹⁵⁻²² These H-bonds are responsible for the unique geometries adopted by biomolecules such as

proteins and nucleic acids.²³⁻²⁸ H-bond was originally believed to be formed between an H atom attached to electronegative atoms (N, O or F), and another electronegative atom (N, O or F). These H-bonds are represented as $AH\cdots D$, where A is the proton donor and D is the proton acceptor, and were initially considered to be one of the N, O or F atoms. But after the decades of theoretical and experimental investigations, following the formulation of definition of H-bond by Linus Pauling²⁹ in 1930, the concept of hydrogen bond has been broadened.³⁰⁻⁴⁷ Less electronegative atoms like Cl, S, P and C atoms are found to act as good proton donors.⁴⁸⁻⁵⁵ Various π systems and metal ions are also involved in hydrogen bonding as proton acceptors.⁵⁶⁻⁵⁸ Even a partially negatively charged hydrogen atom is able to form H-bond with another H atom, usually called a dihydrogen bond.⁵⁹⁻⁶¹ These findings eventually led to the redefinition of H-bonds.⁶²

Hydrogen bonds are usually electrostatic in nature in addition to the charge transfer and dispersion interactions. The charge transfer occurs from the proton acceptor to A-H σ^* antibond orbital of the proton donor. The consequence of the charge transfer can be seen in the stretching of A-H bond length and red shifting of A-H stretching frequency. Not all H-bonds result in the stretching and red shifting of A-H bond, but opposite scenario is found in some H-bonds. One of the most interesting and surprising results are found for H-bonds with CH proton donors. C contains no lone pairs and so does not act as proton acceptor. But it acts as a weak proton donor due to the presence of partial positive charge in H atom attached to it. The CH H-bond strength lies somewhere around 1-3 kcal/mol.⁶³⁻⁶⁶ But the presence of some electron withdrawing groups on the C atom makes it stronger proton donor. Also, the sp and sp_2 hybridized C acts as slightly

better proton donor. In some CH H-bonds, blue shifting of C-H stretching frequency occurs along with the contraction in its bond length.⁶⁷⁻⁷¹

Another noncovalent interaction, which is younger than H-bond, is the halogen bond, and is formed by a simple replacement of bridging H of H-bond by halogen atom.^{30,32,47,72-73} Despite having an overall negative charge, halogen atom contains a small region of positive potential commonly known as σ -hole, and is responsible for the electrostatic attraction with another electronegative atom. In addition, it also contains induction and dispersion components just like in H-bonds. Direct π - π stacking interactions are also observed especially in aromatic amino acids in proteins.⁷⁴

Recent work in this laboratory has identified a fundamentally new sort of noncovalent interaction between two electronegative atoms with no intervening hydrogen or halogen atoms.⁷⁵⁻⁷⁶ For instance, a global minimum search in the potential energy surface of PH_3 and NH_3 yields a direct $\text{P}\cdots\text{N}$ interaction. This direct $\text{P}\cdots\text{N}$ interaction is more stable than other possible H-bonds namely $\text{PH}\cdots\text{N}$ and $\text{NH}\cdots\text{P}$ hydrogen bonds. This interaction is found to be stabilized mostly by the charge transfer from N lone pair to P-H σ^* antibond which lies along the $\text{P}\cdots\text{N}$ axis. This sort of $\text{A}\cdots\text{D}$ interaction (where A is electron acceptor and D is electron donor) also exists within the PH_3 dimer with the formation of direct $\text{P}\cdots\text{P}$ interaction.⁷⁷

Progressive works demonstrated that other atoms like S and Cl are also capable of formation of $\text{A}\cdots\text{D}$ interactions. Substitution of one of the H atoms of PH_3 by F, Cl or NO_2 enhances the $\text{P}\cdots\text{N}$ bond energy, which surpasses the H-bond energy of model water dimer.⁷⁸ Similarly, replacement of one of the H atoms of NH_3 by F atom enables a direct $\text{N}\cdots\text{N}$ interaction with another NH_3 molecule, which was never observed before.⁷⁹ These

interactions are named after the electron acceptor atoms A, viz. pnictogen bond ($P\cdots N$), chalcogen bond ($S\cdots N$) and halogen bond ($Cl\cdots N$). Experimental examination of crystal structures has shown similar sorts of interactions, emphasizing their importance in the crystal packing as well as in the biological systems.⁸⁰⁻⁸¹

So the literature contains some glimpses of involvement of second and third row atoms in direct $A\cdots D$ interaction. Although $A\cdots D$ sorts of interactions are energetically competitive with H-bonds, very little information is available in the literature, and this big void in the literature immediately needs to be filled for the deeper understanding of their importance. Some of those gaps include the measurement of effect of various substituents in second row pnictogen, chalcogen and halogen bond interactions. Similarly, changing the electron donors can have profound effect on these interactions. π -systems are engaged in H-bonding, and it also signals for the formation of $A\cdots\pi$ interactions with first and second row atoms. H-bond is found to be very sensitive towards angular distortion and exists in molecular aggregates, so it is natural to wonder if these properties are also valid for pnictogen, chalcogen, and halogen bonds.

$CH\cdots O$ H-bond is one the most important H-bonds formed via C proton donor. This is due to the prevalence of CH groups alongside the strong proton acceptor $O=C$ of the peptide groups in biomolecules like nucleic acids and proteins. The $CH\cdots O$ H-bonds in many systems are secondary forces, only to $NH\cdots O$ H-bonding.^{33,36,52} Even though several fundamental aspects of these H-bonds are well documented, their prominently applicable roles in binding various amino acid side chains, mechanism and magnitude of presence of charge in the surrounding, and mechanism of enzyme catalysis are still to be discovered. For instance, charge assisted $CH\cdots O$ H-bonding is believed to be involved in

the methyl transfer reaction in some particular enzymatic systems.⁸²⁻⁸³ But the strength, availability, capability and mechanism of such charge enforced CH...O H-bonds are not yet investigated, and requires a thorough computational and experimental examinations for their proper understanding and practical applicability.

Similarly, the formation of α -helices and β -sheets in proteins are governed by the extensive NH...O and CH...O hydrogen bonds.⁸⁴⁻⁸⁸ The CH...O H-bonds are not only the supplementary interaction but contains almost half of the total interaction energy in parallel β -sheets. So, from both experimental and theoretical point of view, it is already affirmed that CH...O H-bonds are competitive with NH...O H-bonds and are considered as the determinant of conformation of biomolecules.⁸⁹ But some lingering questions still remain about the role of CH...O H-bonds in the structure and functions of peptides. For example, even though CH...O H-bonds are involved in peptide-peptide interactions, are they really involved in the initial stages of formation of α -helix and β -sheet? And, are these interactions just important within the major peptide units or are they also crucial in the interaction involving side chains with various heteroatoms? These questions need to be answered to fully understand their role in the biological systems.

Noncovalent interactions, mainly H-bonding influences the properties and functions of several materials. Most importantly, the presence of several oxygen containing functional groups in oxidized carbon nanotubes and graphene allow the formation of H-bonds. The presence of H-bonds alters the energetic and spectroscopic properties, allowing the identification and separation of various nanomaterials. So it is very necessary to study the presence of any sorts of H-bonding and their consequences in these nanomaterials.

This dissertation focuses on exploring and analyzing a wide range of noncovalent interactions; from new sorts of A...D interactions with various A and D atoms, to NH...O and CH...O hydrogen bonds, carbonyl-carbonyl stacking, peptide interactions, and influence of H-bonds in functionalized carbon nanotubes. A brief description of each chapter is provided in the following paragraphs.

Previous research has revealed the absence of a direct S...N interaction on the potential energy surface of H₂S and NH₃ pair.⁹⁰ A putative S...N interaction with an angle frozen was indeed an attractive force, but SH...N hydrogen bond was found to be the stronger force involved. This gives a strong indication of presence of some stronger true S...N interaction in presence of different electronic environment on the electron acceptor. Chapter 2 of this dissertation deals with the comparison of a new sort of S...N interaction with hydrogen and halogen bonds formed by the complexation of halogen substituted H₂S and NH₃ molecules. One of the H-atoms of H₂S is replaced by series of halogen atoms X = F, Cl and Br, and all possible minima on their potential energy surface are searched. This replacement indeed allows the formation of S...N interaction which is competitive with hydrogen and halogen bonds.

Most of the direct A...D interactions studied before relied on the variation of electron acceptor A taking NH₃ as only electron donor.⁷⁵⁻⁷⁸ The replacement of electron acceptor atom P by S, Cl or As did not alter the results dramatically but one might expect a substantial change on replacing the electron donor atom N. Chapter 3 thus tries to explore the ability of various electron donors (D) to form direct P...D interactions by considering PH₂F as an electron acceptor which has served as a good electron acceptor in the past.⁷⁸ The electron donors considered are the single bonded models H₂O, H₂S and

CH₃OH, double bonded models H₂C=O and H₂C=S, and various π -systems like HC \equiv CH, H₂C=CH₂, H₂C=CH-CH=CH₂ and C₆H₆. Each of these systems was allowed to interact with FH₂P molecule, and various starting points for the geometry optimization of each pair were taken so as to find all possible minima. It is found that O and S atom, and carbon π -systems participate in the P \cdots D type of interaction. These interactions are stabilized by the charge transfer from D lone pair to P-F σ^* antibond. The P \cdots D interactions are comparable to and sometimes stronger than H-bonds formed by H₂O molecule. Natural Bond Orbital (NBO), Symmetry Adapted Perturbation Theory (SAPT), electrostatic potential map and electron density shift analyses reveals some unique features of these sorts of interactions.

The earlier investigations of BA \cdots D (B=substituents) interactions were mainly focused on the dimers containing various A and D atoms. Since the molecular aggregates have different environment and properties, it seems absolutely necessary to figure out if these forces are also present in various molecular aggregates. In fact, these interactions are proved to be present in molecular aggregates. This is explained in chapter 4, where various possible minimum structures of homo trimer and tetramer of PH₃, and hetero trimers with one PH₃ replaced by NH₃ and FH₂P, are thoroughly searched. Global minimum of all the trimers and tetramer are held by the direct A \cdots D interactions, and form cyclic structures. Similar to other A \cdots D interactions, these interactions are also stabilized by the charge transfer from the D lone pair to A-B σ^* antibond which lies 180° away from the A \cdots D axis. In addition to A \cdots D interactions, other weaker noncovalent interactions like PH \cdots P, NH \cdots P and NH \cdots F hydrogen bonds, and “reverse hydrogen

bond,” where electron density is transferred from smaller lobe at the tail of the lone pair, are also observed.

One of the important features of hydrogen bond is its directional propensity. H-bonds tend to be linear and any deviation from linearity results in the loss of some of its strength. This directional feature of H-bonds is well studied. But this property is not well documented for newly found A···D sorts of noncovalent interactions. Chapter 5 of this dissertation provides the extent and cause of the directionality of those new sorts of bonds. *Ab initio* calculations are performed for various electron acceptors P, S and Cl with various substituents (B) interacting with N of NH₃ for varying BA···D angles. It is found that P···N, S···N and Cl···N noncovalent interactions are anisotropic and more directional in nature than hydrogen bonds. SAPT decomposition of energy reveals that exchange energy is mainly responsible for this directional nature.

Since the BA···D interactions are stabilized mainly by the charge transfer from D lone pair (or π -bond) to B-A σ^* antibond, one might wonder how the presence of various substituents B on the electron acceptor might affect the binding. Chapter 6 tries to answer this question by thoroughly analyzing the effect of various substituents (electron releasing groups to electron withdrawing groups) on Cl···N, S···N and P···N noncovalent interactions. The binding energy increases in the order of B = CH₃ < NH₂ < CF₃ < OH < Cl < NO₂ < F and becomes as strong as 10 kcal/mol for Cl electron acceptor. A···D type geometries are found to be the most stable structures in many cases, stronger than NH···F, CH···N and SH···N H-bonds. Electrostatics and induction equally contribute to the total energy in weaker complexes but former becomes dominant in stronger complexes.

It can be anticipated that pnicoen atoms are bonded with carbon chains in real systems. So it is essential to explore the strength and nature of pnicoen bonds for various carbon chain substituents. In chapter 7, the effect of various carbon chains in electron acceptor P in P...N interaction is studied. Both saturated and unsaturated alkyl groups with various length, conjugated system and aromatic systems are considered as carbon chain substituents. Saturated alkyl groups tend to weaken the P...N interaction whereas unsaturated system strengthens it. The placement of F atoms in the carbon chain increases the binding energy but the effect decreases with the increase of distance of F from the center of bonding.

In proteins, the presence of peptide units -CONH- offers a variety of noncovalent interactions with peptides and polar side chains. An extensive study has been done to understand their nature, strength and effect on structure and functions. But the study of noncovalent interactions formed by the side chains containing heteroatoms like S is scant. So the main goal of the chapter 8 is to explore the possible noncovalent interactions between peptide unit and sulfur containing amino acid side chains. For this purpose, N-methylacetamide (NMA) is taken as a model peptide unit and is allowed to interact with CH₃SH representing cysteine side chain, CH₃SCH₃ as a prototype methionine and CH₃SSCH₃ as a disulfide bond which connects Cys side chain. All possible interactions on the potential surface of each pair were searched. A complete analysis reveals that there is no single force dominating the conformations. Instead, most of the structures are stabilized by the combinations of various forces. These forces include SH...O, NH...S, CH...O, SH... π , CH... π H-bonds, and charge transfer into σ^* and π^* antibond types of interactions.

Secondary structures of proteins, α -helices and β -sheets, are stabilized by the $\text{NH}\cdots\text{O}=\text{C}$ H-bond formation between two peptide units. In the literature, it is usually found that $\text{NH}\cdots\text{O}=\text{C}$ is the sole interaction that occurs in peptides, either in parallel, antiparallel or in perpendicular fashion. But some other possible interactions may exist in addition to $\text{NH}\cdots\text{O}$ H-bonds. Chapter 9 of this dissertation deals with finding all possible peptide-peptide interactions via high level *ab initio* calculations. Indeed, a new sort of interaction is investigated where carbonyl groups of two peptide units are stacked upon each other. Studied by taking dimer of N-methylacetamide (in its *trans* form), as a model peptide-peptide interaction, both parallel and antiparallel stacking geometries with equivalent stability are found. These stacked geometries are just slightly less stable than $\text{NH}\cdots\text{O}$ H-bonded geometries and are stabilized by the mutual charge transfer from CO π bond to CO π^* antibond, and $\text{CH}\cdots\text{O}$ hydrogen bonds.

Continuation of the interpeptide interaction study in a different basis is the content of chapter 10. Although several works have been done to understand the formation of β -sheets in proteins, there are still some lingering questions about the forces and the mechanism that initiates their formation. It is also unknown whether two peptide fragments coming together form β -sheet instantly or they prefer helical structures. So, a rigorous study is carried out to answer these questions by examining a full potential energy surface of a molecule containing a dipeptide and a single peptide connected via a spacer group. It is found that the most stable structure contains a regular $\text{NH}\cdots\text{O}$ H-bond and couple of $\text{CH}\cdots\text{O}$ H-bonds. It is also figured out that a β -sheet formation requires more peptide units and is not evident in the smaller model.

The presence of charge on one of the proton acceptor or donor group magnifies the hydrogen bond energy of regular H-bonds by some orders.⁹¹⁻⁹² So it is obvious to wonder if there is such a magnification for weak interactions like CH \cdots O H-bonds. In fact there are some experimental as well as theoretical evidences for such enhancement.⁹³⁻⁹⁴ But a detailed investigation is missing and several queries are to be answered. In chapter 11 of this dissertation, a robust examination of the charged CH \cdots O H-bonds is performed for biologically significant systems. N-methylacetamide (NMA) is paired with XR_n⁺ where X = S and N, and R is an alkyl group with various chain lengths. Various queries like strength of ⁺CH \cdots O H-bonds, effect of heteroatom X, distance from the center of positive charge, sensitivity towards linearity, effect of solvents and competition with regular hydrogen bonds are systematically studied.

Hydrogen bonds play very important role in recognition of materials. One of the examples can be seen in oxidized single walled carbon nanotubes.⁹⁵⁻⁹⁶ Oxidative purification of carbon nanotubes introduces some oxygen containing functional groups, and are very important due to their unique properties and various applications like biosensors and biomedical applications.⁹⁷ But the presence of various groups makes experimental characterization very complicated due to the coupling of vibrational modes and hydrogen bonding between various groups. Recent quantum calculations revealed that two different sorts of COOH group lie at the tip of zigzag carbon nanotubes, one of which show C=O stretching frequency around 1650 cm⁻¹, well below the normal CO stretching of other COOH groups at the tip of carbon nanotubes.⁹⁸ One might wonder if the presence of OH group alongside COOH group will bring some changes to the stretching frequency of C=O and OH groups as they are susceptible to the H-bond

formation. And, for the OH...O type of H-bonds, red shifting of C=O and O-H stretching frequency is observed. So, in chapter 12, the possibility and consequences of presence of OH and COOH groups together at the tip of oxidized single walled carbon nanotubes are thoroughly studied.

References

- (1) Hobza, P.; Zahradnik, R. *Weak Intermolecular Interactions in Chemistry and Biology*; Elsevier Scientific: Amsterdam, 1980.
- (2) Kaplan, I. G. *Theory of Molecular Interactions*; Elsevier: Amsterdam, 1986.
- (3) Müller-Dethlefs, K.; Hobza, P. *Chem. Rev.* **2000**, *100*, 143-147.
- (4) Stone, A. J. *The Theory of Intermolecular Forces*; Oxford University Press: Oxford, 2002.
- (5) Hobza, P.; Muller-Dethlefs, K. *Non-Covalent Interactions*; RSC: Cambridge, 2010.
- (6) Hobza, P.; Zahradnik, R.; Müller-Dethlefs, K. *Collect. Czech. Chem. Commun.* **2006**, *71*, 443–531.
- (7) Kollman, P. A. *Acc. Chem. Res.* **1977**, *10*, 365-371.
- (8) Gilson, M. K.; Mihailescu, M. *Biophys. J.* **2004**, *87*, 23-36.
- (9) Lewis, G. N. *J. Am. Chem. Soc.* **1931**, *53*, 1367.
- (10) Beer, P. D.; Gale, P. A.; Smith, D. K. *Supramolecular Chemistry*; Oxford University Press: New York, 1999.
- (11) Lehn, J-M. *Angew. Chem., Int. Ed. Engl.* **1988**, *27*, 89-112; *ibid.* **1990**, *29*, 1304-1319.
- (12) Duncan, R.; Kopecek, J. *Adv. Polym. Sci.* **1984**, *57*, 51-101.

- (13) Huck, W. T. S.; Prins, L. J.; Fokkens, R. H.; Nibbering, N. M.; van Veggel, F. C. J. M.; Reinhoudt, D. N. *J. Am. Chem. Soc.* **1998**, *120*, 6240-6246.
- (14) Warshel, A.; Papazyan, A.; Kollman, P. A. *Science* **1995**, *269*, 102-104.
- (15) Scheiner, S. *Hydrogen Bonding. A Theoretical Perspective*; Oxford University Press: New York, 1997.
- (16) Schuster, P. *Hydrogen Bonds*; Springer-Verlag: Berlin, 1984; Vol. 120.
- (17) Gilli, G.; Gilli, P. *The Nature of the Hydrogen Bond*; Oxford University Press: Oxford, UK, 2009.
- (18) *The Hydrogen Bond. Recent Developments in Theory and Experiments*; Schuster, P.; Zundel, G.; Sandorfy, C., Eds.; North-Holland Publishing Co.: Amsterdam, 1976.
- (19) Jeffrey, G. A.; Saenger, W. *Hydrogen Bonding in Biological Structures*; Springer-Verlag: Berlin, 1991.
- (20) Alabugin, I. V.; Manoharan, M.; Peabody, S.; Weinhold, F. *J. Am. Chem. Soc.* **2003**, *125*, 5973-5987.
- (21) Wieczorek, R.; Dannenberg, J. J. *J. Am. Chem. Soc.* **2003**, *125*, 8124-8129.
- (22) Hernández-Soto, H.; Weinhold, F.; Francisco, J. S. *J. Chem. Phys.* **2007**, *127*, 164102.
- (23) Glowacki, E. D.; Irimia-Vladu, M.; Bauerb, S.; Sariciftcia, N. S. *J. Mater. Chem. B* **2013**, *1*, 3742-3753.
- (24) Cu, Z.; Zambrano, R.; McDermott, A. *J. Am. Chem. Soc.* **1994**, *116*, 6368-6372.
- (25) Nilar, S. H.; Pluta, T. S. *J. Am. Chem. Soc.* **1995**, *117*, 12603-12607.

- (26) Johansson, A.; Kollman, P.; Rothenberg, S.; McKelvey, J. *J. Am. Chem. Soc.* **1974**, *96*, 3794-3800.
- (27) Seaman, F. C.; Hurley, F. C. *J. Am. Chem. Soc.* **1998**, *120*, 13028-13041.
- (28) Lipsitz, R. S.; Sharma, Y.; Brooks, B. R.; Tjandra, N. *J. Am. Chem. Soc.* **2002**, *124*, 10621-10626.
- (29) Pauling L. *J. Am. Chem. Soc.* **1931**, *53*, 1367-1400.
- (30) Alkorta, I.; Rozas, S.; Elguero, J. *J. Phys. Chem. A* **1998**, *102*, 9278-9285.
- (31) Wash, P. L.; Ma, S.; Obst, U.; Rebek, J. *J. Am. Chem. Soc.* **1999**, *121*, 7973-7974.
- (32) Nguyen, H. L.; Horton, P. N.; Hursthouse, M. B.; Legon, A. C.; Bruce, D. W. *J. Am. Chem. Soc.* **2004**, *126*, 16-17.
- (33) Gu, Y.; Kar, T.; Scheiner, S. *J. Mol. Struct.* **2000**, *552*, 17-31.
- (34) *Hydrogen Bonding - New Insights*; Grabowski, S. J., Ed.; Springer: Dordrecht, 2006.
- (35) Desiraju, G. R. *Angew. Chem. Int. Ed.* **2011**, *50*, 52-59.
- (36) Scheiner, S. *Phys. Chem. Chem. Phys.* **2011**, *13*, 13860-13872.
- (37) Takahashi, O.; Kohno, Y.; Nishio, M. *Chem. Rev.* **2010**, *110*, 6049-6076.
- (38) Alkorta, I.; Elguero, J.; Bene, J. E. D. *Chem. Phys. Lett.* **2010**, *489*, 159-163.
- (39) Rizzato, S.; Bergès, J.; Mason, S. A.; Albinati, A.; Kozelka, J. *Angew. Chem. Int. Ed.* **2010**, *49*, 7440-7443.
- (40) Lommerse, J. P. M.; Stone, A. J.; Taylor, R.; Allen, F. H. *J. Am. Chem. Soc.* **1996**, *118*, 3108-3116.

- (41) Arunan, E.; Desiraju, G. R.; Klein, R. A.; Sadlej, J.; Scheiner, S.; Alkorta, I.; Clary, D. C.; Crabtree, R. H.; Dannenberg, J. J.; Hobza, P.; Kjaergaard, H. G.; Legon, A. C.; Mennucci, B.; Nesbitt, D. J. *Pure Appl. Chem.* **2011**, *83*, 1637-1641.
- (42) Veken, B. J. v. d.; Delanoye, S. N.; Michielsens, B.; Herrebout, W. A. *J. Mol. Struct.* **2010**, *976*, 97-104.
- (43) Cavallo, G.; Metrangolo, P.; Pilati, T.; Resnati, G.; Sansotera, M.; Terraneo, G. *Chem. Soc. Rev.* **2010**, *39*, 3772-3783.
- (44) Chudzinski, M. G.; McClary, C. A.; Taylor, M. S. *J. Am. Chem. Soc.* **2011**, *133*, 10559-10567.
- (45) Zierkiewicz, W.; Wieczorek, R.; Hobza, P.; Michalska, D. *Phys. Chem. Chem. Phys.* **2011**, *13*, 5105-5113.
- (46) Walter, S. M.; Kniep, F.; Herdtweck, E.; Huber, S. M. *Angew. Chem. Int. Ed.* **2011**, *50*, 7187-7191.
- (47) Politzer, P.; Murray, J. S.; Clark, T. *Phys. Chem. Chem. Phys.* **2010**, *12*, 7748-7757.
- (48) Grzechnik, K.; Rutkowski, K.; Mielke, Z. *J. Mol. Struct.* **2012**, *1009*, 96-102.
- (49) Bhattacharjee, A.; Matsuda, Y.; Fujii, A.; Wategaonkar, S. *ChemPhysChem* **2013**, *14*, 905-914.
- (50) Biswal, H. S.; Wategaonkar, S. *J. Phys. Chem. A* **2009**, *113*, 12774-12782.
- (51) Howard, N. W.; Legon, A. C. *J. Chem. Phys.* **1986**, *85*, 6898-6904.
- (52) Gu, Y.; Kar, T.; Scheiner, S. *J. Am. Chem. Soc.* **1999**, *121*, 9411-9422.
- (53) You, L.-Y.; Chen, S.-G.; Zhao, X.; Liu, Y.; Lan, W.-X.; Zhang, Y.; Lu, H.-J.; Cao, C.-Y.; Li, Z.-T. *Angew. Chem. Int. Ed.* **2012**, *51*, 1657-1661.

- (54) Scheiner, S., The CH--O Hydrogen Bond. A Historical Account. In *Theory and Applications of Computational Chemistry: The First 40 Years*; Dykstra, C. E.; Frenking, G.; Kim, K. S.; Scuseria, G. E., Eds.; Elsevier: Amsterdam, 2005; pp 831-857.
- (55) Scheiner, S. *Curr. Org. Chem.* **2010**, *14*, 106-128.
- (56) Nishio, M. *Phys. Chem. Chem. Phys.* **2011**, *13*, 13873-13900.
- (57) Nakanaga, T.; Buchhold, K.; Ito, F. *Chem. Phys.* **2003**, *288*, 69-76.
- (58) Takahashi, O.; Kohno, Y.; Nishio, M. *Chem. Rev.* **2010**, *110*, 6049-6076.
- (59) Kar, T.; Scheiner, S. *J. Chem. Phys.* **2003**, *119*, 1473-1482.
- (60) Solimannejad, M.; Scheiner, S. *J. Phys. Chem. A* **2005**, *109*, 11933-11935.
- (61) Belkova, N. V.; Shubina, E. S.; Epstein, L. M. *Acc. Chem. Res.* **2005**, *38*, 624-631.
- (62) Arunan, E.; Desiraju, G.R.; Klein, R.A.; Sadlej, J.; Scheiner, S.; Alkorta, I.; Clary, D.C.; Crabtree, R.H.; Dannenberg, J.J.; Hobza, P.; Kjaergaard, H.G.; Legon, A.C.; Mennucci, B.; Nesbitt, D.J. *Pure Appl. Chem.* **2011**, *83*, 1619-1636.
- (63) Cybulski, S.; Scheiner, S. *J. Am. Chem. Soc.* **1987**, *109*, 4199-4206.
- (64) Seiler, P.; Weisman, G. R.; Glendening, E. D.; Weinhold, F.; Johnson V. B.; Dunitz, J. D. *Angew. Chem. Int. Ed. Engl.* **1987**, *26*, 1175-1177.
- (65) Wiberg, K. B.; Waldron, R. F.; Schulte, G.; Saunders, M. *J. Am. Chem. Soc.* **1991**, *113*, 971-977.
- (66) Vaz, P. D.; Nolasco, M. M.; Gil, F. P. S. C.; Ribeiro-Claro, P. J. A.; Tomkinson, J. *Chem.Eur. J.* **2010**, *16*, 9010-9017.
- (67) Cubero, E.; Orozco, M.; Hobza, P.; Luque, F. J. *J. Phys. Chem. A* **1999**, *103*, 6394-6401.

- (68) Scheiner, S.; Kar, T. *J. Phys. Chem. A* **2008**, *112*, 11854-11860.
- (69) Ford, T. A.; Glasser, L. *J. Mol. Struct.:THEOCHEM* **1997**, 398-399, 381-394.
- (70) Zierkiewicz, W.; Czarnik-Matusiewicz, B.; Michalska, D. *J. Phys. Chem. A* **2011**, *115*, 11362-11368.
- (71) Scheiner, S.; Grabowski, S. J.; Kar, T. *J. Phys. Chem. A* **2001**, *105*, 10607-10612.
- (72) Glaser, R.; Chen, N.; Wu, H.; Knotts, N.; Kaupp, M. *J. Am. Chem. Soc.* **2004**, *126*, 4412-4419.
- (73) Caronna, T.; Liantonio, R.; Logothetis, T. A.; Metrangolo, P.; Pilati, T.; Resnati, G. *J. Am. Chem. Soc.* **2004**, *126*, 4500-4501.
- (74) Mignon, P.; Loverix, S.; Steyaert, J.; Geerlings, P. *Nucleic Acids Res.* **2005**, *33*, 1779-1789.
- (75) Scheiner, S. *Phys. Chem. Chem. Phys.* **2011**, *13*, 13860-13872.
- (76) Solimannejad, M.; Gharabaghi, M.; Scheiner, S. *J. Chem. Phys.* **2011**, *134*, 024312.
- (77) Scheiner, S. *J. Chem. Phys.* **2011**, *134*, 094315.
- (78) Scheiner, S. *J. Phys. Chem. A* **2011**, *115*, 11202-11209.
- (79) Scheiner, S. *Chem. Phys. Lett.* **2011**, *514*, 32-35.
- (80) Rosenfield, R. E.; Parthasarathy, R.; Dunitz, J. D. *J. Am. Chem. Soc.* **1977**, *99*, 4860-4862.
- (81) Iwaoka, M.; Takemoto, S.; Tomoda, S. *J. Am. Chem. Soc.* **2002**, *124*, 10613-10620.
- (82) Horowitz, S.; Yesselman, J. D.; Al-Hashimi, H. M.; Trievel, R. C. *J. Biol. Chem.* **2011**, *286*, 18658-18663.
- (83) Horowitz, S.; Trievel, R. C. *J. Biol. Chem.* **2012**, *287*, 41576-41582.

- (84) Scheiner, S. *J. Phys. Chem. B* **2006**, *110*, 18670-18679.
- (85) Scheiner, S. *J. Phys. Chem. B* **2007**, *111*, 11312-11317.
- (86) Fricke, H.; Gerlach, A.; Unterberg, C.; Wehner, M.; Schrader, T.; Gerhards, M. *Angew. Chem. Int. Ed.* **2009**, *48*, 900-904.
- (87) Fricke, H.; Funk, A.; Schrader, T.; Gerhards, M. *J. Am. Chem. Soc.* **2008**, *130*, 4692-4698.
- (88) Jiang, L.; Lai, L. *J. Biol. Chem.* **2002**, *277*, 37732-37740.
- (89) Jones, C. R.; Baruah, P. K.; Thompson, A. L.; Scheiner, S.; Smith, M. D. *J. Am. Chem. Soc.* **2012**, *134*, 12064-12071.
- (90) Scheiner, S. *J. Chem. Phys.* **2011**, *134*, 164313.
- (91) Deakyne, C. A.; Meot-Ner, M. *J. Am. Chem. Soc.* **1999**, *121*, 1546-1557.
- (92) Shishkin, O. V.; Palamarchuk, G. V.; Gorb, L.; Leszczynski, J. *Chem. Phys. Lett.* **2008**, *452*, 198-205.
- (93) Tatko, C. D.; Waters, M. L. *J. Am. Chem. Soc.* **2004**, *126*, 2028 - 2034.
- (94) Chabynyc, M. L.; Brauman, J. I. *J. Am. Chem. Soc.* **1998**, *120*, 10863-10870.
- (95) Hu, H.; Bhowmick, P.; Zhao, B.; Hamon, M. A.; Itkis, M. E.; Haddon, R. C. *Chem. Phys. Lett.* **2001**, *345*, 25-28.
- (96) Marshall, M. W.; Popa-Nita, S.; Shapter, J. G. *Carbon* **2006**, *44*, 1137-1141.
- (97) Niyogi, S.; Hamon, M. A.; Hu, H.; Zhao, B.; Bhowmick, P.; Sen, R.; Itkis, M. E.; Haddon, R. C. *Acc. Chem. Res.* **2002**, *35*, 1105-1113.
- (98) Kar, T.; Scheiner, S.; Roy, A. K.; Bettinger, H. F. *J. Phys. Chem. C* **2012**, *116*, 26072-26083.

CHAPTER 2

THE S \cdots N NONCOVALENT INTERACTION: COMPARISON WITH HYDROGEN
AND HALOGEN BONDS¹**Abstract**

When one of the H atoms of SH₂ is replaced by a halogen X, the S engages in a strong S \cdots N interaction with the N of NH₃, wherein X lies directly opposite the N. The binding energy varies from 8 kcal/mol for X=F down to 5 kcal/mol for Br. This FS \cdots N geometry represents the global minimum on the HSF/NH₃ potential energy surface, more stable than minima containing either a SH \cdots N or NH \cdots F H-bond. It is equally stable with a SH \cdots N structure for X=Cl, and slightly less stable than SH \cdots N for X=Br. In all cases, the S \cdots N minimum is more stable than geometries containing a halogen bond.

2-1. Introduction

The study of noncovalent forces has a long history [1-3], which has led to their compartmentalization into various categories. The definition of the hydrogen bond [4-8] has undergone a broadening in recent years to include C, Cl, π bonds, σ bonds, metal atoms, or even direct interaction between a pair of H atoms [9-16]. The replacement of the bridging H by a halogen atom leads to another strong sort of interaction but at the same time alters its fundamental nature [17-23].

Recent work in this laboratory [24-27] has identified a fundamentally different sort of noncovalent interaction between a P atom and the N atom on another molecule,

¹ Coauthored by Upendra Adhikari and Steve Scheiner. Reproduced with permission from *Chem. Phys. Lett.* **2011**, 514, 36-39. Copyright 2011, Elsevier.

with no intervening H or halogen atom. This attraction is due in large measure to charge transfer from the N lone pair into the σ^* antibond of the P-H bond. But unlike the PH \cdots N H-bond where this same charge transfer takes place, the pertinent H atom lies directly opposite the N lone pair. In addition to this charge transfer effect, there is also a sizable electrostatic attraction, as well as a dispersion component. This sort of interaction is not unique to P, but is also characteristic [28] of other second-row atoms S and Cl, as well as the third-row congener As, all of which can engage in a direct interaction with an electron-donating N atom. A pair of N atoms will also engage in this sort of attractive interaction, but only [29] if the H atom that lies opposite to the N of the partner molecule is replaced by an electron-withdrawing atom such as F.

In the examination of the putative S \cdots N interaction [28] it was noted that while the force between the S and N atoms of SH₂ and NH₃ is indeed attractive, the electrostatic potential surrounding the SH₂ molecule permitted a displacement of the NH₃ electron donor toward one of the SH₂ protons, so as to engage in a SH \cdots N H-bond, a somewhat stronger interaction. Given the observation that replacement of one of the H atoms of the electron acceptor by a halogen strengthens the direct P \cdots N or N \cdots N interaction [27], the question arises as to whether a similar substitution on SH₂ might stabilize the direct S \cdots N interaction so as to yield a true minimum on the potential energy surface of SH₂/NH₃, and whether this interaction might be competitive in strength with the SH \cdots N H-bond.

The present communication considers this question by replacing one H atom of SH₂ by each of a series of halogens, X=F, Cl, and Br. Each SXH molecule is paired with NH₃ as electron donor and all minima on the potential energy surface identified. As this heterodimer offers the options of hydrogen and halogen bonds which might compete with

direct S \cdots N bonding, it is possible to assess the strengths of each sort of interaction in comparison with the others. The results demonstrate that a S \cdots N interaction is not only feasible if one of the partners has been halogenated, but its strength exceeds that of a SH \cdots N H-bond in the case of X=F and equal to a H-bond when X=Cl. The S \cdots N interaction is also stronger than the NH \cdots X H-bond, or a SX \cdots N halogen bond.

2-2. Computational Methods

Calculations were carried out via the Gaussian 03 package [30]. Geometries were optimized at the ab initio MP2/aug-cc-pVDZ level, an approach which has been shown to be of high accuracy, especially for weak intermolecular interactions of the type of interest here where the data are in close accord with CCSD(T) values [27,31], and in nearly perfect coincidence with experimental energetics [32]. All minima were identified on the potential energy surface of each pair of molecules, by using a variety of different starting points for geometry optimizations. Minima were verified as having all real vibrational frequencies. Interaction energies were corrected for basis set superposition error by the counterpoise procedure [33]. Natural bond orbital (NBO) analysis [34,35] was performed via the procedures contained within Gaussian 03.

2-3. Results

The potential energy surface of each HSX/NH₃ pair contains several minima. The first category, and the one which represents the global minimum for both X=F and Cl, is illustrated in Figure 2-1. Each structure is characterized by the location of the halogen atom almost diametrically opposite the N atom, with θ (XS \cdots N) angles of about 170°. The counterpoise-corrected interaction energies of each complex are included in Figure 2-1

from which it may be seen that the FS \cdots N structure is bound by 7.9 kcal/mol, and small reductions occur as one proceeds from X=F to Cl and then to Br.

Other facets of these structures are reported in Table 2-1, which illustrates that the progressive weakening of the bonding in the order F \rightarrow Cl \rightarrow Br also results in a lengthening of the R(S \cdots N) intermolecular distance. The next row of Table 2-1 displays the stretch of the X-S covalent bond that occurs when the XSH monomer engages in the complex. This elongation is greatest for X=F at 40 mÅ, and is reduced slightly to 36 mÅ for X=Br. The main source of this bond stretch is the shift of electron density from the N lone pair into the S-X antibonding orbital. The energetic measure of this shift is the NBO value of E(2), which is as much as 28 kcal/mol for FSH and is cut in half by the replacement of F by Br. The amount of charge shifted from the N lone pair to the σ^* orbital is reported in the last row of Table 2-1, and likewise undergoes a reduction in the F, Cl, Br sequence.

The second type of complex observed is related to that in Figure 2-1, except that the H and X atoms exchange places, with the H atom now lying opposite to the N. As may be noted in Figure 2-2, the H atom lies between 162° and 169° from the N. The R(S \cdots N) distances are considerably longer than those in Figure 2-1, which is consistent with the much weaker nature of these HS \cdots N complexes. Taking X=F as an example, the HS \cdots N structure pictured in Figure 2-2a is weaker than the FS \cdots N interaction in Figure 2-1a by a factor of ¼. The remainder of the salient features of these structures are reported in Table 2-2 which underscore the weaker binding, less than 2 kcal/mol in all cases. Consequently, the intermolecular distances are longer, the degree of R(S-H) bond

stretching is smaller, less than 7 mÅ, and the NBO charge transfer quantities are much smaller as well. There is only slight dependence upon the nature of the halogen atom, consistent with the idea that this atom is not directly involved in the bonding.

The geometries in Figure 2-2 are such that one might suspect a weak H-bond between the halogen and the H atoms of NH₃. However, there is no such bond. In the first place, the X···H interatomic distances are rather long. Secondly, the $\theta(\text{NH}\cdots\text{X})$ angles are far from linearity. And finally, NBO analysis reveals no significant charge transfer between the halogen lone pairs and the pertinent N-H bonds. One may conclude that the binding here is purely of the HS···N type.

The third category of complex is one which involves a SH···N H-bond. As illustrated in Figure 2-3, there is also present a weak attractive interaction between the halogen and a NH bond which is partly responsible for a small distortion of each SH···N H-bond from linearity. In the H-bonded cases, the X=F complex is the most weakly bound of the three, with the Cl and Br complexes bearing an equally strong total interaction. Comparison of the interaction energies displayed in Figure 2-3 with those in Figure 2-1 leads to the following conclusion about global minima. The FS···N structure 2-1a is clearly more stable than SH···N 2-3a, whereas the opposite is true for X = Br, where SH···N 2-3c is 0.7 kcal/mol more stable than BrS···N 2-3a. The situation for X=Cl is intermediate in that 2-1b and 2-3b are effectively equal in energy.

Each XSH/NH₃ pair contains a fourth minimum on its surface, which are displayed in Figure 2-4. In the X = F case, this minimum 2-4a contains a NH···F H-bond, which is in fact second only to the FS···N complex 2-1a in terms of stability, surpassing that of the SH···N H-bond in 2-3a. The NH₃ molecule rotates around for X = Cl and Br,

so as to form a $SX\cdots N$ halogen bond instead of a $NH\cdots X$ H-bond. As is normally the case, this bond is very nearly linear, and Br engages in a stronger halogen bond than does Cl. The strength of this bond yields a shorter $R(X\cdots N)$ for Br, despite the larger atomic radius of Br. Also consistent with this trend is the greater S-X bond elongation for $X = Br$, 19 me vs 8 me for $X = Cl$. The NBO perturbation energy $E(2)$ for charge transfer into the S-X antibonding orbital is also nearly 3 times greater for Br than for Cl. The failure of F to participate in a halogen bond is not surprising, as this atom is generally reluctant to do so, usually preferring to act as H-bond proton acceptor as in 2-4a. And likewise, the absence of a minimum containing a $NH\cdots Cl$ or $NH\cdots Br$ H-bond is consistent with the lesser electronegativities of Cl and Br relative to F.

Examination of the electrostatic potential that surrounds each monomer can provide some insights into the source of the optimal geometries. These potentials are exhibited in Figure 2-5. Each monomer is arranged as it occurs in the global minima of Figure 2-1. It is immediately obvious that the blue positive potential to the right of the S atom in every case overlaps nicely with the negative (red) region to the left of NH_3 . There is also an extended positive region along the S-H direction of each XSH molecule that helps explain the stability of the $SH\cdots N$ H-bonded complexes in Figure 2-3. There is a much smaller blue region above each S atom in Figure 2-5, directly opposite the S-H bond, which comes into play in the $HS\cdots N$ minima of Figure 2-2. These geometries will also be abetted by an overlap between the negative regions near each halogen atom, perpendicular to the S-X bond. This area can overlap with the blue regions around the H atoms of NH_3 . Finally, one may note a blue positive region directly to the left of the halogen atoms when $X = Cl$ or Br , but not F. This attribute helps explain why a $SX\cdots N$

halogen bond will form for only the two former atoms. It is the absence of this positive region around F, coupled with the particularly prominent negative region to its left, that permits this atom to engage in a $\text{NH}\cdots\text{F}$ H-bond, an interaction that eludes both Cl and Br.

There is one last class of minima on these surfaces. These are very weakly bound, with interaction energies of 1 kcal/mol or less. After zero-point vibrational energies are added, their binding energies are even smaller, roughly 0.2 kcal/mol and some even less. These structures are “shadow minima” of a sort, in that each one resembles a deeper minimum in Figures 2-1 - 2-4. Where they differ is that the NH_3 molecule is rotated about 180° so that its lone pair is turned away from the partner molecule, not toward it. These structures may perhaps best be understood by bearing in mind that the main lobe of the N lone pair has a smaller tail in the opposite direction, much like a hybrid orbital. Indeed, the NH_3 lone pair is categorized as a sp^3 orbital by NBO analysis. This tail can overlap with the requisite antibonds of the partner molecule, and transfer charge into them, in much the same way as the main lobe, albeit to a lesser extent. Any interaction is further weakened by electrostatic effects, since this minor lobe is present on the side of the NH_3 molecule that has a positive electrostatic potential, which would tend to repel certain atoms, like the bridging hydrogen of an approaching proton-donor molecule.

2-4. Conclusions

In summary, the replacement of one of the H atoms of H_2S by a halogen does indeed result in a highly attractive force between the S and a N atom of NH_3 . Whether X = F, Cl, or Br, the $\text{XS}\cdots\text{N}$ structure represents a true minimum on the potential energy

surface of the XSH/NH₃ heterodimer, with binding energies between 7.9 kcal/mol for X = F, down to 4.7 kcal/mol for Br. In the case of X = F, the FS⋯N structure represents the global minimum. Second in stability is the structure which contains a classic NH⋯F H-bond; and slightly less stable is the complex comprising a SH⋯N H-bond.

When F is replaced by other halogens, the stability of the XS⋯N complex diminishes a bit, but remains fairly strong. Cl or Br substitution has the opposite effect of strengthening the SH⋯N H-bond energy. As a result the latter is the global minimum for BrSH/NH₃, stronger than the BrS⋯N bond by some 0.7 kcal/mol. The situation for X=Cl is intermediate, in that the ClS⋯N and SH⋯N geometries are nearly equal in energy.

Related to the XS⋯N structure is one in which the H atom of HSX replaces the halogen as the atom which lies diametrically opposite the N atom. While representing a true minimum for all X = F, Cl, Br, the binding energy is only about 2 kcal/mol. And finally, when the halogen atom is either Cl or Br, but not F, one obtains a fourth minimum on the surface, this time involving a SX⋯N halogen bond. While rather weakly bound for X = Cl, this bond is stronger for HSB_r, amounting to 3.5 kcal/mol.

The literature contains some confirmation of the stability of complexes of the XS⋯N type. Surveys of crystal structures prior to 1980 [36], for example, noted a propensity for nucleophiles to approach a divalent S atom approximately along an extension of a S-X bond, a tendency confirmed [37] later. Some specifics emerge from an N-acetylglycine ethyl dithioester [38] where a S⋯N pair lay less than 3 Å from one another, with a $\theta(\text{CS}\cdots\text{N})$ angle of 161°, close to the angles predicted here by quantum calculations. And although the authors did not carry out a search for the presence of other minima, a calculation [39] of the dimer pairing NH₃ with SF₂ identified a minimum in

which the N atom lies 175° from a S-F bond axis. When S is placed in the context of a 5-membered ring, there is a tendency of a water molecule to position itself between 157° and 166° from a S-C bond [40].

References

- [1] P. Hobza, R. Zahradnik, *Weak Intermolecular Interactions in Chemistry and Biology*, Elsevier Scientific, Amsterdam, 1980.
- [2] A.J. Stone, *The Theory of Intermolecular Forces*, Oxford University Press, Oxford, 2002.
- [3] P. Hobza, K. Muller-Dethlefs, *Non-Covalent Interactions*, RSC, Cambridge, 2010.
- [4] G.C. Pimentel, A.L. McClellan, *The Hydrogen Bond*, Freeman, San Francisco, 1960.
- [5] P. Schuster, G. Zundel, C. Sandorfy (Ed.), *The Hydrogen Bond. Recent Developments in Theory and Experiments*. North-Holland Publishing Co., Amsterdam, 1976.
- [6] G.A. Jeffrey, W. Saenger, *Hydrogen Bonding in Biological Structures*, Springer-Verlag, Berlin, 1991.
- [7] S. Scheiner, *Hydrogen Bonding. A Theoretical Perspective*, Oxford University Press, New York, 1997.
- [8] G. Gilli, P. Gilli, *The Nature of the Hydrogen Bond*, Oxford University Press, Oxford, UK, 2009.

- [9] G.R. Desiraju, T. Steiner, *The Weak Hydrogen Bond in Structural Chemistry and Biology*, Oxford, New York, 1999.
- [10] S. Scheiner, Y. Gu, T. Kar, *J. Mol. Struct. (Theochem)*. 500 (2000) 441.
- [11] S.J. Grabowski (Ed.), *Hydrogen Bonding - New Insights*. Springer, Dordrecht, 2006.
- [12] B.J.v.d. Veken, S.N. Delanoye, B. Michielsens, W.A. Herrebout, *J. Mol. Struct.* 976 (2010) 97.
- [13] O. Takahashi, Y. Kohno, M. Nishio, *Chem. Rev.* 110 (2010) 6049.
- [14] I. Alkorta, J. Elguero, J.E.D. Bene, *Chem. Phys. Lett.* 489 (2010) 159.
- [15] G.R. Desiraju, *Angew. Chem., Int. Ed. Engl.* 50 (2011) 52.
- [16] E. Arunan, G.R. Desiraju, R.A. Klein, J. Sadlej, S. Scheiner, I. Alkorta, D.C. Clary, R.H. Crabtree, J.J. Dannenberg, P. Hobza, H.G. Kjaergaard, A.C. Legon, B. Mennucci, D.J. Nesbitt, *Pure Appl. Chem.* 83 (2011) 1637.
- [17] A. Karpfen, *J. Phys. Chem. A*. 104 (2000) 6871.
- [18] P. Auffinger, F.A. Hays, E. Westhof, P.S. Ho, *Proc. Nat. Acad. Sci., USA*. 101 (2004) 16789.
- [19] G. Cavallo, P. Metrangolo, T. Pilati, G. Resnati, M. Sansotera, G. Terraneo, *Chem. Soc. Rev.* 39 (2010) 3772.
- [20] V.R. Hathwar, T.N.G. Row, *J. Phys. Chem. A*. 114 (2010) 13434.
- [21] P. Politzer, J.S. Murray, T. Clark, *Phys. Chem. Chem. Phys.* 12 (2010) 7748.
- [22] M. Tuikka, M. Niskanen, P. Hirva, K. Rissanen, A. Valkonen, M. Haukka, *Chem. Commun.* 47 (2011) 3427.

- [23] W. Zierkiewicz, R. Wieczorek, P. Hobza, D. Michalska, *Phys. Chem. Chem. Phys.* 13 (2011) 5105.
- [24] M. Solimannejad, M. Gharabaghi, S. Scheiner, *J. Chem. Phys.* 134 (2011) 024312.
- [25] S. Scheiner, *J. Chem. Phys.* 134 (2011) 094315.
- [26] S. Scheiner, *Phys. Chem. Chem. Phys.* 13 (2011) 13860.
- [27] S. Scheiner, *J. Phys. Chem. A.* 115 (2011) 11202-11209.
- [28] S. Scheiner, *J. Chem. Phys.* 134 (2011) 164313.
- [29] S. Scheiner, *Chem. Phys. Lett.* 514 (2011) 32.
- [30] M.J. Frisch, G.W. Trucks, H.B. Schlegel, G.E. Scuseria, M.A. Robb, J.R. Cheeseman, V.G. Zakrzewski, J. Montgomery, J. A., R.E. Stratmann, J.C. Burant, S. Dapprich, J.M. Millam, A.D. Daniels, K.N. Kudin, M.C. Strain, O. Farkas, J. Tomasi, V. Barone, M. Cossi, R. Cammi, B. Mennucci, C. Pomelli, C. Adamo, S. Clifford, J. Ochterski, G.A. Petersson, P.Y. Ayala, Q. Cui, K. Morokuma, D.K. Malick, A.D. Rabuck, K. Raghavachari, J.B. Foresman, J. Cioslowski, J.V. Ortiz, A.G. Baboul, B.B. Stefanov, G. Liu, A. Liashenko, P. Piskorz, I. Komaromi, R. Gomperts, R.L. Martin, D.J. Fox, T. Keith, M.A. Al-Laham, C.Y. Peng, A. Nanayakkara, C. Gonzalez, M. Challacombe, P.M.W. Gill, B. Johnson, W. Chen, M.W. Wong, J.L. Andres, C. Gonzalez, M. Head-Gordon, E.S. Replogle, J.A. Pople, Gaussian03. Gaussian, Inc., Pittsburgh PA, 2003.
- [31] R.M. Osuna, V. Hernández, J.T.L. Navarrete, E. D’Oria, J.J. Novoa, *Theor. Chem. Acc.* 128 (2011) 541.

- [32] D. Hauchecorne, A. Moiana, B.J.v.d. Veken, W.A. Herrebout, *Phys. Chem. Chem. Phys.* 13 (2011) 10204.
- [33] S.F. Boys, F. Bernardi, *Mol. Phys.* 19 (1970) 553.
- [34] A.E. Reed, F. Weinhold, L.A. Curtiss, D.J. Pochatko, *J. Chem. Phys.* 84 (1986) 5687.
- [35] A.E. Reed, L.A. Curtiss, F. Weinhold, *Chem. Rev.* 88 (1988) 899.
- [36] R.E. Rosenfield, R. Parthasarathy, J.D. Dunitz, *J. Am. Chem. Soc.* 99 (1977) 4860.
- [37] M. Iwaoka, S. Takemoto, S. Tomoda, *J. Am. Chem. Soc.* 124 (2002) 10613.
- [38] C.P. Huber, Y. Ozaki, D.H. Pliura, A.C. Storer, P.R. Carey, *Biochem.* 21 (1982) 3109.
- [39] J.S. Murray, P. Lane, T. Clark, P. Politzer, *J. Mol. Model.* 13 (2007) 1033.
- [40] J.S. Murray, P. Lane, P. Politzer, *Int. J. Quantum Chem.* 108 (2010) 2770.

Table 2-1. Energetic (kcal/mol), geometric and electronic aspects of XS⋯N complexes in Figure 2-1

	1a	1b	1c
$-\Delta E$	9.71	6.89	6.20
$-\Delta E^{\text{CP,a}}$	7.91	5.44	4.72
$-\Delta E^{\text{CP+ZPE,b}}$	5.77	3.88	3.32
$R(\text{S-N}), \text{\AA}$	2.467	2.658	2.701
$\Delta r(\text{X-S}), \text{m\AA}$	40.4	38.8	36.3
$E(2)^{\text{c}}$	27.88	15.84	13.84
$\Delta q^{\text{c}}, \text{me}$	57.2	35.8	33.0

^aCP=counterpoise correction

^bZPE= zero-point vibrational correction

^c $N_{\text{lp}} \rightarrow \sigma^*(\text{SX})$

Table 2-2. Energetic (kcal/mol), geometric and electronic aspects of HS⋯N complexes in Figure 2-2

	2a	2b	2c
$-\Delta E$	2.90	2.96	3.17
$-\Delta E^{\text{CP}}$	1.99	1.90	1.78
$-\Delta E^{\text{CP+ZPE}}$	0.74	0.73	0.60
$R(\text{S-N}), \text{\AA}$	3.111	3.161	3.183
$\Delta r(\text{H-S}), \text{m\AA}$	6.5	5.5	4.1
$E(2)^{\text{a}}$	1.45	1.55	1.55
$\Delta q^{\text{a}}, \text{me}$	2.5	2.7	2.7

^a $N_{\text{lp}} \rightarrow \sigma^*(\text{SH})$

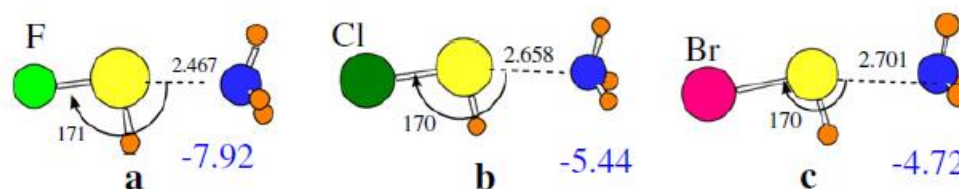


Figure 2-1. Optimized structures of XS⋯N complexes for X= a) F, b) Cl, and c) Br. Counterpoise-corrected interaction energies in kcal/mol, distances in Å, and angles in degs.

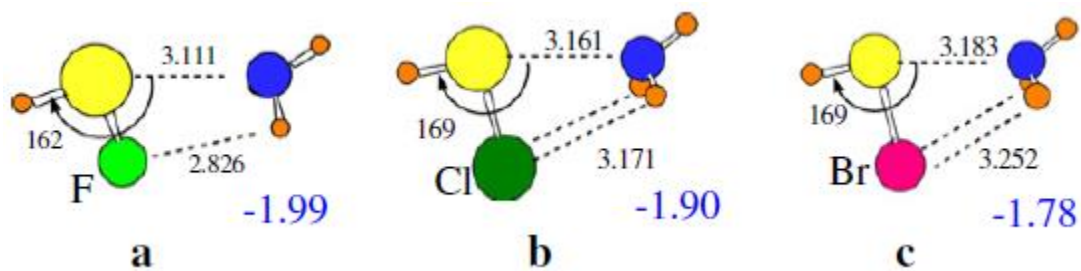


Figure 2-2. Optimized geometries of HS...N complexes. Counterpoise-corrected interaction energies in kcal/mol, distances in Å, and angles in degs.

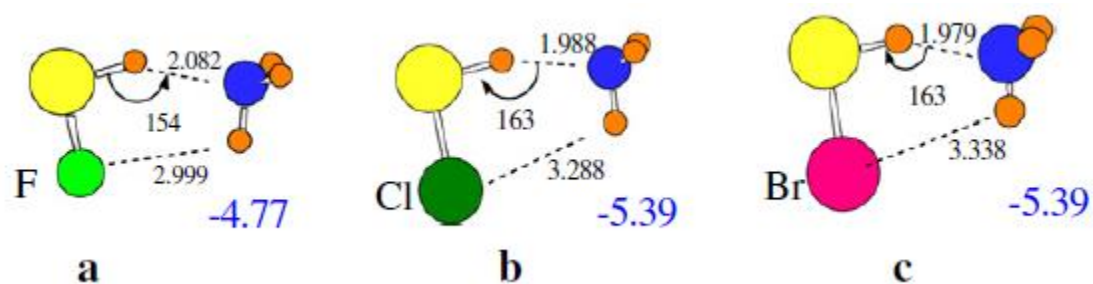


Figure 2-3. Optimized geometries of SH...N complexes. Counterpoise-corrected interaction energies in kcal/mol, distances in Å, and angles in degs.

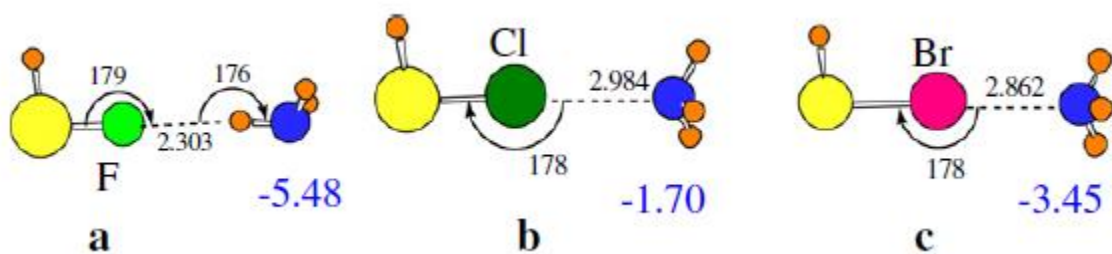


Figure 2-4. Optimized geometries of a) NH...F, b) SCl...N, and c) SBr...N complexes. Counterpoise-corrected interaction energies in kcal/mol, distances in Å, and angles in degs.

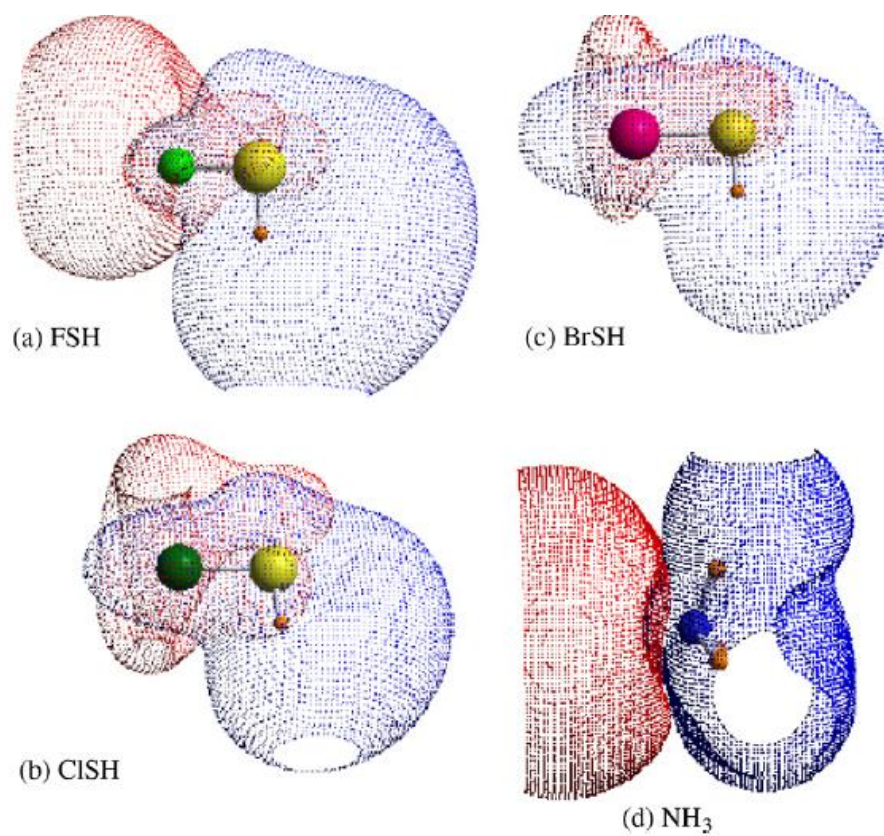


Figure 2-5. Electrostatic potentials of the isolated monomers of XSH and NH₃. Contour shown corresponds to ± 0.01 au, with blue/red indicating positive/negative sign of the potential.

CHAPTER 3

ABILITIES OF DIFFERENT ELECTRON DONORS (D) TO ENGAGE IN A P \cdots D
NONCOVALENT INTERACTION¹**Abstract**

Previous work has documented the ability of the P atom to form a direct attractive noncovalent interaction with a N atom, based in large measure on the charge transfer from the N lone pair into the σ^* antibonding orbital of the P-H that is turned away from the N atom. The present work considers whether other atoms, viz O and S, can also participate as electron donors, and in which bonding environments. Also considered are the π -systems of multiply-bonded C atoms. Unlike earlier observation that the interaction is unaffected by the nature of the electron-acceptor atom, there is strong sensitivity to the donor. The P \cdots D binding energy diminishes in the order D = NH₃ > H₂CO > H₂CS > H₂O > H₂S, different from the patterns observed in both H and halogen bonds. The P \cdots D interactions are comparable to, and in some cases stronger than the analogous H-bonds formed by HOH as proton donor. The carbon π systems form surprisingly strong P \cdots D complexes, augmented by the back donation from the P lone pair to the C-C π^* antibond, which surpass the strengths of H-bonds, even some with HF as proton donor.

3-1. Introduction

The importance of noncovalent forces to chemistry and biology cannot be overstated.¹⁻⁵ As a prominent and important example, hydrogen bonds have motivated a

¹Coauthored by Steve Scheiner and Upendra Adhikari. Reproduced with permission from *J. Phys. Chem. A* **2011**, *115*, 11101-11110. Copyright 2011, American Chemical Society.

long history of study,⁶⁻¹² which has documented that they derive their strength from a combination of electrostatic with covalent forces.¹³⁻²³ While the earliest codification of the H-bond was restricted to electronegative atoms like N and O, the more modern view^{20,24-35} has broadened to include C or Cl as proton donor atom, and the accepting unit can contribute electron density via π bonds, σ bonds, metal atoms, or even another H atom.

Another sort of primary noncovalent interaction, with a shorter history than H-bonds, is the halogen bond wherein the bridging H is replaced by a halogen atom.³⁶⁻⁴⁷ The Coulombic part of the attraction has been attributed to the shape of the electrostatic potential around the halogen atom, which despite an overall negative charge, contains a small positive region that can attract an electronegative partner atom. Yet like the H-bond, there are important contributions of induction and dispersion forces to halogen bonds as well. The literature also contains instances of other attractive forces between non-halogen electronegative atoms such as S and O,⁴⁸⁻⁵⁹ understanding of which continues to grow.

Recent work in this laboratory has identified a fundamentally different sort of noncovalent interaction between a P atom and the N atom on another molecule, with no intervening H or halogen atom.⁶⁰ In an illustrative case, the global minimum on the surface of the PH_3/NH_3 heterodimer⁶¹ eschews any sort of $\text{NH}\cdots\text{P}$ or $\text{PH}\cdots\text{N}$ H-bonding, containing instead a direct interaction between the electronegative P and N atoms. A primary source of the stability of this complex is a certain amount of charge transfer from the N lone pair into the σ^* antibond of the P-H bond. But unlike a $\text{PH}\cdots\text{N}$ H-bond where this same charge transfer might take place, the pertinent H atom is rotated directly away

from the N lone pair, so that the charge is transferred into the other lobe of the σ^* orbital, on the P end of the P-H bond. In addition to this charge transfer effect, there is also a sizable electrostatic attraction, as well as a dispersion component. Subsequent work⁶² has demonstrated that this sort of interaction is not unique to P, but is also characteristic of other second-row atoms S and Cl, as well as the third-row congener As.

With particular regard to $P\cdots N$, it has very recently been shown⁶³ that while this interaction between simple hydride PH_3 and NH_3 molecules is rather weak, less than 2 kcal/mol, it is enhanced if the H atom of the phosphine is replaced by a more electronegative group. For example, even a single Cl, F, or NO_2 substituent multiplies the interaction energy as much as fivefold, to the point where the $P\cdots N$ interaction surpasses the strength of the paradigmatic H-bond in the water dimer. The ability of a substituent to strengthen the attraction has been recently shown⁶⁴ to permit even two N atoms to attract one another, as in the case of $FH_2N\cdots NH_3$, which is bound by 4 kcal/mol, comparable to that of the H-bonded water dimer, even though the unsubstituted NH_3 dimer will not engage in this sort of $N\cdots N$ interaction. Interestingly, double or triple substitution does not further amplify this interaction,⁶⁵ a dramatic difference with H-bonding whose strength continues to grow as more electron-withdrawing substituents are added to the proton donor molecule. Experimental confirmation of these sorts of interactions has arisen from examination⁶³⁻⁶⁵ of a number of crystal structures in the literature. It would thus appear that this particular interaction is an important one, in the same class as H and halogen bonds, that warrants a great deal more study and characterization.

All of the previous investigation of this noncovalent force has been concerned with how it is affected by variation of the electron acceptor molecule. The present work

shifts attention to the electron donor, which has been modeled only by NH_3 to this point. While it might be anticipated that replacement of the N atom with others that are able to donate electrons will affect the interaction, the reader is reminded that, contrary to expectations, earlier study⁶² showed no substantial perturbation caused by replacement of the electron acceptor atom P by S, Cl, or As. In order to examine this question in detail, the N of the electron donor is replaced by O and S. In addition to their single-bonded models HOH, HSH, and CH_3OH , they are also considered in the context of double-bonded valency in $\text{H}_2\text{C}=\text{O}$ and $\text{H}_2\text{C}=\text{S}$. Another sort of system that is known to donate electrons in H-bonded situations is the π -electron cloud of hydrocarbons. Also considered in this light then are $\text{HC}\equiv\text{CH}$, $\text{H}_2\text{C}=\text{CH}_2$, the conjugated system $\text{H}_2\text{C}=\text{CH}-\text{CH}=\text{CH}_2$, and the fully aromatic C_6H_6 .

Each of these molecules is paired with FH_2P as a model electron acceptor molecule. For each pair of molecules, the potential energy is thoroughly searched for all minima, not just that which contains the direct $\text{P}\cdots\text{D}$ ($\text{D} = \text{O}, \text{S}, \text{C}$) interaction. In this way, any such $\text{P}\cdots\text{D}$ interaction can be compared directly with other sorts of molecular interactions that might be present, such as H or halogen bonds or simple dipole-dipole attractions. The results show that O is not quite as strong an electron donor as is N, and S is still weaker, but that both O and S are strengthened by involvement in a double $\text{C}=\text{D}$ bond. The carbon π systems are quite proficient electron donors to P, even more so than when participating in $\text{OH}\cdots\pi$ H-bonds. The uniqueness of the $\text{P}\cdots\text{D}$ interaction is underscored by the observation that the effects of different electron donors on the binding strength are quite different than the patterns observed in H and halogen bonds. Perhaps

most surprisingly, the direct P...D interaction is shown to be stronger than a large number of widely occurring H-bonds, even many with OH as proton donor.

3-2. Computational Methods

The Gaussian 09 package⁶⁶ was applied to all systems. Geometries were optimized at the ab initio MP2/aug-cc-pVDZ level, an approach which has been shown to be of high accuracy, especially for weak intermolecular interactions of the type of interest here^{45,67-73} where the data are in close accord with CCSD(T) values with larger basis sets^{63,74} and in nearly perfect coincidence with experimental energetics.⁷⁵ The potential energy surface of each pair was examined to identify all minima, by using a variety of different starting points for geometry optimizations. Minima were verified as having all real vibrational frequencies. Interaction energies were computed as the difference in energy between the dimer, and the sum of the optimized energies of the isolated monomers, corrected for basis set superposition error by the counterpoise procedure,⁷⁶ and by zero-point vibrational energies. Natural bond orbital (NBO) analysis^{77,78} was carried out via the procedures contained within Gaussian. The interaction energy was decomposed by the symmetry-adapted perturbation theory (SAPT) procedure,^{79,80} implemented via the MOLPRO set of codes,⁸¹ a technique which is subject to less artifact than Kitaura-Morokuma.⁸²

3-3. Results

3-3.1. Donors Containing Electronegative Atoms

The global minima of the dimers pairing FH_2P with HOH , HSH , H_2CO , H_2CS , and CH_3OH are illustrated in Figure 3-1. In all cases, the structure can be described as containing a $\text{FP}\cdots\text{D}$ interaction, in which the P and D atoms approach one another directly, and the F atom stands nearly directly opposite D; these $\theta(\text{FP}\cdots\text{D})$ angles are all in the narrow range between 167° and 172° . The intermolecular distances for the $\text{P}\cdots\text{O}$ interactions are also fairly consistent from one complex to another, varying between 2.65 Å for CH_3OH to 2.76 Å for HOH . The $\text{R}(\text{P}\cdots\text{S})$ distances are a bit longer, consistent with the larger atomic radius of S.

Also displayed in Figure 3-1 are the interaction energies, corrected for basis set superposition error by the counterpoise procedure. These quantities are also reported in the first line of Table 3-1 where it may be seen that the change of the single bonds in HOH to the double bond in H_2CO yields an increase in the interaction energy by some 20%; a slightly larger increment occurs upon replacing one of the H atoms of OH_2 by a methyl group. These energy changes are mirrored by the contractions of the intermolecular distances reported in the next line of Table 3-1. Comparison of the aforementioned values with those reported in the next two columns of Table 3-1 reveals that replacement of O by S reduces the interaction energies. The difference between HOH and HSH of 1 kcal/mol is much larger than the very small difference between H_2CO and H_2CS . As a point of comparison, data are reported in the last column for the reference NH_3 molecule, which may be seen to form a stronger interaction.

As has been described previously,⁸³ the stability of each of these complexes relies to some extent upon the transfer of electron density from the lone pair of the electron donor to the σ^* antibonding orbital of the electron acceptor, in this case FH_2P . Some measures of this process are recorded in the next few rows of Table 3-1. First of these is the amount of density assigned to this particular transfer by the NBO procedure, Δq , followed by $E(2)$ which refers to the second-order perturbation energy of the same process. Since both O and S contain two lone pairs, the quantities listed in Table 3-1 represent the sum of the two. The final row contains the stretch of the F-P bond that occurs upon formation of the complex, which is attributed to the extra density that is transferred into its antibonding orbital.

Examination of the data indicates that all of these measures of electron density increase upon going from HOH to H_2CO and then to CH_3OH , mirroring the rise in the interaction energy. The switching from O to S as electron donor atom results in a sizable increase in Δq and $E(2)$, even though the interaction itself is weakened slightly. The F-P bond stretch, on the other hand, correlates a bit more closely with ΔE , suffering a decline on going from HOH to HSH. The computed data for reference electron donor NH_3 presented in the last column of the table are consistent with the stronger nature of the $\text{FH}_2\text{P}\cdots\text{NH}_3$ binding.

To obtain a deeper understanding of the source of the bonding, the total interaction energy of each complex was decomposed into its various constituent parts. The various SAPT components are displayed in Table 3-2, which shows some strong parallels with the total interaction energies in Table 3-1. Within the O series, the ES component increases in the order $\text{HOH} \ll \text{H}_2\text{CO} < \text{CH}_3\text{OH}$, as does EX, IND, and DISP.

These components are considerably larger for H_2CS than for HSH. With regard to their relative magnitudes, the terms follow the order $\text{ES} > \text{IND} > \text{DISP}$ for the O-molecules, but the induction energy is larger than ES for the S systems, particularly so for H_2CS . The last column pertains to the N electron donor, for which all of the components are larger than those for the O and S systems. The only exception is the large dispersion energy for H_2CS which slightly exceeds that of NH_3 . A final point concerns the induction energies. These quantities in Table 3-2 are fairly similar to the $E(2)$ values in Table 3-1, which reinforces the notion that it is the $\text{D}_{\text{lp}} \rightarrow \sigma^*(\text{PF})$ transfer which accounts for a large portion of the full induction energy. Of course these quantities are not exactly the same, notably for HOH and H_2CS , which reminds us that the full induction energy does contain a number of other terms.

The NBO data reported in Table 3-1 refer explicitly to the transfer of density between certain pairs of orbitals, specifically from the lone pair of the electron donor atom to the F-P σ^* antibond. There are of course a wide array of other shifts that are taking place, including those internal to each molecule. The combined effect of all of these shifts are visualized in Figure 3-2 which represents increases in density by blue contours and decreases by red. Along with the systems considered here, the $\text{FH}_2\text{P} \cdots \text{NH}_3$ prototype system is included in Figure 3-2f for purposes of comparison. Inspection reveals a commonality of patterns in all cases. Focus is drawn to the $\text{P} \cdots \text{D}$ axis, where density is lost immediately to the right of the P atom, and gained to the left of the D atom, whether O, S, or N. There is some gain observed also on both sides of the F atom, as well as around the circumference of P, perpendicular to the $\text{P} \cdots \text{D}$ axis. Density is drained

from the area to the immediate right of D, balancing the gain to its left. This pattern of electron redistribution may be taken as a fingerprint of sorts of this type of P...D interaction.

As noted before,⁸³ it is not entirely surprising that the full density shifts in Figure 3-2 do not affirm the NBO data, as the latter refer to a specific pair of orbitals, and the former to the entire basis set. The charge shifts occurring from one molecule to the other, emphasized by the NBO treatment, are combined with polarizations internal to each molecule in Figure 3-2. It is for this same reason that total electron density rearrangements monitored in H-bonds^{11,84-89} are at odds with the $n \rightarrow \sigma^*$ transfer that is a well-known characteristic of H-bonds. This idea has been confirmed recently⁹⁰ by calculations that divided the electron redistributions that occur upon formation of a H-bonded dimer into two separate contributions. The shifts that are attributed to the transfer of total density from one monomer to the other clearly show the loss of density from the lone pair of the proton acceptor atom, and the gain in the σ^* region of the covalent O-H bond of the proton donor, verifying the predictions of a score of NBO analyses of numerous H-bonds. On the other hand, the pattern that results directly from polarization effects is just the opposite, but larger in magnitude. In other words, the loss of density in the proton acceptor lone pair due to a very real $n \rightarrow \sigma^*$ charge transfer is masked by a larger density increase in this same region associated with intramolecular density rearrangements. The combination of these two effects into a single map of charge density shift thus shows the familiar increase of density in the lone pair area.

The SAPT analysis had indicated a large fraction of the interaction energy is associated with the electrostatic interaction. In order to achieve a better understanding of

this component, the electrostatic potential of each monomer was computed, and these potentials superimposed upon each other as occurs in the equilibrium geometry of each dimer. These potentials are exhibited in Figure 3-3 where it may be seen that the positive (blue) region to the right of P of FH_2P approaches a negative (red) region of each electron donor molecule. Clearly, then, the electrostatic interaction is a favorable one. On the other hand, this potential is not sufficient to explain the equilibrium orientations of the various complexes. Specifically, in the cases of the three O-donors on the left side of Figure 3-3, a clockwise rotation of the right-hand molecule would better align its red region with the blue potential on the left. In other words, electrostatic considerations alone would lead to a larger $\theta(\text{P}\cdots\text{OX})$ angle ($\text{X} = \text{C}, \text{H}$) than is observed. It is likely that the need to align one of the O lone pairs with the P-F σ^* antibond accounts for the more acute angle. In the S cases, the electrostatic potentials of the HSH and H_2CS monomers more closely resemble the directions of the two S lone pairs, so the electrostatic and $n\rightarrow\sigma^*$ transfers have the same requirements, so no such conflict arises.

3-3.2. Carbon-Containing Electron Donors

The π systems of the various unsaturated hydrocarbon molecules can also serve as electron donors. The global minimum of the potential energy surface of FH_2P with $\text{HC}\equiv\text{CH}$, $\text{H}_2\text{C}=\text{CH}_2$, 1,3-butadiene, and benzene are all illustrated in Figure 3-4 where it may be seen that once again, the P-F bond is swung around away from the source of electrons. The binding energies of these complexes are all within the 3-4 kcal/mol regime. The triply bonded $\text{HC}\equiv\text{CH}$ is the most weakly bound, followed by $\text{H}_2\text{C}=\text{CH}_2$, and then by the two conjugated systems. The full aromaticity of benzene does not appear

to add significantly to the energetics of the conjugated C_4H_6 . These binding energies are comparable to, albeit a bit smaller than, those reported in Table 3-1 for the electronegative electron donors. The P atom is located above the midpoint of the C-C bond, but is skewed slightly toward one C atom over the other. (The blue X in each diagram indicates this bond center.) As in the systems described earlier, the intermolecular distance diminishes as the interaction energy climbs, with the exception of the fully aromatic C_6H_6 complex.

The other important properties of these complexes are displayed in Table 3-3. Switching out the molecules of Figure 3-1 by the C-containing partner molecules eliminates the lone pair as electron donor. Instead, the electron density is acquired from the π system. The NBO parameters of the charge transfer from the C-C π bond to the F-P σ^* antibond are reported in Table 3-3 as Δq_{FP} and $E(2)_{FP}$. Like the binding energies, the values of $E(2)$ are slightly smaller than those in Table 3-1. The magnitudes of the charge transferred, Δq_{FP} , however, are in the same range as those for the electronegative atoms.

The carbon π systems add a new factor to the binding of these complexes. The presence of a low-lying C-C π^* orbital permits electron transfer into it from the P lone pair. As may be seen by the relevant measures of this shift, Δq_{CC} and $E(2)_{CC}$, this phenomenon is quite significant, amounting to 35-45% of the dominant $D_{lp \rightarrow \sigma^*(PF)}$ quantities.

As in the earlier cases, the accumulation of electron density in the antibonding P-F region elongates this bond, by between 6 and 11me, again slightly smaller than the stretches reported in Table 3-1. The second, and new, factor in the C systems, whereby

density is added to the C-C π^* system, stretches this bond as well, by amounts listed in the last row of Table 3-3.

There are several interesting observations about the data reported above. In the first place, the single C=C π bond in ethylene makes for a slightly stronger interaction with FH₂P, than does the pair of such π bonds in HC≡CH. One may interpret this distinction as a tentative rule that sp² hybridization is superior to sp in such interactions. The addition of a second C=C bond in butadiene which can conjugate with the first adds to the interaction although nothing further arises from the full aromaticity of benzene. In fact, the two molecules lie a bit further apart in the latter case. It might be noted also that the P atom prefers a position directly above one C=C bond, as opposed to a central location above the middle of the C₆H₆ molecule.

The SAPT components of the interactions reported in Table 3-4 show that each of the elements climb in magnitude from HCCH to H₂C=CH₂, and then to butadiene, pretty much parallel to the rise in the total interaction energy. The benzene terms, in contrast, are surprisingly small, contrasting with the stronger total interaction of this electron donor. It is likely that these smaller terms are due at least in part to the longer intermolecular separation in the FH₂P...C₆H₆ complex. Note, however, that the dispersion energy in this complex is rather large, which might be attributed to the high polarizability of the aromatic π system of benzene.

It is interesting to compare the individual energy components in Table 3-4 with those of the more electronegative donors of Table 3-2. Taking butadiene as a system which has the largest such quantities as one end of the spectrum, its ES, EX, and IND

components are all comparable to those in Table 3-2. The dispersion energy is particularly large for butadiene, greater than the same quantity for any donor of Table 3-2, even those molecules with much stronger total binding strength. Indeed, one distinguishing feature of all the C-containing systems is a disproportionately large contribution from DISP. The latter component is in fact the single largest contributor to the $\text{FH}_2\text{P}\cdots\text{C}_6\text{H}_6$ dimer.

The shifts in total electron density accompanying the formation of the complexes of FH_2P with the C systems are illustrated in Figure 3-5. Comparison with those in Figure 3-2 indicates strong similarities. Once again, the strongest loss is observed to the immediate right of the P atom, and a gain further to its right. In this case, the increment occurs in the region between the two C atoms, to the left of the C-C bond, rather than to the left of a single (O, S, or N) atom. Also in common, accumulations of density occur along the F-P axis. Just as the C-containing systems are somewhat more weakly bound than those in Figure 3-2, the patterns in Figure 3-5 are also slightly attenuated. And again there is the tendency of more strongly bound complexes within this C subset to manifest larger density shifts. These charge shift patterns, then, suggest strong similarities whether the electron-donating entity is a C-C π bond or an electronegative atom like O, S, or N.

A final remaining question concerns whether electrostatic considerations in the C-systems represent a strong influence in the orientation adopted by the two subunits in the global minimum. The electrostatic potentials of the relevant systems are placed in juxtaposition in Figure 3-6. It is immediately obvious that there is a strong overlap between the positive region to the right of the P atom and a negative area that lies directly

above the midpoint of the C-C multiple bonds. Note that the aforementioned negative potential is most prominent above the double bonds of butadiene in Figure 3-6c, so that electrostatic considerations reinforce the charge transfer effect arising from optimal overlap of the appropriate π orbital with the P-F σ^* antibond. The case of benzene is a bit different in that the maximum of its negative density lies directly above the center of the molecule. Nonetheless, the approaching FH_2P molecule forgoes this position for one closer to an individual C-C bond. This latter preference is likely due the fact that whereas the ES potential is most negative above the molecular center, the electron density is larger above the individual C-C bonds. This off-center geometry thus permits a better overlap between the relevant orbitals of the two molecules that engage in $\pi(\text{CC})\rightarrow\sigma^*(\text{PF})$ and $\text{P}_{\text{lp}}\rightarrow\pi^*(\text{CC})$ charge transfers.

3-3.3. Secondary Minima

As indicated above, all of the structures presented to this point represent the global minimum in the potential energy surface of each heterodimer. Examination of secondary minima provides useful insights into the comparative strengths of the $\text{FP}\cdots\text{D}$ interactions with H-bonds or other noncovalent forces. The $\text{FH}_2\text{P}/\text{OH}_2$ heterodimer contains only one secondary minimum, characterized as a cyclic structure containing a pair of H-bonds. The primary interaction is a $\text{OH}\cdots\text{F}$ H-bond, with $R(\text{H}\cdots\text{F}) = 2.02 \text{ \AA}$, complemented by a much longer $\text{PH}\cdots\text{O}$ interaction ($R = 2.71 \text{ \AA}$). Despite the presence of these two H-bonds, this complex is less strongly bound than the primary minimum by 1 kcal/mol. There are two secondary minima when H_2O is replaced by H_2S . Again, both

of these contain a pair of H-bonds ($\text{SH}\cdots\text{F}$ and $\text{SH}\cdots\text{P}$), and again they are both less stable than the $\text{FP}\cdots\text{S}$ structure by 1 kcal/mol.

The double-bonded H_2CX ($\text{X} = \text{O}, \text{S}$) molecules present a few more secondary minima. The most stable of these contains both a $\text{CH}\cdots\text{F}$ and $\text{PH}\cdots\text{X}$ H-bond. Whether O or S, the $\text{CH}\cdots\text{F}$ bond is the shorter of the two, at 2.4 Å. Another minimum, very similar in energy, also contains this same pair of H-bonds, except that the PH approaches the O/S atom from above the plane of the H_2CX molecule, rather than from within its plane as in the former case. The third and least stable of the H_2CO minima is stabilized by a bifurcated pair of $\text{CH}\cdots\text{F}$ H-bonds. This same structure is present also for $\text{X} = \text{S}$, but is complemented by two other minima, even less stable. One of them also sports a bifurcated $\text{CH}\cdots\text{F}$ pair, and the least stable of all contains what appears to be a bifurcated $\text{PH}\cdots\text{S}$ pair, although the two $\text{R}(\text{H}\cdots\text{S})$ distances are rather long at 3.3 Å.

The relative complexity of the CH_3OH molecule leads to 11 minima in addition to the global structure. The most stable quartet of this set all have in common a $\text{OH}\cdots\text{F}$ H-bond, with $\text{R}(\text{H}\cdots\text{F})$ in the 2.0-2.2 Å range, complemented by a much longer (2.7-3.0 Å) $\text{PH}\cdots\text{O}$ interaction. These four have similar energies, all 2 kcal/mol less stable than the global minimum. Another geometry is stabilized by a $\text{OH}\cdots\text{F}$ H-bond without benefit of $\text{PH}\cdots\text{N}$ interactions so is somewhat higher in energy. Two other complexes contain a bifurcated pair of $\text{CH}\cdots\text{F}$ H-bonds, one with and one without an auxiliary $\text{OH}\cdots\text{P}$ interaction. A $\text{PH}\cdots\text{O}$ interaction occurs along with a $\text{CH}\cdots\text{F}$ in another structure. The next two minima both contain a single stabilizing interaction, $\text{OH}\cdots\text{P}$ in one and $\text{CH}\cdots\text{F}$ in the other. The least stable of the minima on this surface, only 0.4 kcal/mol more stable than the isolated monomers, is most interesting in some sense. While there are no H-

bonds of any sort, the $\text{FP}\cdots\text{C}$ alignment is reminiscent of the global minimum, with the O replaced by the methyl C atom. And indeed, NBO analysis reveals a charge transfer from a methyl C-H bond to the P-F σ^* antibond, with $E(2) = 0.89$ kcal/mol. This transfer is complemented by another ($E(2) = 0.50$ kcal/mol) from the P lone pair to the C-O σ^* antibond, enabled by the proper alignment of the C-O bond.

In summary, the $\text{FP}\cdots\text{D}$ interaction is clearly the dominant one in these dimers. Its binding energy surpasses those of a wide range of different sorts of H-bonds that occur in the secondary minima, including $\text{OH}\cdots\text{F}$, $\text{PH}\cdots\text{O}$, $\text{CH}\cdots\text{F}$, and $\text{OH}\cdots\text{P}$. This greater binding strength is notable first in that the F substituent on the P atom is expected to strengthen the proton-donating power of the phosphine. Secondly, the single $\text{FP}\cdots\text{D}$ interaction must compete with other structures which contain not one but two or more H-bonds.

Turning next to the C-containing species, alternate minima contain weak H-bonds. The fairly high acidity of the sp-hybridized CH group of $\text{HC}\equiv\text{CH}$ results in a $\text{CH}\cdots\text{F}$ H-bond which amounts to 1.9 kcal/mol, weaker than the $\text{FP}\cdots\pi$ interaction of the global minimum by 1.1 kcal/mol. Still weaker is a $\text{CH}\cdots\text{P}$ H-bond. The sp^2 hybridization of C_2H_4 yields a weaker CH proton donor. The two secondary minima on the surface both contain a pair of $\text{CH}\cdots\text{F}$ H-bonds to the single F atom. In the more stable of the two, the participating H atoms are on different C atoms while they are bound to the same C in the highest energy structure. Like CH_3OH , the butadiene molecule also is associated with a number of different secondary minima, nine in this case. Two of these are much like the global minimum of Figure 3-3, containing a $\text{FP}\cdots\pi$ interaction, except that the FH_2P

molecule is rotated a bit. The next group of three minima rotates FH_2P so that one of its two H atoms is oriented away from the C-C π bond, instead of the F. These structures are about 1.5 kcal/mol less stable than the $\text{FP}\cdots\pi$ structure. The remaining minima each contain a pair of $\text{CH}\cdots\text{F}$ H-bonds, usually fairly long in the range between 2.6 and 2.8 Å. One of the two alternate minima of the complexes with benzene is nearly identical to the global minimum, containing the same $\text{FP}\cdots\pi$ interaction, with only slight differences in orientation, but essentially identical in energy. The other minimum is 1 kcal/mol higher and has the FH_2P molecule oriented in such a way that a P-H bond is turned toward the benzene π system, in what is primarily a $\text{PH}\cdots\pi$ interaction. It is clear then that the $\text{FP}\cdots\pi$ interaction is favored in all cases, being more stable than $\text{HP}\cdots\pi$, $\text{PH}\cdots\pi$, or $\text{CH}\cdots\text{F}$ H-bonds, even when there are two of the latter.

3-4. Discussion and Conclusions

Some of these $\text{FP}\cdots\text{D}$ interactions might be considered surprisingly strong. For example, the water molecule forms an interaction with FH_2P that is very nearly as strong as that with another water. That is, the 4.03 kcal/mol binding energy of $\text{FH}_2\text{P}\cdots\text{OH}_2$ is within only 0.4 kcal/mol of the strength of the prototypical H-bond in the water dimer, computed at the same level of theory. In order to further explore this comparison between $\text{FP}\cdots\text{D}$ and H-bonding the various electron donors in Figures 3-1 and 3-4 were paired with HF and HOH. These two molecules represent powerful proton donors in the H-bonds in which they participate, in particular HF which forms some of the strongest H-bonds known.

The binding energies of all complexes are collected in Table 3-5 which illustrates some interesting points. In terms of the electron donors in the first six rows that contain electronegative atoms, formation of a H-bond with FH is substantially preferred over a $\text{FP}\cdots\text{D}$ interaction. This margin of difference is smallest for S donors but is present nonetheless. There is also a preference for the CC π bonds of acetylene and ethylene to interact with HF over FH_2P . However, this order reverses for the more extended π systems of 1,3-butadiene and benzene, where there is a slight preference for the $\text{FP}\cdots\pi$ bond over $\text{FH}\cdots\pi$. HOH is a somewhat weaker proton donor than is HF, so the binding energies in the last column of Table 3-5 are uniformly smaller than those in the preceding column. Indeed, the $\text{OH}\cdots\text{D}$ H-bonds formed by water are similar to, and usually smaller than, the $\text{FP}\cdots\text{D}$ binding energies in the first column.

Visualization of these data in Figure 3-7 exhibits some important patterns. There is some generality in that NH_3 forms the strongest complexes, followed by the O-containing electron donors, and then the S analogues. There are discrepancies as well. For example, H_2CO forms a weaker complex with HF than does OH_2 , but the reverse is true for HOH and FH_2P ; H_2CS engages more strongly with all three electron acceptors than does SH_2 . Whereas HF is a uniformly stronger electron acceptor, FH_2P and OH_2 are fairly similar to one another, although FH_2P emerges as superior for S-donors. Within the subset of C-donors, the binding energy climbs in the sequence $\text{HC}\equiv\text{CH} < \text{H}_2\text{C}=\text{CH}_2 < \text{butadiene} < \text{benzene}$. Perhaps most interesting is the strength of the complexes of FH_2P with the C-donors. The $\text{P}\cdots\pi$ interaction is substantially stronger than $\text{OH}\cdots\pi$ for all four carbon donors, and is even competitive with $\text{FH}\cdots\pi$. In fact, a recent calculation⁹¹

enhanced the proton donating power of HOH by replacing one H atom by a halogen (X = F, Cl, Br, or I). Even with this boost, the $\text{XOH}\cdots\text{C}_6\text{H}_6$ H-bonding energy remained lower than the value computed here for $\text{FH}_2\text{P}\cdots\text{C}_6\text{H}_6$ for all halogen atoms save I.

One may conclude that the $\text{FP}\cdots\text{D}$ interaction is competitive with even some of the strongest H-bonds. FH_2P is superior to HOH as an electron acceptor from π bonds, and can even surpass HF for conjugated systems. The $\text{FP}\cdots\text{D}$ interaction is as strong as $\text{OH}\cdots\text{D}$ for electronegative donors, and is in fact better for S-containing systems. Only the very powerful HF proton donor surpasses FH_2P as electron acceptor, but even that distinction evaporates for C-donors. Comparison of the geometries of the global minimum in each case with secondary minima also demonstrates the superiority of the $\text{FP}\cdots\text{D}$ interaction over various other sorts of H-bonds such as $\text{OH}\cdots\text{F}$, $\text{PH}\cdots\text{O}$, $\text{CH}\cdots\text{F}$, $\text{CH}\cdots\text{P}$, $\text{OH}\cdots\text{P}$, or $\text{PH}\cdots\pi$. Electron donors are not limited to only very electronegative atoms. In addition to the C atoms examined here, even P can act in this capacity⁶¹ so as to form a $\text{P}\cdots\text{P}$ interaction. Indeed, the binding energy of such a $\text{P}\cdots\text{P}$ complex can exceed 4 kcal/mol with certain substituents.⁹²

A major component of the $\text{P}\cdots\text{D}$ binding arises from the charge transfer from the lone pair(s) of the donor atom into the σ^* antibond of the P-F bond that lies opposite the donor atom. This transfer is disproportionately larger for second-row S than for O and N, presumably due to the greater polarizability of S-compounds. The latter property is also responsible for the large contribution of induction energy for S, greater than ES or DISP, whereas ES represents the greatest contributor for O and N. When the electron donation occurs from a C π system, there is a tendency of the P atom to hover immediately above the midpoint of one particular C=C bond, rather than locating itself above the center of

the entire molecule. In addition to the $\pi \rightarrow \sigma^*$ transfer, there is a back transfer from the P lone pair into a C-C π^* antibond. This second factor may account for the unexpected strength of the $P \cdots \pi$ binding energies. The largest contribution to the interaction is made in three of these four cases by the induction energy, followed by ES and DISP. The exception occurs for the benzene donor in which the dispersion energy is largest, and the electrostatic term the smallest. Consideration of the three-dimensional disposition of the electrostatic potentials of each monomer is consistent with the equilibrium geometries but not fully predictive, as the alignment of the donor lone pair, or C=C density maximum, with the acceptor σ^* orbital is another important issue

The concept of a stabilizing charge transfer from a lone pair of one molecule to a σ^* antibond of another has strong precedent and is a foundation of some other noncovalent interactions. It has been invoked, for example, to help explain H and halogen bonding⁹³⁻⁹⁶ and has been applied also to chalcogen atoms such as O and S.^{48,50,51,53,59,97-101} Its participation in the $P \cdots D$ interactions here should thus not be entirely surprising. Adding to this primary $D_{lp} \rightarrow \sigma^*(PF)$ effect is the back transfer that occurs when the P atom interacts with the carbon π systems. It is likely that this auxiliary $P_{lp} \rightarrow \pi^*(CC)$ charge transfer is at least partially responsible for the large interaction energies in these σ^* complexes, as compared to the analogous H-bonded complexes in Figure 3-7. This idea of transfer to π^* antibonds is not without precedent either. A similar sort of phenomenon has been invoked^{55,56,102} to explain certain close contacts between carbonyl groups in proteins, which has been attributed to a purported transfer of charge from an O lone pair of one subunit to the C=O π^* antibonding orbital of the other.

Summarizing the potency of the various electron donors for participation in a P...D bond, N is stronger than O which is in turn a better donor than is S. The double-bonded O and S atoms in H₂C=D are superior to the single bonded HDH analogues; replacement of a H atom by a methyl group enhances the electron-donating ability. The π systems of multiply bonded C atoms form surprisingly strong P... π bonds, notably superior to OH... π interactions and even comparable to FH... π . These P... π interactions are better for CC double than for triple bonds, particularly if the double bond is part of a conjugated π system. Indeed the P...benzene binding is essentially equivalent to the standard OH...O H-bond in the water dimer.

It is reiterated finally that the P...D interaction studied here is fundamentally distinct from both halogen and H-bonds in a number of important ways. Some of the differences have been discussed previously,^{61-63,65,83} and include the patterns of charge density shift, energy component magnitudes, internal geometry perturbations, sensitivity to angular distortion, dependence upon identity of electron-accepting atom, and the effect of multiple halogenation. Another distinction arises from the work presented here, concerning the way in which the binding energy varies with the particular electron donor molecule. These differences with H-bonds are exhibited in Figure 3-7. While these differences are not overly dramatic, comparison with halogen bonds leads to more striking contrasts. It was found previously¹⁰³ that halogen bonds weaken as the donor is changed in the order: H₂CS > H₂CO > NH₃ > H₂S > H₂O. This pattern is quite different for P...D interactions which, as illustrated in Table 3-5, is: NH₃ > H₂CO > H₂CS > H₂O > H₂S. There is some similarity as well. Halogen bonds to the π -clouds of C-containing

systems, like the $P \cdots \pi$ interactions considered here, are also stronger for doubly bonded $H_2C=CH_2$, as compared to the triple bond in $HC \equiv CH$.⁷³

One might expect that the much greater electronegativity of F as compared to P would lead to a P-F σ^* antibonding orbital that is biased heavily toward the P. However, NBO evaluation of this orbital indicates a surprising lack of such bias; the shape of this orbital is very little affected by the electronegativity of the group bonded to P, whether F, H, OH, or CF_3 .⁶³

There are a number of chemical situations where such interactions may be important. Phosphines are a common ligand in inorganic systems,¹⁰⁴⁻¹⁰⁶ which typically interacts with nearby groups in the solid state. As one example, a synthetic catalyst has recently been developed which can produce molecular H_2 at an unprecedented rate.¹⁰⁷ The efficiency of this catalyst relies upon a pair of pendant seven-membered cyclic diphosphine amine ligands. Interactions of these two ligands with each other, or those between separate catalyst molecules might take advantage of the sort of $P \cdots N$ interactions under consideration here. In the context of biological situations, the electron donor groups considered here are all representative of functional groups within proteins. HSH, for example, is a model of the Cys residue, CH_3OH of hydroxyl groups in Ser or Thr, and benzene approximates the functional group of Phe. The P atom of the phosphate group is bonded to four very electronegative O atoms, so would be unlikely to interact in the fashion indicated. However, trivalent phosphines are a common structural and enzymatic element and their interaction with other molecular units might be controlled by the forces that are the subject of this work.

References

- (1) Hobza, P.; Zahradnik, R. *Weak Intermolecular Interactions in Chemistry and Biology*; Elsevier Scientific: Amsterdam, 1980.
- (2) Kaplan, I. G. *Theory of Molecular Interactions*; Elsevier: Amsterdam, 1986.
- (3) Müller-Dethlefs, K.; Hobza, P. *Chem. Rev.*, **2000**, *100*, 143.
- (4) Stone, A. J. *The Theory of Intermolecular Forces*; Oxford University Press: Oxford, UK, 2002.
- (5) Hobza, P.; Müller-Dethlefs, K. *Non-Covalent Interactions*; RSC: Cambridge, 2010.
- (6) Pimentel, G. C.; McClellan, A. L. *The Hydrogen Bond*; Freeman: San Francisco, 1960.
- (7) *The Hydrogen Bond. Recent Developments in Theory and Experiments*; Schuster, P.; Zundel, G.; Sandorfy, C., Eds.; North-Holland Publishing Co.: Amsterdam, 1976.
- (8) Hadzi, D.; Bratos, S. Vibrational spectroscopy of the hydrogen bond. In *The Hydrogen Bond. Recent Developments in Theory and Experiments*; Schuster, P., Zundel, G., Sandorfy, C., Eds.; North-Holland Publishing Co.: Amsterdam, 1976; Vol. 2; pp 565.
- (9) Schuster, P. *Hydrogen Bonds*; Springer-Verlag: Berlin, 1984; Vol. 120.
- (10) Jeffrey, G. A.; Saenger, W. *Hydrogen Bonding in Biological Structures*; Springer-Verlag: Berlin, 1991.
- (11) Scheiner, S. *Hydrogen Bonding. A Theoretical Perspective*; Oxford University Press: New York, 1997.

- (12) Gilli, G.; Gilli, P. *The Nature of the Hydrogen Bond*; Oxford University Press: Oxford, UK, 2009.
- (13) Wiczorek, R.; Dannenberg, J. J. *J. Am. Chem. Soc.*, **2003**, *125*, 8124.
- (14) Alabugin, I. V.; Manoharan, M.; Peabody, S.; Weinhold, F. *J. Am. Chem. Soc.*, **2003**, *125*, 5973
- (15) Hernández-Soto, H.; Weinhold, F.; Francisco, J. S. *J. Chem. Phys.*, **2007**, *127*, 164102.
- (16) Li, Q.; Liu, H.; An, X.; Gong, B.; Cheng, J. *J. Mol. Struct. (Theochem)*, **2008**, *861*, 14.
- (17) Bhate, M. P.; Woodard, J. C.; Mehta, M. A. *J. Am. Chem. Soc.*, **2009**, *131*, 9579.
- (18) Samanta, A. K.; Pandey, P.; Bandyopadhyay, B.; Chakraborty, T. *J. Phys. Chem. A*, **2010**, *114*, 1650–1656.
- (19) Wang, W.; Zhang, Y.; Ji, B. *J. Phys. Chem. A*, **2010**, *114*, 7257–7260.
- (20) Alkorta, I.; Elguero, J.; Bene, J. E. D. *Chem. Phys. Lett.*, **2010**, *489*, 159.
- (21) Bene, J. E. D.; Alkorta, I.; Elguero, J. *Phys. Chem. Chem. Phys.*, **2011**, *13*, 13951.
- (22) Thakur, T. S.; Kirchner, M. T.; Bläser, D.; Boese, R.; Desiraju, G. R. *Phys. Chem. Chem. Phys.*, **2011**, *13*, 14076.
- (23) McDowell, S. A. C.; Buckingham, A. D. *Phys. Chem. Chem. Phys.*, **2011**, *13*, 14097.
- (24) Desiraju, G. R.; Steiner, T. *The Weak Hydrogen Bond in Structural Chemistry and Biology*; Oxford: New York, 1999.
- (25) Scheiner, S.; Gu, Y.; Kar, T. *J. Mol. Struct. (Theochem)*, **2000**, *500*, 441.
- (26) Gu, Y.; Kar, T.; Scheiner, S. *J. Mol. Struct.*, **2000**, *552*, 17.

- (27) *Hydrogen Bonding - New Insights*; Grabowski, S. J., Ed.; Springer: Dordrecht, 2006.
- (28) Orlova, G.; Scheiner, S. *J. Phys. Chem. A*, **1998**, *102*, 4813.
- (29) Desiraju, G. R. *Angew. Chem., Int. Ed. Engl.*, **2011**, *50*, 52.
- (30) Arunan, E.; Desiraju, G. R.; Klein, R. A.; Sadlej, J.; Scheiner, S.; Alkorta, I.; Clary, D. C.; Crabtree, R. H.; Dannenberg, J. J.; Hobza, P.; Kjaergaard, H. G.; Legon, A. C.; Mennucci, B.; Nesbitt, D. J. *Pure Appl. Chem.*, **2011**, *83*, 1637.
- (31) Vaz, P. D.; Nolasco, M. M.; Gil, F. P. S. C.; Ribeiro-Claro, P. J. A.; Tomkinson, J. *Chem. Eur. J.*, **2010**, *16*, 9010.
- (32) Veken, B. J. v. d.; Delanoye, S. N.; Michielsens, B.; Herrebout, W. A. *J. Mol. Struct.*, **2010**, *976*, 97.
- (33) Takahashi, O.; Kohno, Y.; Nishio, M. *Chem. Rev.*, **2010**, *110*, 6049.
- (34) Rizzato, S.; Bergès, J.; Mason, S. A.; Albinati, A.; Kozelka, J. *Angew. Chem., Int. Ed. Engl.*, **2010**, *49*, 7440.
- (35) Falvello, L. R. *Angew. Chem., Int. Ed. Engl.*, **2010**, *49*, 10045.
- (36) Lommerse, J. P. M.; Stone, A. J.; Taylor, R.; Allen, F. H. *J. Am. Chem. Soc.*, **1996**, *118*, 3108.
- (37) Alkorta, I.; Rozas, S.; Elguero, J. *J. Phys. Chem. A*, **1998**, *102*, 9278.
- (38) Wash, P. L.; Ma, S.; Obst, U.; Rebek, J. *J. Am. Chem. Soc.*, **1999**, *121*, 7973.
- (39) Glaser, R.; Chen, N.; Wu, H.; Knotts, N.; Kaupp, M. *J. Am. Chem. Soc.*, **2004**, *126*, 4412.
- (40) Nguyen, H. L.; Horton, P. N.; Hursthouse, M. B.; Legon, A. C.; Bruce, D. W. *J. Am. Chem. Soc.*, **2004**, *126*, 16.

- (41) Caronna, T.; Liantonio, R.; Logothetis, T. A.; Metrangolo, P.; Pilati, T.; Resnati, G. *J. Am. Chem. Soc.*, **2004**, *126*, 4500.
- (42) Cavallo, G.; Metrangolo, P.; Pilati, T.; Resnati, G.; Sansotera, M.; Terraneo, G. *Chem. Soc. Rev.*, **2010**, *39*, 3772.
- (43) Sarwar, M. G.; Dragisic, B.; Salsberg, L. J.; Gouliaras, C.; Taylor, M. S. *J. Am. Chem. Soc.*, **2010**, *132*, 1646.
- (44) Politzer, P.; Murray, J. S.; Clark, T. *Phys. Chem. Chem. Phys.*, **2010**, *12*, 7748.
- (45) Chudzinski, M. G.; McClary, C. A.; Taylor, M. S. *J. Am. Chem. Soc.*, **2011**, *133*, 10559.
- (46) Zierkiewicz, W.; Wieczorek, R.; Hobza, P.; Michalska, D. *Phys. Chem. Chem. Phys.*, **2011**, *13*, 5105.
- (47) Walter, S. M.; Kniep, F.; Herdtweck, E.; Huber, S. M. *Angew. Chem. Int. Ed.*, **2011**, *50*, 7187.
- (48) Rosenfield, R. E.; Parthasarathy, R.; Dunitz, J. D. *J. Am. Chem. Soc.*, **1977**, *99*, 4860.
- (49) Burling, F. T.; Goldstein, B. M. *J. Am. Chem. Soc.*, **1992**, *114*, 2313.
- (50) Nagao, Y.; Hirata, T.; Goto, S.; Sano, S.; Kakehi, A.; Iizuka, K.; Shiro, M. *J. Am. Chem. Soc.*, **1998**, *120*, 3104.
- (51) Iwaoka, M.; Takemoto, S.; Tomoda, S. *J. Am. Chem. Soc.*, **2002**, *124*, 10613.
- (52) Werz, D. B.; Gleiter, R.; Rominger, F. *J. Am. Chem. Soc.*, **2002**, *124*, 10638.
- (53) Bleiholder, C.; Werz, D. B.; Koppel, H.; Gleiter, R. *J. Am. Chem. Soc.*, **2006**, *128*, 2666.

- (54) Aakeröy, C. B.; Fasulo, M.; Schultheiss, N.; Desper, J.; Moore, C. *J. Am. Chem. Soc.*, **2007**, *129*, 13772.
- (55) Choudhary, A.; Gandla, D.; Krow, G. R.; Raines, R. T. *J. Am. Chem. Soc.*, **2009**, *131*, 7244.
- (56) Jakobsche, C. E.; Choudhary, A.; Miller, S. J.; Raines, R. T. *J. Am. Chem. Soc.*, **2010**, *132*, 6651.
- (57) Vener, M. V.; Egorova, A. N.; Tsirelson, V. G. *Chem. Phys. Lett.*, **2010**, *500*, 272.
- (58) Wang, W.; Xin, J.; Zhang, Y.; Wang, W.; Lu, Y. *Int. J. Quantum Chem.*, **2011**, *111*, 644.
- (59) Junming, L.; Yunxiang, L.; Subin, Y.; Weiliang, Z. *Struct. Chem.*, **2011**, *22*, 757.
- (60) Solimannejad, M.; Gharabaghi, M.; Scheiner, S. *J. Chem. Phys.*, **2011**, *134*, 024312.
- (61) Scheiner, S. *J. Chem. Phys.*, **2011**, *134*, 094315.
- (62) Scheiner, S. *J. Chem. Phys.*, **2011**, *134*, 164313.
- (63) Scheiner, S. *J. Phys. Chem. A*, **2011**, *115*, in press DOI: 10.1021/jp203964b.
- (64) Scheiner, S. *Chem. Phys. Lett.*, **2011**, in press DOI: 10.1016/j.cplett.2011.08.028.
- (65) Scheiner, S. *Chem. Phys.*, **2011**, *387*, 79.
- (66) Frisch, M. J.; Trucks, G. W.; Schlegel, H. B.; Scuseria, G. E.; Robb, M. A.; Cheeseman, J. R.; Zakrzewski, V. G.; Montgomery, J., J. A.; Stratmann, R. E.; Burant, J. C.; Dapprich, S.; Millam, J. M.; Daniels, A. D.; Kudin, K. N.; Strain, M. C.; Farkas, O.; Tomasi, J.; Barone, V.; Cossi, M.; Cammi, R.; Mennucci, B.; Pomelli, C.; Adamo, C.; Clifford, S.; Ochterski, J.; Petersson, G. A.; Ayala, P. Y.; Cui, Q.; Morokuma, K.; Malick, D. K.; Rabuck, A. D.; Raghavachari, K.;

Foresman, J. B.; Cioslowski, J.; Ortiz, J. V.; Baboul, A. G.; Stefanov, B. B.; Liu, G.; Liashenko, A.; Piskorz, P.; Komaromi, I.; Gomperts, R.; Martin, R. L.; Fox, D. J.; Keith, T.; Al-Laham, M. A.; Peng, C. Y.; Nanayakkara, A.; Gonzalez, C.; Challacombe, M.; Gill, P. M. W.; Johnson, B.; Chen, W.; Wong, M. W.; Andres, J. L.; Gonzalez, C.; Head-Gordon, M.; Replogle, E. S.; Pople, J. A. *Gaussian 03*; D.01 ed.; Gaussian, Inc.: Pittsburgh PA, 2003.

- (67) Hermida-Ramón, J. M.; Cabaleiro-Lago, E. M.; Rodríguez-Otero, J. *J. Chem. Phys.*, **2005**, *122*, 204315.
- (68) Riley, K. E.; Op't Holt, B. T.; Merz, K. M. *J. Chem. Theory Comput.*, **2007**, *3*, 407.
- (69) Lu, Y.-X.; Zou, J.-W.; Fan, J.-C.; Zhao, W.-N.; Jiang, Y.-J.; Yu, Q.-S. *J. Comput. Chem.*, **2008**, *30*, 725.
- (70) Hyla-Kryspin, I.; Haufe, G.; Grimme, S. *Chem. Phys.*, **2008**, *346*, 224.
- (71) Biswal, H. S.; Wategaonkar, S. *J. Phys. Chem. A*, **2009**, *113*, 12774.
- (72) Osuna, R. M.; Hernández, V.; Navarrete, J. T. L.; D'Oria, E.; Novoa, J. J. *Theor. Chem. Acc.*, **2011**, *128*, 541.
- (73) Zeng, Y.; Zhang, X.; Li, X.; Zheng, S.; Meng, L. *Int. J. Quantum Chem.*, **2011**, *111*, 3725.
- (74) Zhao, Q.; Feng, D.; Sun, Y.; Hao, J.; Cai, Z. *Int. J. Quantum Chem.*, **2011**, *111*, 3881.
- (75) Hauchecorne, D.; Moiana, A.; Veken, B. J. v. d.; Herrebout, W. A. *Phys. Chem. Chem. Phys.*, **2011**, *13*, 10204.
- (76) Boys, S. F.; Bernardi, F. *Mol. Phys.*, **1970**, *19*, 553.

- (77) Reed, A. E.; Weinhold, F.; Curtiss, L. A.; Pochatko, D. J. *J. Chem. Phys.*, **1986**, *84*, 5687.
- (78) Reed, A. E.; Curtiss, L. A.; Weinhold, F. *Chem. Rev.*, **1988**, *88*, 899.
- (79) Szalewicz, K.; Jeziorski, B. Symmetry-adapted perturbation theory of intermolecular interactions. In *Molecular Interactions. From Van der Waals to Strongly Bound Complexes*; Scheiner, S., Ed.; Wiley: New York, 1997; p 3.
- (80) Moszynski, R.; Wormer, P. E. S.; Jeziorski, B.; van der Avoird, A. *J. Chem. Phys.*, **1995**, *103*, 8058.
- (81) Werner, H.-J.; Knowles, P. J.; Manby, F. R.; Schütz, M.; P. Celani; Knizia, G.; Korona, T.; Lindh, R.; Mitrushenkov, A.; Rauhut, G.; Adler, T. B.; Amos, R. D.; Bernhardsson, A.; Berning, A.; Cooper, D. L.; Deegan, M. J. O.; Dobbyn, A. J.; Eckert, F.; Goll, E.; Hampel, C.; Hesselmann, A.; G. Hetzer; Hrenar, T.; Jansen, G.; Köppl, C.; Liu, Y.; Lloyd, A. W.; Mata, R. A.; May, A. J.; McNicholas, S. J.; Meyer, W.; Mura, M. E.; Nicklaß, A.; Palmieri, P.; Pflüger, K.; Pitzer, R.; Reiher, M.; Shiozaki, T.; Stoll, H.; Stone, A. J.; Tarroni, R.; Thorsteinsson, T.; Wang, M.; Wolf, A. MOLPRO; Version 2006 ed., 2010.
- (82) Cybulski, S. M.; Scheiner, S. *Chem. Phys. Lett.*, **1990**, *166*, 57.
- (83) Scheiner, S. *Phys. Chem. Chem. Phys.*, **2011**, *13*, 13860.
- (84) Morokuma, K.; Kitaura, K. Variational approach (SCF ab-initio calculations) to the study of molecular interactions: the origin of molecular interactions. In *Molecular Interactions*; Ratajczak, H., Orville-Thomas, W. J., Eds.; Wiley: New York, 1980; Vol. 1; p 21.

- (85) Vanquickenborne, L. G. Quantum chemistry of the hydrogen bond. In *Intermolecular Forces*; Huyskens, P. L., Luck, W. A. P., Zeegers-Huyskens, T., Eds.; Springer-Verlag: Berlin, 1991; p 31.
- (86) Sokalski, W. A. *J. Chem. Phys.*, **1982**, *77*, 4529.
- (87) Gu, Y.; Kar, T.; Scheiner, S. *J. Am. Chem. Soc.*, **1999**, *121*, 9411.
- (88) Morokuma, K. *Acc. Chem. Res.*, **1977**, *10*, 294.
- (89) Scheiner, S.; Kar, T. *J. Phys. Chem. A*, **2002**, *106*, 1784.
- (90) Mo, Y.; Bao, P.; Gao, J. *Phys. Chem. Chem. Phys.*, **2011**, *13*, 6760.
- (91) Zhao, Q.; Feng, D.; Sun, Y.; Hao, J.; Cai, Z. *J. Mol. Model.*, **2011**, *17*, 1935.
- (92) Zahn, S.; Frank, R.; Hey-Hawkins, E.; Kirchner, B. *Chem. Eur. J.*, **2011**, *22*, 6034.
- (93) Romaniello, P.; Lelj, F. *J. Phys. Chem. A*, **2002**, *106*, 9114.
- (94) Wang, W.; Tian, A.; Wong, N.-B. *J. Phys. Chem. A*, **2005**, *109*, 8035.
- (95) Alkorta, I.; Blanco, F.; Solimannejad, M.; Elguero, J. *J. Phys. Chem. A*, **2008**, *112*, 10856.
- (96) Amezaga, N. J. M.; Pamies, S. C.; Peruchena, N. M.; Sosa, G. L. *J. Phys. Chem. A*, **2010**, *114*, 552.
- (97) Iwaoka, M.; Komatsu, H.; Katsuda, T.; Tomoda, S. *J. Am. Chem. Soc.*, **2004**, *126*, 5309.
- (98) Bleiholder, C.; Gleiter, R.; Werz, D. B.; Köppel, H. *Inorg. Chem.*, **2007**, *46*, 2249.
- (99) Gleiter, R.; Werz, D. B.; Rausch, B. *J. Chem. Eur. J.*, **2006**, *9*, 2676–2683.
- (100) Hayashi, S.; Nakanishi, W.; Furuta, A.; Drabowicz, J.; Sasamori, T.; Tokitoh, N. *New J. Chem.*, **2009**, *33*, 196.

- (101) Sarma, B. K.; Muges, G. *ChemPhysChem.*, **2009**, *10*, 3013.
- (102) Pal, T. K.; Sankararamakrishnan, R. *J. Phys. Chem. B*, **2010**, *114*, 1038–1049.
- (103) Lu, Y.-X.; Zou, J.-W.; Wang, Y.-H.; Jiang, Y.-J.; Yu, Q.-S. *J. Phys. Chem. A*, **2007**, *111*, 10781.
- (104) Crestani, M. G.; Manbeck, G. F.; Brennessel, W. W.; McCormick, T. M.; Eisenberg, R. *Inorg. Chem.*, **2011**, *50*, 7172–7188.
- (105) Hu, J.; Nguyen, M.-H.; Yip, J. H. K. *Inorg. Chem.*, **2011**, *50*, 7429–7439.
- (106) Platel, R. H.; White, A. J. P.; Williams, C. K. *Inorg. Chem.*, **2011**, *50*, 7718–7728.
- (107) Helm, M. L.; Stewart, M. P.; Bullock, R. M.; DuBois, M. R.; DuBois, D. L. *Science*, **2011**, *333*, 863.

Table 3-1. Energetic, geometric, and electronic aspects of FP...D complexes, all with FH₂P as electron acceptor.

	HOH	H ₂ CO	CH ₃ OH	HSH	H ₂ CS	NH ₃
-ΔE, kcal/mol	4.03	4.78	5.00	3.07	4.68	6.19
R(P...D), Å	2.759	2.670	2.651	3.239	3.061	2.624
Δq ^a , me	11.6	17.3	19.0	17.3	33.8	33.3
E(2) ^b kcal/mol	7.69	9.70	10.91	8.44	14.85	18.18
Δr(F-P), mÅ	11.3	11.5	14.1	8.9	13.2	26.5

^aD_{lp}→σ*(F-P) charge transfer, summed over both lone pairs of O or S

^bNBO perturbation energy corresponding to D_{lp}→σ*(F-P), summed over both lone pairs of O or S

Table 3-2. SAPT decompositions (kcal/mol) of the complexation energies of the FP...D complexes, all with FH₂P as partner molecule.

	HOH	H ₂ CO	CH ₃ OH	HSH	H ₂ CS	NH ₃
ES	-8.38	-11.16	-11.54	-6.72	-12.43	-18.21
EX	8.16	12.08	13.51	8.98	16.74	22.07
IND	-4.87	-8.61	-9.16	-8.41	-18.11	-19.91
IND+EXIND	-1.32	-1.91	-2.03	-1.19	-2.42	-4.08
DISP	-3.25	-4.80	-5.43	-3.97	-6.50	-6.39
DISP+EXDIS	-2.69	-3.92	-4.46	-3.25	-5.14	-4.90
P						

Table 3-3. Energetic, geometric, and electronic aspects of FP...D complexes, for carbon-containing donors, all with FH₂P as partner molecule.

	HCCH	H ₂ CCH ₂	CH ₂ CHCHCH ₂	C ₆ H ₆
-ΔE, kcal/mol	3.04	3.47	4.11	4.16
R(P...C), Å	3.075	2.974	2.922	3.186
Δq _{FP} ^a , me	10.9	18.9	18.8	31.3
E(2) _{FP} ^a , kcal/mol	5.06	8.01	8.02	7.68
Δq _{CC} ^b , me	3.8	7.1	7.6	c
E(2) _{CC} ^b , kcal/mol	2.07	3.52	3.58	c
Δr(F-P), mÅ	6.2	9.2	11.0	8.1
Δr(C-C), mÅ	1.8	3.8	5.2	2.0

^aπ(C-C)→σ*(F-P)

^bP_{1p}→π*(CC) charge transfer

^cNBO treatment suffers partial breakdown with C₆H₆

Table 3-4. SAPT decompositions (kcal/mol) of the complexation energies of the FP...D complexes, all with FH₂P as partner molecule.

	HCCH	H ₂ CCH ₂	CH ₂ CHCHCH ₂	C ₆ H ₆
ES	-6.94	-9.62	-10.61	-6.75
EX	9.71	15.03	17.75	11.73
IND	-7.77	-14.43	-16.65	-7.46
IND+EXIND	-1.13	-1.78	-2.12	-1.17
DISP	-4.68	-6.54	-8.17	-7.60
DISP+EXDISP	-3.83	-5.23	-6.61	-6.36

Table 3-5. FP•••D binding energies (kcal/mol) with FH₂P compared with H-bonds formed with FH and HOH.

	FH ₂ P	FH	HOH
NH ₃	6.19	11.64	5.81
HOH	4.03	7.86	4.43
H ₂ CO	4.78	7.43	4.73
CH ₃ OH	5.00	8.93	5.05
HSH	3.07	4.54	2.55
H ₂ CS	4.68	5.52	3.84
HCCH	3.04	3.72	2.05
H ₂ CCH ₂	3.47	4.08	2.27
C ₄ H ₆	4.11	4.06	2.68
C ₆ H ₆	4.16	3.92	2.88

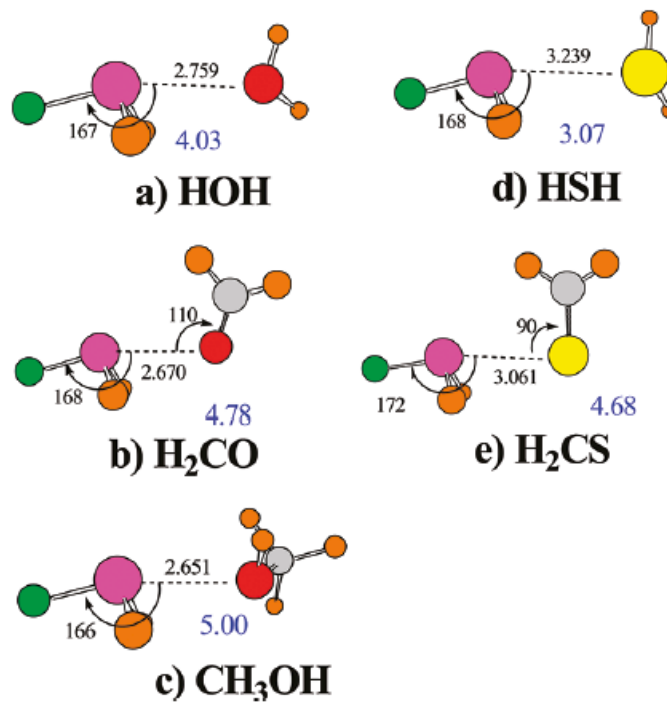


Figure 3-1. Optimized geometries of complexes pairing FH₂P with various electron donor molecules. Distances in Å, and angles in degs. Counterpoise-corrected binding energy reported as blue number.

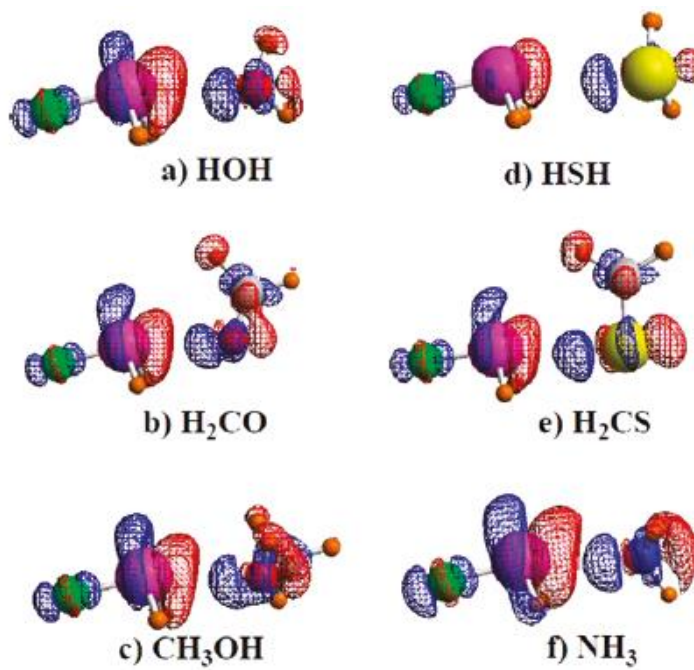


Figure 3-2. Density shifts occurring in the indicated $\text{FH}_2\text{P}\cdots\text{D}$ complexes upon formation of each complex. Blue regions indicate density increase, red a decrease. Contours are shown at the 0.001 au level.

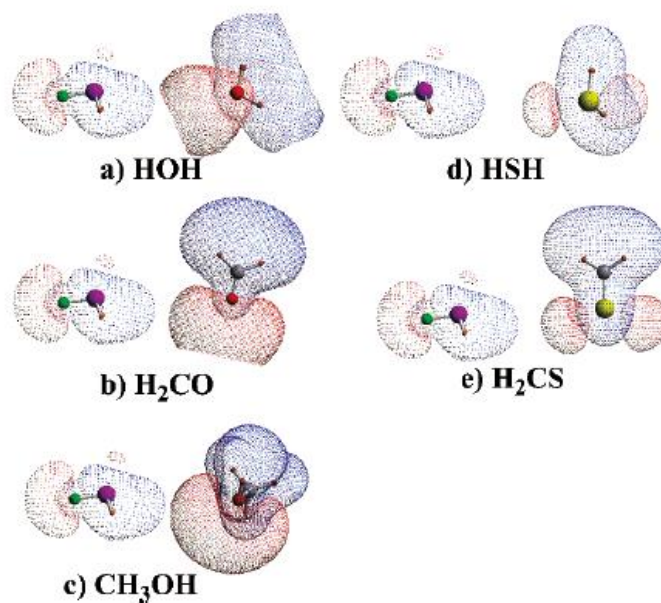


Figure 3-3. Electrostatic potentials of isolated monomers, oriented as they are within the optimized complexes with FH₂P. Blue and red regions indicate positive and negative potentials, respectively; contours at the ± 0.02 au level.

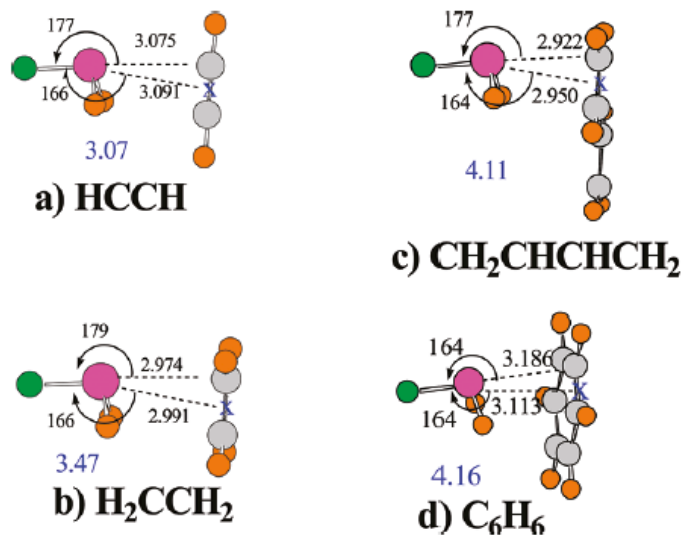


Figure 3-4. Optimized geometries of complexes pairing FH₂P with each of several unsaturated C-containing molecules. Distances in Å, and angles in degs. Blue X represents center of indicated C-C bond. Counterpoise-corrected binding energy reported as blue number.

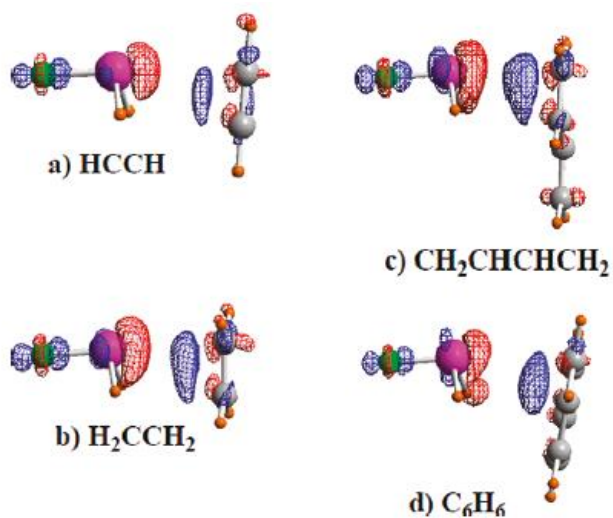


Figure 3-5. Density shifts occurring in the indicated $\text{FH}_2\text{P}\cdots\text{D}$ structures upon formation of each complex. Blue regions indicate density increase, red a decrease. Contours are shown at the 0.001 au level.

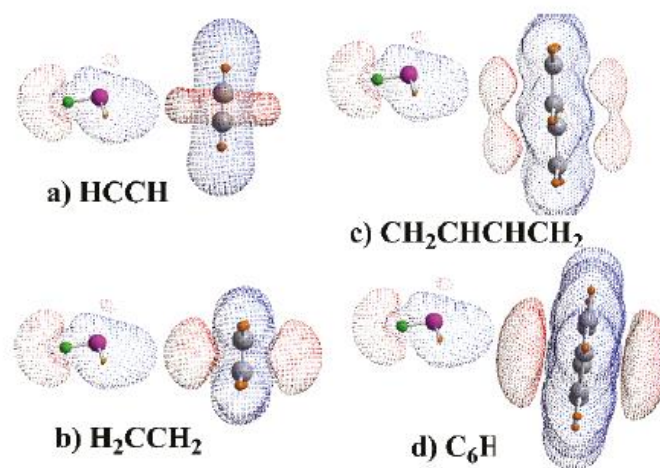


Figure 3-6. Electrostatic potentials of isolated monomers, oriented as they are within the optimized complexes with FH_2P . Blue and red regions indicate positive and negative potentials, respectively; contours at the ± 0.02 au level.

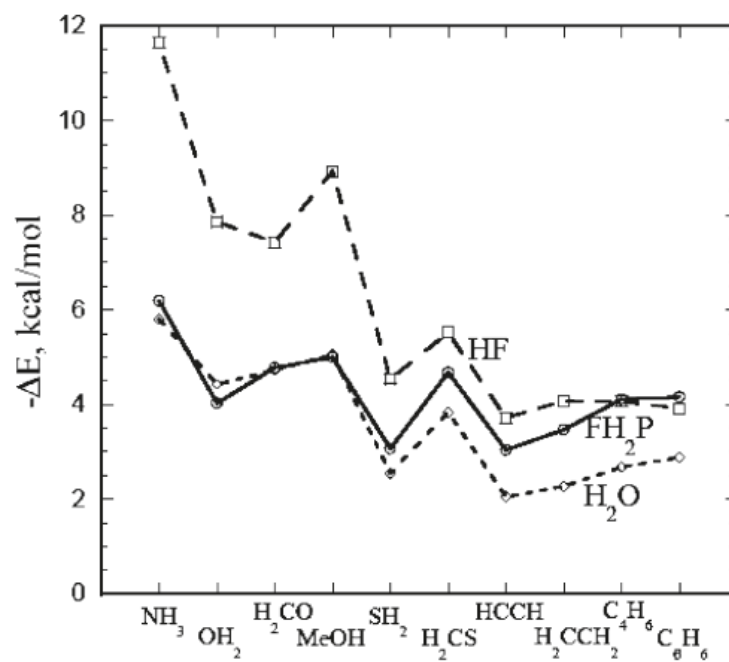


Figure 3-7. Interaction energies of each of the complexes formed by HF, H₂O, and FH₂P with various electron donors. Broken lines refer to H-bonds and solid to P···D.

CHAPTER 4
COMPARISON OF P···D (D=P,N) WITH OTHER NONCOVALENT BONDS IN
MOLECULAR AGGREGATES¹

Abstract

All the minima on the potential energy surfaces of homotrimers and tetramers of PH₃ are identified and analysed as to the source of their stability. The same is done with mixed trimers in which one PH₃ molecule is replaced by either NH₃ or PFH₂. The primary noncovalent attraction in all global minima is the BP···D (D=N,P) bond which is characterized by the transfer of charge from a lone pair of the donor D to a σ^* B-P antibond of the partner molecule which is turned away from D, the same force earlier identified in the pertinent dimers. Examination of secondary minima reveals the presence of other weaker forces, some of which do not occur within the dimers. Examples of the latter include PH···P, NH···P and PH···F H-bonds, and “reverse” H-bonds in which the source of the electron density is the smaller tail lobe of the donor lone pair. The global minima are cyclic structures in all cases, and exhibit some cooperativity, albeit to a small degree. The energy spacing of the oligomers is much smaller than that in the corresponding strongly H-bonded complexes such as the water trimer.

4-1. Introduction

Noncovalent forces have been recognized as a dominant phenomenon in chemistry and biology for many years.¹⁻⁴ There is a long history of examination of the

¹Coauthored by Upendra Adhikari and Steve Scheiner. Reproduced with permission from *J. Chem. Phys.* **2011**, *135*, 184306. Copyright 2011, AIP Publishing LLC.

hydrogen bond⁵⁻¹⁰ which has undergone an evolution from the early ideas of involvement of only O, N and F, to a more modern view¹¹⁻¹⁹ that has added C or Cl as potential proton donor atom, and π bonds, σ bonds, metal atoms, or another H atom as a source of electron density. Halogen bonds have certain similarities to H-bonds and can be competitive in strength. The Coulombic part of the attraction has been attributed²⁰⁻²⁹ to the shape of the electrostatic potential around the halogen atom, which despite an overall negative charge, contains a small positive region that can attract an electronegative partner atom. The literature also contains instances of other attractive forces between non-halogen electronegative atoms such as S and O,³⁰⁻³⁷ understanding of which continues to grow.

Recent work in this laboratory has identified a fundamentally different sort of noncovalent interaction between an assortment of atoms, with no intervening H or halogen atom between them.^{38,39} In an illustrative case, there is neither a $\text{NH}\cdots\text{P}$ nor $\text{PH}\cdots\text{N}$ H-bond in the global minimum of the PH_3/NH_3 heterodimer.⁴⁰ This complex is bound instead by a direct interaction between the electronegative P and N atoms. A large part of the attraction arises when a certain amount of charge from the occupied lone pair of the N atom is transferred into the vacant σ^* antibonding orbital of a P-H bond that is turned away from the N nucleus. (This sort of interaction is denoted below as $\text{BA}\cdots\text{D}$ where A and D refer respectively to the electron acceptor and donor atoms, and B represents a group bound to A.)

Subsequent work^{41,42} has demonstrated that this sort of $\text{BA}\cdots\text{D}$ interaction is not unique to $\text{A} = \text{P}$, but is also characteristic of other second-row atoms S and Cl, as well as the third-row congener As. Given a single substitution, even two highly electronegative first-row N atoms can be made to approach one another in an attractive fashion.⁴³ These

forces can be quite strong. Calculations have shown⁴⁴ that even a single B = Cl, F, or NO₂ substituent on the electron acceptor molecule multiplies the interaction energy as much as fivefold, to the point where the P...N interaction surpasses the strength of the paradigmatic H-bond in the water dimer. In addition, there are a range of different atoms, other than N, that can serve as the source of electron density, including carbon-containing π systems.⁴⁵ Experimental confirmation of these sorts of interactions has arisen from examination^{43,44,46} of a number of crystal structures in the literature. It would thus appear that this particular interaction is an important one, in the same class as H and halogen bonds.

The question then arises as to whether this type of interaction will also play a major role in the structure and energetics of larger aggregates of these molecules. This issue has obvious importance for condensed phases where static dimer equilibrium geometries are not necessarily indicative of the fluctuating molecular orientations. There may well be alternate types of interactions, that do not represent minima within the context of dimers, but that might become more important within larger aggregates. For instance, while one of the two minima of the PH₃/NH₃ heterodimer system is characterized by a PH...N H-bond, there is no such minimum corresponding to the reverse NH...P interaction. Likewise for the PH₃ homodimer, where there is no PH...P minimum. So in the context of dimers, neither NH...P nor PH...P H-bonds would be said to exist. However, might either of these H-bonds become a contributing factor in a trimer or larger aggregate? As another example, both the P...N and PH...N minima of the heterodimer attribute their stability in part to charge transfer originating in the N lone

pair. Could other orbitals also act as electron donors? Some obvious candidates might include an occupied PH or NH bonding orbital.

Another issue concerns the shape of the aggregates. It is known that small H-bonded trimers usually adopt either a triangular cyclic structure, with all three molecules essentially equivalent, or an open-chain where a central molecule is connected to two end molecules.⁴⁷⁻⁵⁰ The relative stabilities of these two types of structures change as the size of the aggregate grows beyond the trimer level. One must thus wonder whether the same is true for BA···D bonds. Do these sorts of shapes pertain there as well, and what factors might favor open chain versus closed cycles?

A very important phenomenon that arises in complexes containing more than two molecules is cooperativity. It is understood that the total binding energy of a H-bonded chain of molecules exceeds the sum of the H-bond energies that are associated with each dimer of which it is comprised.^{9,51-53} It is partly for this reason that the liquid state of water is so stable. On the other hand, this cooperativity can become negative, exerting a weakening effect, if the central molecule acts as double electron donor or acceptor. However, there has been no examination of this issue in the case of BA···D interactions. Does this interaction exhibit cooperativity, and if so how strongly?

The work presented here attempts to answer these questions. The numbers of molecules are built up beyond the dimer level to trimers and tetramers. In each case, all minima on the potential energy surface are identified, and analyzed as to the source of stability of each, with an eye toward other sorts of interactions that might compete with the BA···D bond, such as H-bonds, dipole-dipole or dispersion-dominated interactions, and other attractive forces that might appear only in the larger aggregates. The energy

differences between the minima also provide information as to the rapidity with which the structure of the aggregate will oscillate over time.

The systems considered include first the homotrimer and tetramer of PH_3 . The work then replaces one PH_3 molecule by NH_3 . The latter molecule was shown earlier to engage in a $\text{HP}\cdots\text{N}$ interaction with PH_3 , but its secondary minimum was different than that in the PH_3 homodimer, in that it contained a $\text{PH}\cdots\text{N}$ H-bond. The consideration of these larger aggregates will provide some insight into how these sorts of interactions compete with one another on the larger scale. And finally, a PH_3 molecule is replaced by FPH_2 . This fluorosubstitution was demonstrated earlier^{44,46} to ramp up the strength of the $\text{FP}\cdots\text{D}$ interaction, while also acting to make PH a more potent proton donor in a H-bond. The competition between these two sorts of forces could thus become very interesting as the number of molecules rises.

The direct $\text{P}\cdots\text{P}$ and $\text{P}\cdots\text{N}$ interactions which are the principal forces within the dimers are shown to dominate these larger oligomers as well. But by considering secondary minima, a range of other attractive forces are observed, many of which are not present in the dimers. These secondary interactions include weak H-bonds where P and F act as proton acceptors. Also making an appearance are “reverse” H-bonds in which the electron donation originates in the smaller tail lobe of the lone pair, or from a σ -bonding P-H orbital.

4-2. Computational Methods

The GAUSSIAN 09 package⁵⁴ was applied to all systems. Geometries were optimized at the *ab initio* MP2/aug-cc-pVDZ level, an approach which has been shown to

be of high accuracy, especially for weak intermolecular interactions of the type of interest here^{27,55-60} where the data are in close accord with CCSD(T) values with larger basis sets⁴⁴ and in nearly perfect coincidence with experimental energetics.⁶¹ The potential energy surface of each aggregate was examined to identify all minima, by using a wide range of different starting points for geometry optimizations. Minima were verified as having all real vibrational frequencies. Interaction energies were computed as the difference in energy between the complex, and the sum of the optimized energies of the isolated monomers, corrected for basis set superposition error by the counterpoise procedure,⁶² and by zero-point vibrational energies. Natural bond orbital (NBO) analysis^{63,64} was carried out via the procedures contained within Gaussian.

4-3. Results

There are two minima on the surface of the PH₃ dimer.⁴⁰ The more stable of the two, with a counterpoise-corrected binding energy of 1.14 kcal/mol, has the two P atoms facing one another directly, and one H atom of each molecule is turned nearly 180° away from the other P. The primary binding here is derived from a pair of HP···P interactions, with a NBO value of E(2) of 1.04 kcal/mol for each of the two P_{1p}→σ*(PH) transfers. The other minimum is dominated by dispersion, and there is no appreciable intermolecular charge transfer. The total binding energy is only 0.74 kcal/mol. The orientations can be characterized by the directions of the two P lone pairs: One points directly away from the other molecule, and the other perpendicular to the P···P axis. For shorthand purposes, the latter sort of interaction will be denoted below as a “dispersion bond”, but it should be understood that electrostatics and induction make contributions to

binding in this dimer, albeit small ones. For reference purposes, the R(P···P) distances in the HP···P and dispersion-dominated dimers were optimized⁴⁰ to 3.654 and 4.099 Å, respectively.

4-3.1. (PH₃)₃

The eight minima located on the surface of the PH₃ trimer are displayed in Fig. 4-1. Along with each is illustrated its counterpoise-corrected binding energy, followed by this same quantity after zero point vibrations have been added. This binding energy is defined as the energy required to separate the trimer into three isolated, fully optimized monomers. The most stable such trimer in Fig. 4-1(a) may be seen to be nearly an equilateral triangle, with all three R(P···P) distances equal to 3.84 Å. The binding can be characterized as three HP···P charge transfers. That is, one H atom of each molecule is disposed 158° away from a P···P axis, and the NBO value of E(2) for each such interaction is equal to 1.15 kcal/mol, as indicated by the red numbers near each of these H atoms. These observations confirm the importance of the HP···P bond to the trimer, as was true in the dimer.

The total binding energy of this trimer is 2.91 kcal/mol. This value is slightly less than the 3.42 kcal/mol that is equal to 3 times the binding energy in a fully optimized dimer, also stabilized by a HP···P bond. The optimized R(P···P) distances of 3.84 Å in 4-1(a) are somewhat longer than the corresponding separation of 3.65 Å in the dimer. In addition, the $\theta(\text{HP}\cdots\text{P})$ angles, critical to the charge transfer stabilization, are 158° in 4-1(a), as compared to the more nearly linear 178° in the dimer. On the other hand, the three values of E(2) in the trimer, 1.16 kcal/mol, are slightly larger than the two values of

1.04 kcal/mol in the optimized dimer. Evidently, the geometric distortions associated with forming the trimer, and any 3-body effects, yield a slight negative cooperativity in this trimer. Another factor to consider is that the optimized dimer contains a pair of equivalent $P_{lp} \rightarrow \sigma^*(PH)$ transfers, one going in each direction. This contrasts with the single transfer between each pair of molecules in 4-1(a), and may also contribute to the 0.2 Å longer $R(P \cdots P)$ in the trimer.

This behavior can be contrasted with the water trimer, which also adopts an equilateral triangle as its equilibrium structure. In order to maximize its cooperativity, each molecule in this structure acts simultaneously as both electron donor and acceptor, just as each molecule in 4-1(a) is both donor and acceptor. At this same level of theory, the total binding energy of this trimer is equal to 13.9 kcal/mol, which is slightly larger, by 0.6 kcal/mol, than three times the binding energy of the dimer. Like the PH_3 trimer, the water trimer also exhibits angular strain, in that each $\theta(OH \cdots O)$ angle is 151° , much further from linearity than the angle of 175° in the dimer. Unlike the increased intermolecular distance in the PH_3 trimer, however, $R(O \cdots O)$ contracts from dimer to trimer, by 0.23 Å. So despite its angular distortions the water trimer exhibits positive cooperativity in both R and E, while the reverse is true for the PH_3 trimer.

The next most stable trimer in Fig. 4-1(b) loses its equilateral character as one of the $R(P \cdots P)$ distances is 4.443 Å, considerably longer than the other two. This distance, as well as all others, is listed in Table 4-1 along with the important $E(2)$ values for the various trimer configurations in summary form. And in fact, there is no appreciable amount of charge transfer between these two molecules, 1 and 3. Indeed, this separation

is even larger than the 4.1 Å distance when a pair of PH₃ molecules are held together by dispersion alone. This lack of a source of attraction is indicated by the absence of a connecting line between molecules 1 and 3 in Fig. 4-1(b). Instead, one H atom of each of molecules 1 and 3 is turned away from P₂, by some 170°. There are two H atoms of molecule 2 that are turned away from another P, one away from P₁ (by 165°) and one from P₃ (by 177°). Altogether then, there are four E(2) contributions, by amounts varying from 0.82 to 1.25 kcal/mol. It might also be noted that two of the R(P···P) distances in 4-1(b) are shorter than the 3.84 Å in 4-1(a), which is consistent with the presence of two HP···P bonds between each such pair, as compared to only one in 4-1(a). Geometry 4-1(b) thus resembles a pair of dimers, 1-2 and 2-3, in that each pair contains two HP···P charge transfers. The two corresponding R(P···P) separations of 3.66 and 3.67 Å are also rather close to the distance of 3.65 Å in the optimized dimer. Structure 4-1(c) is very similar to 4-1(b), with comparable geometrical parameters, and is also bound by the same four HP···P charge transfers. Thus the HP···P bond appears to be the dominant form of interaction in the three most stable minima.

Structure 4-1(d) adds a new feature to these complexes. It contains two separate HP···P interactions, one from 2 to 3 and the other from 1 to 2. What is new here is the type of interaction between molecules 1 and 3, which adopt the relative orientation of the second and less stable of the two optimized PH₃ dimers, dominated by dispersion attraction. This orientation is designated by the blue hatched line between these two molecules and the parenthetical d in Table 4-1. Note that the R(P···P) distance is 4.18 Å, only 0.08 Å longer than the optimized interphosphorous distance in the corresponding optimized dimer. These distances represent a pattern that is repeated for dimers and

higher order oligomers of PH_3 . The $\text{R}(\text{P}\cdots\text{P})$ separations for $\text{HP}\cdots\text{P}$ bonds lie in the 3.6-3.8 Å range, and dispersion bonds are roughly 4.1-4.2 Å; longer distances indicate little appreciable attraction. Apparently, the exchange of a $\text{HP}\cdots\text{P}$ for a dispersion bond requires some 0.4 kcal/mol, the difference in energy between structures 4-1(a) and 4-1(d). It is likely no coincidence that this is also the energy difference between the two dimers, one bound by $\text{HP}\cdots\text{P}$ and the other by dispersion.

It was noted earlier that no minimum on the PH_3 dimer surface contains a $\text{PH}\cdots\text{P}$ H-bond. Nonetheless, such an interaction appears for the first time in trimer 4-1(e) between molecules 2 and 3. The $\text{R}(\text{H}\cdots\text{P})$ distance is rather long at 3.23 Å, but there is a sizable amount of charge transfer involved, with $E(2) = 0.74$ kcal/mol. The other two stabilizing interactions in 4-1(e) occur between molecules 1 and 2, both of which are of the stronger $\text{HP}\cdots\text{P}$ variety. As was the case for 4-1(b) and 4-1(c), the presence of two such bonds between this pair of molecules results in a short $\text{R}(\text{P}\cdots\text{P})$ contact, close to that in the dimer. In comparison to global minimum 4-1(a), the exchange of one $\text{HP}\cdots\text{P}$ for a dispersion bond, and another for a $\text{PH}\cdots\text{P}$ H-bond in 4-1(e) destabilizes the system by 0.6 kcal/mol. Structure 4-1(f) has the distinction of being held together only by the dispersion bonds of the less stable PH_3 dimer; one between molecules 1 and 2, and the other between 1 and 3. This pair of bonds places complex 4-1(f) above 4-1(a) in energy by 0.9 kcal/mol.

It is not until structure 4-1(g), held together by 1.93 kcal/mol, that the triangular structure distorts into an open chain geometry. Molecules 2 and 3 interact via a pair of $\text{HP}\cdots\text{P}$ interactions, with the standard short $\text{R}(\text{P}\cdots\text{P})$, and 1 is held to 2 via a dispersion bond. Thus the transition from cyclic (4-1(a)) to open chain trimer costs 1.0 kcal/mol.

The least stable of the minima, 4-1(h), contains a dispersion attraction between molecules 1 and 2. Molecules 1 and 3 are held together by an unusual sort of H-bond. The H atom lies very nearly along the P...P axis as usual. However, the electron-donating molecule 1 is turned so that the main lobe of its lone pair points away from the bridging proton, not toward it. Nevertheless, the charge transfer accounts for a NBO E(2) value of a non-negligible 0.60 kcal/mol. This sort of reverse H-bond, involving a lone pair minor lobe, or tail, has been noted recently⁴² in related systems.

4-3.2. *PH₃ tetramer*

Searches for minima on the surface of the PH₃ tetramer yielded a total of 23 such structures, with binding energies varying between a maximum of 4.8 to a minimum of 2.1 kcal/mol. Inclusion of zero-point vibrations lowers this range to 0.4-2.5 kcal/mol. The most stable nine of these, those with binding energies greater than 4 kcal/mol, are displayed in Fig. 4-2 where it may first be observed that there are only small energy differences that separate them. For example, these nine minima span an energy range of only 0.8 kcal/mol, an average gap of some 0.1 kcal/mol. This separation is even smaller than was observed in the trimer above. It is clear then that the cluster will freely oscillate between these minima, unless the temperature is very low indeed.

These geometries exhibit many of the same binding patterns that arose in the trimers. Global minimum 4-2(a), for example, is a close analogue of trimer 4-1(a). Like the latter, it is bound by four, instead of three, equivalent P_{lp}→σ*(PH) bonds, with E(2) values of 1.2 kcal/mol, and with R(P...P) separations of 3.84 Å, displayed also in Table 4-2. The total binding energy of 4.83 kcal/mol can be compared with four times the

interaction energy of 1.14 kcal/mol within the optimized PH_3 homodimer, a slight cooperative enhancement of 0.27 kcal/mol. But perhaps this cooperativity can be considered somewhat larger in that each pair of molecules in 4-2(a) is bound by a single $\text{P}_{\text{lp}} \rightarrow \sigma^*(\text{PH})$ transfer, rather than the two holding together the dimer.

There are also four such transfers in 4-2(b), three of which involve molecule 1. This triple interaction would be expected to have a weakening influence on each one, and another interaction, a dispersion bond between molecules 3 and 4, makes up for much of this difference. As a result 4-2(b) is only 0.1 kcal/mol higher in energy than 4-2(a). Structure 4-2(c) is much like 4-2(b), except that one of the $\text{P}_{\text{lp}} \rightarrow \sigma^*(\text{PH})$ transfers is lost, raising the energy another 0.2 kcal/mol. Geometry 4-2(d) resembles 4-2(c) except that the interaction between molecules 1 and 2 is associated with two transfers, as is the case in 4-2(f). This double transfer causes the ensuing interphosphorous distance to shrink down a bit, below 3.7 Å. In fact, it might be worth stressing at this point that the various $\text{R}(\text{P} \cdots \text{P})$ distances in the tetramer fit the patterns noted in the trimers. The shortest intermolecular distances of 3.6-3.7 Å are associated with double transfers, single transfer slightly longer at about 3.8 Å, and dispersion bonds are roughly 4.1 Å long.

Complex 4-2(e) contains a binding across the diagonal of the square, between molecules 1 and 3, a pattern first observed in 4-2(b). This structure might best be described as a trimer involving molecules 1, 3, and 4, plus an interaction of molecule 2 with one of the molecules of the triangle. The absence of any substantial attraction between molecules 2 and 3 is confirmed by the interphosphorous distance of 4.622 Å, considerably longer than even those molecules held together primarily by dispersion. This same sort of pattern, wherein not all of the vertex molecules are bound together,

becomes the rule rather than the exception as the total stabilization energies continue to diminish. Molecules 3 and 4 in structure 4-2(g) are separated by 4.384 Å, even further apart than the 1,2 pair which are held together only by dispersion. Molecules 1 and 4 are even further separated, by 4.517 Å, in 4-4(h) which contains two dispersion bonds. The stability of this complex is due at least in part to the presence of a PH...P H-bond between molecules 1 and 3. Complex 4-2(i) is interesting in that it contains a multitude of different sorts of attractive forces. The 1,4 and 2,3 pairs are connected by dispersion bonds with the usual intermolecular separations. There are also three HP...P bonds, one of which cuts across a diagonal of the square, and all three of which contain the expected R(P...P) distances.

As higher-energy tetramers are considered, there is a continuation of the tendency to replace HP...P bonds by weaker dispersion or PH...P H-bonds. For example, the next complex, bound by 3.92 kcal/mol, contains three dispersion bonds and a PH...P H-bond, in addition to a single HP...P. Slightly higher in energy is another minimum which contains only two HP...P and one dispersion bond.

4-3.3. $NH_3-PH_3-PH_3$

The PH_3/NH_3 heterodimer potential energy surface contains two minima.⁴⁰ The more stable of the two, bound by 1.43 kcal/mol, has each of the two molecules turned so that one of its H atoms is pointing away from the other molecule. The less stable dimer contains a PH...N H-bond, and is bound by 0.83 kcal/mol. Again, for reference purposes, the optimized R(P...N) distance in the more stable dimer is 3.302 Å while the R(H...N) separation within the H-bonded dimer is 2.629 Å.

Both of these themes can be seen in a number of the twelve minima identified on the $\text{NH}_3(\text{PH}_3)_2$ trimer surface illustrated in Fig. 4-3. The most stable of these configurations in Fig. 4-3(a) is characterized by three interactions. The lone pair of NH_3 donates charge to a H atom bound to P3, with $E(2)=1.60$ kcal/mol. This quantity, reported also in Table 4-3, is larger than that which occurs in the fully optimized dimer where $E(2)$ for $\text{N}_{\text{lp}} \rightarrow \sigma^*(\text{PH})$ is equal to 1.18 kcal/mol. The $R(\text{P} \cdots \text{N})$ distance of 3.324 Å, on the other hand, is slightly longer than the 3.302 Å in the dimer, probably a result of the angular strain within the trimer. The lone pair of this same PH_3 molecule donates charge to a $\sigma^*(\text{PH})$ antibond of P2, characterized by $E(2)=1.29$ kcal/mol, again larger than the 1.04 kcal/mol within the PH_3 homodimer, and again $R(\text{P} \cdots \text{P})$ is longer within the trimer than the dimer. And finally there is transfer from P2 to the NH_3 molecule via a $\text{NH} \cdots \text{P}$ H-bond. It is worth noting that such a $\text{NH} \cdots \text{P}$ H-bond does not occur in either of the minima on the surface of the NH_3/PH_3 heterodimer, so is a feature that first occurs within the context of the trimer. The evidence for the presence of this H-bond is strong. The $\theta(\text{NH} \cdots \text{P})$ bond is reasonably close to linearity, the $R(\text{H} \cdots \text{P})$ distance is less than 3 Å, and the $E(2)$ for this transfer is rather large, at 2.15 kcal/mol. Each of the three molecules in trimer 4-3(a) acts simultaneously as both electron donor and acceptor, which would suggest some positive cooperativity. However, it is difficult to assess the energetic impact as there is no minimum present in the PH_3/NH_3 heterodimer surface with a $\text{NH} \cdots \text{P}$ H-bond, so no definite value can be assigned to the third of the attractive interactions.

The nature of trimer 4-3(c) is much like that of 4-3(a), in that each of the three molecules is both donor and acceptor. The geometries differ in that the P3-H antibond which is accepting the density from NH_3 does so in the form of a $\text{PH} \cdots \text{N}$ H-bond in 4-

3(c), as compared to a $N_{lp} \rightarrow \sigma^*(PH)$ transfer in 4-3(a). This distinction destabilizes the system by some 0.6 kcal/mol, identical to the energy difference between the two relevant dimers.

Minimum 4-3(b) lies 0.5 kcal/mol higher in energy than the global minimum and contains only two clear interactions. In both of these, the N lone pair is transferring charge to a P-H σ^* bond, one on each of the two PH_3 molecules. Even though the NH_3 is acting as double electron donor, the interaction energy of 3.15 kcal/mol in this trimer is fairly high, more than double the value of a $N_{lp} \rightarrow \sigma^*(PH)$ interaction energy in the pertinent optimized dimer. It is likely that there is some attractive contribution arising between the two PH_3 molecules, although there is no appreciable charge transfer between them, and $R(P \cdots P) = 4.617 \text{ \AA}$. Minimum 4-3(d) brings into the picture the dispersion-dominated interaction that occurs as one of the minima in the PH_3 dimer. The two P atoms are separated by 4.19 \AA in this interaction which is indicated by the hashed blue line. Complex 4-3(d) also contains both a $NH \cdots P$ H-bond and a $N_{lp} \rightarrow \sigma^*(PH)$ interaction, both of which have fairly large values of $E(2)$. Structure 4-3(e) is similar, but the $NH \cdots P$ H-bond of 4-3(d) has been turned into a $PH \cdots N$ H-bond, destabilizing the system by 0.1 kcal/mol. 4-3(g) is similar as well, but contains a pair of $PH \cdots N$ H-bonds which make the N atom a double proton acceptor. The resulting negative cooperativity raises the energy of 4-3(g) by 0.6 kcal/mol, relative to 4-3(e). Like 4-3(g), structure 4-3(h) also contains a $P \cdots P$ dispersion bond, and a $PH \cdots N$ H-bond. However, the $PH \cdots N$ H-bond of 4-3(g) has altered to a $NH \cdots P$ H-bond, but with the PH_3 molecule rotated so that its lone pair faces away from the approaching NH. Earlier work⁴² has shown that this orientation allows the

tail of the lone pair orbital to interact with the approaching proton to engage in a weak H-bond. This sort of weaker arrangement costs the trimer 0.1 kcal/mol, relative to 4-3(g).

The remaining five complexes represent open chains with the terminal molecules distant from one another. NH_3 occupies the central position in 4-3(f), where it serves as both electron donor and acceptor. The same is true in 4-3(i), except that the righthand PH_3 molecule has turned its major lone pair lobe away from the NH bond. The resulting $\text{NH}\cdots\text{P}$ H-bond is 0.2 Å longer than that in 4-3(f), and the value of $E(2)$ has diminished three-fold. The other three open-chain configurations place the NH_3 on a terminus of the chain, where it acts as electron donor to the central PH_3 unit, either as a $\text{PH}\cdots\text{N}$ H-bond as in 4-3(j) and 4-3(l) or in the $\text{N}_{\text{lp}}\rightarrow\sigma^*(\text{PH})$ bond of 4-3(k). The latter structure is interesting in the “face-off” between the two H atoms along the $\text{PH}\cdots\text{HP}$ axis, a geometry reminiscent of dihydrogen bonds.

4-3.4. $\text{FPH}_2\text{-PH}_3\text{-PH}_3$

As was demonstrated earlier,⁴⁴ the substitution of one of the H atoms of PH_3 by an electron-withdrawing group strengthens its $\text{P}\cdots\text{N}$ bond severalfold. For example, the 1.4 kcal/mol binding energy of $\text{H}_3\text{P}\cdots\text{NH}_3$ rises to 6.2 in $\text{FH}_2\text{P}\cdots\text{NH}_3$. Other calculations have indicated a like enhancement when the electron donor is another P atom.^{65,66} At the level of theory applied here, the counterpoise-corrected binding energy of the $\text{FH}_2\text{P}\cdots\text{PH}_3$ complex is 3.23 kcal/mol, as compared to 1.14 kcal/mol in $\text{H}_3\text{P}\cdots\text{PH}_3$.

One would therefore anticipate that the overall binding energy of the $(\text{PH}_3)_3$ trimer will increase when one of the PH_3 molecules is replaced by FPH_2 . And indeed, whereas the global minimum of the homotrimer is bound by 2.9 kcal/mol, this

replacement of a single molecule nearly doubles the total interaction energy. This global minimum is illustrated in Fig. 4-4(a) where four different charge transfers are observed. By far the largest of these is the value of 11.8 kcal/mol for E(2) that arises from the transfer from the P2 lone pair into the P1-F σ^* antibond, reported along with the interphosphorous distances in Table 4-4. Note that this strong interaction leads to a short R(P \cdots P) distance of only 3.168 Å, much shorter than any of the other interphosphorous distances noted to this point. This distance is only very slightly shorter than the R(P \cdots P) separation of 3.172 Å in the FH₂P \cdots PH₃ dimer. Also very close to the dimer value is the θ (FP \cdots P) angle of 168°, altered by only 3°. There are three other transfers from P lone pairs to σ^* (PH) antibonds, all with values of E(2) around 1 kcal/mol.

This same major P2_{lp} $\rightarrow\sigma^*$ (PF) interaction arises also in 4-4(b), complemented again by a pair of P_{lp} $\rightarrow\sigma^*$ (PH) transfers to the lower right PH₃ molecule. It is worth noting that E(2) is larger for the transfer from the P1 lone pair than from P3, even though the θ (P1 \cdots P2H) angle is much further from linearity. This difference may be due to the shorter R(P \cdots P) distance in the former case. Structure 4-4(d) is very much like 4-4(a) and 4-4(b), except that the lower left PH₃ molecule is rotated around so that its interaction with the lower right PH₃ is of the dispersion-dominated sort. It is consequently of higher energy, nearly 1 kcal/mol less stable than 4-3(a).

Geometries 4-4(c), 4-4(e), and 4-4(f) are all of the open-chain variety. All have in common the stabilizing P_{lp} $\rightarrow\sigma^*$ (PF) transfer, with E(2) between 11 and 12 kcal/mol. A new sort of interaction is encountered for the first time in 4-4(c), wherein it is the F, rather than the P lone pair, that donates charge to a neighboring PH σ^* antibond.

Structure 4-4(e) contains a dispersion bond between molecules 2 and 3, while a $\text{PH}\cdots\text{F}$ H-bond makes its maiden appearance in 4-4(f). The next three minima all have binding energies of roughly 3 kcal/mol, and all are triangular. Notably, 4-4(f) is the last of the minima which has a large energetic contribution due to charge transfer into the $\text{PF } \sigma^*$ antibond, which probably accounts for the 0.8 kcal/mol jump in energy to 4-4(g). In 4-4(g) and 4-4(h), the F atom again replaces P as the source of charge for transfer from its lone pairs to $\text{PH } \sigma^*$ antibonds. While there may be a superficial resemblance, this arrangement does not fit the usual pattern of a halogen bond in a number of respects. First in terms of geometry, halogen bonds would be expected to have a $\theta(\text{PF}\cdots\text{P})$ angle very close to linearity which is far from the case in 4-4(g) and 4-4(h), which exhibit angles between 93° and 105° . Secondly, in a halogen bond the transfer would move density into the $\text{P-F } \sigma^*$ antibond; the opposite occurs in 4-4(g) and 4-4(h) where the F atom is the source of the charge transfer into the partner molecule.

Structure 4-4(i) is stabilized in part by a $\text{P}_{\text{lp}} \rightarrow \sigma^*(\text{PF})$ transfer, but with the new wrinkle that the charge comes from the smaller, minor lobe of the P lone pair on molecule 2. It is for this reason that $E(2)$ is only 0.50 kcal/mol for this interaction, and that the $\text{R}(\text{P}\cdots\text{P})$ distance of 3.85 Å is so much longer than the 3.14-3.19 Å range in 4-4(a) - 4-4(f), where the charge arises from the larger lobe of the P lone pair. It is in 4-4(i) that one sees a different sort of charge transfer for the first time. Another transfer occurs from molecule 2 to 1, with $E(2) = 0.58$, but this time the source of the charge is a $\text{P-H } \sigma$ bond. The F atom of molecule 1 lies 167° from the $\text{H}\cdots\text{P}$ axis, and $E(2)$ is 0.58 kcal/mol, exceeding the value of 0.50 kcal/mol for the transfer from the P lone pair tail. Structure 4-

4(j) resembles 4-4(h) geometrically but there are some important distinctions. Molecule 1 is turned a bit so that F is somewhat removed from the other two molecules, and this entity has no appreciable charge transfer interactions with the others. Molecule 1 is thus tied to the other two by dispersion bonds, rather than $\text{HP}\cdots\text{F}$. What remains from 4-4(h) is only the transfer from the P lone pair of molecule 2 into the σ^* PH antibond of molecule 3.

Structure 4-4(k) looks quite a bit like 4-4(i), and is within 0.2 kcal/mol of it. What is missing in 4-4(k) is the charge transfer from molecule 1 to 3, which is corroborated by the much longer intermolecular distance in 4-4(k), 4.62 Å vs 3.84 Å in 4-4(i). Also like 4-4(i), 4-4(k) is stabilized by a second transfer between 1 and 2, again from a PH bonding orbital. Geometry 4-4(l) resembles 4-4(f) in that the PH_2F molecule lies at the center of an open chain trimer. But its resemblance is superseded by differences in terms of the specific interactions. In the first place the transfer into the PF σ^* orbital comes from the minor, rather than the major, lobe of the P lone pair of molecule 2, making it an order of magnitude smaller. Additional transfer into this same antibond originates in a PH bonding orbital of molecule 2. As in 4-4(i), there is transfer into a PH antibond of molecule 3 from 1, but this charge arises from a F lone pair, not P.

There were six more minima located on the $\text{FH}_2\text{P}(\text{PH}_3)_2$ surface, with stabilization energies ranging from 2.71 down to 1.51 kcal/mol. The four most stable of this group are triangular. The charge transfer interactions are largely repeats of those enunciated above. The minima with binding energies 2.71 and 2.49 both include a transfer from an F lone pair to a PH σ^* orbital, while those lying at 2.57 and 2.05 kcal/mol are stabilized

primarily by the $P_{lp} \rightarrow \sigma^*(PF)$ which involves the minor lobe of the P lone pair. The less stable of these two contains also a transfer from a PH σ bonding orbital to the PF σ^* antibond. The last and least stable of the minima are open chain. The structure bound by 1.77 kcal places the PH_2F in the center. Charge is transferred into its PF σ^* orbital from two sources; both a PH σ bond and the minor lobe of the P lone pair. PH σ bonds are also the recipients of charge, from both a F and P lone pair. The highest energy structure contains only a single transfer, from a F lone pair into a PH σ^* antibond.

4-4. Discussion

The primary noncovalent attraction which prevails in the dimers is a $BP \cdots D$ interaction, which is characterized by the transfer of charge from a lone pair of the donor D to the σ^* antibond of the B-P bond. This same bond remains the dominating attractive force within the context of the trimers and tetramers. The dimers each contain a secondary minimum whose energy is not far above that of the global minimum. Specifically, a $PH \cdots N$ H-bond occurs in the secondary minimum of the NH_3/PH_3 mixed dimer, whereas the PH_3 homodimer secondary minimum is characterized by a dispersion-dominated attraction. Both of these dimer-derived interactions are observed in the various minima of the oligomers.

In addition, this study of the larger aggregates has highlighted a number of other sorts of attractive interactions, forces that do not occur in any of the minima of the dimers, and which are consequently unexplored to this point. There is a variant of the $BP \cdots D$ interaction in which a halogen atom F replaces the usual P or N atom as the electron donor. Another set of interactions that arise only in the higher oligomers are the

PH...P, NH...P and PH...F H-bonds. There are also “reverse” H-bonds present in which the larger, primary lobe of the electron donor lone pair is turned away from the bridging proton, so that the overlap occurs with the smaller lone pair lobe. As one would anticipate, these reverse H-bonds are considerably longer and weaker than normal H-bonds. This lone pair tail can also act as electron donor into a HP...P bond, again leading to a much weakened interaction. Two other sources of electron density make their presence known in some of the higher energy minima, again leading to weak attractions. One of these is the occupied σ lobe of a P-H bond, and the other is a F lone pair.

Some of the properties of aggregates of PH₃ and related molecules are related to the energy spectrum of the various minima. In that regard, it should be noted that the energy gap between the lowest and next lowest energy PH₃ homotrimers is 0.3 kcal/mol. This same gap is equal to 0.1 kcal/mol for the tetramer. Replacement of one of the PH₃ molecules of the trimer by NH₃ or FH₂P raises this increment to 0.5 and 0.4 kcal/mol, respectively. Eight minima of the homotrimer all lie within 1.3 kcal/mol of one another, which yields an average energy gap of 0.2 kcal/mol. The dozen minima obtained when one of the PH₃ molecules of the trimer is replaced by NH₃ are separated by a total of 3.6 kcal/mol, for an average energy gap of 0.2 kcal/mol; a similar gap occurs in the FH₂P(PH₃)₂ mixed trimer. In the case of the homotetramer, there are more such minima, and the average energy difference drops to 0.1 kcal/mol. It would seem then that these aggregates can easily transition from one structure to another on a fairly rapid time scale.

This behavior stands in marked contrast to aggregates of molecules that are more tightly bound. Taking the water trimer as a counterexample, the global minimum is cyclic, and is bound by 13.9 kcal/mol. There is another very similar structure, 0.7

kcal/mol higher in energy, which differs from the global minimum only in an alternate position of one of the non H-bonding protons. The other two minima are of open-chain type, one with a double proton acceptor molecule and the other with a double donor, both bound by 7.9 kcal/mol. The energy gap between the lowest and next lowest energy structures is thus more than 6 kcal/mol, an order of magnitude larger than in any of the PH₃-containing oligomers considered here.

With respect to the shape of the minima, all of the trimers and tetramers examined here opt for a cyclic global minimum, in preference to an open chain geometry. Indeed, the open structure is of rather high energy: It represents the seventh of eight minima of the PH₃ homotrimer, and 22nd out of 23 in the case of the tetramer. After zero-point vibrational energies are included, their binding energies are less than one kcal/mol. The advantage of this sort of cyclic structure is the presence of one additional attractive interaction, between what would be the terminal molecules of the open chain. This extra stabilizing interaction comes with the energetic cost of deforming the individual interactions so that the ring can be closed. As indicated above, the extra H-bond in the cyclic water trimer outweighs any deformation energy, making it 6 kcal/mol more stable than the open chain. The balance is a bit finer in the cases of the various molecular attractions involved in the oligomers examined here, with much smaller energy gaps separating cyclic from open-chain structures.

In terms of the well known cooperativity of H-bonds, the BA...D forces that are the primary vehicles of oligomerization would appear to exhibit this property too. Of course, any such cooperativity that would arise in a cyclic structure is tamped down by the aforementioned intermolecular stretching and angular distortions within the rings.

These two competing effects are illustrated by the water trimer as a prototype H-bonded complex. The total binding energy of the global minimum cyclic geometry is greater, but only slightly so (0.6 kcal/mol), than the sum of three H-bonds, each computed within the context of an optimized dimer. The two trends are in rough balance in the global minima of the PH₃ homotrimers and tetramers as well, where the total binding energy is approximately equal to the sum of n HP \cdots P bonds associated with the undistorted dimer.

References

- ¹ P. Hobza and R. Zahradnik, *Weak Intermolecular Interactions in Chemistry and Biology* (Elsevier Scientific, Amsterdam, 1980).
- ² I. G. Kaplan, *Theory of Molecular Interactions* (Elsevier, Amsterdam, 1986).
- ³ A. J. Stone, *The Theory of Intermolecular Forces* (Oxford University Press, Oxford, 2002).
- ⁴ P. Hobza and K. Muller-Dethlefs, *Non-Covalent Interactions* (RSC, Cambridge, 2010).
- ⁵ G. C. Pimentel and A. L. McClellan, *The Hydrogen Bond* (Freeman, San Francisco, 1960).
- ⁶ *The Hydrogen Bond. Recent Developments in Theory and Experiments*, edited by P. Schuster, G. Zundel, and C. Sandorfy (North-Holland Publishing Co., Amsterdam, 1976).
- ⁷ D. Hadzi and S. Bratos, in *The Hydrogen Bond. Recent Developments in Theory and Experiments*, edited by P. Schuster, G. Zundel, and C. Sandorfy (North-Holland Publishing Co., Amsterdam, 1976), Vol. 2, p. 565.

- ⁸ G. A. Jeffrey and W. Saenger, *Hydrogen Bonding in Biological Structures* (Springer-Verlag, Berlin, 1991).
- ⁹ S. Scheiner, *Hydrogen Bonding. A Theoretical Perspective* (Oxford University Press, New York, 1997).
- ¹⁰ G. Gilli and P. Gilli, *The Nature of the Hydrogen Bond* (Oxford University Press, Oxford, UK, 2009).
- ¹¹ G. R. Desiraju and T. Steiner, *The Weak Hydrogen Bond in Structural Chemistry and Biology* (Oxford, New York, 1999).
- ¹² Y. Gu, T. Kar, and S. Scheiner, *J. Mol. Struct.* **552**, 17 (2000).
- ¹³ *Hydrogen Bonding - New Insights*, edited by S. J. Grabowski (Springer, Dordrecht, 2006).
- ¹⁴ S. Scheiner, *J. Phys. Chem. B* **110**, 18670 (2006).
- ¹⁵ E. Arunan, G. R. Desiraju, R. A. Klein, J. Sadlej, S. Scheiner, I. Alkorta, D. C. Clary, R. H. Crabtree, J. J. Dannenberg, P. Hobza, H. G. Kjaergaard, A. C. Legon, B. Mennucci, and D. J. Nesbitt, *Pure Appl. Chem.* **83**, 1637 (2011).
- ¹⁶ B. J. v. d. Veken, S. N. Delanoye, B. Michielsen, and W. A. Herrebout, *J. Mol. Struct.* **976**, 97 (2010).
- ¹⁷ O. Takahashi, Y. Kohno, and M. Nishio, *Chem. Rev.* **110**, 6049 (2010).
- ¹⁸ T. Kar and S. Scheiner, *J. Chem. Phys.* **119**, 1473 (2003).
- ¹⁹ S. Rizzato, J. Bergès, S. A. Mason, A. Albinati, and J. Kozelka, *Angew. Chem., Int. Ed. Engl.* **49**, 7440 (2010).
- ²⁰ J. P. M. Lommerse, A. J. Stone, R. Taylor, and F. H. Allen, *J. Am. Chem. Soc.* **118**, 3108 (1996).

- ²¹ I. Alkorta, s. Rozas, and J. Elguero, *J. Phys. Chem. A* **102**, 9278 (1998).
- ²² P. L. Wash, S. Ma, U. Obst, and J. Rebek, *J. Am. Chem. Soc.* **121**, 7973 (1999).
- ²³ H. L. Nguyen, P. N. Horton, M. B. Hursthouse, A. C. Legon, and D. W. Bruce, *J. Am. Chem. Soc.* **126**, 16 (2004).
- ²⁴ G. Cavallo, P. Metrangolo, T. Pilati, G. Resnati, M. Sansotera, and G. Terraneo, *Chem. Soc. Rev.* **39**, 3772 (2010).
- ²⁵ M. G. Sarwar, B. Dragisic, L. J. Salsberg, C. Gouliaras, and M. S. Taylor, *J. Am. Chem. Soc.* **132**, 1646 (2010).
- ²⁶ P. Politzer, J. S. Murray, and T. Clark, *Phys. Chem. Chem. Phys.* **12**, 7748 (2010).
- ²⁷ M. G. Chudzinski, C. A. McClary, and M. S. Taylor, *J. Am. Chem. Soc.* **133**, 10559 (2011).
- ²⁸ W. Zierkiewicz, R. Wieczorek, P. Hobza, and D. Michalska, *Phys. Chem. Chem. Phys.* **13**, 5105 (2011).
- ²⁹ S. M. Walter, F. Kniep, E. Herdtweck, and S. M. Huber, *Angew. Chem. Int. Ed.* **50**, 7187 (2011).
- ³⁰ Y. Nagao, T. Hirata, S. Goto, S. Sano, A. Kakehi, K. Iizuka, and M. Shiro, *J. Am. Chem. Soc.* **120**, 3104 (1998).
- ³¹ M. Iwaoka, S. Takemoto, and S. Tomoda, *J. Am. Chem. Soc.* **124**, 10613 (2002).
- ³² D. B. Werz, R. Gleiter, and F. Rominger, *J. Am. Chem. Soc.* **124**, 10638 (2002).
- ³³ C. Bleiholder, D. B. Werz, H. Koppel, and R. Gleiter, *J. Am. Chem. Soc.* **128**, 2666 (2006).
- ³⁴ C. E. Jakobsche, A. Choudhary, S. J. Miller, and R. T. Raines, *J. Am. Chem. Soc.* **132**, 6651 (2010).

- ³⁵ M. V. Vener, A. N. Egorova, and V. G. Tsirelson, *Chem. Phys. Lett.* **500**, 272 (2010).
- ³⁶ W. Wang, J. Xin, Y. Zhang, W. Wang, and Y. Lu, *Int. J. Quantum Chem.* **111**, 644 (2011).
- ³⁷ L. Junming, L. Yunxiang, Y. Subin, and Z. Weiliang, *Struct. Chem.* **22**, 757 (2011).
- ³⁸ M. Solimannejad, M. Gharabaghi, and S. Scheiner, *J. Chem. Phys.* **134**, 024312 (2011).
- ³⁹ S. Scheiner, *Phys. Chem. Chem. Phys.* **13**, 13860 (2011).
- ⁴⁰ S. Scheiner, *J. Chem. Phys.* **134**, 094315 (2011).
- ⁴¹ S. Scheiner, *J. Chem. Phys.* **134**, 164313 (2011).
- ⁴² U. Adhikari and S. Scheiner, *Chem. Phys. Lett.* **514**, 36 (2011).
- ⁴³ S. Scheiner, *Chem. Phys. Lett.* **514**, 32 (2011).
- ⁴⁴ S. Scheiner, *J. Phys. Chem. A* **115**, 11202 (2011).
- ⁴⁵ S. Scheiner and U. Adhikari, *J. Phys. Chem. A* **115**, 11101 (2011).
- ⁴⁶ S. Scheiner, *Chem. Phys.* **387**, 79 (2011).
- ⁴⁷ Z. Latajka and S. Scheiner, *Chem. Phys.* **122**, 413 (1988).
- ⁴⁸ G. Chalasinski, S. M. Cybulski, M. M. Szczesniak, and S. Scheiner, *J. Chem. Phys.* **91**, 7048 (1989).
- ⁴⁹ G. Chalasinski, M. M. Szczesniak, P. Cieplak, and S. Scheiner, *J. Chem. Phys.* **94**, 2873 (1991).
- ⁵⁰ Z. Latajka and S. Scheiner, *Chem. Phys.* **216**, 37 (1997).
- ⁵¹ T. Kar and S. Scheiner, *J. Phys. Chem. A* **108**, 9161 (2004).
- ⁵² S. Scheiner, *J. Mol. Struct.* **976**, 49 (2010).
- ⁵³ T. Kar and S. Scheiner, *Int. J. Quantum Chem.* **106**, 843 (2006).

- ⁵⁴ M. J. Frisch, G. W. Trucks, H. B. Schlegel *et al.*, Pople, GAUSSIAN 03, Version D.01, Gaussian, Inc., Pittsburgh PA, 2003.
- ⁵⁵ J. M. Hermida-Ramón, E. M. Cabaleiro-Lago, and J. Rodríguez-Otero, *J. Chem. Phys.* **122**, 204315 (2005).
- ⁵⁶ K. E. Riley, B. T. Op't Holt, and K. M. J. Merz, *J. Chem. Theory Comput.* **3**, 407 (2007).
- ⁵⁷ Y.-X. Lu, J.-W. Zou, J.-C. Fan, W.-N. Zhao, Y.-J. Jiang, and Q.-S. Yu, *J. Comput. Chem.* **30**, 725 (2008).
- ⁵⁸ I. Hyla-Kryspin, G. Haufe, and S. Grimme, *Chem. Phys.* **346**, 224 (2008).
- ⁵⁹ H. S. Biswal and S. Wategaonkar, *J. Phys. Chem. A* **113**, 12774 (2009).
- ⁶⁰ R. M. Osuna, V. Hernández, J. T. L. Navarrete, E. D'Oria, and J. J. Novoa, *Theor. Chem. Acc.* **128**, 541 (2011).
- ⁶¹ D. Hauchecorne, A. Moiana, B. J. v. d. Veken, and W. A. Herrebout, *Phys. Chem. Chem. Phys.* **13**, 10204 (2011).
- ⁶² S. F. Boys and F. Bernardi, *Mol. Phys.* **19**, 553 (1970).
- ⁶³ A. E. Reed, F. Weinhold, L. A. Curtiss, and D. J. Pochatko, *J. Chem. Phys.* **84**, 5687 (1986).
- ⁶⁴ A. E. Reed, L. A. Curtiss, and F. Weinhold, *Chem. Rev.* **88**, 899 (1988).
- ⁶⁵ S. Zahn, R. Frank, E. Hey-Hawkins, and B. Kirchner, *Chem. Eur. J.* **22**, 6034 (2011).
- ⁶⁶ J. E. D. Bene, I. Alkorta, G. Sanchez-Sanz, and J. Elguero, *Chem. Phys. Lett.* **512**, 184 (2011).

Table 4-1. Intermolecular R(P··P) distances, Å, and NBO E(2), kcal/mol, for trimers illustrated in Fig 1.^a

-ΔE, kcal/mol			
a) 2.91	3.836/ 1.15	3.837/ 1.15	3.837/ 1.16
b) 2.60	3.671/ 1.25, 0.82	3.660/ 0.89, 1.05	4.443
c) 2.56	3.713/ 0.91, 0.74	3.649/0.96, 1.19	4.355
d) 2.51	3.797/ 0.87	3.801/ 1.06	4.180 (d)
e) 2.31	3.663/ 0.86, 1.16	4.607 (PH-P)/ 0.74	4.123 (d)
f) 2.00	4.089 (d)	4.131 (d)	4.384
g) 1.93	3.643/ 1.02, 1.03	4.077 (d)	
h) 1.60	3.994 (d)	4.708 (PH-P)/ 0.60	

^avalues after / refer to E(2); d indicates dispersion-dominated interaction

Table 4-2. Intermolecular R(P··P) distances, Å, and NBO E(2), kcal/mol, for tetramers illustrated in Fig 2.^a

-ΔE, kcal/mol					
a) 4.83	3.838/ 1.17	3.840/ 1.18	3.841/ 1.18	3.840/ 1.16	
b) 4.73	3.786/ 1.25	3.789/ 1.44	3.784/ 0.89	3.843/ 0.84	4.147 (d)
c) 4.50	3.766/ 0.93	3.784/ 1.18	3.885/ 1.16	4.123 (d)	
d) 4.42	3.696/ 1.14, 0.68	3.713/1.19	3.802/ 0.93	4.146 (d)	
e) 4.41	3.640/0.96, 1.29	3.784/1.25	3.801/ 1.15	3.823/1.15	
f) 4.30	3.657/ 1.17, 0.79	3.775/ 1.31	3.797/1.09	4.064 (d)	
g) 4.25	3.752/ 0.96	3.822/1.11	3.891/0.72	4.103 (d)	
h) 4.07	3.654/1.40, 0.75	4.088 (d)	4.093 (d)	4.586 (PH-P)/ 0.83	
i) 4.05	3.788/1.19	3.819/1.01	3.883/0.70	4.130 (d)	4.160 (d)

^avalues after / refer to E(2); d indicates dispersion-dominated interaction

Table 4-3. Intermolecular R(P⋯N) and R(P⋯P) distances, Å, and NBO E(2), kcal/mol for trimers illustrated in Fig 3.^a

-ΔE, kcal/mol	P⋯N	P⋯N	P⋯P
a) 3.63	3.801 (NH-P)/2.15	3.324/ 1.60	3.834/ 1.29
b) 3.15	3.309/ 1.15	3.326/ 0.97	4.617
c) 3.02	3.877 (NH-P)/1.99	3.919 (PH-N)/2.00	3.831/ 0.91
d) 2.90	3.792 (NH-P)/1.35	3.346/1.46	4.190 (d)
e) 2.77	4.038 (PH-N)/2.71	3.374/0.57	4.140 (d)
f) 2.60	3.822 (NH-P)/1.79	3.286/1.58	
g) 2.13	4.078 (PH-N)/2.34	4.080 (PH-N)/1.21	4.083 (d)
h) 2.02	4.054 (NH-P)/0.66	3.990 (PH-N)/2.01	3.939 (d)
i) 1.97	4.047 (NH-P)/0.68	3.294/1.37	
j) 1.94	4.052 (PH-N)/2.57		3.679/1.08,0.75
k) 1.69	3.293/ 1.31		5.139
l) 1.52	4.066 (PH-N)/2.52		4.321 (PH-P)/0.70

^avalues after / refer to E(2); d indicates dispersion-dominated interaction

Table 4-4. Intermolecular R(P⋯P) and R(F⋯P) distances, Å, and NBO E(2), kcal/mol for trimers illustrated in Fig 4.^a

-ΔE, kcal/mol			
a) 5.32	3.168/11.8, 1.01	3.746/1.45, 1.15	3.750
b) 4.94	3.138/12.2, 2.00	3.732/1.54	4.364 (d)
c) 4.73	3.147/12.0, 1.92	3.194(P-F)/0.52	
d) 4.41	3.190/10.9, 0.65	4.017 (d)	4.318
e) 3.99	3.169/11.0, 1.86	4.068 (d)	
f) 3.92	3.156/11.5, 1.92	3.880 (PH-F)/0.78	
g) 3.11	3.189(P-F)/0.68	3.198(P-F)/0.53	4.541 (d)
h) 3.01	3.232(P-F)/0.54	3.785/0.66	4.511
i) 2.95	3.776/0.81	3.837/0.77	3.848/0.58, 0.50
j) 2.94	3.801/0.73	4.039 (d)	4.228 (d)
k) 2.76	3.714/1.06	3.810/0.85, 0.62	4.617
l) 2.75	3.696/0.61, 0.64	3.804/0.70, 0.85	

^avalues after / refer to E(2); d indicates dispersion-dominated interaction

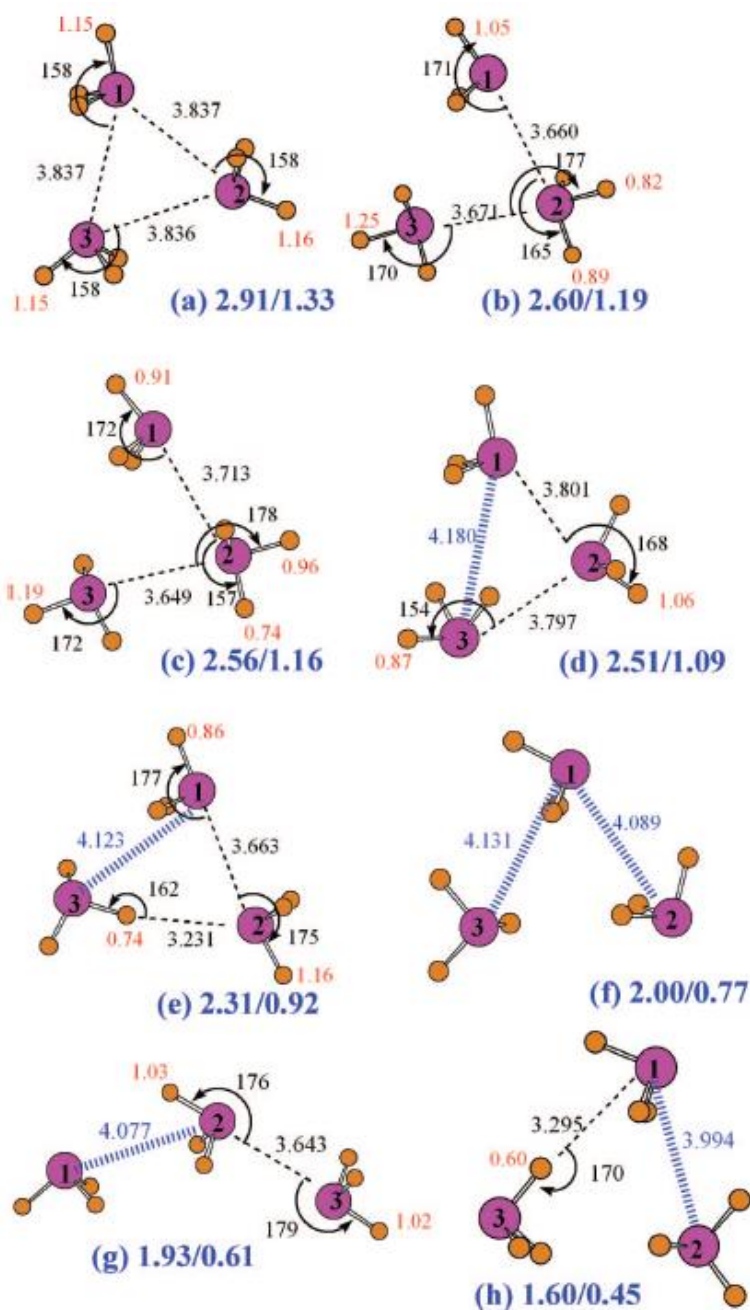


FIG. 4-1. Optimized geometries of the eight minima on the surface of the PH₃ trimer. Binding energies are reported as the large blue numbers, followed by the same quantity including zero point vibrations. Broken lines indicate HP...P bonds, dispersion-dominated interactions are denoted by blue hatched lines. Small red numbers indicate the NBO value of E(2), in kcal/mol, for each charge transfer; values displayed when in excess of 0.5. Distances in Å, angles in degs.

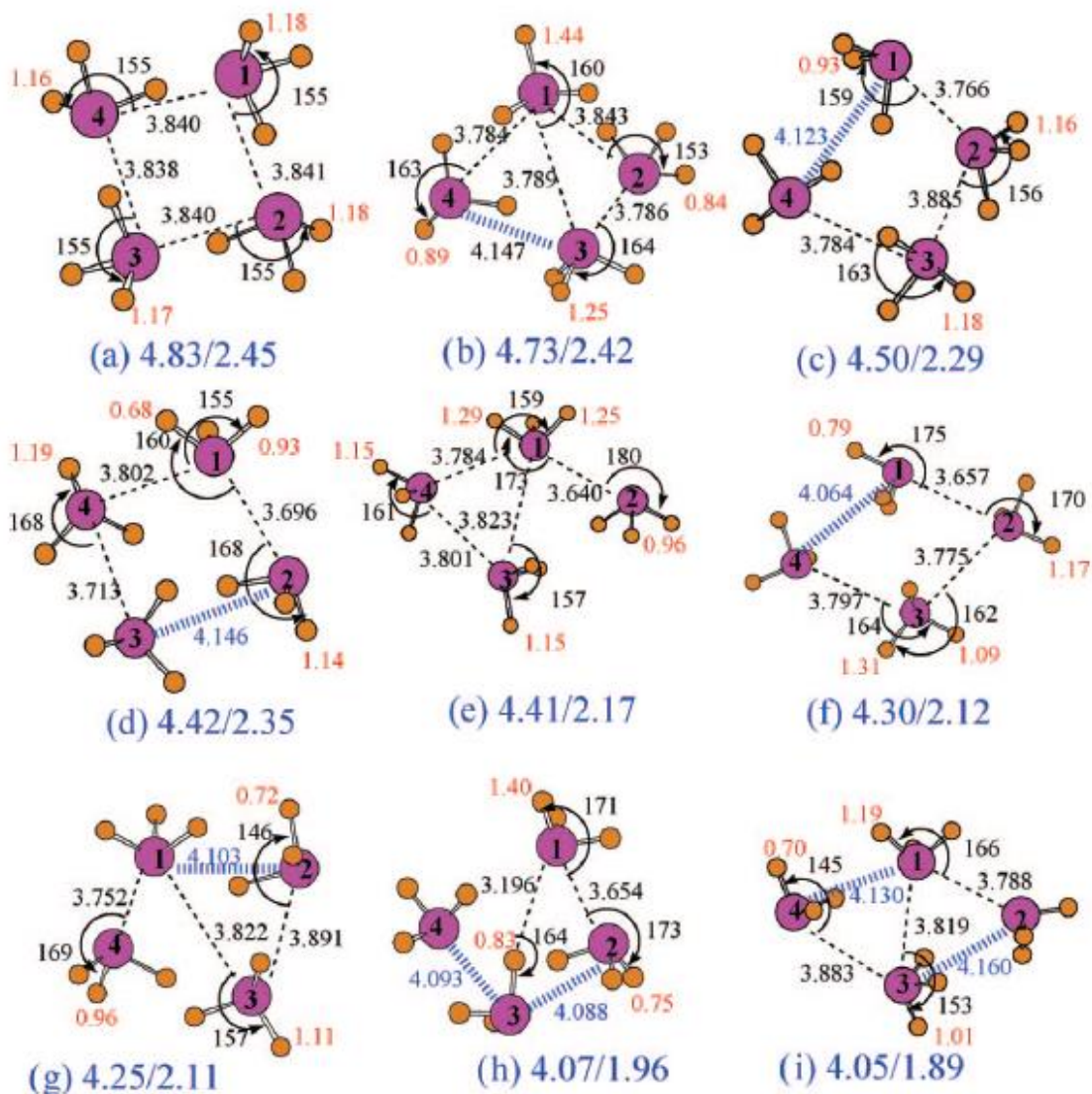


FIG. 4-2. Optimized geometries of nine minima on the surface of the PH_3 tetramer with binding energies in excess of 4 kcal/mol. Binding energies are indicated by the large blue numbers, followed by the same quantity including zero point vibrations. Broken lines indicate $\text{HP}\cdots\text{P}$ bonds, dispersion-dominated interactions are denoted by blue hatched lines. Small red numbers indicate the NBO value of $E(2)$, in kcal/mol, for each charge transfer; values displayed when in excess of 0.5. Distances in Å, angles in degs.

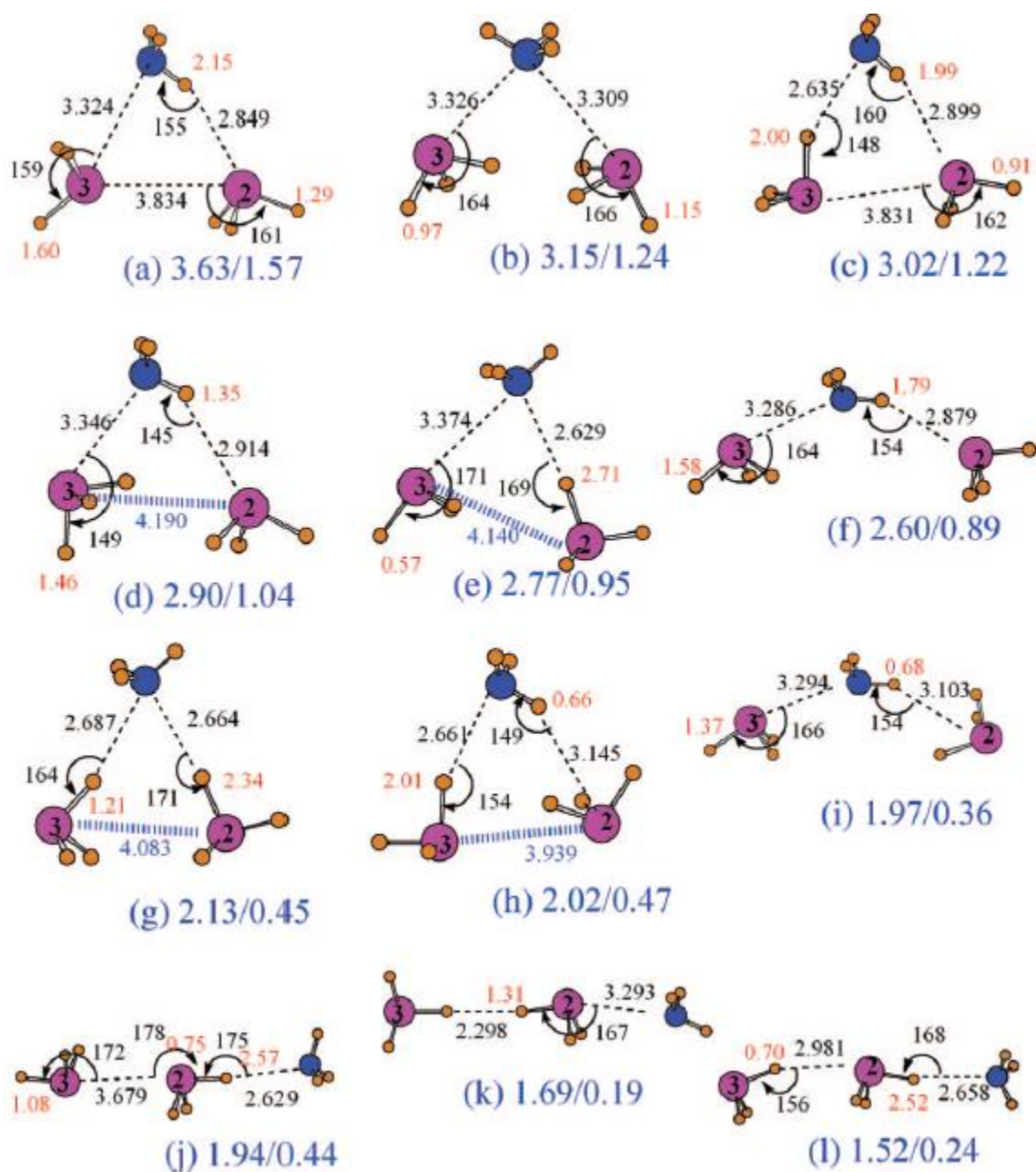


FIG. 4-3. Optimized geometries of the twelve minima on the surface of the $\text{NH}_3\text{-PH}_3\text{-PH}_3$ mixed heterotrimer. Binding energies are denoted by the large blue numbers, followed by the same quantity including zero point vibrations. Broken lines indicate $\text{HA}\cdots\text{D}$ bonds where $\text{A}, \text{D} = \text{P}, \text{N}$ and dispersion bonds are denoted by blue hatched lines. Small red numbers indicate the NBO value of $E(2)$, in kcal/mol, for each charge transfer; values displayed when in excess of 0.5. Distances in Å, angles in degs.

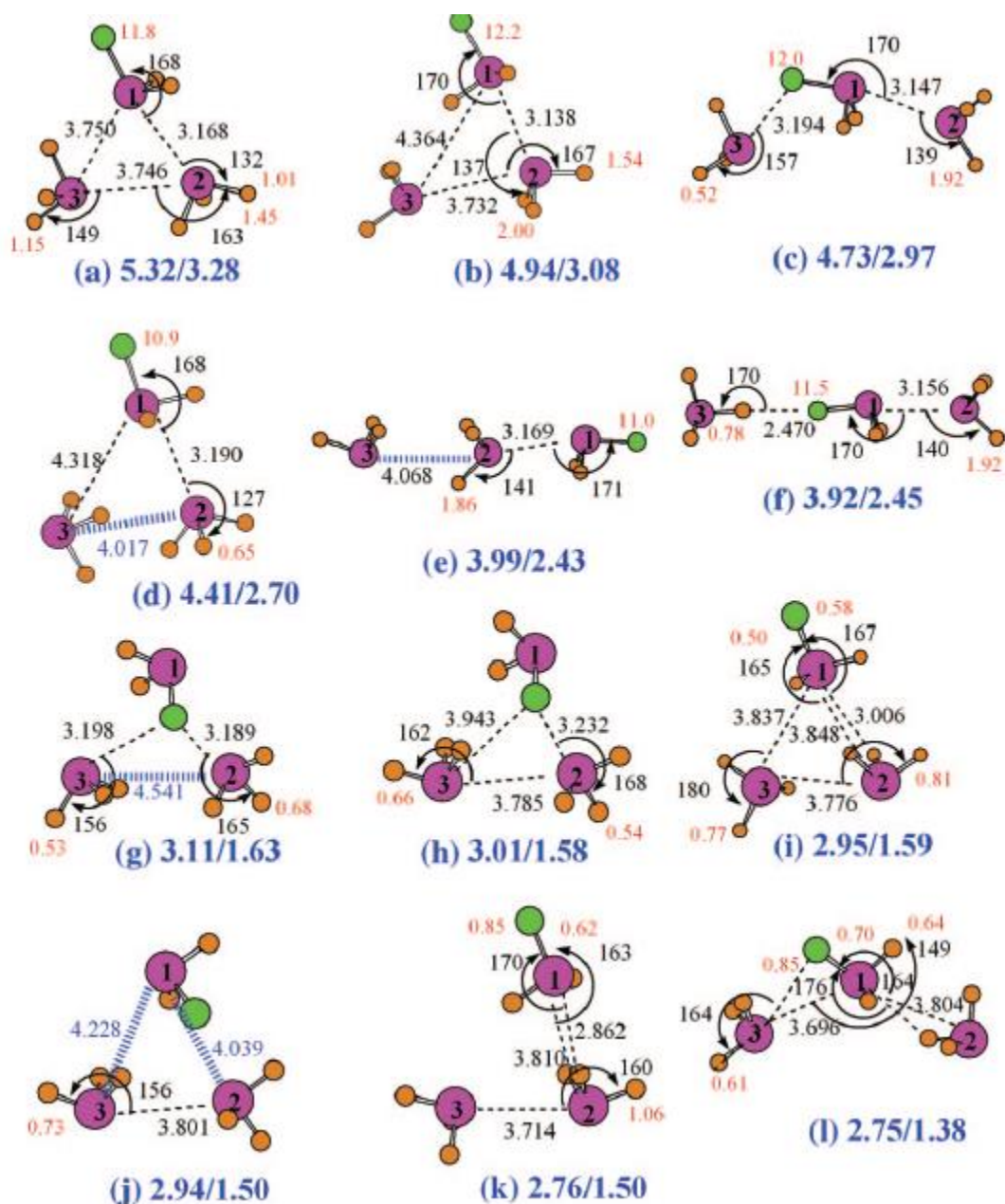


FIG. 4-4. Optimized geometries of twelve minima on the surface of the $\text{FH}_2\text{P}-\text{PH}_3-\text{PH}_3$ mixed heterotrimer. Binding energies are denoted by large blue numbers, followed by the same quantity including zero point vibrations. Small red numbers indicate the NBO value of $E(2)$, in kcal/mol, for each charge transfer; values displayed when in excess of 0.5. Distances in Å, angles in degs.

CHAPTER 5
SENSITIVITY OF PNICOGEN, CHALCOGEN, HALOGEN AND H-BONDS TO
ANGULAR DISTORTIONS¹

Abstract

Pnicogen, chalcogen, and halogen atoms have been shown previously to have some elements in common with H-bonds, including charge transfer into a σ^* antibonding orbital. While H-bonds are known to have a strong propensity toward linearity, there is little known about the angular sensitivity of the former interactions. Ab initio calculations are performed that show that the noncovalent bonds formed between P, S, and Cl atoms with a N electron donor are strongly anisotropic, more sensitive to angular distortion than are H-bonds. Energy decomposition implicates exchange repulsion as the force that is chiefly responsible for this pattern.

5-1. Introduction

There are a wide range of intermolecular forces that fall under the rubric of noncovalent interactions. The hydrogen bond [1-4] is perhaps best known and understood, as a result of decades of study. This interactions may be considered one of a larger and more general group of three-center, four-electron (3c-4e) hypervalent bonds [5,6]. The replacement of the bridging hydrogen by a halogen atom leads to another sort of interaction that has come to be called a halogen bond (X-bond) [7-12]. The attraction between this halogen atom and an electronegative electron-donating atom is due at least

¹ Coauthored by Upendra Adhikari and Steve Scheiner. Reproduced with permission from *Chem. Phys. Lett.* **2012**, 532, 31-35. Copyright 2012, Elsevier.

in part to the presence of a “sigma-hole” of positive electrostatic potential that lies directly along the extension of the C-X bond.

Recent work has shown that it is not only H and halogen atoms that can interact with an electron-donor in this way but also pnicogens and chalcogens, e.g. P, N, O, S [13-18]. For example, our own group has shown that the PH_3/NH_3 heterodimer [19] contains a direct interaction between the electronegative P and N atoms. A primary source of the stability arises from a certain amount of charge transfer from the N lone pair into the σ^* antibond of the P-H bond that is turned away from the N. It was later shown [20] that while this interaction between simple hydride PH_3 and NH_3 molecules is rather weak, less than 2 kcal/mol, it is magnified if the pertinent H atom of the phosphine is replaced by a more electronegative group. For example, even a single Cl, F, or NO_2 substituent multiplies the interaction energy as much as fivefold. The ability of a substituent to strengthen the attraction permitted even two electronegative N atoms to attract one another, as in the case of $\text{FH}_2\text{N}\cdots\text{NH}_3$ which is bound by 4 kcal/mol [21]. Surprisingly, in striking contrast with H-bonding, double or triple halogenation does not further amplify this interaction [22]. Continuing work extended this noncovalent interaction to electron donor atoms other than N. O and S can also participate, and electron density may also be extracted from the C-C π bonds of alkenes, alkynes and conjugated systems such as benzene. The strength of the interaction is fairly insensitive to the nature of the electron-acceptor atom [23], whether P, S, Cl, or As. These particular 3c-4e interactions are not confined only to dimers in certain well defined geometries but persist even in larger aggregates [24] such as trimers and tetramers. Experimental confirmation of these sorts

of interactions has arisen from examination of a number of crystal structures [25-32] in the literature. It is clear then that this particular interaction is an important one, in the same class as the better known H and halogen bonds, that certainly warrants a comparable level of understanding.

One of the more important and well-cited properties of the H-bond is its propensity toward linearity. That is, the $\theta(\text{BH}\cdots\text{D})$ angle tends toward 180° , and there is a high energetic cost to variations therefrom, which has been attributed to both electrostatic and charge transfer arguments. There is far less understanding of other 3c-4e interactions. Previous study of halogen, pnictogen, and chalcogen bonding has largely been restricted to optimal geometries, minima upon the potential energy surface, with little data available concerning the cost of angular distortion. The present work is aimed toward rectification of this omission. A series of 3c-4e interactions are considered, of varying strength and involving differing atoms. The change in energy that arises with bending from the optimal angle is computed, which permits a comparison of the linearity constraints of pnictogen, chalcogen, and halogen bonding with each other and with the like properties of H-bonds. The surprising result obtained is that the latter sorts of interactions are more rigidly held in an optimal intermolecular orientation than are H-bonds. Partitioning of the total interaction energy facilitates an analysis as to the underlying cause of this sharper anisotropy.

5-2. Computational Methods

Calculations were carried out via the Gaussian 09 package [33]. Geometries were optimized at the ab initio MP2/aug-cc-pVDZ level which has been shown to be of high

accuracy, especially for weak intermolecular interactions of the type of interest here [12,34-37] where the data are in close accord with CCSD(T) values with larger basis sets [20,38,39] and in excellent agreement with experimental energetics [40]. Interaction energies were computed as the difference in energy between the dimer, and the sum of the optimized energies of the isolated monomers, corrected for basis set superposition error by the counterpoise procedure [41]. The interaction energy was decomposed by the symmetry-adapted perturbation theory (SAPT) procedure [42,43] implemented via the MOLPRO set of codes [44], a technique which is subject to less artifact than Kitaura-Morokuma [45].

NH₃ was taken as the universal electron donor. Electron accepting atoms (A) considered were second-row atoms P, S, and Cl. Substituents (B) on these atoms spanned the range from F which is associated with very strong BA...N bonds, to the weaker Cl, and the CF₃ group which is weaker still. So as to establish a basis for comparison with H-bonds, HOH, FOH, FH, and ClH were all evaluated as proton donors to NH₃. The equilibrium geometries of several of these dimers are displayed in Figure 5-1, which also shows the definitions of important geometrical parameters.

In order to measure sensitivity to angular distortion, each complex was distorted from its fully optimized geometry in 1-10° increments. Holding this angle frozen, as well as the intermolecular distance, the remainder of the geometry was fully optimized. The data were found to adhere fairly well to a parabolic shape, characteristic of harmonic motion. The force constant k for this angular distortion was taken as that value which best fit the expression

$$E = \frac{1}{2} k(\Delta\theta)^2 \tag{1}$$

where $\Delta\theta$ refers to the deviation of the angle from its optimized value.

5-3. Results

The rise in energy that accompanies angular distortions from the optimal geometry are pictured in Figure 5-2 for several of the dimers examined here. The parabolas which are best-fit to the calculated data points are depicted by the curves, and may be seen to represent the data very well. The broken curves correspond to the H-bonding proton donors HF and HOH, while the halogen (FCl), chalcogen (FSH) and pnictogen (FPH₂) electron acceptors are represented by the solid parabolas. It is evident that the latter three curves are considerably steeper than those of the former H-bonds. This sharper rise with energy is true whether the fully optimized interaction energy (the bottom of each curve) is as weak as HOH or nearly as strong as HF.

The salient aspects of the energetic data for all systems are summarized in Table 5-1 where the first column shows that the F substituent is associated with the sharpest rise in energy with angular distortion, with bending force constant $k = 61\text{-}70 \text{ kcal mol}^{-1} \text{ rad}^{-2}$ for electron acceptor atoms P, S and Cl. This quantity undergoes a drop when the F substituent is changed to Cl, and then another especially sharp decrease for CF₃. k is characteristically smaller for the four H-bonded systems, falling in the range between 10 and 23 $\text{kcal mol}^{-1} \text{ rad}^{-2}$. The optimum binding energies of each system, prior to any angular distortion, are displayed in the next column of Table 5-1. The trends are generally similar to those for k , again obeying the pattern $F > Cl > CF_3$. The H-bonds vary in strength from 5.8 kcal/mol for HOH up to 11.6 kcal/mol for FH.

It is generally considered that a stronger interaction will likewise exhibit a larger bending force constant. For that reason, it is perhaps most interesting to consider the ratio between k and ΔE , reported in the final column of Table 5-1. The H-bonding systems all have roughly equivalent $k/\Delta E$ ratios between 1.6 and 2.8 rad^{-2} . The comparable quantities for the various $\text{BA}\cdots\text{N}$ systems are considerably larger. For example, the ratio is equal to 12 rad^{-2} for the ClPH_2 electron acceptor. In fact, the P acceptor has generally larger angular sensitivity than S, which is in turn greater than that for Cl. There is a tendency for smaller values for the $\text{B} = \text{CF}_3$ substituent, but F and Cl have rather similar effects to one another. But the most important conclusion is that, regardless of the A atom, the $\text{BA}\cdots\text{N}$ interaction is considerably more sensitive to angular distortions than are any of the H-bonded systems examined here, including even the very strong proton donor HF. This conclusion is based not only on k itself, but also when the ratio between k and the optimized binding energy is considered.

Another measure of the resistance of each complex to angular distortion arises from the harmonic vibrational frequencies that are associated with such motion. These quantities are imperfect first because they are not pure angular distortion modes but are mixed with other intermolecular and intramolecular motions such as torsions and bond stretches. Secondly, these frequencies are highly sensitive to the effective mass of each motion. And third, these low-frequency modes are subject to fairly large anharmonicity effects. Nonetheless, the frequencies reported in Table 5-2 do obey trends that are not dissimilar from those of the pure deformation force constant k in Table 1. One again sees the diminishing trend for each A atom as the substituent B is changed from F to Cl to

CF₃. On the other hand, the frequencies of the H-bonded systems are somewhat inflated due in large part to the very small mass of the bridging H atom that is undergoing the motion in these systems.

In order to check for sensitivity of the results to basis set, another set of d-functions was added to the basis set of the second row atoms, in line with the recommendation of Dunning et al. [46] that a tight d-function can improve results. This aug-ccpV(D + d)Z basis set was applied to the complexes pairing FPH₂, FSH, and FCl with NH₃ and yielded results little different than those described above for the non-supplemented aug-cc-pVDZ basis set. The depths of the minima, DE, remained stable within 2%, becoming slightly more attractive. More importantly, the force constants reported in Table 5-1 were increased by less than 5% in all cases, and uniformly such that the relative results were unchanged.

Having found that pnictogen, chalcogen, and halogen bonds are all more sensitive to angular distortion than are H-bonds, it would be interesting to identify the underlying reason for this difference. In an effort to achieve this goal, the interaction energy of each complex was partitioned into its constituent electrostatic, induction, dispersion, and exchange terms via the commonly applied symmetry-adapted perturbation theory (SAPT). The behavior of each component was monitored as angular distortions are introduced into each dimer. The electrostatic component is fairly insensitive to the distortions, and in fact does not necessarily become less attractive as the distortion progresses. For example, ES favors such distortions in the dimers containing FCl, ClSH, and CF₃SH, as well as the H-bonded systems containing HF and HCl. The induction energy is similarly inconsistent, mirroring ES to a certain degree. Nor is dispersion the

deciding factor, as the distortions lead to a more stabilizing DISP component, opposite the rise in the total energy.

It is the exchange repulsion whose sensitivity to angular distortion most closely mimics that of the total energy. The variation in this quantity that accompanies the bending is illustrated in Figure 5-3 for the same systems presented in Figure 5-2. It may be noted first that the two H-bonded systems contain a smaller amount of exchange repulsion, than do the three others. Even though HF forms the strongest complex with NH₃, its exchange repulsion is smaller than that of the latter three electron acceptor molecules. More germane to the topic at hand, the exchange energy of these H-bonded systems rises more gradually than that of the dimers containing FCl, FSH or FPH₂.

This relationship can be placed on a more quantitative footing through Table 5-3 which displays the change in each component which occurs when the angle is distorted by 30°. The inconsistency of the signs of the ES, IND, and DISP components from one system to the next are evident, which contrasts with the rise in total energy which characterizes each and every dimer. It is the exchange repulsion which consistently destabilizes the system as the geometry is deformed. In fact, the increase in the exchange energy is comparable to that of the total energy, reported in the final column of Table 5-3, for many of the systems. Probably the biggest exception to this similarity occurs in the CF₃SH...NH₃ and ClSH...NH₃ dimers where the ES, IND, and DISP terms all favor the 30° distortion, opposed only by EX. One may conclude then that the rise in energy caused by angular distortion may be attributed largely to the exchange repulsion energy. This component tends to be smaller in magnitude for the H-bonded systems, but more

importantly undergoes a more gradual increase as the H-bond is deformed, as compared to the pnictogen, chalcogen, and halogen bonds.

The forgoing conclusion concerning the importance of exchange repulsion leads to the immediate question as to why that should be. As this component of the interaction energy arises in part from the steric repulsion between electron clouds on the two monomers, some clue can be gained by considering the total electron density of the various electron acceptor molecules. Figure 5-4 illustrates this density for the five molecules included in Figure 5-1, all at the same contour of 10^{-4} au. One might note a difference in shape between the P, S, and Cl molecules in the upper half of this figure, as compared to the two H-bonding molecules in the lower half. In the former three cases, the density does not change much as one rotates away from the blue dashed line, and one might even suggest a small increase in density. In contrast, the density in Figure 5-4d and e has a sort of oblong egg shape, with the narrow end along the direction of the H-bond to the right. Consequently, as a partner molecule is rotated away from the blue dotted line the density diminishes significantly, which would mitigate any rise in the steric repulsion. So the lesser sensitivity of H-bonds to angular distortion, in comparison to $BA \cdots N$ interactions, may be attributed at least in part to the narrower shape of the electron density of the proton donor along the H-bond axis direction.

Some confirmation of some of these results may be drawn from a very recently published set of ab initio calculations by Tsuzuki et al. [47] who concluded that halogen bonds are more sensitive to angular distortions than are H-bonds. Unfortunately, their comparison cannot be taken as fully conclusive, as the halogen bonds involved a pair of aromatic systems containing a halogen drawn from the fourth row of the periodic table

(C₆H₅I or C₆F₅I with pyridine), whereas the H-bonds involved small molecules containing oxygen (HOH + OH₂ and OCH₂).

References

- [1] G. A. Jeffrey, W. Saenger, *Hydrogen Bonding in Biological Structures*, Springer-Verlag, Berlin, 1991.
- [2] S. Scheiner, *Hydrogen Bonding. A Theoretical Perspective*, Oxford University Press, New York, 1997.
- [3] G. Gilli, P. Gilli, *The Nature of the Hydrogen Bond*, Oxford University Press, Oxford, UK, 2009.
- [4] H. Hernández-Soto, F. Weinhold, J. S. Francisco, *J. Chem. Phys.* 127 (2007) 164102.
- [5] G. C. Pimentel, *J. Chem. Phys.* 19 (1951) 446.
- [6] J. I. Musher, *Angew. Chem., Int. Ed. Engl.* 8 (1969) 54–68.
- [7] I. Alkorta, S. Rozas, J. Elguero, *J. Phys. Chem. A* 102 (1998) 9278.
- [8] G. Cavallo, P. Metrangolo, T. Pilati, G. Resnati, M. Sansotera, G. Terraneo, *Chem. Soc. Rev.* 39 (2010) 3772.
- [9] W. Zierkiewicz, R. Wieczorek, P. Hobza, D. Michalska, *Phys. Chem. Chem. Phys.* 13 (2011) 5105.
- [10] K. E. Riley, J. S. Murray, J. i. Fanfrlík, J. Rezáč, R. J. Solá, M. C. Concha, F. M. Ramos, P. Politzer, *J. Mol. Model.* 17 (2011) 3309.
- [11] S. L. Stephens, N. R. Walker, A. C. Legon, *Phys. Chem. Chem. Phys.* 13 (2011) 21093.

- [12] D. Hauchecorne, N. Nagels, B. J. v. d. Veken, W. A. Herrebout, *Phys. Chem. Chem. Phys.* 14 (2012) 681.
- [13] S. Zahn, R. Frank, E. Hey-Hawkins, B. Kirchner, *Chem. Eur. J.* 22 (2011) 6034.
- [14] M. Bühl, P. Kilian, J. D. Woollins, *ChemPhysChem.* 12 (2011) 2405.
- [15] G. Sánchez-Sanz, I. Alkorta, J. Elguero, *Mol. Phys.* 109 (2011) 2543.
- [16] J. J. Scepaniak, C. G. Margarit, J. N. Harvey, J. M. Smith, *Inorg. Chem.* 50 (2011) 9508.
- [17] J. E. D. Bene, I. Alkorta, G. Sanchez-Sanz, J. Elguero, *Chem. Phys. Lett.* 512 (2011) 184.
- [18] J. E. D. Bene, I. Alkorta, G. Sanchez-Sanz, J. Elguero, *J. Phys. Chem. A* 115 (2011) 13724.
- [19] S. Scheiner, *J. Chem. Phys.* 134 (2011) 094315.
- [20] S. Scheiner, *J. Phys. Chem. A* 115 (2011) 11202.
- [21] S. Scheiner, *Chem. Phys. Lett.* 514 (2011) 32.
- [22] S. Scheiner, *Chem. Phys.* 387 (2011) 79.
- [23] S. Scheiner, *J. Chem. Phys.* 134 (2011) 164313.
- [24] U. Adhikari, S. Scheiner, *J. Chem. Phys.* 135 (2011) 184306.
- [25] G. Muller, J. Brand, S. E. Jetter, *Z. Naturforsch, B: Chem. Sci.* 56 (2001) 1163.
- [26] S. B. Bushuk, F. H. Carre, D. M. H. Guy, W. E. Douglas, Y. A. Kalvinkovskya, L. G. Klapshina, A. N. Rubinov, A. P. Stupak, B. A. Bushuk, *Polyhedron* 23 (2004) 2615.
- [27] S. Tschirschwitz, P. Lönnecke, E. Hey-Hawkins, *Dalton Trans.* 2007 (2007) 1377.
- [28] P. Kilian, A. M. Z. Slawin, J. D. Woollins, *Chem. Eur. J.* 9 (2003) 215.

- [29] M. R. Sundberg, R. Ugglä, C. Viñas, F. Teixidor, S. Paavola, R. Kivekäs, *Inorg. Chem. Commun.* 10 (2007) 713.
- [30] M. Widhalm, C. Kratky, *Chem. Ber.* 125 (1992) 679.
- [31] R. J. Butcher, R. Gilardi, K. Baum, N. J. Trivedi, *Thermochim. Acta* 384 (2002) 219.
- [32] P. V. Bernhardt, G. A. Lawrance, T. W. Hambley, *Inorg. Chem.* 31 (1992) 631.
- [33] M. J. Frisch et al., *Gaussian03*. Gaussian, Inc., Pittsburgh PA, 2003.
- [34] R. M. Osuna, V. Hernández, J. T. L. Navarrete, E. D’Oria, J. J. Novoa, *Theor. Chem. Acc.* 128 (2011) 541.
- [35] M. G. Chudzinski, C. A. McClary, M. S. Taylor, *J. Am. Chem. Soc.* 133 (2011) 10559.
- [36] Y. Zeng, X. Zhang, X. Li, S. Zheng, L. Meng, *Int. J. Quantum Chem.* 111 (2011) 3725.
- [37] J. Wu, *Int. J. Quantum Chem.* 111 (2011) 4247.
- [38] Q. Zhao, D. Feng, Y. Sun, J. Hao, Z. Cai, *Int. J. Quantum Chem.* 111 (2011) 3881.
- [39] E. Munusamy, R. Sedlak, P. Hobza, *ChemPhysChem.* 12 (2011) 3253.
- [40] D. Hauchecorne, A. Moiana, B. J. v. d. Veken, W. A. Herrebout, *Phys. Chem. Chem. Phys.* 13 (2011) 10204.
- [41] S. F. Boys, F. Bernardi, *Mol. Phys.* 19 (1970) 553.
- [42] K. Szalewicz, B. Jeziorski, in: S. Scheiner (Ed.), *Molecular Interactions. From Van der Waals to Strongly Bound Complexes*, Wiley, New York, 1997, p. 3.

- [43] R. Moszynski, P. E. S. Wormer, B. Jeziorski, A. van der Avoird, *J. Chem. Phys.* 103 (1995) 8058.
- [44] H.-J. Werner, et al., *MOLPRO*, 2010.
- [45] S. M. Cybulski, S. Scheiner, *Chem. Phys. Lett.* 166 (1990) 57.
- [46] T.H. Dunning, K.A. Peterson, A.K. Wilson, *J. Chem. Phys.* 114 (2001) 9244.
- [47] S. Tsuzuki, A. Wakisaka, T. Ono, T. Sonoda, *Chem. Eur. J.* 18 (2012) 951.

Table 5-1. Measures of sensitivity of interaction energy to angular distortion for complexes pairing various electron acceptors with NH₃.

EA	k ^a kcal mol ⁻¹ rad ⁻²	-ΔE kcal mol ⁻¹	k/-ΔE rad ⁻²
BA···N bonds			
FPH ₂	68.9	6.18	11.2
CIPH ₂	64.3	5.35	12.0
CF ₃ PH ₂	25.6	3.40	7.5
FSH	61.1	7.92	7.7
CISH	51.2	5.44	9.4
CF ₃ SH	9.2	3.38	2.7
FCl	70.3	10.36	6.8
ClCl	33.5	4.98	6.7
CF ₃ Cl	9.8	2.38	4.1
H-bonds			
HOH	10.5	5.81	1.8
FOH	15.8	9.98	1.6
FH	22.3	11.63	1.9
ClH	23.0	8.27	2.8

^aforce constant: $E=1/2 k(\Delta\theta)^2$

Table 5-2. Harmonic vibrational frequencies (cm^{-1}) associated with intermolecular nonlinear distortions.

EA	ν_1	ν_2
BA...N bonds		
FPH ₂	155.6	170.0
CIPH ₂	114.1	133.7
CF ₃ PH ₂	56.2	59.4
FSH	172.4	188.2
CISH	109.0	118.5
CF ₃ SH	31.4	43.8
FCI	195.5	195.8
CICI	107.8	108.4
CF ₃ CI	44.3	44.5
H-bonds		
HOH	169.4	180.1
FOH	81.6	250.8
FH	269.9	270.1
CIH	238.9	239.3

Table 5-3. Changes incurred by various SAPT components of the total interaction energy (kcal/mol) as a result of 30° angular distortion for complexes pairing various electron acceptors with NH₃.

	ES	IND	DISP	EX	EXIND	EXDISP	ΔE^a
FPH ₂	1.4	-2.1	-0.7	7.4	2.3	0.5	10.0
FSH	1.2	1.0	-0.3	5.6	-0.4	0.2	7.9
FCI	-1.4	-1.2	-0.8	9.7	1.8	0.5	9.7
CIPH ₂	1.6	-1.3	-0.5	5.5	1.5	0.4	5.4
CISH	-3.2	-2.3	-1.3	9.1	2.0	0.5	7.0
CICI	0.4	0.8	-0.4	3.2	-0.2	0.2	4.6
CF ₃ PH ₂	1.4	0.3	-0.3	2.5	0.7	0.2	3.1
CF ₃ SH	-4.8	-2.5	-1.7	8.6	1.5	0.4	0.7
CF ₃ CI	0.7	-0.1	-0.1	0.8	0.1	0.1	1.5
HF	-0.7	-1.4	-0.4	3.0	1.5	0.2	2.5
HCI	-0.9	-2.0	-0.5	3.6	1.9	0.2	2.7
HOH	0.0	-0.7	-0.3	1.6	0.8	0.1	1.1
FOH	-0.1	-0.4	-0.1	1.5	0.5	0.1	1.9

^achange in full interaction energy

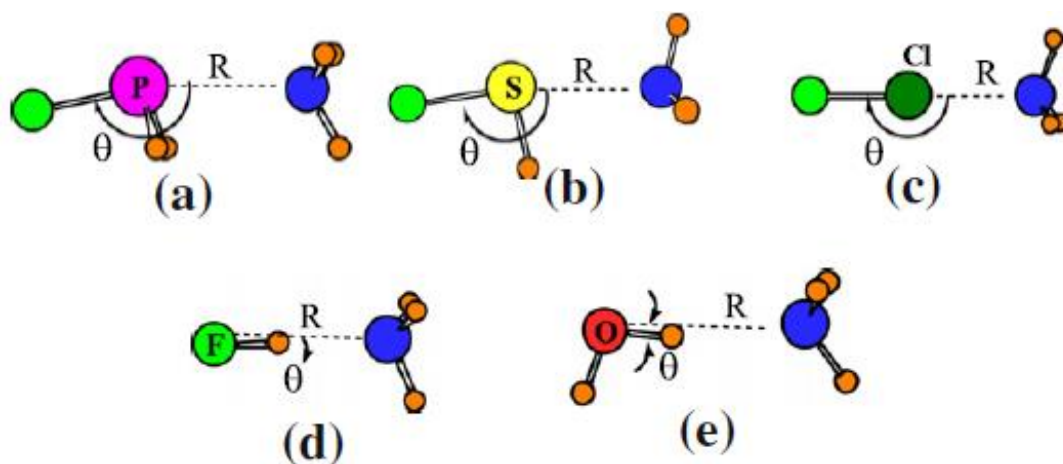


Figure 5-1. Optimized geometries of various complexes, all involving NH_3 as electron donor.

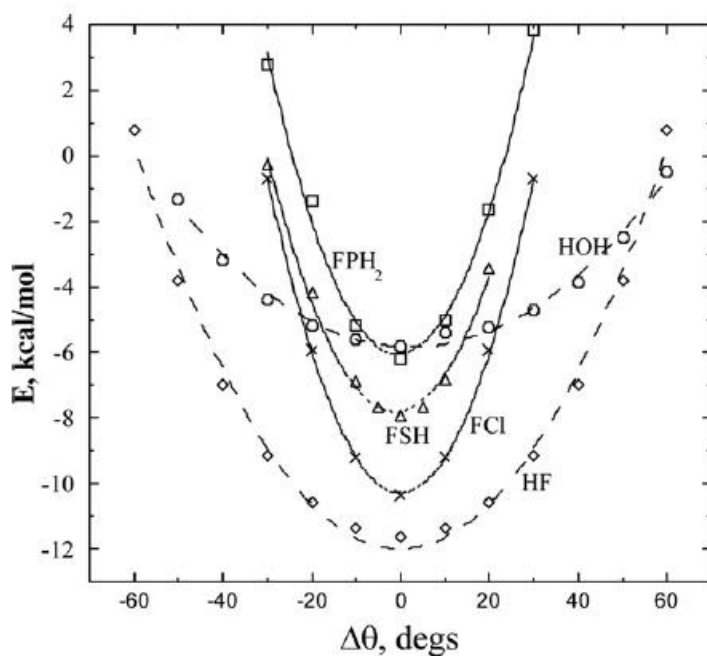


Figure 5-2. Rise in energy that accompanies angular distortion in the complex of each indicated electron acceptor with NH_3 . Curves represent parabola that are fit to the data points shown. H-bonding systems denoted by broken curves.

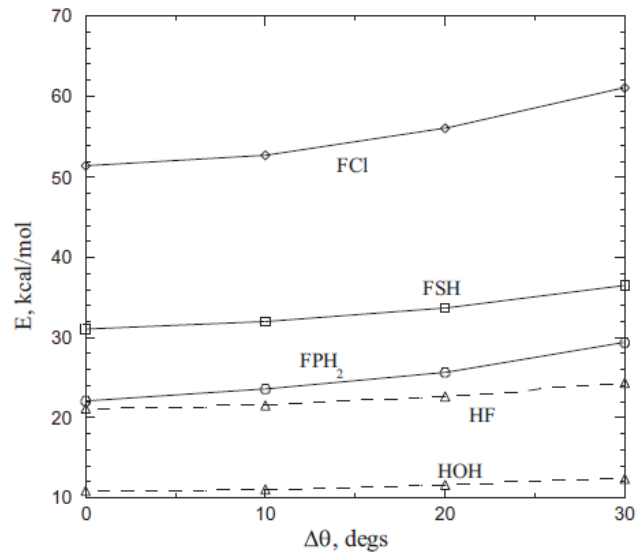


Figure 5-3. Rise in the SAPT exchange repulsion energy that accompanies angular distortion in the dimer of each indicated electron acceptor with NH_3 . H-bonding systems denoted by broken curves.

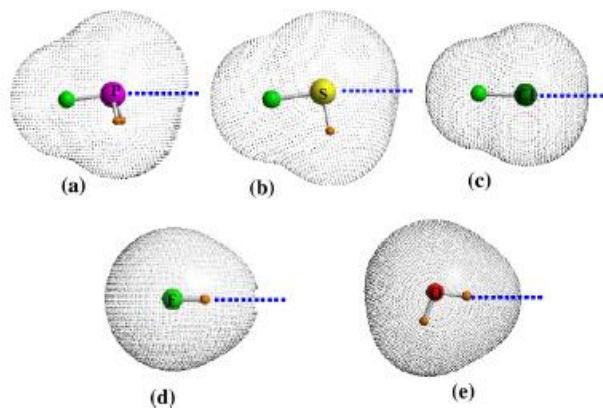


Figure 5-4. Electron densities of (a) FPH_2 , (b) FSH , (c) FCl , (d) FH , (e) HOH , all at the 0.0001 au contour. Blue dashed lines represent alignment adopted by NH_3 electron donor in optimized dimer geometry.

CHAPTER 6

SUBSTITUENT EFFECTS ON CL \cdots N, S \cdots N, AND P \cdots N NONCOVALENT BONDS¹**Abstract**

Cl, S, and P atoms have previously been shown capable of engaging in a noncovalent bond with the N atom on another molecule. The effects of substituents B on the former atoms upon the strength of this bond are examined, and it is found that the binding energy climbs in the order B= CH₃ < NH₂ < CF₃ < OH < Cl < NO₂ < F. However, there is some variability in this pattern, particularly for the NO₂ group. The A \cdots N bonds (A= Cl, S, P) can be quite strong, amounting to as much as 10 kcal/mol. The binding energy arises from approximately equal contributions from its induction and electrostatic components, although the former becomes more dominant for the stronger bonds. The induction energy is due in large measure to the transfer of charge from the N lone pair to a B-A σ^* antibonding orbital of the electron acceptor molecule containing Cl, S, or P. These A \cdots N bonds typically represent the lowest-energy structure on each potential energy surface, stronger than H-bonds such as NH \cdots F, CH \cdots N, or SH \cdots N.

6-1. Introduction

Within the context of noncovalent interactions, the hydrogen bond¹⁻¹¹ has undergone the most exhaustive examination over the years. Its original formulation as involving only electronegative atoms like O, N and F has broadened considerably as a result of work over the last couple of decades.¹²⁻¹⁹ While its history is perhaps somewhat

¹ Coauthored by Upendra Adhikari and Steve Scheiner. Reproduced with permission from *J. Phys. Chem. A* **2012**, *116*, 3487-3497. Copyright 2012, American Chemical Society.

less venerable than that of H-bonds, the halogen bond has been the subject of thorough study as well.²⁰⁻²⁸ The fundamental origins of both sorts of interactions are now well understood for the most part.

Unlike these interactions wherein either a H or halogen (X) atom occupies a bridging position between two other atoms, recent work in this laboratory^{29,30} has identified a fundamentally different sort of noncovalent interaction, one which was originally conceived between P and N atoms on different molecules, with no such intervening H or X atom. For example, the PH₃/NH₃ heterodimer³¹ contains a direct interaction between the electronegative P and N atoms. A primary source of the stability of this complex arises from a certain amount of charge transfer from the N lone pair into the σ^* antibond of the P-H bond. But unlike a PH \cdots N H-bond where this same charge transfer might take place, the pertinent H atom is rotated roughly 180° away from the N lone pair, so that the charge is transferred into the other lobe of the σ^* orbital, on the P end of the P-H bond. It was later shown³² that while this interaction between simple hydride PH₃ and NH₃ molecules is rather weak, less than 2 kcal/mol, it is magnified if the pertinent H atom of the phosphine is replaced by a more electronegative group. For example, even a single Cl, F, or NO₂ substituent multiplies the binding energy as much as fivefold. The ability of a substituent to strengthen the attraction permitted even two electronegative N atoms to attract one another, as in the case of FH₂N \cdots NH₃ which is bound by 4 kcal/mol.³³ Interestingly, double or triple halogenation does not further amplify this interaction,³⁴ a dramatic difference with H-bonding whose strength continues to grow as more electron-withdrawing substituents are added to the proton donor molecule.

Continuing work demonstrated that this noncovalent interaction is not limited to N as electron donor atom. Indeed, recent calculations³⁵ have shown that viable electron donors (D) extend beyond the traditional lone pairs of N and O atoms, and that S can also participate. More interesting perhaps, electron density may also be extracted from the C-C π bonds of alkenes, alkynes and conjugated systems such as benzene. The latter P $\cdots\pi$ interaction is augmented by a secondary electron back transfer, from the P lone pair to the π^* antibonds of the C systems. Together, these two charge transfer effects make such P $\cdots\pi$ bonds quite strong, competitive with the H-bonds associated with even a very strong proton donor such as HF.

P \cdots D interactions are not confined only to dimers in certain well defined geometries. Very recent work³⁶ has shown that they persist in larger aggregates, accounting for the structure of the global minimum, as well as making their presence felt in a number of low-lying secondary minima on the potential energy surfaces. Experimental confirmation of these sorts of interactions has arisen from examination of a number of crystal structures³⁷⁻⁴⁵ in the literature. It would thus appear that this particular interaction is an important one, in the same class as H and halogen bonds, that warrants detailed scrutiny.

Adding to its generality, the P atom of these P \cdots D interactions can be replaced by other electron acceptors (A). In particular, P's neighbors in the second row of the periodic table, S and Cl are also viable acceptors, as is third-row As.⁴⁶ In fact, the strength of these A \cdots N interactions were barely altered by these replacements. On the other hand, these alternate electron-acceptor units studied to this point were limited to the simple

hydrides, e.g. SH_2 and HCl , which work shows to be particularly weak acceptors. While the dependence of the $\text{P}\cdots\text{N}$ interaction upon the nature of substituents on the P atom has been systematically studied,³² there is no information available as to how substituents might affect the strength or nature of the interaction with other electron-acceptor atoms. Although it might be tempting to anticipate that the sensitivity of other atoms should mirror that of P, this type of interaction has exhibited some surprises in the past, such as the absence of any significant dependence upon the *number* of substituents.³⁴

The principal thrust of the present work is an elucidation of how the $\text{A}\cdots\text{N}$ interaction is affected by various substituents upon the A atom, with $\text{A} = \text{S}, \text{Cl}$. So as to span a wide range of properties, substituents (B) examined include $\text{CH}_3, \text{CF}_3, \text{NH}_2, \text{Cl}, \text{OH}, \text{F},$ and NO_2 . NH_3 is taken as the common electron donor, so as to permit comparison with past study of the $\text{P}\cdots\text{N}$ bond. For each pair of molecules, the potential energy is thoroughly searched for all minima, not just that which contains the direct $\text{BA}\cdots\text{N}$ interaction, permitting direct comparison with other sorts of molecular interactions that might be present, such as H or halogen bonds. The results show that there is a certain degree of commonality between S, Cl, and P as electron acceptor atoms for different substituents, just as in the case of unsubstituted hydrides. Regardless of the atom type, the interactions are composed largely of electrostatic and induction energy in roughly equal measure, with a smaller contribution from dispersion. On the other hand, the three atoms differ considerably in the case of F and NO_2 substituents, even to the point of reversing trends observed for the other substituents. The $\text{BA}\cdots\text{N}$ interaction can be quite strong, more than 10 kcal/mol in the case of $\text{FCl}\cdots\text{NH}_3$, which can exceed even strong H-bonds as in $\text{ClOH}\cdots\text{NH}_3$.

6-2. Computational Methods

Calculations were carried out via the Gaussian 09 package.⁴⁷ Geometries were optimized at the ab initio MP2/aug-cc-pVDZ level which has been shown to be of high accuracy, especially for weak intermolecular interactions of the type of interest here^{26,48-55} where the data are in close accord with CCSD(T) values with larger basis sets^{32,56} and in excellent agreement with experimental energetics.⁵⁷ The potential energy surface of each dimer was examined to identify all minima, by using a variety of different starting points for geometry optimizations. Minima were verified as having all real vibrational frequencies. As in the earlier work, ΔE was computed as the difference in energy between the dimer, and the sum of the optimized energies of the isolated monomers, corrected for basis set superposition error by the counterpoise procedure,⁵⁸ and by zero-point vibrational energies. (While many authors refer to ΔE as the interaction energy,⁵⁹⁻⁶⁴ it has alternately been denoted as dissociation,^{65,66} stabilization,^{67,68} binding,^{69,70} complexation⁷¹ and intermolecular energy.⁷²)

Natural bond orbital (NBO) analysis^{73,74} was carried out via the procedures contained within Gaussian. The interaction energy was decomposed by the symmetry-adapted perturbation theory (SAPT) procedure,^{75,76} implemented via the MOLPRO set of codes,⁷⁷ a technique which is subject to less artifact than Kitaura-Morokuma.⁷⁸ For purposes of comparison, some of the dimers were re-optimized within the framework of density functional theory, using a number of different variants, as detailed below.

NH_3 was taken as the universal electron donor, paired first with various substituted BSH monomers where B = CH_3 , NH_2 , CF_3 , HO, Cl, NO_2 , and F. The same set

of seven substituents were added to the BCl monomer so that S and Cl can be directly compared as electron acceptor atoms. When coupled with the earlier results involving BPH₂, the entire data set allows a systematic comparison across the second row of the periodic table.

6-3. Results

The potential energy surface of each pair of molecules contained one or more minima. Those in which the substituent B was pointed away from the N atom of the electron donor are of particular interest, and are illustrated in Figure 6-1 for the S acceptor. Although each of these represents a true minimum (with one exception), they are not always the global minimum on the surface. (The other minima obtained for each dimer are discussed in a later section.) In the single case of CH₃SH, the structure illustrated in Figure 6-1a is not a true minimum. Like the earlier case of SH₂⋯NH₃,⁴⁶ the structure was optimized by enforcing a single restriction that the $\theta(\text{CS}\cdots\text{N})$ angle be held to 180°. Indeed, this particular angle is not far from those that were optimized in the other structures in Figure 6-1, with $\theta(\text{BS}\cdots\text{N})$ angles that vary between 171° and 159°. Also reported in Figure 6-1 is the counterpoise-corrected binding energy of each structure, which varies from a minimum of 1.52 kcal/mol for CH₃HS⋯NH₃ up to 7.92 kcal/mol for FHS⋯NH₃.

The analogous geometries of the BCl⋯NH₃ systems are displayed in Figure 6-2 where there are some strong similarities. Intermolecular distances are comparable to the S analogues in Figure 6-1, although the Cl-systems have a stronger tendency toward linearity, with $\theta(\text{BCl}\cdots\text{N})$ angles closer to 180°. The primary exception is the weakly

bound $\text{CH}_3\text{Cl}\cdots\text{NH}_3$ with a deviation of 31° from linearity. This structure is also unique in that the C_3 axis of the NH_3 molecule, coincident with its lone electron pair, is turned away from the Cl atom, much as in the analogous $\text{CH}_3\text{HS}\cdots\text{NH}_3$ case in Figure 6-1a.

The energetics of these complexes are displayed in Tables 6-1 and 6-2 which also report the binding energy following incorporation of zero-point vibrational energy corrections in the second row. The next row of each table lists the intermolecular distance. The range is somewhat wider for the Cl complexes, varying from a maximum of 3.391 Å for $\text{CH}_3\text{Cl}\cdots\text{NH}_3$ down to 2.271 Å for $\text{FCl}\cdots\text{NH}_3$. Following the measures of linearity, the next three rows involve the charge transfer from the N lone pair to the BS or BCl σ^* antibonding orbital. The NBO second-order perturbation energy, $E(2)$, for this transfer is quite sensitive to the identity of the B substituent, varying from less than 1 kcal/mol for the methyl substituent, all the way up to 51 kcal/mol for $\text{FCl}\cdots\text{NH}_3$. The NBO charge transfer, directly related to $E(2)$ and the orbital energy difference, is reported in the next row as Δq and is similarly sensitive to B, achieving a maximum of 120 me for the same complex. The succeeding row displays the change in the population of the σ^* orbital that is the purported recipient of the charge originating from the N lone pair. Comparison of this quantity, Δocc , with Δq in the preceding row shows a fairly close correspondence in most cases, supporting the notion that the N lone pair is indeed the primary source of the increase in the population of this σ^* orbital. (There are some important exceptions, e.g. the NO_2 substituent, which is discussed in more detail below.) The last row of Tables 6-1 and 6-2 contains the change in the length of the covalent bond which is the recipient of the charge transfer into its σ^* antibond. In most cases, this bond

elongates, as much as 40-70 mÅ in some cases, but there are exceptions, also discussed in more detail below.

The dependence of the energetics of binding upon the identity of the substituent is illustrated graphically in Figure 6-3. In order to make the comparison more thorough the data for the S and Cl electron acceptors in Tables 6-1 and 6-2 are supplemented by data computed earlier for the P acceptors, with the same substituents.³² For the three most weakly bound complexes, those binding through Cl are significantly weaker than those for S and P which are quite similar to one another. In the middle of the spectrum, for substituents OH and Cl, there is little difference between any of the three. The largest differences are observed for the NO₂ and F substituents. In the former case, the P serves as strongest electron acceptor and Cl the weakest, but the situation reverses for F, where the Cl atom forms the tightest interaction with NH₃. Indeed, the FCl...NH₃ complex is the most strongly bound of all those examined here, and by a sizable margin. In other words, for the NO₂ substituent, the binding strength of the various electron acceptor atoms with NH₃ follows the trend Cl < S < P, but this pattern reverses for the F substituent.

The energetics reported in Tables 6-1 and 6-2 included counterpoise correction of the energy of each complex. The geometry optimizations did not itself include counterpoise at each step. As a test as to whether including counterpoise correction into the optimization algorithm might affect the results, several complexes were taken as test cases. The results found almost identical results, with complexation energies differing by only 0.1 kcal/mol or less for the two prescriptions.

6-3.1. Analysis of Binding Energetics

Decomposition of the total binding energy into its various components permits a helpful analysis of the contributing factors. The elements arising from a SAPT decomposition are contained in Tables 6-3 and 6-4. The first point that is apparent is the rise in each quantity from left to right. In other words, all components, whether attractive or repulsive, grow as the total binding energy climbs. In more detail, both the induction and electrostatic contributions follow precisely the same trend as in Figure 6-3. These patterns are more obvious when these quantities are plotted. Figures 6-4 and 6-5 illustrate the behavior of the electrostatic and induction energies, respectively. Comparison with Figure 6-3 verifies the very close coincidence of the patterns. Both ES and IND duplicate the binding energy observation that for the NO₂ substituents, the quantities rise in the order Cl < S < P, whereas the order is reversed for the F substituent. And with regard to the induction energy, the NBO value of E(2) that corresponds to the transfer of charge from the N lone pair to the B-A σ^* antibonding orbital, the prime contributor to the induction energy, obeys the same pattern as well. One might thus conclude that the trends exhibited in Figure 6-3 arise from a combination of factors, particularly electrostatic and induction energies.

A scan of the SAPT data reveals that the largest contributing factors in the binding of these complexes are ES and IND in roughly equal measure. There is a general trend for ES to exceed IND for the more weakly bound complexes, but the latter becomes more dominant for the complexes with the stronger substituents on the right side of the tables. This dominance by IND is particularly notable in the FCl \cdots NH₃ complex where

IND is nearly twice the magnitude of ES. Although DISP is comparable in magnitude to ES and IND for the weakly bound complexes, it rises considerably more slowly than the latter two components as the complexes are strengthened. Consequently, DISP is a more minor contributor for these strongly bound complexes, whether P, S, or Cl.

There are discrepancies between the counterpoise-corrected MP2 binding energies in Tables 6-1 and 6-2, and the totals of the SAPT components displayed in the last row of Tables 6-3 and 6-4. These differences are due in part to the different methodologies of the supermolecule approach for MP2 values and the perturbation theory strategy which computes each component directly. There are also distinctions as to how the two methods evaluate each segment of the correlation energy. Further, the SAPT total requires the geometries of the separate monomers to match their structures in the complex, whereas the MP2 binding energy ΔE allows for relaxation of the monomer geometries.

Earlier work³² had indicated that there is a characteristic density shift pattern for complexes such as these. More specifically, an increase of density is observed on the N lone pair when the complex is formed, in tandem with a larger area of charge loss immediately to the right of the electron acceptor atom. Buildup is observed also within the B-A bond, as well as on the far side of most of the substituents. The far right, on the remote side of the N atom, suffers a substantial loss of charge. While the patterns are very much the same for all substituents, there is a general enlargement of the magnitudes as one progresses from the weaker to the stronger substituents. This same pattern is noted for the S \cdots N and Cl \cdots N complexes as well. Figure 6-6 illustrates these shifts for a weakly (B=NH₂) and strongly (B=F) bound complex of both electron acceptor S and Cl type. All four contain the same common elements as those described earlier, and the more strongly

bound complexes magnify these effects. The most intense charge shifts arise in the $\text{FCl}\cdots\text{NH}_3$ complex, the most strongly bound of any considered here. These changes are large enough that the sectors of charge loss on the two sides of the NH_3 molecule, most plainly visible in $\text{FHS}\cdots\text{NH}_3$ in Figure 6-6b, coalesce into one extended red region in $\text{FCl}\cdots\text{NH}_3$. Note that the charge loss on the right side of the NH_3 electron donor is too weak to be visible at the 0.0005 au contour for the two complexes in which $\text{B} = \text{NH}_2$.

It was noted in Figure 6-3 that the binding energy climbs as the substituent B is changed incrementally from CH_3 to F, with minor exceptions. For the Cl electron acceptor, the NO_2 substituent causes a substantial drop, with an interaction smaller than might otherwise be expected. Figure 6-4 shows that this anomaly occurs in the electrostatic component as well, and in fact ES drops for the S acceptor atom as well as Cl. The electrostatic potential that surrounds each of the electron-accepting molecules, displayed in Figure 6-7, provides some useful cues as to the origin of these trends. The three molecules on the left side of Figure 6-7 all include the $\text{B} = \text{NH}_2$ substituent that leads to a fairly weak interaction with the P, S, and Cl electron acceptor atoms in a, b, and c, respectively. The three on the far right represent the strong $\text{B} = \text{F}$ substituent, and the NO_2 substituent is displayed in the center. Also reported in Figure 6-7 is the SAPT electrostatic component of the interaction of each molecule with NH_3 .

The most important section of the potential is to the immediate right of each molecule, where the lone pair of the NH_3 molecule, with its negative potential, is approaching. This region is blue, i.e. positive, in all three cases where $\text{B} = \text{NH}_2$, consistent with an attractive electrostatic term. However, this attraction is compromised to some extent by the negative red regions that are nearby, so the ES components are not

overly negative. There are no such red regions to the right of the other six molecules in Figure 6-7. When combined with the larger, more extensive blue contours, this observation accounts for the more negative ES quantities. The lack of such red regions immediately surrounding the Cl, S, and P atoms in some cases might be at first surprising given their electronegativity. On the other hand, these atoms are bound to very electron-withdrawing groups in some cases, which act to pull density away from them, and thus impart to them a positive partial charge which can be very substantial.

It is tempting to try to take a further step in this analysis by comparing the various values in each column of Figure 6-7. However, the correlation is not immediately obvious. Taking the B = F substituent as an example, ES grows quickly, approximately doubling, as one progresses from P to S to Cl. However, comparison of the contours to the right of Figures 6-7g-i do not show any striking dissimilarities, not enough to account for such a large change in ES. Nor is it clear from Figures 6-7f and i why the ES term for FCl is more than thrice the value for NO₂Cl. Of course, ES is very sensitive to the intermolecular separation as well. The much shorter distance of 2.271 vs 2.791 Å for the complexes of FCl and NO₂Cl with NH₃ most certainly contribute to the larger ES in the former complex. But in summary, the differences in the monomer electrostatic potentials do not in and of themselves fully explain the trends in the various systems.

And indeed, Figure 6-5 shows that the induction energy makes quite an important contribution, larger in some cases than ES, especially for the more strongly bound complexes. As mentioned above, the primary contributor to the induction energy is the transfer of charge from the N lone pair to the B-A σ* antibonding orbital of the electron acceptor molecule. Just as the ES term is considerably larger for FCl⋯NH₃ than for

$\text{NO}_2\text{Cl}\cdots\text{NH}_3$, by a factor of 3.5, this magnification is even greater for the IND term, a factor of 6. There is a similar amplification factor in the NBO E(2) terms, which are 9.1 and 51.5 kcal/mol, respectively. Again, some of this enlargement is due to the much shorter intermolecular separation, but one is still left wondering as to the ultimate cause of this much stronger interaction. This stronger charge transfer for FCl cannot be attributed to a better energetic alignment with the N lone pair. The NBO energy of the σ^* orbital rises on going from NO_2Cl to FCl, which would have the opposite effect of reducing the $\text{N}_{\text{lp}}/\sigma^*(\text{BA})$ interaction.

Another distinction between the P, S, and Cl atoms as partners in complexes with NH_3 has to do with pendant H atoms. In principle, such atoms could form a H-bond with the N atom, supplementing the strength of the interaction. However, such H-bonds are ruled out by NBO analysis which indicates none of the $\text{N}_{\text{lp}}\rightarrow\sigma^*(\text{AH})$ charge transfer that is characteristic of such a bond. And the absence of such a H-bond is also supported by geometrical principles. Whereas a $\text{AH}\cdots\text{N}$ H-bond is expected to be approximately linear, the nonlinearity for the structures in Figure 6-1 is quite large, varying between 71° and 89° . The $r(\text{H}\cdots\text{N})$ distances are also longer than anticipated for H-bonds, in the 2.54 - 3.34 Å range.

6-3.2. Source of Behavior of NO_2 Substituent

Comparison of the Δq and Δocc rows of Tables 6-1 and 6-2 aids in understanding the source of this discrepancy. Whereas these two values are reasonably close in value to one another for most complexes, this is not the case for the NO_2 substituents. Δocc is only half the value of Δq for $\text{NO}_2\text{HS}\cdots\text{NH}_3$; these two quantities actually have different

sign for $\text{NO}_2\text{Cl}\cdots\text{NH}_3$. More detailed inspection of the orbital occupations reveals a possible source of this discrepancy. While the NBO perturbation treatment reveals that some charge does indeed transfer into the Cl-N σ^* orbital, it does not remain there. A good deal of charge moves on to the O lone pairs of the NO_2 group. A lone pair on each of these two oxygens shows a charge increase of 36 me, for a total of 72 me, which exceeds the 26 me originally deposited into the Cl-N σ^* orbital. As a result the latter antibond actually suffers a *loss* of population, with Δocc dropping by 50 me. It is this diminished occupation of this antibond which is the origin of the shortening of the Cl-N bond when the $\text{NO}_2\text{Cl}\cdots\text{NH}_3$ complex is formed, contrary to the usual observation of a stretch of the B-Cl bond, as seen in the other complexes. There is a similar pattern in the NO_2SH analogue, albeit to a smaller extent. In this case, only 26 me winds up on the NO_2 O lone pairs. Progressing along the periodic table row, there is no such noticeable effect for the NO_2PH_2 complex, as Δq and Δocc are nearly identical.

As another indication of this phenomenon, the formation of the $\text{NO}_2\text{Cl}\cdots\text{NH}_3$ complex raises the natural negative charges of the O atoms by 44 me, but only half that amount in the S and P analogues. This diminishing effect from Cl to S to P may be associated with the eigenvalues of the $\sigma^*(\text{A}-\text{NO}_2)$ antibonding orbital. As one progresses from Cl to S to P, this energy rises from -0.01 to +0.16 to +0.20 au. This rise takes this orbital further away from the energies of the relevant O lone pairs, which lie at -0.5 au. The deteriorating energy match would be expected to reduce the ability of the orbitals to interact, thereby decreasing the ability of charge to transfer away from the $\sigma^*(\text{A}-\text{NO}_2)$ antibonding orbital. And finally, a simplistic Lewis-type view of the NO_2 substituent is

based on a pair of resonance diagrams in each of which the O atom with the negative charge is connected to the N by a single bond, and the other by a double bond. This picture is consistent with the lengthened N-O bonds in the $\text{NO}_2\text{Cl}\cdots\text{NH}_3$ complex since the O atoms acquire more negative charge, and more single (longer) bond character.

One last consideration has to do with the use of the singlet state for the NO_2 derivatives. A number of other research groups^{59,79-81} have also treated the singlet state in the same molecules considered here: ClNO_2 and SHNO_2 and PH_2NO_2 , and the closely related FNO_2 , CH_3SNO_2 , BrNO_2 , SeHNO_2 , and AsH_2NO_2 , including their complexes with electron donors, all to good effect, and with no hints that a triplet might be more appropriate or would seriously contaminate the results. Our own calculations confirm the findings of the earlier groups, as the singlet is more stable than the triplet by more than 90 kcal/mol. The HOMO-LUMO separation is 13 eV, also arguing against substantial contamination.

6-3.3. Alternate Minima

As mentioned earlier, the structures illustrated in Figures 1 and 2 are not necessarily the global minimum for each complex. Examination of the alternate minima in the potential energy surfaces enable a comparison of the $\text{BA}\cdots\text{N}$ type of interaction with others which these molecules are capable of engaging in. Taking the ClOH molecule as an example, the hydroxyl group represents a potent proton donor. It hence comes as no surprise that a structure containing a $\text{OH}\cdots\text{NH}_3$ H-bond is more than twice as strongly bound as the $\text{OCl}\cdots\text{N}$ complex in Figure 6-2d, with a binding energy of 10.0 kcal/mol. While not quite as strong a proton donor, the amino group too engages in H-bonds, so the

$\text{ClNH}\cdots\text{NH}_3$ H-bonded structure represents the global minimum on the $\text{NH}_2\text{Cl}\cdots\text{NH}_3$ surface, bound by 5.5 kcal/mol. Hence, while the $\text{OCl}\cdots\text{N}$ and $\text{NCl}\cdots\text{N}$ bonds are reasonably strong, with binding energies of 4.1 and 1.5 kcal/mol, respectively, they are both overshadowed by conventional H-bonds.

It should be mentioned at this point that the surfaces also contain what have been termed “reverse” H-bonds^{36,82} in which the NH_3 molecule is rotated 180° from its normal orientation. More specifically, this reorientation replaces the large lobe of the N lone pair by its smaller partner lobe, also oriented along the C_3 axis, but pointing toward the three H atoms, rather than away from them. Such reverse H-bonds are understandably much weaker than their more standard cousins. For example, the reverse $\text{OH}\cdots\text{N}$ H-bond amounts to 1.6 kcal/mol, only 15% that of the regular $\text{OH}\cdots\text{N}$ complex. There is also a minimum on the ClOH/NH_3 surface which corresponds to a reverse $\text{OCl}\cdots\text{N}$ bond, bound by 1.0 kcal/mol, compared to 4.1 kcal/mol for the stronger $\text{OCl}\cdots\text{N}$ interaction. Like the OH substituent, the NH_2 group too is involved in such reverse bonds. Both the $\text{NCl}\cdots\text{N}$ complex in Figure 6-2 and the more strongly bound $\text{NH}\cdots\text{N}$ structure mentioned above have reverse analogues, both of which are bound by 1 kcal/mol or less.

The CF_3 group presents some additional options as well. The F atom is a reasonably strong proton acceptor, so can engage in $\text{NH}\cdots\text{F}$ H-bonds with NH_3 . There are indeed several minima on the surface of $\text{CF}_3\text{Cl}\cdots\text{NH}_3$, but even two or more $\text{NH}\cdots\text{F}$ H-bonds cannot compete with the $\text{CCl}\cdots\text{N}$ interaction in Figure 6-2c, all bound by less than 1 kcal/mol. One might expect the O atoms of the nitro group could form fairly strong $\text{NH}\cdots\text{O}$ H-bonds with NH_3 . However, no minima of this sort appear on the $\text{NO}_2\text{Cl}\cdots\text{NH}_3$ surface, leading to the conclusion that the $\text{NCl}\cdots\text{N}$ interaction will

predominate over any competing structures that might contain $\text{NH}\cdots\text{Cl}$ H-bonds. As in the earlier discussions, the NO_2 group behaves somewhat uniquely. There is an extensive region of positive electrostatic potential above the plane of the ClNO_2 molecule, particularly above the N atom. This region attracts the lone pair of the NH_3 molecule to form a complex about 1 kcal/mol more strongly bound than that illustrated in Figure 6-2f. The most stable structure in this dimer can thus be characterized as dominated by electrostatics, since there are no other specific interactions present in this complex.

The situation is simpler for the Cl-Cl and Cl-F dihalides where there is less variety in terms of possible interacting groups. The structures in Figure 6-2 are thus global minima, and by a sizable margin.

A glance at the structure in Figure 6-2a suggests that the NH_3 lone pair is not pointing toward the Cl atom, but is turned upward, leading to a null value of the corresponding $E(2)$. This misalignment can be attributed primarily to electrostatics. In contrast to the other BCl monomers, the CH_3 group is insufficiently electronegative to create a region of positive potential near the Cl atom, a so-called σ -hole. The ensuing negative potential there repels the N lone pair, causing it to rotate in the direction illustrated in Figure 6-2a. In fact, the global minimum for the $\text{CH}_3\text{Cl}\cdots\text{NH}_3$ complex, bound by 2.8 kcal/mol, is one which contains a pair of weak H-bonds, $\text{NH}\cdots\text{F}$ and $\text{CH}\cdots\text{N}$. A secondary minimum, also more strongly bound than that in Figure 6-2a, has the NH_3 lone pair approaching the end of the CH_3Cl molecule directly opposite Cl, forming what might be described as a trifurcated set of $\text{CH}\cdots\text{N}$ H-bonds. This structure is quite consistent with the electrostatic potential of CH_3Cl , positive on the methyl end, so

could alternately be described as the simple interaction between the dipole moments of the two monomers.

Rather similar arguments pertain to the CH_3SH analogue. As indicated above, the weakly bound complex between CH_3SH and NH_3 in Figure 6-1a is not a true minimum, but is obtained only after the $\theta(\text{CS}\cdots\text{N})$ angle is held fixed at 180° . Just as in Figure 6-2a, the NH_3 lone pair is not pointing toward the S atom, but is turned upward toward the SH proton, and again this is due to the failure of the methyl group to induce a positive σ -hole near the S atom. The SH group differs in an important and fundamental way from Cl in that the former is a potential proton donor, which leads to additional possibilities. And indeed, the global minimum of the $\text{CH}_3\text{SH}/\text{NH}_3$ dimer, bound by 2.8 kcal/mol, is stabilized primarily by a $\text{SH}\cdots\text{N}$ H-bond. Another minimum, slightly less stable, would appear to be largely electrostatic in nature, with positive regions of one molecule overlapping negative areas of its partner. Finally, as in the CH_3Cl analogue, the NH_3 lone pair approaches the CH_3 group directly in another minimum which can be described as a trifurcated set of $\text{CH}\cdots\text{N}$ H-bonds.

Even in the case of the simple halogen substituents, the proton on the SH group adds more options. In addition to the global minima pictured in Figures 6-1e and 6-1g, there are alternate minima for FSH/NH_3 and ClSH/NH_3 where the primary $\text{SH}\cdots\text{N}$ H-bond is supplemented by another that occurs between the halogen and a NH of the NH_3 molecule. In the case of $\text{ClSH}\cdots\text{NH}_3$, this structure is within only 0.1 kcal/mol of the global minimum in Figure 6-1e. Both heterodimers also contain minima that are similar to the primary $\text{XS}\cdots\text{N}$ bond, except that the halogen atom is exchanged with a H to form a

weaker HS \cdots N complex. Unlike Cl, the strongly electronegative F atom can engage in a linear NH \cdots F H-bond, a structure which is second in stability only to the FS \cdots N complex in Figure 6-1g.

This SH group also adds further minima to the cases of the OH and NH₂ substituents, structures which contain a pair of bent H-bonds. In the case of OHSH/NH₃, for example, SH \cdots N and NH \cdots O H-bonds are present, and the complex is bound by a total of 3.9 kcal/mol, but still less stable than the structure of interest in Figure 6-1d. The SH donor group plays a more important role in the case of CF₃SH. Several weak NH \cdots F H-bonds are combined with a stronger SH \cdots N interaction to yield a structure that is more stable than that in Figure 6-1c by 2.6 kcal/mol.

It was mentioned above that there is a minimum in the NO₂Cl/NH₃ surface in which the N lone pair approaches above the plane of the NO₂Cl molecule. There is a similar minimum in the case of the HSNO₂ analogue, but less stable since the positive region above the plane of this molecule is much less extensive. Instead, the global minimum for HSNO₂/NH₃, more stable than that in Figure 6-1f, is one which contains both a NH \cdots O and a SH \cdots N H-bond.

In summary, then, OH and NH₂ are potent proton donors, and will generally form OH \cdots N and NH \cdots N H-bonds that are stronger than the OCl \cdots N and NCl \cdots N interactions. The halogens are weak proton acceptors so that any possible NH \cdots X H-bonds, whether in XCl or in F₃CCl cannot compete effectively with the XCl \cdots N interaction. The NO₂ substituent prefers to interact with NH₃ via an almost purely electrostatic interaction, taking advantage of the large positive region above the molecular plane of ClNO₂. These same trends are true as well when the Cl electron acceptor is replaced by the SH group.

However, the latter group is capable of forming SH \cdots N H-bonds which, although weaker than most of the BS \cdots N bonds, nonetheless contribute to the stability of certain secondary minima. The primary distinction occurs in the case of the NO₂ substituent which strengthens SH as proton donor to the point where the global minimum contains a SH \cdots N H-bond, supplemented by an weaker NH \cdots O interaction. There are a number of reverse minima, all of which are rather weakly bound.

6-3.4. Test of Various DFT Functionals

As indicated above, MP2/aug-cc-pVDZ calculations of the sort applied here have an excellent record of handling a variety of noncovalent interactions. The computed data can hence be used as a benchmark by which to assess the accuracy of an assortment of DFT approaches, all of which are anticipated to be much more parsimonious of computer resources, and might be used to perform calculations on much larger systems. In order to test the reliability of potential DFT approaches, two separate systems were considered. The dimer containing HSF and NH₃ was taken as representative of those which contain a very strong FS \cdots N interaction. On the other end of the continuum, calculations were also performed for a much more weakly bound complex, that between NH₂SH and NH₃. So as to provide a balanced approach, it is important that any method accurately portray not only the BS \cdots N configuration which is the focus of this work, but also any other minima that lie upon each potential energy surface, some of which may contain H or halogen bonds. Beginning with all the minima previously optimized at the MP2/aug-cc-pVDZ level, each structure was subjected to a full geometry optimization with a variety of DFT functionals. The particular methods chosen for examination included B3LYP,^{83,84} BP86,⁸⁵

PBEPBE,⁸⁶ and M06⁸⁷ and M05-2X.^{88,89} The binding energies were all corrected for basis set superposition error by the counterpoise technique.

Table 6-5 reports the binding energies computed by each such method for the FSH/NH₃ heterodimer, all corrected by the counterpoise procedure. The first column numbers each such structure in order of diminishing stability at the MP2/aug-cc-pVDZ level, and the next column reports the dominant attractive interaction(s) in the structure. There are several points on which all methods agree. The FS···N bond displayed in Figure 6-1g represents the most stable of all minima. All the DFT methods overestimate its binding energy, particularly PBEPBE. The latter method, as well as B3LYP, does not predict a minimum corresponding to structure 2, stabilized by a NH···F H-bond, although it is second only to FS···N in stability. The other DFT procedures are little better in this regard, all computing binding energies less than 1 kcal/mol, compared to 5.5 kcal/mol for MP2. The next two minima are better handled by the DFT procedures, despite a small degree of overestimation for structure 3. Note that these two minima, like geometry 2, all contain a NH···F H-bond, so this inability to handle the latter structure seems inconsistent.

The last three minima in Table 6-5 contain “reverse” bonds in which the NH₃ molecule is turned 180° from its normal orientation, so that the smaller lobe of the N lone pair takes the place of the major lobe which is the usual electron donor in H-bonds. In the case of minimum 5, the smaller N lobe donates charge to the SF σ* orbital, and is hence designated as reverse FS···N; replacement of the F by H leads to minimum 7 with its reverse HS···N. As one might expect, such reverse bonds are considerably weaker than their more common cousins, here producing a binding energy on the order of 1 kcal/mol

at the MP2 level, even when augmented by a secondary H-bond. Most of the DFT methods, with the exception of B3LYP, exaggerate the strength of the reverse FS \cdots N of minimum 5. On the other hand B3LYP finds no minimum for structure 7, true also of M05-2X and BP86 (although the latter identifies a minimum with energy equal to that of the isolated monomers). In general, then, the concept of reverse noncovalent bonds is supported by the DFT calculations, with some exceptions. In summary, all the DFT methods have difficulties with minimum 2 which is dominated by a NH \cdots F H-bond. With that understood, the B3LYP method probably offers the best overall balance in terms of reproducing the MP2 data.

Turning next to the NH₂SH/NH₃ heterodimer, the NS \cdots N complex of primary interest is not the global minimum, and is in fact the least stable of the four minima on the potential energy surface. The data in the last row of Table 6-6 indicate that B3LYP and BP86 underestimate the stability of this structure, which is most accurately portrayed by PBEPBE. The M06 stability is slightly overestimated, but perhaps most surprising, the M05-2X procedure finds no minimum with this sort of bonding. All the DFT procedures agree with MP2 that the global minimum is a cyclic structure containing both a NH \cdots N and NH \cdots S H-bond, and there is reasonably close coincidence concerning its binding energy. The same is generally true for the other two minima on the surface, although BP86 mistakenly finds structures 2 and 3 to be of equal energy. One might note the presence of another reverse H-bond, this one of the SH \cdots N type, in minimum 3. As in the earlier dimer, the various DFT methods perform credibly with this type of interaction. In summary, the various DFT methods are reasonably reliable, and place the four minima in the correct order. There is an exception for M05-2X which cannot be used to examine the

NS \cdots N geometry; the B3LYP and BP86 functionals correctly identify this structure, but underestimate its strength.

6-4. Summary

As was shown earlier in the case of simple hydrides, the Cl, S, and P atoms can all participate in a direct noncovalent bond with an electron donor N atom. Substitution of the H atoms by progressively stronger electron withdrawing substituents enhances the strength of the interaction. The order of strengthening follows the general pattern $\text{CH}_3 < \text{NH}_2 < \text{CF}_3 < \text{OH} < \text{Cl} < \text{NO}_2 < \text{F}$, but this pattern is not uniform for all three atoms. The bond strengths are nearly identical among S and P for the first three substituents, with a weaker Cl \cdots N interaction; the bond strengths for B = OH and Cl are similar for all three atoms. The greatest divergence occurs for NO₂ and F. Whereas the Cl \cdots N bond is anomalously weak for B=NO₂, the situation reverses entirely for B = F where the FCl \cdots NH₃ complex is strongest of all, bound by more than 10 kcal/mol. In contrast, the P \cdots N bond is stronger than the other two for NO₂ but weakest for B = F.

The BA \cdots N bond has similar origins for all three A atoms. Electrostatic and induction energies are roughly equal contributors, although the latter becomes progressively more important as the strength of the bond increases. Dispersion plays a smaller role, particularly for the most strongly bound complexes. All three of these components follow trends similar to that of the total binding energy. The dominant contributor to the induction energy arises from the charge transfer from the N lone pair into the vacant BA σ^* antibonding orbital. The increased occupation of this orbital is responsible for the observed stretch of the corresponding covalent bond.

Three-dimensional maps of the shifts of total electron density that accompany formation of each complex are very similar regardless of the identity of the electron-accepting A atom. Consideration of the electrostatic potentials surrounding each subunit provide useful insights into the geometries adopted by each complex as well as the binding energy.

The behavior of the NO₂ substituent is different than that of the other substituents in a number of ways. For example, the Cl-N bond of ClNO₂ is shortened, rather than lengthened by its interaction with NH₃. These differences appear to arise from the fact that this group contains multiple non-hydrogen atoms. The electronic structure of the entire substituent, not just the B atom, adjusts to the incoming density from the NH₃ electron donor. In the case of NO₂, a good deal of this new density bypasses the Cl and N atoms and winds up on the lone pairs of the two O atoms. Further study will be required to determine whether this distinctive behavior is characteristic only of the NO₂ group, with its internal resonance, or is common to other larger substituents.

Comparison of the stabilities of the various minima on each surface enable detailed scrutiny of the different sorts of noncovalent bonds that can be present. For example, the rather strong OH...N H-bond that might occur in the case of the OH substituent is preferred over the alternative OHA...N interaction; similar considerations apply to the amino group, although the preference for the weaker NH...N H-bond is correspondingly weaker. The weaker proton-accepting ability of the F atom makes any potential NH...F H-bonds too weak to compete with the BA...N bonds, also true of the CH...N H-bonds that could arise with the methyl substituent. Contrary to what one might expect, the O atoms of the NO₂ group serve as surprisingly weak proton acceptors.

Instead, this group interacts with a NH_3 molecule via its positive electrostatic potential region, located above the molecular plane. Although not the strongest of proton donors, the SH group can engage in $\text{SH}\cdots\text{N}$ H-bonds. These H-bonds can compete with $\text{BS}\cdots\text{N}$ interactions, but only when combined with a secondary H-bond as well. Exhaustive examination of the potential energy surfaces also reveals the presence of minima which contain “reverse” H-bonds, in which the NH_3 molecule is oriented so that the major N lone pair lobe is replaced in the interaction by its smaller counterpart lobe. These interactions are weak and in no case represent a global minimum.

Given the similarities of the properties of the complexes in which $\text{A}=\text{P}$, S with $\text{A}=\text{Cl}$, it is tempting to consider halogen bonds as a subset of the $\text{BA}\cdots\text{N}$ noncovalent bonds under discussion here. Of course, such a designation may be premature, as the only halogen atom subjected to this particular detailed analysis to this point is Cl. Furthermore, the various electron-acceptor molecules have been paired only with a very small and simple N-containing NH_3 . There may be important differences that will be revealed for larger and more complex subunits. For example, an earlier work³¹ noted some fundamental distinctions between $\text{H}_3\text{P}\cdots\text{NH}_3$ and $\text{CH}_3\text{Br}\cdots\text{OCH}_2$. A more systematic and thorough comparison might be in order, one in which the same electron acceptor molecule is used for both complexes, and the A atoms in the two complexes come from the same row of the periodic table.

References

- (1) *The Hydrogen Bond. Recent Developments in Theory and Experiments*; Schuster, P., Zundel, G., Sandorfy, C., Eds.; North-Holland Publishing Co.: Amsterdam, 1976.
- (2) Schuster, P. *Hydrogen Bonds*; Springer-Verlag: Berlin, 1984; Vol. 120.
- (3) Jeffrey, G. A.; Saenger, W. *Hydrogen Bonding in Biological Structures*; Springer-Verlag: Berlin, 1991.
- (4) Scheiner, S. *Hydrogen Bonding. A Theoretical Perspective*; Oxford University Press: New York, 1997.
- (5) Gilli, G.; Gilli, P. *The Nature of the Hydrogen Bond*; Oxford University Press: Oxford, UK, 2009.
- (6) Wiczorek, R.; Dannenberg, J. J. *J. Am. Chem. Soc.* **2003**, *125*, 8124-8129.
- (7) Alabugin, I. V.; Manoharan, M.; Peabody, S.; Weinhold, F. *J. Am. Chem. Soc.* **2003**, *125*, 5973-5987.
- (8) Hernández-Soto, H.; Weinhold, F.; Francisco, J. S. *J. Chem. Phys.* **2007**, *127*, 164102.
- (9) Bene, J. E. D.; Alkorta, I.; Elguero, J. *Phys. Chem. Chem. Phys.* **2011**, *13*, 13951-13961.
- (10) Thakur, T. S.; Kirchner, M. T.; Bläser, D.; Boese, R.; Desiraju, G. R. *Phys. Chem. Chem. Phys.* **2011**, *13*, 14076-14091.
- (11) McDowell, S. A. C.; Buckingham, A. D. *Phys. Chem. Chem. Phys.* **2011**, *13*, 14097-14100.
- (12) Gu, Y.; Kar, T.; Scheiner, S. *J. Mol. Struct.* **2000**, *552*, 17-31.

- (13) *Hydrogen Bonding - New Insights*; Grabowski, S. J., Ed.; Springer: Dordrecht, 2006.
- (14) Desiraju, G. R. *Angew. Chem., Int. Ed. Engl.* **2011**, *50*, 52-59.
- (15) Arunan, E.; Desiraju, G. R.; Klein, R. A.; Sadlej, J.; Scheiner, S.; Alkorta, I.; Clary, D. C.; Crabtree, R. H.; Dannenberg, J. J.; Hobza, P.; Kjaergaard, H. G.; Legon, A. C.; Mennucci, B.; Nesbitt, D. J. *Pure Appl. Chem.* **2011**, *83*, 1637-1641.
- (16) Veken, B. J. v. D.; Delanoye, S. N.; Michielsens, B.; Herrebout, W. A. *J. Mol. Struct.* **2010**, *976*, 97-104.
- (17) Takahashi, O.; Kohno, Y.; Nishio, M. *Chem. Rev.* **2010**, *110*, 6049-6076.
- (18) Alkorta, I.; Elguero, J.; Bene, J. E. D. *Chem. Phys. Lett.* **2010**, *489*, 159-163.
- (19) Rizzato, S.; Bergès, J.; Mason, S. A.; Albinati, A.; Kozelka, J. *Angew. Chem., Int. Ed. Engl.* **2010**, *49*, 7440-7443.
- (20) Lommerse, J. P. M.; Stone, A. J.; Taylor, R.; Allen, F. H. *J. Am. Chem. Soc.* **1996**, *118*, 3108-3116.
- (21) Alkorta, I.; Rozas, S.; Elguero, J. *J. Phys. Chem. A* **1998**, *102*, 9278-9285.
- (22) Wash, P. L.; Ma, S.; Obst, U.; Rebek, J. *J. Am. Chem. Soc.* **1999**, *121*, 7973-7974.
- (23) Nguyen, H. L.; Horton, P. N.; Hursthouse, M. B.; Legon, A. C.; Bruce, D. W. *J. Am. Chem. Soc.* **2004**, *126*, 16-17.
- (24) Cavallo, G.; Metrangolo, P.; Pilati, T.; Resnati, G.; Sansotera, M.; Terraneo, G. *Chem. Soc. Rev.* **2010**, *39*, 3772-3783.
- (25) Politzer, P.; Murray, J. S.; Clark, T. *Phys. Chem. Chem. Phys.* **2010**, *12*, 7748-7757.

- (26) Chudzinski, M. G.; McClary, C. A.; Taylor, M. S. *J. Am. Chem. Soc.* **2011**, *133*, 10559-10567.
- (27) Zierkiewicz, W.; Wieczorek, R.; Hobza, P.; Michalska, D. *Phys. Chem. Chem. Phys.* **2011**, *13*, 5105-5113.
- (28) Walter, S. M.; Kniep, F.; Herdtweck, E.; Huber, S. M. *Angew. Chem. Int. Ed.* **2011**, *50*, 7187-7191.
- (29) Scheiner, S. *Phys. Chem. Chem. Phys.* **2011**, *13*, 13860-13872.
- (30) Solimannejad, M.; Gharabaghi, M.; Scheiner, S. *J. Chem. Phys.* **2011**, *134*, 024312.
- (31) Scheiner, S. *J. Chem. Phys.* **2011**, *134*, 094315.
- (32) Scheiner, S. *J. Phys. Chem. A* **2011**, *115*, 11202-11209.
- (33) Scheiner, S. *Chem. Phys. Lett.* **2011**, *514*, 32-35.
- (34) Scheiner, S. *Chem. Phys.* **2011**, *387*, 79-84.
- (35) Scheiner, S.; Adhikari, U. *J. Phys. Chem. A* **2011**, *115*, 11101-11110.
- (36) Adhikari, U.; Scheiner, S. *J. Chem. Phys.* **2011**, *135*, 184306.
- (37) Muller, G.; Brand, J.; Jetter, S. E. *Z. Naturforsch., B: Chem. Sci.* **2001**, *56*, 1163-1171.
- (38) Bushuk, S. B.; Carre, F. H.; Guy, D. M. H.; Douglas, W. E.; Kalvinkovskya, Y. A.; Klapshina, L. G.; Rubinov, A. N.; Stupak, A. P.; Bushuk, B. A. *Polyhedron* **2004**, *23*, 2615-2623.
- (39) Tschirschwitz, S.; Lönnecke, P.; Hey-Hawkins, E. *Dalton Trans.* **2007**, *2007*, 1377-1382.
- (40) Kilian, P.; Slawin, A. M. Z.; Woollins, J. D. *Chem. Eur. J.* **2003**, *9*, 215-222.

- (41) Sundberg, M. R.; Uggla, R.; Viñas, C.; Teixidor, F.; Paavola, S.; Kivekäs, R. *Inorg. Chem. Commun.* **2007**, *10*, 713-716.
- (42) Widhalm, M.; Kratky, C. *Chem. Ber.* **1992**, *125*, 679-689.
- (43) Dalinger, I. L.; Vinogradov, V. M.; Shevelev, S. A.; Kuz'min, V. S. *Mendeleev Comm.* **1996**, *6*, 13-15.
- (44) Butcher, R. J.; Gilardi, R.; Baum, K.; Trivedi, N. J. *Thermochim. Acta* **2002**, *384*, 219-227.
- (45) Bernhardt, P. V.; Lawrance, G. A.; Hambley, T. W. *Inorg. Chem.* **1992**, *31*, 631-634.
- (46) Scheiner, S. *J. Chem. Phys.* **2011**, *134*, 164313.
- (47) Frisch, M. J.; Trucks, G. W.; Schlegel, H. B.; Scuseria, G. E.; Robb, M. A.; Cheeseman, J. R.; Scalmani, G.; Barone, V.; Mennucci, B.; Petersson, G. A.; et al. Gaussian 09; Revision B.01 ed.; Gaussian, Inc: Wallingford CT, 2009.
- (48) Hermida-Ramón, J. M.; Cabaleiro-Lago, E. M.; Rodríguez-Otero, J. J. *Chem. Phys.* **2005**, *122*, 204315.
- (49) Riley, K. E.; Op't Holt, B. T.; Merz, K. M. *J. Chem. Theory Comput.* **2007**, *3*, 407-433.
- (50) Lu, Y.-X.; Zou, J.-W.; Fan, J.-C.; Zhao, W.-N.; Jiang, Y.-J.; Yu, Q.-S. *J. Comput. Chem.* **2008**, *30*, 725-732.
- (51) Hyla-Kryspin, I.; Haufe, G.; Grimme, S. *Chem. Phys.* **2008**, *346*, 224-236.
- (52) Biswal, H. S.; Wategaonkar, S. *J. Phys. Chem. A* **2009**, *113*, 12774-12782.
- (53) Osuna, R. M.; Hernández, V.; Navarrete, J. T. L.; D'Oria, E.; Novoa, J. J. *Theor. Chem. Acc.* **2011**, *128*, 541-553.

- (54) Zeng, Y.; Zhang, X.; Li, X.; Zheng, S.; Meng, L. *Int. J. Quantum Chem.* **2011**, *111*, 3725-3740.
- (55) Wu, J. *Int. J. Quantum Chem.* **2011**, *111*, 4247-4254.
- (56) Zhao, Q.; Feng, D.; Sun, Y.; Hao, J.; Cai, Z. *Int. J. Quantum Chem.* **2011**, *111*, 3881-3887.
- (57) Hauchecorne, D.; Moiana, A.; Veken, B. J. v. d.; Herrebout, W. A. *Phys. Chem. Chem. Phys.* **2011**, *13*, 10204-10213.
- (58) Boys, S. F.; Bernardi, F. *Mol. Phys.* **1970**, *19*, 553-566.
- (59) Junming, L.; Yunxiang, L.; Subin, Y.; Weiliang, Z. *Struct. Chem.* **2011**, *22*, 757-763.
- (60) Riley, K. E.; Murray, J. S.; Fanfrlík, J.; Rezáč, J.; Solá, R. J.; Concha, M. C.; Ramos, F. M.; Politzer, P. *J. Mol. Model.* **2011**, *17*, 3309-3318.
- (61) Li, Q.; Li, R.; Yi, S.; Li, W.; Cheng, J. *Struct. Chem.* **2012**, *23*, 411-416.
- (62) Lu, Y.; Li, H.; Zhu, X.; Liu, H.; Zhu, W. *Int. J. Quantum Chem.* **2012**, *112*, 1421-1430.
- (63) Wang, Z.; Liu, Z.; Ding, X.; Yu, X.; Hou, B.; Yi, P. *Comput. Theor. Chem.* **2012**, *981*, 1-6.
- (64) Tsuzuki, S.; Wakisaka, A.; Ono, T.; Sonoda, T. *Chem. Eur. J.* **2012**, *18*, 951-960.
- (65) Zahn, S.; Frank, R.; Hey-Hawkins, E.; Kirchner, B. *Chem. Eur. J.* **2011**, *17*, 6034-6038.
- (66) Feng, G.; Evangelisti, L.; Gasparini, N.; Caminati, W. *Chem. Eur. J.* **2012**, *18*, 1364-1368.
- (67) Karthikeyan, S.; Sedlak, R.; Hobza, P. *J. Phys. Chem. A* **2011**, *115*, 9422-9428.

- (68) Munusamy, E.; Sedlak, R.; Hobza, P. *ChemPhysChem*. **2011**, *12*, 3253-3261.
- (69) Zierkiewicz, W.; Czarnik-Matusiewicz, B.; Michalska, D. *J. Phys. Chem. A* **2011**, *115*, 11362-11368.
- (70) Grabowski, S. J. *J. Phys. Chem. A* **2012**, *116*, 1838-1845.
- (71) Szostak, R. *Chem. Phys. Lett.* **2011**, *516*, 166-170.
- (72) Lu, X.; Shi, H.; Chen, J.; Ji, D. *Comput. Theor. Chem.* **2012**, *982*, 34-39.
- (73) Reed, A. E.; Weinhold, F.; Curtiss, L. A.; Pochatko, D. J. *J. Chem. Phys.* **1986**, *84*, 5687-5705.
- (74) Reed, A. E.; Curtiss, L. A.; Weinhold, F. *Chem. Rev.* **1988**, *88*, 899-926.
- (75) Szalewicz, K.; Jeziorski, B., Symmetry-adapted perturbation theory of intermolecular interactions. In *Molecular Interactions. From Van der Waals to Strongly Bound Complexes*; Scheiner, S., Ed.; Wiley: New York, 1997; pp 3-43.
- (76) Moszynski, R.; Wormer, P. E. S.; Jeziorski, B.; van der Avoird, A. *J. Chem. Phys.* **1995**, *103*, 8058-8074.
- (77) Werner, H.-J.; Knowles, P. J.; Manby, F. R.; M. Schütz, Celani, P.; Knizia, G.; Korona, T.; Lindh, R.; Mitrushenkov, A.; Rauhut, G.; et al. MOLPRO; Version 2006 ed., 2010.
- (78) Cybulski, S. M.; Scheiner, S. *Chem. Phys. Lett.* **1990**, *166*, 57-64.
- (79) Murray, J. S.; Concha, M. C.; Lane, P.; Hobza, P.; Politzer, P. *J. Mol. Model.* **2008**, *14*, 699-704.
- (80) Murray, J. S.; Lane, P.; Politzer, P. *Int. J. Quantum Chem.* **2008**, *108*, 2770-2781.
- (81) Murray, J. S.; Lane, P.; Clark, T.; Riley, K. E.; Politzer, P. *J. Mol. Model.* **2012**, *18*, 541-548.

- (82) Adhikari, U.; Scheiner, S. *Chem. Phys. Lett.* **2011**, *514*, 36-39.
- (83) Becke, A. D. *Phys. Rev. A* **1988**, *38*, 3098-3100.
- (84) Lee, C.; Yang, W.; Parr, R. G. *Phys. Rev. B* **1988**, *37*, 785-789.
- (85) Perdew, J. P. *Phys. Rev. B* **1986**, *33*, 8822-8824.
- (86) Perdew, J. P.; Burke, K.; Ernzerhof, M. *Phys. Rev. Lett.* **1996**, *77*, 3865-3868.
- (87) Zhao, Y.; Truhlar, D. G. *Theor. Chem. Acc.* **2008**, *120*, 215-241.
- (88) Zhao, Y.; Truhlar, D. G. *J. Chem. Theory Comput.* **2006**, *2*, 1009-1018.
- (89) Zhao, Y.; Truhlar, D. G. *J. Chem. Theory Comput.* **2007**, *3*, 289-300.

Table 6-3. SAPT components, kcal/mol, of interaction energies for BHS...NH₃ complexes.

	CH ₃	NH ₂	CF ₃	OH	Cl	NO ₂	F
ES	-2.37	-4.65	-6.28	-10.00	-15.16	-13.85	-24.35
EX	2.80	5.37	5.34	11.70	18.91	13.65	30.97
IND	-1.13	-3.72	-3.97	-10.35	-17.85	-13.31	-33.86
IND + EXIND	-0.22	-0.65	-0.82	-1.70	-3.15	-2.57	-6.08
DISP	-2.02	-2.76	-2.56	-4.19	-5.53	-4.45	-7.34
DISP+EXDISP	-1.75	-3.61	-2.10	-3.29	-4.24	-3.50	-5.52
TOTAL	-1.54	-3.54	-3.86	-3.29	-3.64	-6.27	-4.98

Table 6-4. SAPT components, kcal/mol, of interaction energies for BCl...NH₃ complexes.

	CH ₃	NH ₂	CF ₃	OH	Cl	NO ₂	F
ES	-0.98	-3.73	-5.10	-11.53	-16.33	-9.97	-35.93
EX	1.55	5.92	5.07	15.70	23.27	10.91	51.43
IND	-0.49	-5.15	-4.58	-16.38	-24.77	-11.32	-67.20
IND + EXIND	-0.09	-0.73	-0.70	-2.11	-3.43	-1.77	-11.14
DISP	-1.34	-2.55	-2.19	-4.44	-5.61	-3.65	-8.98
DISP + EXDISP	-1.19	-2.05	-1.78	-3.42	-4.23	-2.87	-6.59
TOTAL	-0.71	-0.59	-2.51	-1.36	-0.72	-3.7	-2.23

Table 6-5. Counterpoise corrected interaction energies (ΔE , kcal/mol) computed by MP2 and various DFT methods, for FSH/NH₃ heterodimer, all with aug-cc-pVDZ basis set. Second column indicates primary molecular interactions present in each structure.

		MP2	B3LYP	BP86	PBEPBE	M05-2X	M06
1	FS...N	-7.92	-8.36	-10.58	-11.66	-9.00	-9.75
2	NH...F	-5.48	-	-0.13	-	-0.98	-0.61
3	SH...N NH...F	-4.77	-4.68	-5.29	-6.19	-5.24	-5.35
4	HS...N NH...F	-1.99	-1.15	-0.98	-2.01	-2.55	-2.57
5	reverse FS...N	-1.26	-1.20	-2.70	-3.68	-2.39	-2.78
6	NH...F reverse SH...N	-0.98	-0.46	-0.23	-1.25	-1.40	-1.12
7	NH...F reverse HS...N	-0.91	-	+0.01	-0.96	-	-1.10

Table 6-6. Counterpoise corrected interaction energies (ΔE , kcal/mol) computed by MP2 and various DFT methods, for NH₂SH/NH₃ heterodimer, all with aug-cc-pVDZ basis set. Second column indicates primary molecular interactions present in each structure.

		MP2	B3LYP	BP86	PBEPBE	M05-2X	M06
1	NH...N NH...S	-4.80	-4.04	-4.10	-5.12	-5.12	-5.25
2	NH...N SH...N	-4.05	-2.85	-3.09	-4.18	-4.32	-4.28
3	NH...N reverse SH...N	-2.36	-1.73	-3.09	-2.44	-2.66	-2.55
4	NS...N	-2.30	-1.31	-1.27	-2.17	-	-2.62

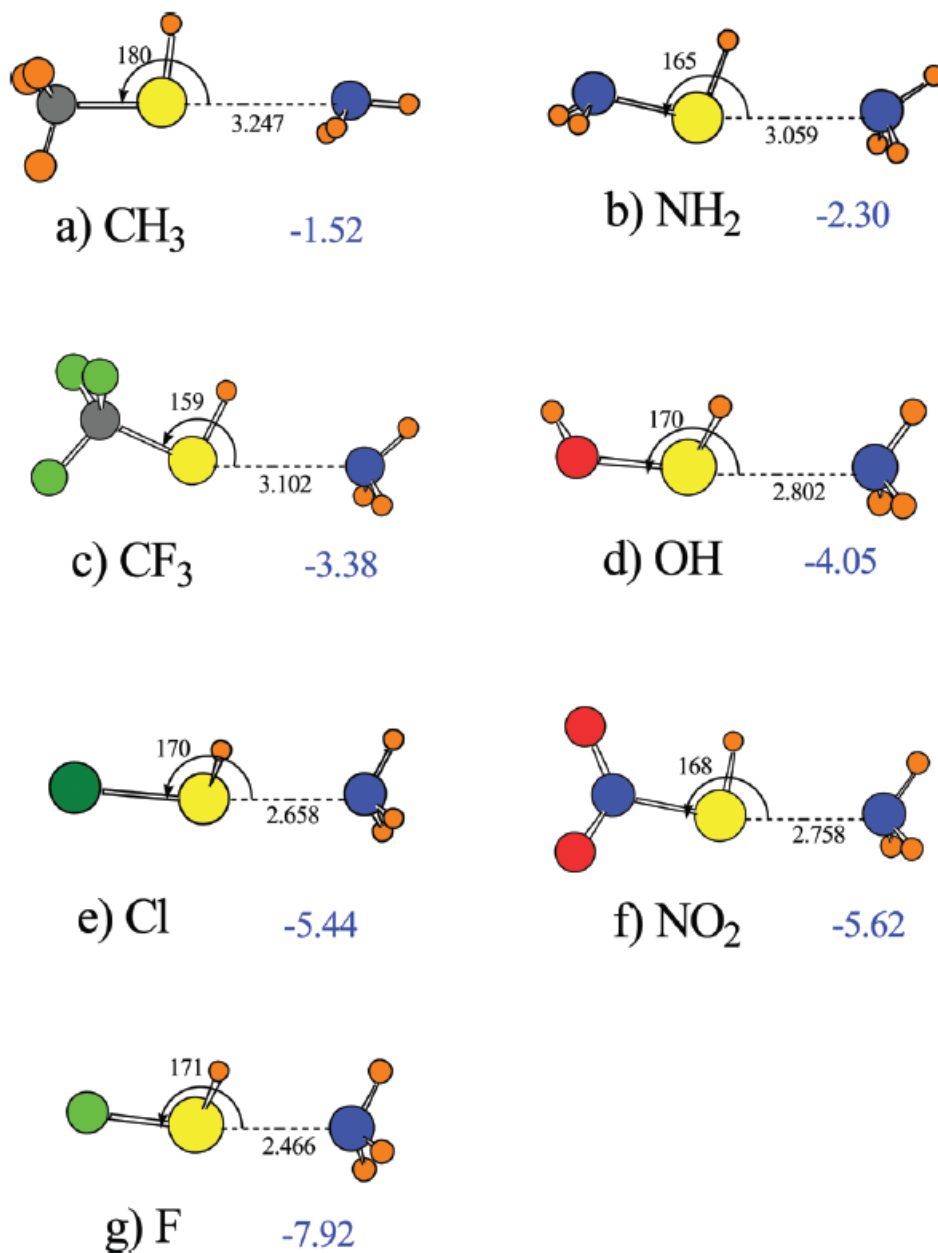


Figure 6-1. Optimized geometries of the BHS \cdots NH₃ complexes for B = a) CH₃, b) NH₂, c) CF₃, d) OH, e) Cl, f) NO₂, and g) F. Distances in Å and angles in degrees. Counterpoise-corrected binding energies ΔE (kcal/mol) in blue.

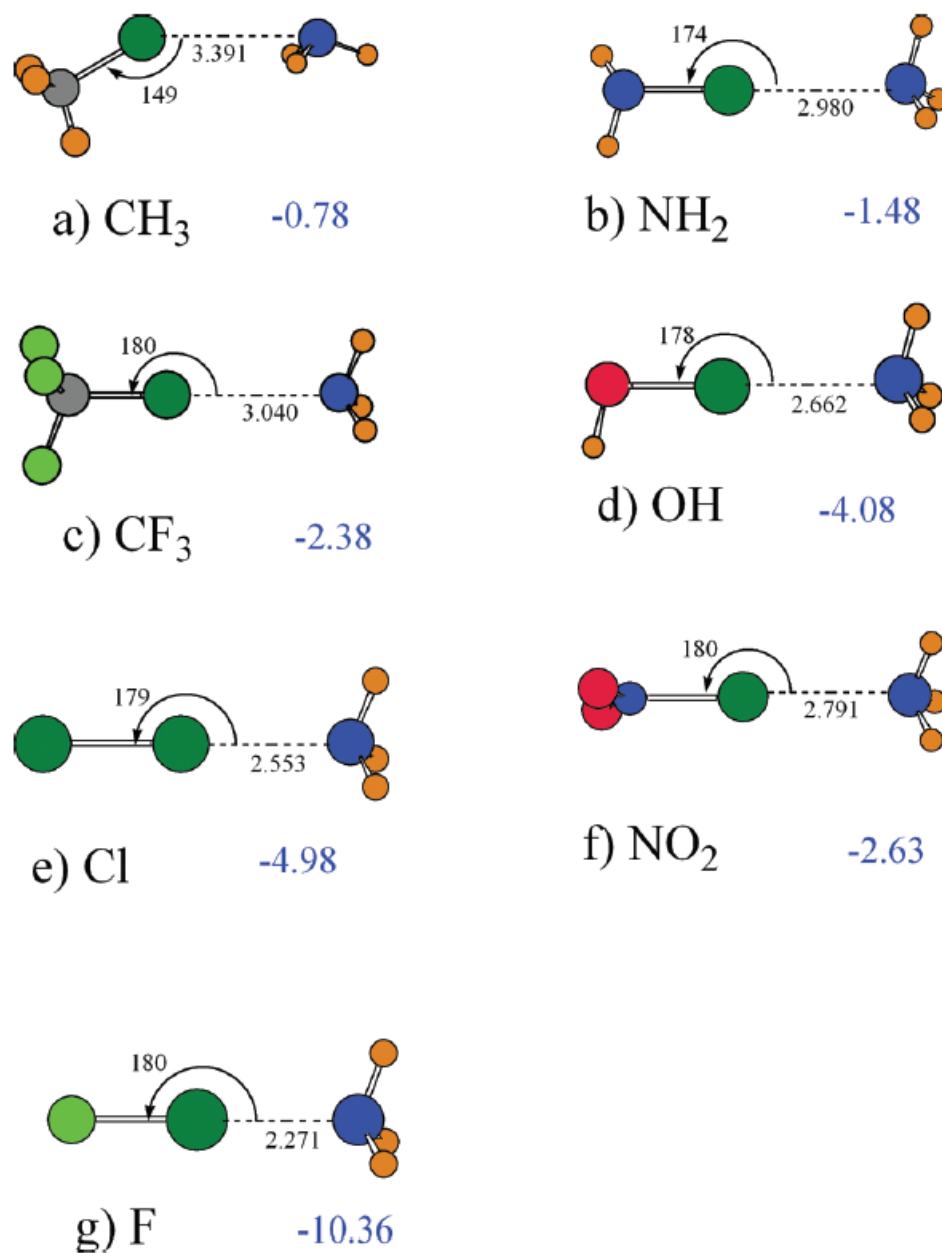


Figure 6-2. Optimized geometries of the $\text{BCl}\cdots\text{NH}_3$ complexes for B = a) CH_3 , b) NH_2 , c) CF_3 , d) OH , e) Cl , f) NO_2 , and g) F . Distances in Å and angles in degrees. Counterpoise-corrected binding energies ΔE (kcal/mol) in blue.

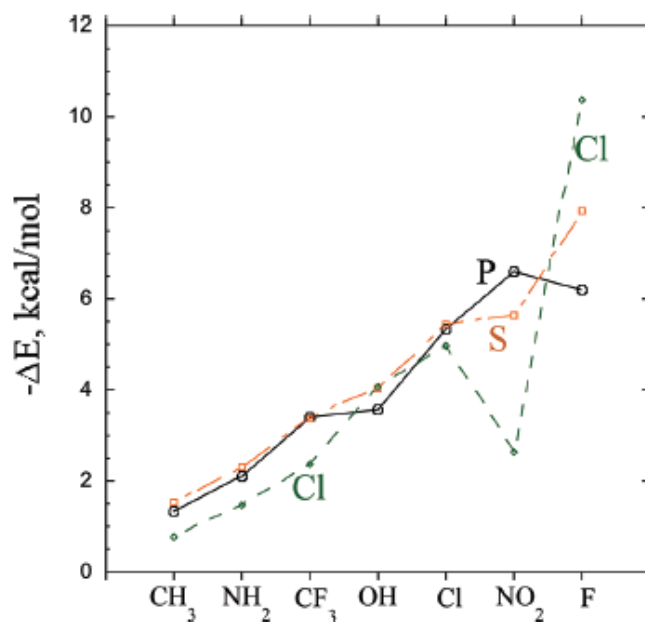


Figure 6-3. Binding energies of the $BA \cdots NH_3$ complexes for various B substituents. Electron acceptor atoms are as indicated Cl, S, and P.

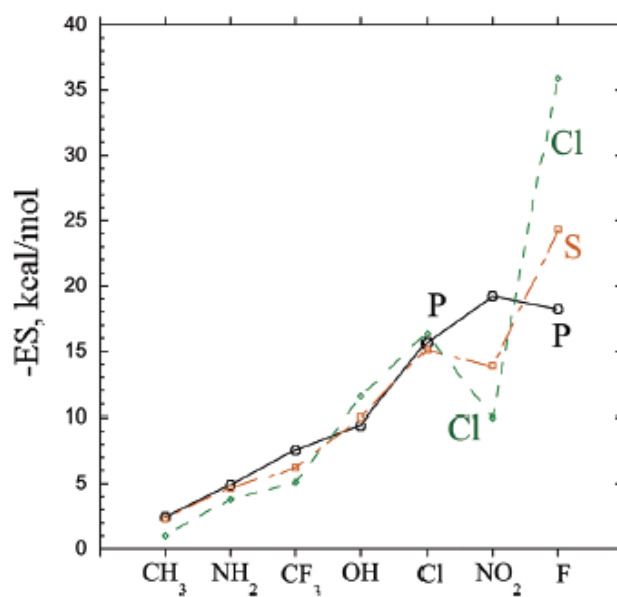


Figure 6-4. Electrostatic components of the $BA \cdots NH_3$ complexes for various B substituents. Electron acceptor atoms are as indicated Cl, S, and P.

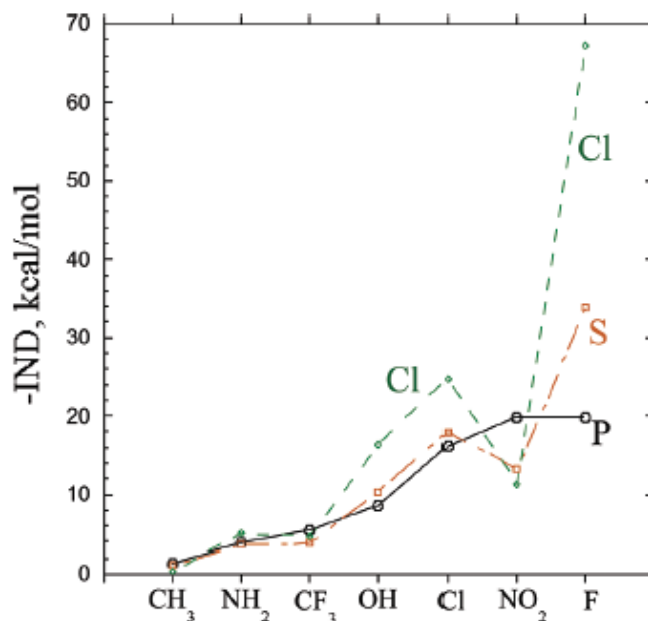


Figure 6-5. Induction energies of the BA...NH₃ complexes for various B substituents. Electron acceptor atoms are as indicated Cl, S, and P.

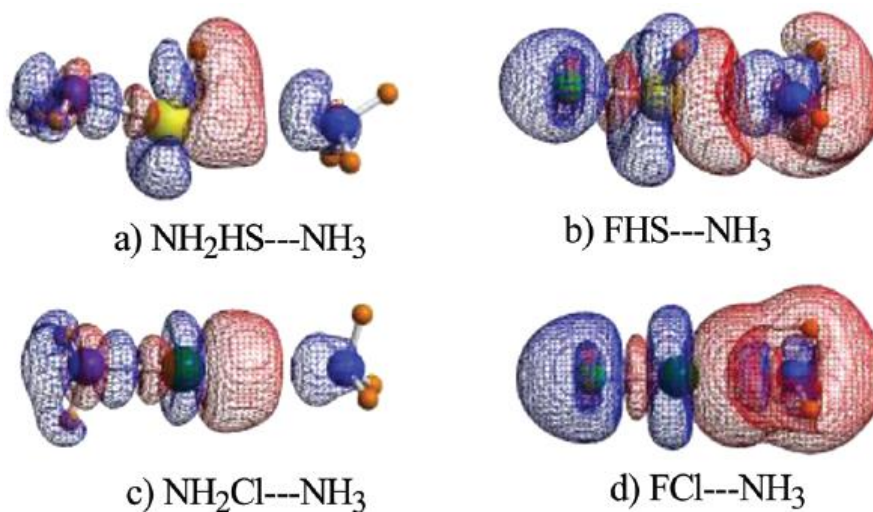


Figure 6-6. Density shifts occurring in the indicated BA...NH₃ complexes upon formation of each complex. Blue regions indicate density increase, red a decrease. Contours are shown at the 0.0005 au level.

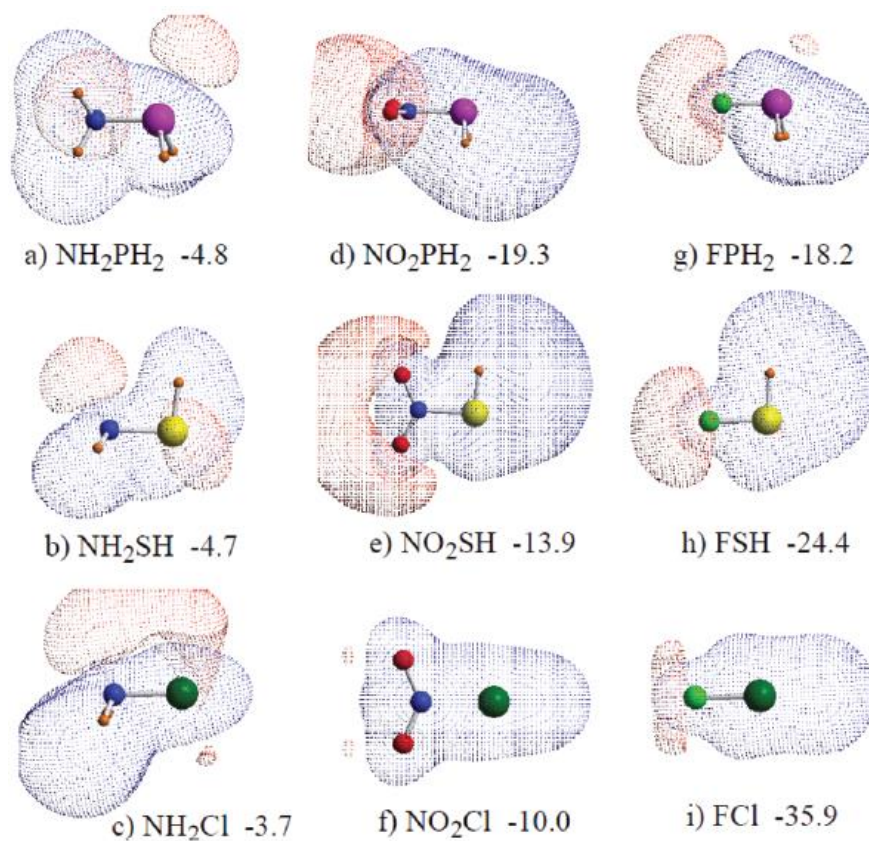


Figure 6-7. Electrostatic potentials around several of the electron acceptor molecules. Blue regions indicate positive potential, negative by red. Contours are shown at the 0.02 au level. Numbers refer to SAPT ES components (kcal/mol) of the interaction of each monomer with NH_3 .

CHAPTER 7

EFFECTS OF CARBON CHAIN SUBSTITUENTS ON THE P···N NONCOVALENT
BOND¹**Abstract**

The effects of carbon chains placed on the electron-accepting P atom of a P···N bond are examined via ab initio calculations. Saturated alkyl groups have a mild weakening effect, regardless of chain length. In contrast, incorporation of double bonds into the chain strengthens the interaction, C≡C triple bonds even more so. These effects are only slightly enhanced by additional conjugated double bonds or an aromatic ring. Placing F atoms onto the carbon chains strengthens the P···N bond, but only by a small amount, which wanes as the F atom is displaced further from the P along the chain.

7-1. Introduction

The H-bond is one of the most venerated and well studied sorts of molecular interaction [1-3]. The attractive nature of this bond is due in large part to a transfer of charge from the lone pair of the proton-acceptor molecule to the A-H σ^* antibond of the proton donor. Later observations have shown that such a transfer can also take place to a C-X antibond in which X represents atoms Cl, Br, or I, known more commonly as a halogen bond [4-12]. Other work [13-17] suggested that chalcogens (e.g. S and Se) might be able to replace halogens, which has been confirmed more recently [18-20] (although there remains some lingering question about S···S bonds [21]).

¹ Coauthored by Upendra Adhikari and Steve Scheiner. Reproduced with permission from *Chem. Phys. Lett.* **2012**, 536, 30-33. Copyright 2012, Elsevier.

Following up on some earlier indications [22-26], our own group considered the possibility that pnictogens such as P and N might also participate in noncovalent interactions of a similar type. It was found, for example, that the PH_3/NH_3 heterodimer [27] contains a direct interaction between the electronegative P and N atoms, relying upon charge transfer from the N lone pair into the σ^* antibond of the P-H bond that is turned away from the N. It was later shown [28] that interaction is magnified if the pertinent H atom of the phosphine is replaced by a more electronegative group. The ability of a substituent to strengthen the attraction permitted even two electronegative N atoms to attract one another, as in the case of $\text{FH}_2\text{N}\cdots\text{NH}_3$ which is bound by 4 kcal/mol [29]. The pnictogen bond is persistent enough to represent the dominant form of interaction in clusters of relevant molecules [30]. Surprisingly, and in striking contrast with H-bonding, double or triple halogenation does not further amplify this interaction [31]. This noncovalent interaction is not limited to electron donor N, as O and S can also participate, and electron density may also be extracted from the C-C π bonds of alkenes, alkynes and conjugated systems such as benzene. The strength of the interaction is fairly insensitive to the nature of the electron-acceptor atom [32], whether P, S, Cl, or As.

Computations since that time have verified many of the above conclusions. The attractive nature of the $\text{P}\cdots\text{P}$ pnictogen bond was confirmed [33] at high levels of theory, as was the ability of electron-withdrawing substituents to strengthen the bond. The potency of FH_2P to serve as electron acceptor, and the importance of induction energy, was verified by Del Bene et al [34,35] as was the correlation between the binding energy

and the intermolecular distance. Buhl et al. [36] have extended the concept of a pnictogen $P \cdots P$ bond to an intramolecular context.

Most of the substituents that have been added to the electron-accepting pnictogen atom to this point have been fairly electronegative, e.g. F, NO_2 , and Cl. From a practical standpoint, it is anticipated that the pnictogen will commonly be bonded to carbon-containing chains. However, the only such groups that have been considered to this point are the methyl groups. There thus remain a number of unanswered questions. How might the pnictogen bond be affected if the alkyl chain is lengthened, e.g. ethyl, propyl, etc? What would be the effects of unsaturated chains which contain double or triple bonds? How might addition of halogen atoms to the carbon chain alter the pnictogen bond?

The present work is an attempt to answer the above questions. The base system considered contains the pnictogen bond formed between RPH_2 and an electron donor (NH_3). As the R group, methyl, ethyl, and propyl allow us to monitor the pnictogen bond in terms of the length of the chain. Double and triple bonds are considered via $-\text{CH}=\text{CH}_2$ and $-\text{C}\equiv\text{CH}$, with elongations considered by adding methyl groups to the growing chain. The possibility of conjugation is taken into account via the butadienyl $-\text{CH}=\text{CH}-\text{CH}=\text{CH}_2$ group, and aromaticity via a phenyl group. In each case, F atoms were added at various locations on the chain so as to provide information about how the proximity of these atoms affects the system.

7-2. Computational Methods

The Gaussian 09 package [37] was used to perform all calculations. Geometries were optimized at the ab initio MP2/aug-cc-pVDZ level which has been shown to be of

high accuracy, especially for weak intermolecular interactions of the type of interest here [11,38-41] where the data are in close accord with CCSD(T) values with larger basis sets [28,42,43] and in excellent agreement with experimental energetics [44]. Interaction energies were computed as the difference in energy between the dimer, and the sum of the optimized energies of the isolated monomers, corrected for basis set superposition error by the counterpoise procedure [45]. Natural bond orbital (NBO) analysis [46,47] was carried out via the procedures contained within Gaussian.

7-3. Results

RH₂P was taken as the electron acceptor in complexes with NH₃ as the common electron donor. The R designation refers to a number of different sorts of carbon chains of varying length. Saturated alkyl groups considered were methyl, ethyl, and propyl. A double bond was introduced into the chain via vinyl and -CH=CHCH₃. Similarly, triple bonds were considered via -C≡CH and -C≡CCH₃. Conjugated systems of π bonds were studied via -CH=CH-CH=CH₂ and full aromaticity by a phenyl ring. The optimized structures of representative samples of each complex are illustrated in Figure 7-1 which indicate the near linearity of the C-P···N bond. As shown in previous studies, this sort of arrangement permits optimal charge transfer from the N lone pair to the C-P σ* antibonding orbital, an important ingredient of the attractive force.

The third row of Table 7-1 indicates this θ(C-P···N) angle varies within the fairly narrow range of 165° to 173° for the various systems, with the smallest angles occurring for the alkynyl groups. The preceding row indicates a similarly narrow range of intermolecular R(P···N) distances, between 3.1 and 3.3 Å. The shortest distances, like the

smaller angles, are associated with the alkynyl groups. The first row of Table 7-1 indicates the various interaction energies are smallest for the alkyl groups, about 1.3 kcal/mol, and grow as multiple bonds are introduced. The most strongly bound complex in this set is that containing the simple $C\equiv CH$ group, about twice the binding energy as the alkanes. A double bond produces an intermediate effect, but it might be noted that the introduction of additional double bonds, as in the conjugated C_4H_5 and C_5H_6 groups, has very little cumulative effect. With regard to chain lengthening, the addition of methyl groups tends to weaken the interaction, albeit by only a small amount.

Previous work has documented the importance of the $N_{lp}\rightarrow\sigma^*(C-P)$ charge transfer to the $P\cdots N$ bond. Several relevant parameters are reported in the next three rows of Table 7-1. The NBO perturbation energy associated with this charge transfer, $E(2)$, very nearly parallels the total interaction energies. This quantity grows as one progresses from single to double and then to triple bonds. Like ΔE , $E(2)$ also diminishes as the chain grows longer. The conjugated systems on the right side of Table 7-1 manifest values similar to the unconjugated double bonds, perhaps slightly larger. The NBO measure of the charge transferred, Δq follows an identical pattern. The last row of Table 7-1 reports the change in the C-P bond length is caused by the formation of the complex with NH_3 . Due to the transfer of charge into the corresponding antibond, this bond is expected to lengthen, and approximately in parallel with $E(2)$ and Δq . In fact, this expectation is confirmed. There is a small bond contraction noted for two of the alkyl groups, but this shortening is less than 0.0001 Å.

Earlier work had shown that the introduction of electron-withdrawing substituents like F onto the P atom result in a marked strengthening of the $P\cdots N$ bond. In order to

examine how these effects might be attenuated if the F atoms are placed on the R chain, rather than directly on the P atom, one or more F atoms were placed in various locations on the chains.

Table 7-2 displays the results when the F atom is placed first on the C of propyl adjacent to P, then the next C, and finally on the methyl group that is most remote. The placing of the F on the first C increases the binding energy from -1.28 to -1.70 kcal/mol. This quantity diminishes as the F is moved further from the P, but only slowly, remaining at -1.52 kcal/mol even when the F is three C atoms down. In fact, there is little change upon moving F from the second to the third C, either in ΔE or any of the other data reported in Table 7-2.

Similar patterns are noted in the F-substitution on the conjugated butadienyl system in Table 7-3. The interaction energy of -1.62 kcal/mol climbs to -2.38 kcal/mol when the F is placed on the adjacent carbon, and then diminishes slowly as the F is moved further away. There is an interesting “bump” for $-\text{CH}_2=\text{CH}-\text{CF}=\text{CH}_2$ where the displacement of the F from C2 to C3 yields small increases in the various parameters $E(2)$, Δq , and Δr . One might expect a similar attenuation as the F atom is moved further from the P in the monofluorosubstituted phenyl group. In fact, Table 7-4 shows that this anticipation is confirmed as the F moves from the ortho to meta to para position. A full perfluorosubstitution of the ring produces a larger effect, raising the binding energy from 1.57 to 2.87 kcal/mol, as indicated in the last column of Table 7-3.

To place these data in a deeper context, it was shown earlier [28] that elimination of all substituents led to a ΔE of -1.43 kcal/mol, greater by 0.10 than the result with a

methyl group. So one can say that all the saturated alkyl groups weaken the interaction to a small degree. In another context, placement of F directly on the P atom raised the binding energy to 6.2 kcal/mol [28]. So displacement to even the first C atom severely damps the effects of the F. Adding three F atoms on the first adjacent C led to a binding energy of 3.4 kcal/mol in $\text{CF}_3\text{PH}_2\cdots\text{NH}_3$, considerably larger than the single F-substitution considered here. On the other hand, even pentafluorosubstitution of the phenyl ring yields a fairly small effect, raising the binding energy from 1.57 to 2.87 kcal/mol, smaller than the effect of perfluorosubstitution of a methyl group, even though the latter reflects only 3 F atoms instead of 5. This surprisingly small effect of pentafluorosubstitution of the phenyl ring is consistent with a recent examination [9] of halogen bonds.

In summary, saturated alkyl groups have only a very modest weakening effect upon the $\text{P}\cdots\text{N}$ pnictogen bond, which is virtually insensitive to chain length. Incorporation of $\text{C}=\text{C}$ double bonds into the chain, on the other hand, has the opposite effect of strengthening the interaction. The addition of several conjugated double bonds yields only a marginal further change, as does an aromatic phenyl ring. Triple $\text{C}\equiv\text{C}$ bonds have the largest effect, producing a pnictogen bond that is roughly twice the strength of the unsubstituted $\text{P}\cdots\text{N}$ system. Lengthening any of these chains tends to weaken the $\text{P}\cdots\text{N}$ bond. Fluorosubstitution of the carbon chain strengthens the interaction, although much less than if the F is placed directly on the P atom. Even adding multiple F atoms to the carbon chain is less effective than a single F situated on the P.

References

- [1] G.A. Jeffrey, W. Saenger, *Hydrogen Bonding in Biological Structures*, Springer-Verlag, Berlin, 1991.
- [2] S. Scheiner, *Hydrogen Bonding. A Theoretical Perspective*, Oxford University Press, New York, 1997.
- [3] G. Gilli, P. Gilli, *The Nature of the Hydrogen Bond*, Oxford University Press, Oxford, UK, 2009.
- [4] O. Hassel, *Science* 170 (1970) 497.
- [5] J.P.M. Lommerse, A.J. Stone, R. Taylor, F.H. Allen, *J. Am. Chem. Soc.* 118 (1996) 3108.
- [6] I. Alkorta, S. Rozas, J. Elguero, *J. Phys. Chem. A* 102 (1998) 9278.
- [7] T. Clark, M. Hennemann, J.S. Murray, P. Politzer, *J. Mol. Model.* 13 (2007) 291.
- [8] P. Metrangolo, G. Resnati, *Science* 321 (2008) 918.
- [9] K.E. Riley et al., *J. Mol. Model.* 17 (2011) 3309.
- [10] S.L. Stephens, N.R. Walker, A.C. Legon, *Phys. Chem. Chem. Phys.* 13 (2011) 21093.
- [11] D. Hauchecorne, N. Nagels, B.J.v.d. Veken, W.A. Herrebout, *Phys. Chem. Chem. Phys.* 14 (2012) 681.
- [12] G. Feng, L. Evangelisti, N. Gasparini, W. Caminati, *Chem. Eur. J.* 18 (2012) 1364.
- [13] R.E. Rosenfield, R. Parthasarathy, J.D. Dunitz, *J. Am. Chem. Soc.* 99 (1977) 4860.
- [14] F.T. Burling, B.M. Goldstein, *J. Am. Chem. Soc.* 114 (1992) 2313.

- [15] Y. Nagao et al., *J. Am. Chem. Soc.* 120 (1998) 3104.
- [16] M. Iwaoka, S. Takemoto, S. Tomoda, *J. Am. Chem. Soc.* 124 (2002) 10613.
- [17] D.B. Werz, R. Gleiter, F. Rominger, *J. Am. Chem. Soc.* 124 (2002) 10638.
- [18] C. Bleiholder, D.B. Werz, H. Koppel, R. Gleiter, *J. Am. Chem. Soc.* 128 (2006) 2666.
- [19] J.S. Murray, P. Lane, T. Clark, P. Politzer, *J. Mol. Model.* 13 (2007) 1033.
- [20] Q.-Z. Li, R. Li, P. Guo, H. Li, W.-Z. Li, J.-B. Cheng, *Comp. Theor. Chem.* 980 (2011) 56.
- [21] F.R. Knight, A.L. Fuller, M. Bühl, A.M.Z. Slawin, J.D. Woollins, *Chem. Eur. J.* 16 (2010) 7503.
- [22] G. Muller, J. Brand, S.E. Jetter, *Z. Naturforsch., B: Chem. Sci.* 56 (2001) 1163.
- [23] C. Jones, P.C. Junk, A.F. Richards, M. Waugh, *New J. Chem.* 26 (2002) 1209.
- [24] S.B. Bushuk et al., *Polyhedron* 23 (2004) 2615.
- [25] P. Politzer, J.S. Murray, P. Lane, *Int. J. Quantum Chem.* 107 (2007) 3046.
- [26] J. Moilanen, C. Ganesamoorthy, M.S. Balakrishna, H.M. Tuononen, *Inorg. Chem.* 48 (2009) 6740.
- [27] S. Scheiner, *J. Chem. Phys.* 134 (2011) 094315.
- [28] S. Scheiner, *J. Phys. Chem. A* 115 (2011) 11202.
- [29] S. Scheiner, *Chem. Phys. Lett.* 514 (2011) 32.
- [30] U. Adhikari, S. Scheiner, *J. Chem. Phys.* 135 (2011) 184306.
- [31] S. Scheiner, *Chem. Phys.* 387 (2011) 79.
- [32] S. Scheiner, *J. Chem. Phys.* 134 (2011) 164313.
- [33] S. Zahn, R. Frank, E. Hey-Hawkins, B. Kirchner, *Chem. Eur. J.* 17 (2011) 6034.

- [34] J.E.D. Bene, I. Alkorta, G. Sanchez-Sanz, J. Elguero, *Chem. Phys. Lett.* 512 (2011) 184.
- [35] J.E.D. Bene, I. Alkorta, G. Sanchez-Sanz, J. Elguero, *J. Phys. Chem. A* 115 (2011) 13724.
- [36] M. Bühl, P. Kilian, J.D. Woollins, *ChemPhysChem* 12 (2011) 2405.
- [37] M.J. Frisch et al., GAUSSIAN 09. Gaussian, Inc., Pittsburgh PA, 2009.
- [38] R.M. Osuna, V. Hernández, J.T.L. Navarrete, E. D’Oria, J.J. Novoa, *Theor. Chem. Acc.* 128 (2011) 541.
- [39] M.G. Chudzinski, C.A. McClary, M.S. Taylor, *J. Am. Chem. Soc.* 133 (2011) 10559.
- [40] Y. Zeng, X. Zhang, X. Li, S. Zheng, L. Meng, *Int. J. Quantum Chem.* 111 (2011) 3725.
- [41] J. Wu, *Int. J. Quantum Chem.* 111 (2011) 4247.
- [42] Q. Zhao, D. Feng, Y. Sun, J. Hao, Z. Cai, *Int. J. Quantum Chem.* 111 (2011) 3881.
- [43] E. Munusamy, R. Sedlak, P. Hobza, *ChemPhysChem* 12 (2011) 3253.
- [44] D. Hauchecorne, A. Moiana, B.J.v.d. Veken, W.A. Herrebout, *Phys. Chem. Chem. Phys.* 13 (2011) 10204.
- [45] S.F. Boys, F. Bernardi, *Mol. Phys.* 19 (1970) 553.
- [46] A.E. Reed, F. Weinhold, L.A. Curtiss, D.J. Pochatko, *J. Chem. Phys.* 84 (1986) 5687.
- [47] A.E. Reed, L.A. Curtiss, F. Weinhold, *Chem. Rev.* 88 (1988) 899.

Table 7-1. Energetic, geometric, and electronic aspects of RPH₂•••NH₃ complexes.

	alkyl			alkenyl		alkynyl		Conjugated	
	CH ₃	C ₂ H ₅	C ₃ H ₇	CH= CH ₂	CH=C HCH ₃	C≡C- H	C≡C- CH ₃	C ₄ H ₅	C ₆ H ₅
ΔE ^a , kcal/mol	-1.33	-1.29	-1.28	-1.56	-1.45	-2.54	-2.13	-1.62	-1.57
R(P•••N), Å	3.353	3.323	3.330	3.249	3.269	3.112	3.142	3.238	3.232
θ(CP•••N), degs	173	173	173	170	171	165	167	170	170
E(2) ^b , kcal/mol	0.76	0.90	0.85	1.70	1.37	4.24	3.51	1.83	1.87
Δq ^c , me	1.4	1.6	1.5	2.8	2.2	6.9	5.6	3.1	3.3
Δr(C-P), mÅ	0.2	-0.8	-0.9	1.2	0.9	9.9	8.5	1.4	0.6

^aCorrected by counterpoise procedure

^bNBO perturbation energy corresponding to N_{lp}→σ*(C-P) charge transfer

^cN_{lp}→σ*(C-P) charge transfer, computed as 2*(F_{ij}/Δε_{ij})²

Table 7-2. Energetic, geometric, and electronic aspects of FC₃H₆-PH₂•••NH₃ complexes.

	-CHFCH ₂ CH ₃	-CH ₂ CHFCH ₃	-CH ₂ CH ₂ CH ₂ F
ΔE, kcal/mol	-1.70	-1.54	-1.52
R(P•••N) Å	3.231	3.276	3.262
θ(CP•••N), degs	169	171	170
E(2), kcal/mol	1.84	1.26	1.52
Δq, me	3.31	2.27	2.57
Δr(C-P), mÅ	-1.01	0.07	1.23

Table 7-3. Energetic, geometric, and electronic aspects of C₄H₅(F)-PH₂...NH₃ complexes.

	-CFH=CH- CH=CH ₂	-CH ₂ =CF- CH=CH ₂	-CH ₂ =CH- CF=CH ₂	-CH ₂ =CH- CH=CFH
ΔE, kcal/mol	-2.38	-1.85	-1.84	-1.70
R(P...N) Å	3.262	3.193	3.141	3.212
θ(XP...N), degs	170	168	165	168
E(2), kcal/mol	3.42	2.31	2.45	1.96
Δq, me	5.76	3.83	4.01	3.30
Δr(C-P), mÅ	3.63	1.99	3.05	1.63

Table 7-4. Energetic, geometric, and electronic aspects of fluorophenyl complexes.

	o-FC ₆ H ₄	m-FC ₆ H ₄	p-FC ₆ H ₄	C ₆ F ₅
ΔE, kcal/mol	-1.96	-1.81	-1.72	-2.87
R(P...N) Å	3.170	3.188	3.219	3.068
θ(XP...N), degs	167	168	169	162
E(2), kcal/mol	2.79	2.55	2.08	5.02
Δq, me	4.79	4.38	3.62	8.99
Δr(C-P), mÅ	3.2	1.54	2.13	11.43

o-, m-, and p- refer respectively to ortho, meta and para position of F with respect to -PH₂ group.

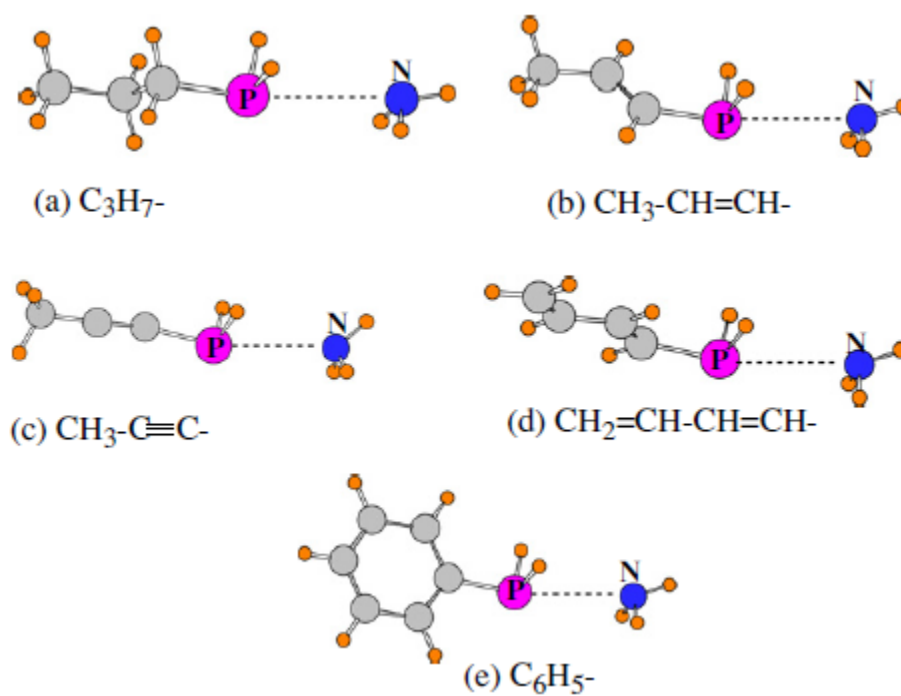


Figure 7-1. Optimized $RH_2P\cdots NH_3$ complexes with various carbon chains taken as R group.

CHAPTER 8
CONTRIBUTIONS OF VARIOUS NONCOVALENT BONDS TO THE
INTERACTION BETWEEN AN AMIDE AND S-CONTAINING
MOLECULES¹

Abstract

N-methylacetamide, a model of the peptide unit in proteins, is allowed to interact with CH₃SH, CH₃SCH₃, and CH₃SSCH₃ as models of S-containing amino acid residues. All of the minima are located on the ab initio potential energy surface of each heterodimer. Analysis of the forces holding each complex together identifies a variety of different attractive forces, including SH···O, NH···S, CH···O, CH···S, SH···π, and CH···π H-bonds. Other contributing noncovalent bonds involve charge transfer into σ* and π* antibonds. Whereas some of the H-bonds are strong enough that they represent the sole attractive force in several dimers, albeit not usually in the global minimum, charge-transfer type noncovalent bonds play only a supporting role. The majority of dimers are bound by a collection of several of these attractive interactions. The SH···O and NH···S H-bonds are of comparable strength, followed by CH···O and CH···S.

8-1. Introduction

Because of its prevalence in proteins, the peptide linkage has been studied extensively, and there is a great deal of information available about its proclivity toward planarity, its flexibility, and its electronic structure. The peptide group involves itself in a

¹ Coauthored by Upendra Adhikari and Steve Scheiner. Reproduced with permission from *ChemPhysChem* **2012**, *13*, 3535-3541. Copyright 2012, Wiley-VCH Verlag & Co. KGaA.

multitude of H-bonds within proteins, which are largely responsible for a great deal of secondary structure, as in α -helices and β -sheets. For this reason, a large amount of effort has been expended in elucidating details about the ability of both the NH and C=O groups of the peptide to engage in H-bonds, not only with other peptide groups, but also with some of the more widely occurring amino acid side chains.

Whereas many of the polar side chains, e.g. Ser, Lys, His, would of course form H-bonds with the proton-donating and accepting sites of the -CONH- peptide group, the situation is less clear for those containing S. The SH group of Cys certainly offers the possibility of a SH \cdots O or SH \cdots N H-bond, but SH is not known as a strong proton donor.^[1-3] In the case of Met, with no SH the only H-bonding opportunity would utilize S as proton-acceptor, in the capacity of which this atom is again not very potent. Another option might utilize a CH as a proton donor, which previous work has suggested can provide a fairly strong H-bond under certain circumstances^[4-12] including protein models.^[13-15] This CH might arise from the C $^{\alpha}$ H element of the protein skeleton^[16-18] or from the alkyl chains which are part of the S-containing residues.

There are options for attractive contacts other than H-bonding. As an example, there have been numerous observations of pairs of carbonyl groups^[19] wherein the two groups are oriented either perpendicular or parallel to one another, a pattern that was originally attributed to dipolar interactions.^[20-22] This idea was further elaborated, invoking the concept of anisotropy of the electrostatic field around the O atom.^[23,24] Other work^[25-27] suggested that the transfer of charge from an O lone pair to a CO π^* antibonding orbital was a major contributor as well.

Molecules containing sulfur are also capable of interactions other than H-bonds. Early analyses of crystal structures^[28] revealed a tendency of nucleophiles to approach S along an extension of one of its covalent bonds, a pattern that won some initial support from calculations.^[29] Subsequent crystal database analyses^[30,31] confirmed this geometric preference within the context of both proteins and smaller molecules. Other groups^[32-35] attributed the attraction, at least in part, to charge transfer from the nucleophilic atom's lone pair to the antibonding orbital of the C-S bond, although induction and dispersion can be important as well.^[36] Very recent research in this laboratory^[37-41] has amplified and generalized the concept of charge transfer from the lone pair of an atom on one molecule to a σ^* antibonding orbital on its partner, to a range of atoms that include P and Cl. The S atom too has been shown to be a prime candidate for accepting this charge into a S-X antibond to form surprisingly strong noncovalent bonds.^[42-45] The range of possibilities for interactions with an amide group could thus be expanded to include a noncovalent bond between S and the O or N atoms of the amide.

The principal purpose of the present communication is an exploration of the full variety of different sorts of interactions that may occur between the peptide linkage of a protein and S-containing amino acid residues, and to sort out which noncovalent bonds might predominate. The N-methylacetamide (NMA) molecule in its trans geometry, which brackets an amide by a pair of C atoms as would occur along the protein backbone, is taken as a model of the peptide unit. CH_3SH is used to represent the Cys side chain, and CH_3SCH_3 is a prototype of Met. The disulfide bond that frequently connects Cys side chains is modeled by CH_3SSCH_3 . For each pair of molecules, the potential energy surface is thoroughly searched for all minima. Comparisons of the energetics of the various

structures provide information about the relative strength of each sort of interaction contained therein. The analysis also brings to light some new noncovalent bonds that have not been previously reported.

8-2. Computational Methods

Ab initio calculations were carried out via the Gaussian 09 package.^[46] Geometries were optimized at the ab initio MP2/aug-cc-pVDZ level which has been shown to be of high accuracy, especially for weak intermolecular interactions of the type of interest here^[35,47-52] where the data are in close accord with CCSD(T) values with larger basis sets^[38,53,54] and in excellent agreement with experimental energetics.^[55] Binding energies were computed as the difference in energy between the dimer, and the sum of the optimized energies of the isolated monomers, corrected for basis set superposition error by the counterpoise procedure.^[56] For purposes of identifying all stabilizing interactions within each dimer, and estimating the strength of each, natural bond orbital (NBO) analysis^[57,58] was carried out via the procedures contained within Gaussian.

8-3. Results

Each of the three S-containing molecules was paired with NMA, and the potential energy surface was thoroughly searched so as to identify all minima.

8-3.1. *CH₃SH*

Perhaps emblematic of this entire problem, the global minimum of the complex between NMA and CH₃SH is a product of a number of contributing noncovalent bonds,

none of which are dominant by any means. This structure, illustrated in Figure **8-1a**, has a total binding energy of 4.60 kcal/mol. Based upon the NBO E(2) values reported in Table 8-1, a CH \cdots O H-bond makes the strongest contribution, which arises in part from an interaction with the O lone pairs (CH \cdots O) in Table 8-1 of 1.53 kcal/mol, combined with 1.11 kcal/mol from electron donation by the CO π -bonding orbital. This fairly strong interaction is consistent with the close R(H \cdots O) contact of 2.31 Å, shorter than a typical CH \cdots O H-bond, particularly one involving a methyl group. Also contributing to the binding energy is a CH \cdots S H-bond, with a value of E(2) of 1.06 kcal/mol, even though the H and S atoms are separated by 3.02 Å. The last component with an E(2) above the 0.5 kcal/mol threshold is one involving electron donation from the S lone pairs to the CO π^* antibonding orbital, with S separated from the pertinent O atom by 3.39 Å, and an even closer R(S \cdots C) contact of 3.30 Å. This latter interaction is rather unusual, one that is not commonly observed. Its absence from the literature is understandable as it occurs only in tandem with other, stronger, noncovalent bonds, which would normally mask its presence.

An SH \cdots O H-bond makes an appearance in the second most stable minimum, **8-1b**, which is bound by 4.27 kcal/mol. This H-bond arises from two elements. Electron donation to the σ^* (SH) orbital from the O lone pairs amounts to 2.77 kcal/mol, which accounts for the normal SH \cdots O H-bond. This H-bond is fairly long, with R(H \cdots O)=2.23 Å, and is further weakened by its 39° deviation from linearity. This attraction is complemented by a value of E(2) of 1.84 kcal/mol for the density extracted from the CO π orbital, surprisingly strong for what amounts to a SH $\cdots\pi$ H-bond. This complex also

contains a secondary CH \cdots S H-bond, allowing the S atom to serve as both proton donor and acceptor. A SH \cdots O H-bond dominates the next minimum on the surface, slightly less stable than its predecessor. In fact, there are no discernible secondary interactions in **8-1c**, and E(2) for this H-bond is 10.2 kcal/mol, facilitated in part by a very nearly linear $\theta(\text{SH}\cdots\text{O})$ of 177°. Comparison of **8-1b** and **8-1c** indicates that the benefit of forming CH \cdots S and SH $\cdots\pi$ H-bonds, even weak ones, is worth the stretching and bending of the SH \cdots O in **8-1b**.

The next minimum on the surface, bound by 4.06 kcal/mol, is reminiscent of the global minimum in terms of its constituent stabilizing forces. It too contains CH \cdots O and CH \cdots S H-bonds, and a repeat of a charge transfer from the S lone pairs to the π^* CO orbital. It also contains a very weak SH $\cdots\pi$ H-bond.

Structure **8-1e** is unique from the others. Bound by 4.03 kcal/mol, its strongest component arises from a CH H-bond to the amide O atom, with both the O lone pairs and the CO π orbital donating charge. But **8-1e** also contains a contribution whereby charge is transferred from the N lone pair into the σ^* antibonding orbital of the SH bond. This transfer is facilitated by the overlap of the N lone pair with the lobe of the σ^* orbital proximate to the S atom, not the usual H as in a H-bond. This overlap is facilitated by the rotation of the S-H bond some 168° away from the N atom. Nonetheless, the latter HS \cdots N noncovalent bond contributes only 0.55 kcal/mol, much smaller than the combined E(2) of 2.82 kcal/mol for the CH \cdots O H-bond, so is not dominating by any means.

There were six other minima identified on the surface of the NMA/CH₃SH heterodimer, with binding energies varying from 3.99 down to 3.38 kcal/mol. The contributing interactions are largely repeats of those incorporated into the more stable minima, albeit weaker versions. The only new interaction is the NH···S H-bond in **8-1h** which is the only contributor to the dimer in which it occurs. Another weakly bound minimum is of interest as it contains a CH···O H-bond as its sole contributor. Comparison of these two complexes with **8-1c** leads to an estimation of the SH···O, NH···S, and CH···O H-bond energies of 4.12, 3.95, and 3.52 kcal/mol, respectively.

8-3.2. CH₃SCH₃

Replacement of the SH of CH₃SH by a second methyl group eliminates the possibility of a SH···O H-bond which is probably the strongest single noncovalent bond, present in several of the lower-energy minima of its complex with NMA. As illustrated in Figure 8-2, the global minimum of the NMA/CH₃SCH₃ heterodimer is stabilized by a single interaction, a NH···S H-bond, with E(2)=12.34 kcal/mol. This NH···S H-bond is stronger than the same interaction in CH₃SH, 4.93 vs 3.95 kcal/mol, and R(H···S) equal to 2.455 Å as compared to 2.534 Å. This enhanced H-bond is likely due to the effect of the second methyl group bound to S.

Only slightly higher in energy is structure **8-2b** which contains a number of different interactions, listed in Table 8-2. One of them involves charge transfer from S lone pairs to the π* CO antibonding orbital. The O atom serves as proton acceptor for two methyl CH groups, both less than 2.5 Å in length. These same H-bonds are both supplemented by charge transfer from the CO π orbital, so can be termed CH···π.

A charge transfer from the N lone pair of NMA to a SC σ^* antibonding orbital is observed in the third minimum **8-2c**, higher in energy than **8-2a** by 0.7 kcal/mol. The R(N \cdots S) distance is 3.28 Å, and θ (CS \cdots N) within 4° of linearity, both of which assist the formation of this bond. However, a CH \cdots O H-bond may be more important, with an E(2) of 1.81 kcal/mol, as compared to 0.75 kcal/mol for the CS \cdots N bond. A bond of similar CS \cdots N type is contained within the next minimum **2e** as well. However, its smaller E(2) of 0.57 kcal/mol is overshadowed by both NH \cdots S and CH \cdots S H-bonds. Somewhat higher in energy is configuration **8-2f** with only one primary source of stability, a CH \cdots O H-bond, but a short and strong one, with R(H \cdots O) = 2.28 Å and E(2)=4.41 kcal/mol. The binding energy of this pure CH \cdots O H-bond of 3.46 kcal/mol is understandably quite similar to the value of 3.52 kcal/mol for this same interaction with CH₃SH.

The next two minima are also stabilized by CH \cdots O H-bonds, followed by a weaker complex, with a stabilization energy of 1.91 kcal/mol, that contains a number of different noncovalent interactions, but E(2) of all of which are only around 0.52 kcal/mol.

The comparison of the complexes of NMA with CH₃SH and CH₃SCH₃ indicates that the loss of the possibility of a SH \cdots O H-bond in the latter case does not necessarily result in a weaker complex. On the contrary, the NH \cdots S H-bond that occurs in **8-2a** makes for a stronger interaction than any involving CH₃SH. The structure which contains a NH \cdots S H-bond for NMA/CH₃SH is somewhat weaker, and represents only the eighth most stable complex on its potential energy surface. It would appear that the second methyl group makes S a stronger proton acceptor, such that the NH \cdots S H-bond is the predominant factor in the global minimum of NMA/CH₃SCH₃.

8-3.3. CH_3SSCH_3

Like CH_3SCH_3 , CH_3SSCH_3 too cannot form a $\text{SH}\cdots\text{O}$ H-bond. However, unlike CH_3SCH_3 , a $\text{NH}\cdots\text{S}$ H-bond is not involved in the global minimum of $\text{NMA}/\text{CH}_3\text{SSCH}_3$. The presence of a second S atom adjacent to the first weakens S as proton acceptor, such that a $\text{NH}\cdots\text{S}$ H-bond appears for the first time only in the eighth minimum in its surface. In the only geometry in which $\text{NH}\cdots\text{S}$ acts as the sole binding agent, its H-bond energy is 4.40 kcal/mol, intermediate between the CH_3SH and CH_3SCH_3 cases.

The global minimum in the $\text{CH}_3\text{SSCH}_3/\text{NMA}$ heterodimer is characterized by the multiple stabilizing interactions indicated in Table 8-3. As illustrated in Figure **8-3a**, there is a $\text{CH}\cdots\text{O}/\pi$ H-bond, in which electrons are donated not only by the O lone pairs (1.22 kcal/mol) but even more so by the CO π bond (2.75 kcal/mol). A methyl group on the NMA engages in a $\text{CH}\cdots\text{O}$ H-bond with S, and there is another contribution involving charge transfer from the S lone pairs to the CO π^* antibonding orbital. Altogether, these interactions add up to a total stabilization energy of more than 5 kcal/mol, the largest of any of the complexes considered here. There is another minimum, **8-3b**, almost a mirror image of the first, that contains very similar interactions, and a binding energy only 0.1 kcal/mol smaller.

The next minimum **8-3c** also contains $\text{CH}\cdots\text{O}$ and $\text{CH}\cdots\text{S}$ H-bonds, as well as $\pi^*\text{CO}\cdots\text{S}$. What is new here, however, are a pair of interactions that involve charge transfer into the SS σ^* antibonding orbital. Some density is extracted from the CO π bond, but some also from the CO π^* antibond. As is true for most NBO virtual orbitals, the π^* CO is partially occupied. Nonetheless, its willingness to part with a portion of its

small occupation to the benefit of the SS σ^* orbital is unexpected. Indeed, both the π and π^* orbitals contribute a like amount of 0.79 kcal/mol to the overall stability of this complex. It is these two charge transfer interactions that compensate for the weaker CH \cdots O and CH \cdots S H-bonds, imparting a stabilization energy of 4.90 kcal/mol to this structure. Indeed, CH \cdots O and CH \cdots S H-bonds occur in pretty much all of the minima of this pair of molecules, whether charge is extracted from just the proton acceptor lone pairs or from the CO π bond as well.

A NH \cdots S H-bond makes its first appearance in the complex **8-3h** with a binding energy of 4.48 kcal/mol, 0.6 kcal/mol less than that of the global minimum. It is supplemented by a CH \cdots S H-bond in that structure, but is fully responsible for the binding of 4.40 kcal/mol of the next minimum **8-3i**. The next minimum **8-3j** repeats some of the prior interactions, including the donation from both the π and π^* CO orbitals into $\sigma^*(SS)$.

A new interaction arises in structure **8-3l**, one in which charge is transferred from the N lone pair into a $\sigma^*(CS)$ antibonding orbital. But despite the $\theta(N\cdots SC)$ angle of 170°, $E(2)$ is only 0.65 kcal/mol for this bond, far less than the 7.37 kcal/mol arising from the NH \cdots S H-bond. Rather than the CS antibond, the SS σ^* orbital is the recipient of charge in the next minimum **8-3m**, this time extracted from both the N lone pair and the CO π^* orbital. A $N_{lp} \rightarrow \sigma^*(CS)$ transfer occurs in the next minimum as well, this time supplemented by a much stronger NH \cdots S H-bond. The remaining minima in the potential energy surface of this heterodimer all contain some combination of NH \cdots S, CH \cdots N,

CH \cdots O, and CH \cdots S H-bonds. The binding energies of these last few minima vary from 4.1 down to 2.1 kcal/mol.

With particular respect to CH \cdots O H-bonds, the geometry with this as its sole contributor leads to an estimate of CH \cdots O H-bond energy of 3.74 kcal/mol, slightly greater than those for CH₃SH and CH₃SCH₃. The S-S linkage may thus be considered to slightly strengthen the proton-donating ability of a neighboring methyl group. But in no case is a CH \cdots O H-bond strong enough to dominate the global minimum of any of these dimers.

8-4. Discussion

The CH₃SH/NMA heterodimer has available to it a number of specific interactions in which it might engage. In terms of H-bonds, the SH group can serve as a potent proton donor, and S can offer a proton-accepting site. The methyl hydrogens of CH₃SH are activated to some extent by the neighboring electronegative S atom. The same can be said of the methyl groups of NMA which are both adjacent to the electron-withdrawing amide group. And of course the NH group of NMA represents a likely proton source. The carbonyl O is a prime proton acceptor, as is the N. One usually thinks of the lone pairs of O as the source of charge transfer, but the C-O π bond offers an alternative, given its concentration of density. The structures of the various minima, and their relative energies, allow a detailed comparison of the competitive strengths of each type of interaction, and an identification of any that might dominate.

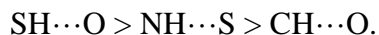
The stability of the global minimum of the CH₃SH/NMA heterodimer rests not on one, but on several of these elements. The strongest component is a H-bond involving a

methyl CH of CH₃SH. The O lone pairs act as proton acceptor from the methyl group, as does the CO π bond. This CH \cdots O interaction is supplemented by a CH \cdots S H-bond, in this case involving a methyl group on the NMA. The fourth, and apparently weakest, interaction is not a H-bond at all. It involves a charge transfer from the S lone pairs, not to a CH group, but rather to the π^* antibonding orbital of the C-O bond. The next minimum also incorporates a CH \cdots S H-bond, but substitutes the various other interactions of the global minimum for a SH \cdots O H-bond, sacrificing 0.3 kcal/mol in the exchange. By losing the CH \cdots S interaction, the third minimum is able to build a shorter and more linear SH \cdots O H-bond, forgoing any other noncovalent bonds, but in so doing rises in energy by 0.15 kcal/mol. One may conclude therefore that a SH \cdots O H-bond is not sufficiently strong, even if fully linear, that it can override those structures containing a number of different noncovalent bonds, even if each of the latter is individually weaker than a linear SH \cdots O bond.

The fourth minimum combines a large number of the various possible interactions. In addition to both CH \cdots O and CH \cdots S H-bonds, there are also CH $\cdots\pi$ and SH $\cdots\pi$ H-bonds wherein both protons extract density from the CO π bond, all combined with a $S_{lp}\rightarrow\pi^*(CO)$ charge transfer. It is not until the fifth minimum, 0.6 kcal/mol less stable than the global structure, that one sees for the first time the charge transfer from a N lone pair to a $\sigma^*(SH)$ antibonding orbital. And even here in this case, the strength of this interaction is overshadowed by a CH \cdots O/CH $\cdots\pi$ H-bond, so cannot be considered the primary stabilizing force.

It is only for the higher-energy minima that complexes characterized by a single stabilizing noncovalent bond become more prevalent. These isolated elements include a

SH··O, NH··S, and CH··O H-bond. In summary, structures characterized by a combination of stabilizing forces are generally more stable than those containing a single element, even when the latter is able to attain its most stable geometry. If one were to consider only those structures with a single stabilizing force, then an order of diminishing strength can be obtained:



The pattern changes when the SH group is replaced by a second methyl in CH₃SCH₃. The enhancement of the S atom's proton-accepting ability strengthens the NH··S H-bond to the point where it is the sole contributor to the global minimum in the CH₃SCH₃/NMA heterodimer, with a binding energy of nearly 5 kcal/mol. The structures of higher energy rely on multiple noncovalent bonds which again include combinations of CH··O, CH··π, CH··S, and S_{lp}→π*(CO). A charge transfer from the N lone pair to a CS σ* antibonding orbital contributes to several of these lower-lying minima, albeit not as much as do the forgoing H-bonds which occur in combination with it. Other than the NH··S H-bond occurring in the global minimum, the CH··O H-bond is the only other that occurs on its own in any of the structures, allowing an assessment of this H-bond energy of some 3.3-3.5 kcal/mol in this system.

When a second S atom is added to the monomer, as in CH₃SSCH₃, most of the minima, and certainly those of lowest energy, rely on multiple stabilizing interactions. The global minimum contains CH··π, CH··O, CH··S, as well as a S_{lp}→π*(CO) interaction, as do many of the other structures. Another minimum, 0.2 kcal/mol higher than the first, adds another pair of charge transfers, both into the SS σ* antibonding

orbital. Some of the charge is extracted from the CO π bond, but a roughly equal amount comes from the CO π^* orbital which is not completely vacant in the NMA monomer.

It is only for higher-energy structures that single interactions arise. The NH \cdots S H-bond in structure **8-3i** amounts to 4.40 kcal/mol, just slightly less than the same interaction where CH₃SCH₃ acts as proton acceptor. Minima containing only a CH \cdots O H-bond lead to an estimate of its binding energy of 3.6-3.7 kcal/mol, slightly higher than in the CH₃SCH₃/NMA heterodimer. Transfer into the CS σ^* antibond from the N lone pair does not occur until structure **8-3l**, and is overshadowed by the much stronger NH \cdots S H-bond.

Numerical values of the H-bond energies are displayed in Table 8-4 for each of the S-containing molecules, derived from those structures in which that H-bond is the only stabilizing force. While SH \cdots O is the strongest H-bond in which CH₃SH engages with NMA, it is only slightly stronger than NH \cdots S. Indeed, the latter H-bond is strengthened in CH₃SCH₃ and CH₃SSCH₃, invalidating any general statement about the relative strengths of SH \cdots O and NH \cdots S. On the other hand, it would be fair to claim that the CH \cdots O H-bond is weaker than either of the other two. Note however, that even here, one cannot ignore a H-bond energy of nearly 4 kcal/mol, only slightly weaker than that in the water dimer. In contrast to CH \cdots O, there are no values reported in Table 4 for the energies of CH \cdots S H-bonds. This absence is due to the fact that although the latter sort of interaction does occur in a number of minimum energy structures, it is not strong enough to represent the sole binding force in any. Likewise for the interactions involving charge transfers into the S-H or S-C antibonds.

With regard to some of the non-H-bonding sorts of noncovalent bonds, the binding energy for a CS \cdots N bond was calculated earlier^[44] to be 0.7 kcal/mol when CH₃SH was combined with NH₃; the corresponding HS \cdots N bond is slightly weaker, 0.5 kcal/mol.^[42] Given the lesser ability of the amide N lone pair to donate electrons, one would expect the noncovalent CS \cdots N and HS \cdots N bonds in the complexes pairing NMA with CH₃SH and CH₃SCH₃ to be even weaker. It is for this reason that these noncovalent interactions are not primary factors in any of the complexes in which they occur. The insertion of a second S atom into CH₃SCH₃ might be expected to strengthen the potential SS \cdots N interaction by a small amount. But nonetheless, this bond remains weaker than other possible interactions, not making an appearance until structure **8-3m**, and even then it is eclipsed by a stronger CH \cdots π CO H-bond. In fact, it would appear that the CO π bond serves as a superior source of electrons to the amide N lone pair, as the former yields higher values of E(2) and SS \cdots π (CO) bonds occur in more stable minima than does SS \cdots N.

There has been one previous computational study of complexes of NMA with S-containing systems of these sorts. Iwaoka et al^[30,31] first paired NMA with CH₃SCH₃, and identified only two minima, in contrast to our own finding of 10 distinct minima. Their global minimum C is stabilized by 2.9 kcal/mol, while our most stable minimum has a binding energy of nearly twice that value. Their structure C appeared to be similar to our dimer **8-2c** in that it contained both a CH \cdots O and CS \cdots N pair of stabilizing interactions. Their secondary minimum D is similar to our own global minimum **8-2a**, containing a NH \cdots S H-bond.

The same research group also considered^[30,31] the NMA/CH₃SSCH₃ heterodimer, again identifying only two minima on a surface that our calculations indicate contains 21 such minima. Their global minimum appears to correspond most closely to our own geometry **8-3c**, the third most stable structure. Our binding energy for **8-3c** is 4.9 kcal/mol, higher by 1.7 kcal/mol than their global minimum. The only other minimum identified by Iwaoka et al is rather similar to their global minimum, also seeming to contain a CH···O and SS···O pair of interactions. It would appear then that their superficial examination of the surface led them to ignore structures that are considerably more stable, bound by other interactions including CH··· π , CH···S, $\pi^*(\text{CO})\cdots\text{S}$, SS··· π , and NH···S noncovalent bonds.

Some of the discrepancies may be due to their use^[30,31] of a 6-31G* basis set, much smaller and less flexible than the aug-cc-pVDZ set used here. There was apparently no attempt made to thoroughly search the potential energy surface for all minima, leaving the researchers with a suboptimal set. Also of note, their determination of the contributing factors in the stability of each structure was based primarily on geometric criteria, without a systematic evaluation of charge transfer energies.

A statistical analysis of protein crystal structures^[30,31] had suggested a propensity of the S atom to lie above the amide plane when interacting with the amide O atom. This trend is confirmed by our calculations. For example in the complexes with CH₃SCH₃, the $\phi(\text{NCO}\cdots\text{S})$ dihedral angle in **8-2b** is 91°, and 76° in **8-2i**. Structures involving CH₃SSCH₃ had a similar tendency: the dihedral angle ranges from 68° in **8-3a** to 95° in **8-3b**. This

placement of the S atom is consistent with the concept of transfer from the π CO bond which is a common feature of these O \cdots S interactions.

It is worthwhile to consider how the results presented here might be altered if the model systems were enlarged to more accurately represent the actual protein segments. The CH₃SH and CH₃SCH₃ models of Cys and Met, respectively, would probably not change much if their methyl groups were replaced by longer alkyl chains. Nor would one expect any changes in the CH₃SSCH₃ model of a disulfide linkage to affect the results by a significant amount. The replacement of NMA by a longer protein skeleton would probably have little influence upon the -CO-NH- amide segment. On the other hand, the CH groups of the NMA would be surrounded on both sides by peptide groups, which would likely make them somewhat stronger proton donors. One might therefore anticipate some small strengthening of the CH \cdots S H-bonds which occur in structures **8-1b**, **8-2b**, and **8-3a**, to name just a few.

8-5. Conclusions

There is no single type of noncovalent bond that dominates the interactions of a peptide group with S-containing protein residues. Most of the minima are characterized by the presence of multiple stabilizing interactions, all contributing to the total binding. In addition to H-bonds of the SH \cdots O, NH \cdots S, CH \cdots O, and CH \cdots S-types there are also SH \cdots π and CH \cdots π interactions where π bonds act as electron donors. Smaller contributions arise from noncovalent bonds in which charge is transferred from a nitrogen lone pair or CO π bond into a CS or SS σ^* antibonding orbital.

References

- [1] G. A. Jeffrey, W. Saenger, *Hydrogen Bonding in Biological Structures*, Springer, Berlin, **1991**.
- [2] S. Scheiner, *Hydrogen Bonding: A Theoretical Perspective*, Oxford University Press, New York, **1997**.
- [3] G. Gilli, P. Gilli, *The Nature of the Hydrogen Bond*, Oxford University Press, Oxford, **2009**.
- [4] S. Scheiner, Y. Gu, T. Kar, *J. Mol. Struct.: THEOCHEM* **2000**, *500*, 441–452.
- [5] S. A. C. McDowell, *Chem. Phys. Lett.* **2006**, *424*, 239–242.
- [6] Y. Gu, T. Kar, S. Scheiner, *J. Mol. Struct.* **2000**, *552*, 17–31.
- [7] S. Scheiner, S. J. Grabowski, T. Kar, *J. Phys. Chem. A* **2001**, *105*, 10607–10612.
- [8] E. S. Kryachko, S. Scheiner, *J. Phys. Chem. A* **2008**, *112*, 1940–1945.
- [9] B. J. van der Veken, S. N. Delanoye, B. Michielsen, W. A. Herrebout, *J. Mol. Struct.* **2010**, *976*, 97–104.
- [10] T. S. Thakur, M. T. Kirchner, D. Bläser, R. Boese, G. R. Desiraju, *Phys. Chem. Chem. Phys.* **2011**, *13*, 14076–14091.
- [11] S. J. Grabowski, *J. Phys. Chem. A* **2011**, *115*, 12789–12799.
- [12] A. Karpfen, A. J. Thakkar, *J. Chem. Phys.* **2006**, *124*, 224313.
- [13] N. G. Mirkin, S. Krimm, *J. Phys. Chem. B* **2008**, *112*, 15267–15268.
- [14] S. M. LaPointe, S. Farrag, H. J. Bohórquez, R. J. Boyd, *J. Phys. Chem. B* **2009**, *113*, 10957–10964.
- [15] S. Scheiner, T. Kar, J. Pattanayak, *J. Am. Chem. Soc.* **2002**, *124*, 13257–13264.
- [16] S. Scheiner, T. Kar, Y. Gu, *J. Biol. Chem.* **2001**, *276*, 9832–9837.

- [17] S. Scheiner, *J. Phys. Chem. B* **2005**, *109*, 16132–16141.
- [18] S. Scheiner, *J. Phys. Chem. B* **2006**, *110*, 18670–18679.
- [19] F. H. Allen, C. A. Baalham, J. P. M. Lommerse, P. R. Raithby, *Acta Crystallogr. Sect. B* **1998**, *54*, 320–329.
- [20] R. Paulini, K. Müller, F. Diederich, *Angew. Chem.* 2005, *117*, 1820–1839; *Angew. Chem. Int. Ed.* **2005**, *44*, 1788–1805.
- [21] F. R. Fischer, P. A. Wood, F. H. Allen, F. Diederich, *Proc. Natl. Acad. Sci. USA* **2008**, *105*, 17290–17294.
- [22] C. Fähr, L. A. Hardegger, M.-O. Ebert, W. B. Schweizer, F. Diederich, *Chem. Commun.* **2010**, *46*, 67–69.
- [23] J. S. Murray, P. Lane, T. Clark, P. Politzer, *J. Mol. Model.* **2007**, *13*, 1033–1038.
- [24] T. Clark, J. S. Murray, P. Lane, P. Politzer, *J. Mol. Model.* **2008**, *14*, 689–697.
- [25] M. L. DeRider, S. J. Wilkens, M. J. Waddell, L. E. Bretscher, F. Weinhold, R. T. Raines, J. L. Markley, *J. Am. Chem. Soc.* **2002**, *124*, 2497–2505.
- [26] T. K. Pal, R. Sankararamkrishnan, *J. Phys. Chem. B* **2010**, *114*, 1038–1049.
- [27] C. E. Jakobsche, A. Choudhary, S. J. Miller, R. T. Raines, *J. Am. Chem. Soc.* **2010**, *132*, 6651–6653.
- [28] R. E. Rosenfield, R. Parthasarathy, J. D. Dunitz, *J. Am. Chem. Soc.* **1977**, *99*, 4860–4862.
- [29] F. T. Burling, B. M. Goldstein, *J. Am. Chem. Soc.* **1992**, *114*, 2313–2320.
- [30] M. Iwaoka, S. Takemoto, S. Tomoda, *J. Am. Chem. Soc.* **2002**, *124*, 10613–10620.

- [31] M. Iwaoka, S. Takemoto, M. Okada, S. Tomoda, *Bull. Chem. Soc. Jpn.* **2002**, *75*, 1611–1625.
- [32] Y. Nagao, T. Hirata, S. Goto, S. Sano, A. Kakehi, K. Iizuka, M. Shiro, *J. Am. Chem. Soc.* **1998**, *120*, 3104–3110.
- [33] C. Bleiholder, D. B. Werz, H. Koppel, R. Gleiter, *J. Am. Chem. Soc.* **2006**, *128*, 2666–2674.
- [34] R. Gleiter, D. B. Werz, B. J. Rausch, *Chem. Eur. J.* **2003**, *9*, 2676–2683.
- [35] L. Junming, L. Yunxiang, Y. Subin, Z. Weiliang, *Struct. Chem.* **2011**, *22*, 757–763.
- [36] C. Bleiholder, R. Gleiter, D. B. Werz, H. Köppel, *Inorg. Chem.* **2007**, *46*, 2249–2260.
- [37] S. Scheiner, *J. Chem. Phys.* **2011**, *134*, 094315.
- [38] S. Scheiner, *J. Phys. Chem. A* **2011**, *115*, 11202–11209.
- [39] S. Scheiner, *Chem. Phys.* **2011**, *387*, 79–84.
- [40] S. Scheiner, U. Adhikari, *J. Phys. Chem. A* **2011**, *115*, 11101–11110.
- [41] U. Adhikari, S. Scheiner, *J. Chem. Phys.* **2011**, *135*, 184306.
- [42] S. Scheiner, *J. Chem. Phys.* **2011**, *134*, 164313.
- [43] U. Adhikari, S. Scheiner, *Chem. Phys. Lett.* **2011**, *514*, 36–39.
- [44] U. Adhikari, S. Scheiner, *J. Phys. Chem. A* **2012**, *116*, 3487–3497.
- [45] U. Adhikari, S. Scheiner, *Chem. Phys. Lett.* **2012**, *532*, 31–35.
- [46] Gaussian 09 (Rev. B.01), M. J. Frisch, G. W. Trucks, H. B. Schlegel, G. E. Scuseria, M. A. Robb, J. R. Cheeseman, G. Scalmani, V. Barone, B. Mennucci,

G. A. Petersson, H. Nakatsuji, M. Caricato, X. Li, H. P. Hratchian, A. F. Izmaylov, J. Bloino, G. Zheng, J. L. Sonnenberg, M. Hada, M. Ehara, K. Toyota, R. Fukuda, J. Hasegawa, M. Ishida, T. Nakajima, Y. Honda, O. Kitao, H. Nakai, T. Vreven, J. A. Montgomery, J. E. Peralta, F. Ogliaro, M. Bearpark, J. J. Heyd, E. Brothers, K. N. Kudin, V. N. Staroverov, R. Kobayashi, J. Normand, K. Raghavachari, A. Rendell, J. C. Burant, S. S. Iyengar, J. Tomasi, M. Cossi, N. Rega, J. M. Millam, M. Klene, J. E. Knox, J. B. Cross, V. Bakken, C. Adamo, J. Jaramillo, R. Gomperts, R. E. Stratmann, O. Yazyev, A. J. Austin, R. Cammi, C. Pomelli, J. W. Ochterski, R. L. Martin, K. Morokuma, V. G. Zakrzewski, G. A. Voth, P. Salvador, J. J. Dannenberg, S. Dapprich, A. D. Daniels, O. Farkas, J. B. Foresman, J. V. Ortiz, J. Cioslowski, D. J. Fox, Gaussian, Inc., Wallingford, CT, **2009**.

- [47] R. M. Osuna, V. Hernandez, J. T. L. Navarrete, E. D’Oria, J. J. Novoa, *Theor. Chem. Acc.* **2011**, *128*, 541–553.
- [48] M. G. Chudzinski, C. A. McClary, M. S. Taylor, *J. Am. Chem. Soc.* **2011**, *133*, 10559–10567.
- [49] D. Hauchecorne, N. Nagels, B. J. van der Veken, W. A. Herrebout, *Phys. Chem. Chem. Phys.* **2012**, *14*, 681–690.
- [50] Y. Zeng, X. Zhang, X. Li, L. Meng, S. Zheng, *ChemPhysChem* **2011**, *12*, 1080–1087.
- [51] J. Wu, *Int. J. Quantum Chem.* **2011**, *111*, 4247–4254.
- [52] J. S. Murray, P. Lane, T. Clark, K. E. Riley, P. Politzer, *J. Mol. Model.* **2012**, *18*, 541–548.

- [53] Q. Zhao, D. Feng, Y. Sun, J. Hao, Z. Cai, *Int. J. Quantum Chem.* **2011**, *111*, 2428–2435.
- [54] E. Munusamy, R. Sedlak, P. Hobza, *ChemPhysChem* **2011**, *12*, 3253–3261.
- [55] D. Hauchecorne, A. Moiana, B. J. van der Veken, W. A. Herrebout, *Phys. Chem. Chem. Phys.* **2011**, *13*, 10204–10213.
- [56] S. F. Boys, F. Bernardi, *Mol. Phys.* **1970**, *19*, 553–566.
- [57] A. E. Reed, F. Weinhold, L. A. Curtiss, D. J. Pochatko, *J. Chem. Phys.* **1986**, *84*, 5687–5705.
- [58] A. E. Reed, L. A. Curtiss, F. Weinhold, *Chem. Rev.* **1988**, *88*, 899–926.

Table 8-1. Total interaction energy ΔE and NBO second-order perturbation energy $E(2)$ of its primary component interactions in complexes of NMA with CH_3SH . Energies in kcal/mol.

	$-\Delta E$	interaction	$E(2)$	interaction	$E(2)$
a	4.60	$\text{CH}\cdots\text{O}$	1.53	$\text{CH}\cdots\text{S}$	1.06
		$\text{CH}\cdots\pi\text{CO}$	1.11	$\pi^*\text{CO}\cdots\text{S}$	0.70
b	4.27	$\text{SH}\cdots\text{O}$	2.77	$\text{CH}\cdots\text{S}$	1.42
		$\text{SH}\cdots\pi\text{CO}$	1.84		
c	4.12	$\text{SH}\cdots\text{O}$	10.19		
d	4.06	$\text{CH}\cdots\text{O}$	1.04	$\text{CH}\cdots\pi\text{CO}$	0.56
		$\pi^*\text{CO}\cdots\text{S}$	0.99	$\text{SH}\cdots\pi\text{CO}$	0.50
		$\text{CH}\cdots\text{S}$	0.76		
e	4.03	$\text{CH}\cdots\pi\text{CO}$	2.11	$\text{HS}\cdots\text{N}$	0.55
		$\text{CH}\cdots\text{O}$	0.71		
h	3.95	$\text{NH}\cdots\text{S}$	10.05		

Table 8-2. Total interaction energy ΔE and NBO second-order perturbation energy $E(2)$ of its primary component interactions in complexes of NMA with CH_3SCH_3 . Energies in kcal/mol.

	$-\Delta E$	interaction	$E(2)$	interaction	$E(2)$
a	4.93	$\text{NH}\cdots\text{S}$	12.34		
b	4.88	$\pi^*\text{CO}\cdots\text{S}$	1.40	$\text{CH}^{\text{a}}\cdots\pi\text{CO}$	0.81
		$\text{CH}^{\text{a}}\cdots\text{O}$	1.24	$\text{CH}^{\text{b}}\cdots\pi\text{CO}$	0.61
		$\text{CH}^{\text{b}}\cdots\text{O}$	0.90		
c	4.22	$\text{CH}\cdots\pi\text{CO}$	1.81	$\text{CS}\cdots\text{N}$	0.75
e	4.10	$\text{NH}\cdots\text{S}$	2.53	$\text{CS}\cdots\text{N}$	0.57
		$\text{CH}\cdots\text{S}$	0.81		
f	3.46	$\text{CH}\cdots\text{O}$	4.41		

Table 8-3. Total interaction energy ΔE and NBO second-order perturbation energy $E(2)$ of its primary component interactions in complexes of NMA with CH_3SSCH_3 . Energies in kcal/mol.

	$-\Delta E$	interaction	$E(2)$	interaction	$E(2)$
a	5.07	$\text{CH}\cdots\pi\text{CO}$	2.75	$\text{CH}\cdots\text{O}$	1.22
		$\text{CH}\cdots\text{S}$	2.35	$\pi^*\text{CO}\cdots\text{S}$	0.76
c	4.90	$\text{CH}\cdots\text{O}$	1.49	$\text{SS}\cdots\pi\text{CO}$	0.79
		$\pi^*\text{CO}\cdots\text{S}$	1.00	$\text{SS}\cdots\pi^*\text{CO}$	0.79
		$\text{CH}\cdots\text{S}$	0.98	$\text{CH}\cdots\pi\text{CO}$	0.67
d	4.73	$\text{CH}\cdots\text{S}$	2.82	$\text{CH}^a\cdots\pi\text{CO}$	0.86
		$\text{CH}^a\cdots\text{O}$	2.19	$\text{CH}^b\cdots\text{O}$	0.62
		$\text{CH}^b\cdots\pi\text{CO}$	1.67		
e	4.57	$\text{CH}\cdots\text{S}$	1.86	$\text{CH}^b\cdots\text{O}$	0.96
		$\text{CH}^b\cdots\pi\text{CO}$	1.27	$\text{CH}^a\cdots\pi\text{CO}$	0.80
		$\text{CH}^a\cdots\text{O}$	1.87	$\pi^*\text{CO}\cdots\text{S}$	0.55
f	4.52	$\text{CH}\cdots\text{S}$	3.59	$\text{CH}\cdots\pi\text{CO}$	2.26
		$\text{CH}\cdots\text{O}$	3.44		
g	4.50	$\text{CH}^a\cdots\text{O}$	3.80	$\text{CH}^b\cdots\pi\text{CO}$	2.56
		$\text{CH}\cdots\text{S}$	3.59	$\text{CH}^b\cdots\text{O}$	0.60
h	4.48	$\text{NH}\cdots\text{S}$	3.98	$\text{CH}\cdots\text{S}$	0.73
i	4.40	$\text{NH}\cdots\text{S}$	8.73		
j	4.39	$\pi^*\text{CO}\cdots\text{S}$	1.05	$\text{SS}\cdots\pi^*\text{CO}$	0.77
		$\text{CH}\cdots\text{O}$	1.05	$\text{SS}\cdots\pi\text{CO}$	0.62
		$\text{CH}\cdots\text{S}$	0.91	$\text{CH}\cdots\pi\text{CO}$	0.61
l	4.34	$\text{NH}\cdots\text{S}$	7.37	$\text{CS}\cdots\text{N}$	0.65
m	4.21	$\text{CH}\cdots\pi\text{CO}$	2.17	$\text{CH}\cdots\text{O}$	0.70
		$\text{SS}\cdots\text{N}$	1.08	$\text{SS}\cdots\pi^*\text{CO}$	0.61
n	4.13	$\text{NH}\cdots\text{S}$	6.49	$\text{CS}\cdots\text{N}$	0.55
		$\text{CO}\pi^*\cdots\text{S}$	0.57		

Table 8-4. H-Bond energies (kcal/mol) of S-containing molecules coupled with NMA.

	$\text{SH}\cdots\text{O}$	$\text{NH}\cdots\text{S}$	$\text{CH}\cdots\text{O}$
CH_3SH	4.12	3.95	3.52
CH_3SCH_3	-	4.93	3.46
CH_3SSCH_3	-	4.40	3.74

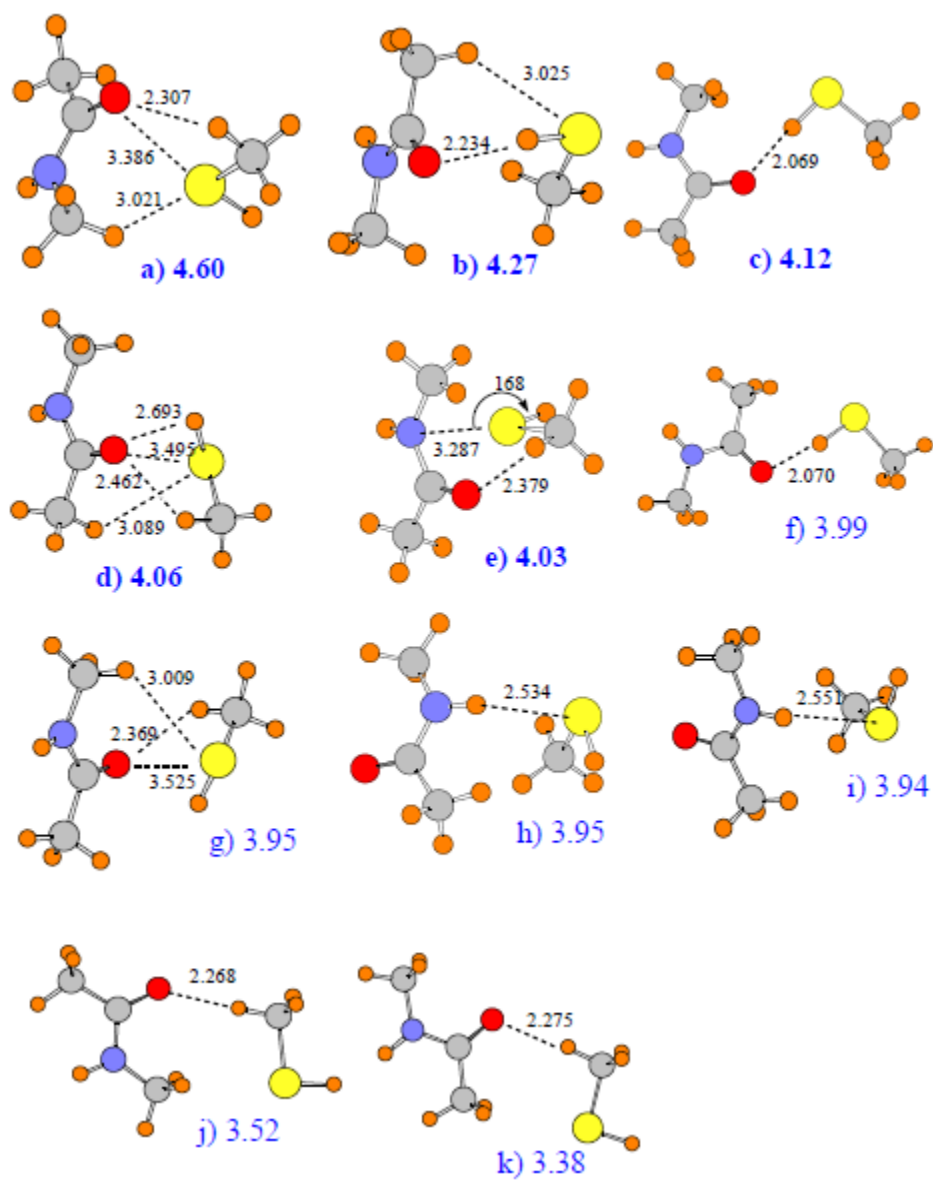


Figure 8-1. Optimized geometries of various minima on the potential energy surface of the CH₃SH/NMA heterodimer. Large blue numbers represent binding energies, in kcal/mol. Distances in Å and angles in degrees.

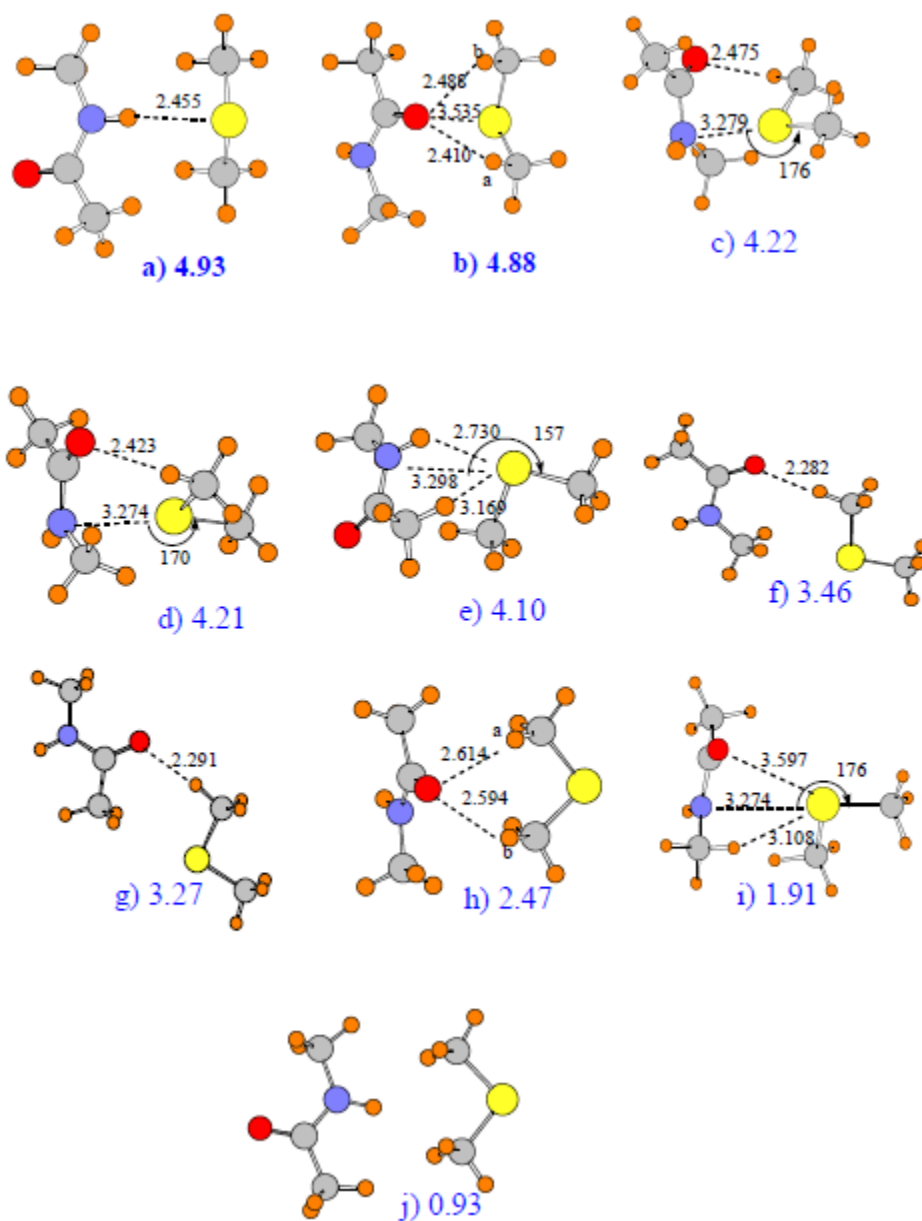


Figure 8-2. Optimized geometries of various minima on the potential energy surface of the $\text{CH}_3\text{SCH}_3/\text{NMA}$ heterodimer. Large blue numbers represent binding energies, in kcal/mol. Distances in Å and angles in degrees.

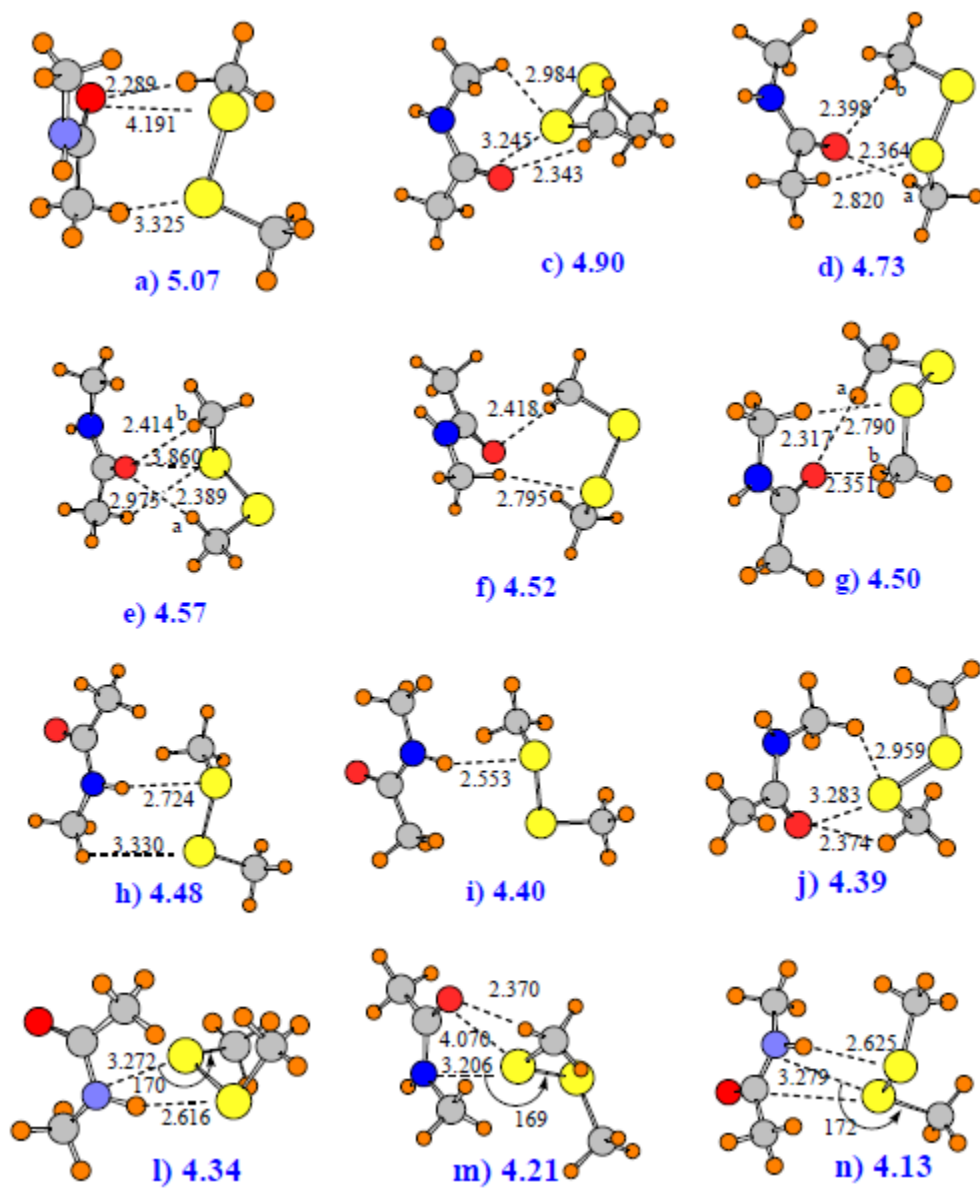


Figure 8-3. Optimized geometries of various minima on the potential energy surface of the $\text{CH}_3\text{SSCH}_3/\text{NMA}$ heterodimer. Large blue numbers represent binding energies, in kcal/mol. Distances in Å and angles in degrees.

CHAPTER 9

PREFERRED CONFIGURATIONS OF PEPTIDE-PEPTIDE INTERACTIONS¹**Abstract**

The natural and fundamental proclivities of interaction between a pair of peptide units is examined using high-level ab initio calculations. The NH \cdots O H-bonded structure is found to be the most stable configuration of the N-methylacetamide (NMA) model dimer, but only slightly more so than a stacked arrangement. The H-bonded geometry is destabilized by only a small amount if the NH group is lifted out of the plane of the proton-accepting amide. This out-of-plane motion is facilitated by a stabilizing charge transfer from the CO π bond to the NH σ^* antibonding orbital. The parallel and anti-parallel stacked dimers are nearly equal in energy, both only slightly less stable than the NH \cdots O H-bonded structure. Both are stabilized by a combination of CH \cdots O H-bonding and a $\pi\rightarrow\pi^*$ transfer between the two CO bonds. There are no minima on the surface that are associated with O_p $\rightarrow\pi^*(\text{CO})$ transfers, due in large part to strong electrostatic repulsion between the two O atoms which resists an approach of a carbonyl O from above the C=O bond of the other amide.

9-1. Introduction

Amidst a broad range of phenomena in which H-bonding plays a prominent role, perhaps none are so important as the H-bonds occurring in proteins. These noncovalent bonds are one of the prime ingredients in protein structure and function. They are widely

¹ Coauthored by Upendra Adhikari and Steve Scheiner. Reproduced with permission from *J. Phys. Chem. A* **2013**, *117*, 489-496. Copyright 2013, American Chemical Society.

accepted to be largely responsible for such prevalent secondary structures as α -helices and β -sheets, wherein pairs of peptide units engage in stabilizing $\text{NH}\cdots\text{O}=\text{C}$ H-bonds. Their influence is exerted also in other less common structural units within proteins, some particular to a given molecule.

While there is widespread agreement concerning the value of these interpeptide H-bonds, there remain some lingering but important questions as to the relative geometries that a pair of peptide units would prefer to approach one another. It is commonly thought, for example, that the $\theta(\text{NH}\cdots\text{O})$ angle tends toward linearity as is the case with other H-bonds. But even that being the case, does the NH favor an approach along the C=O axis, or would it be preferable for the NH to lie along one of the two carbonyl “rabbit ear” lone pairs? The latter idea implies that the NH ought to lie in the plane of the proton-accepting peptide unit. However, there are a host of crystal structure surveys that suggest that placement of the NH out of this plane is quite a common occurrence, more frequent than would be explained simply by other forces of the protein pulling the NH out of the plane against its wishes.

In addition to the presumed $\text{NH}\cdots\text{O}$ H-bonds, there have been several other mechanisms of attraction that have found support in the literature. The notion of attractive interactions between simple carbonyl groups derives from crystal structure analyses^{1,2} which point toward parallel, antiparallel, and perpendicular arrangements, and were attributed to simple dipolar interactions.³ Calculations⁴ of pairs of esters pointed toward charge transfer from the lone pair of one O to the π^* antibond of the other. A perpendicular arrangement of carbonyl groups was tested via model systems⁵ where it

was found to be stabilizing albeit only weakly, comparable to a $\text{CH}\cdots\pi$ H-bond. However, the calculations assumed a particular orientation, and did not test to determine whether or not this was a true minimum in the surface.

Recent work by the Raines group⁶⁻⁹ has made a case that $n\rightarrow\pi^*$ electron transfer from a carbonyl O lone pair to the $\pi^*(\text{CO})$ antibonding orbital of the partner peptide can exert a strong influence, particularly in helical structures and β -sheets,¹⁰ and one that is stronger in true peptide-peptide interactions than in many peptidomimics.¹¹ It is proposed that this force enables a surprisingly close approach of the O atoms of the two peptide groups, and bypasses the idea of a $\text{NH}\cdots\text{O}$ H-bond. Another work¹² found orthogonal $\text{C}=\text{O}\cdots\text{C}=\text{O}$ interactions to be “a substantial intermolecular association force capable of inducing self-assembly in apolar, non-competing solvents.”

A second, and more recent, concept that underlies interpeptide attraction arises from studies of small oligopeptides in the gas phase.¹³⁻¹⁶ In some of the conformations observed, pairs of peptide units arrange themselves parallel to one another, in a stacked geometry. In addition to an electrostatic attraction that might arise from the antiparallel arrangement, a charge transfer to a CO π^* antibonding orbital is suggested here. But unlike the aforementioned carbonyl-carbonyl attraction, in this case the source of the density is the N lone pair. Zwier et al suggest¹⁴ that this stacking motif might not be limited to small di and tripeptides but may well contribute to the folding of the much larger proteins. There was some precedent for this parallel arrangement derived from studies of pairs of carboxyl groups¹⁷ where again a parallel arrangement was observed.

The authors explained the attraction by a combination of dipole-dipole and of $n \rightarrow \pi^*$ charge transfer.

These ideas lead to the obvious question as to what exactly are the preferred arrangements of peptide groups. Is a coplanar pair with a linear $\text{NH} \cdots \text{O}$ H-bond truly energetically superior to the approach of the NH from above the plane of the partner peptide? Is a H-bonded structure indeed preferred, as is commonly supposed, to the approach of the two carbonyl groups toward one another? And how does a stacked arrangement fit into the broader picture; are there occasions in which such a geometry might actually be superior? These are issues which can be addressed in a straightforward manner by quantum chemical calculations.

And as one might expect, the importance of the peptide-peptide interaction has motivated a good deal of prior theoretical scrutiny.¹⁸⁻²⁴ Due to the delicacy involved in comparisons of different sorts of geometries, with differing origins of stability, it would be injudicious to base any decisions of relative stability on any but high-level correlated calculations, of which there have been several performed in recent years. Concerning studies of peptide analogues such as formamide and N-methylacetamide, the majority were limited primarily to standard H-bonded geometries,²⁵⁻²⁹ especially those wherein the two molecules occupied the same plane.³⁰⁻³⁴ There have been a handful of works that went beyond this simple paradigm and noted dimer geometries that had significant elements of nonplanarity,³⁵⁻³⁹ but did not pursue this issue in any detail. Others considered only specific orientations that occur in protein secondary structures such as α -helix and β -sheet⁴⁰ without determining whether or not they correspond to minima on the

potential energy surface, nor making comparisons to such minima. Although receiving only scant attention, stacked arrangements have not been entirely ignored. Vargas et al.⁴¹ for example, considered stacked pairs of dimethylformamide, but their analysis of the origin of the stability of this structure was superficial. The authors did not consider electrostatic or charge transfer effects explicitly, rationalizing the geometry purely on the basis of purported CH \cdots O H-bonds, despite their highly distorted nature, leaving in question their categorization as H-bonds.

The present work comprises a comprehensive examination of the various attractive interactions that may occur between a pair of peptide groups. The N-methylacetamide (NMA) molecule, CH₃NHCOCH₃, is taken as a model of the peptide unit, as the amide group is surrounded on both sides by the C atom that occurs within the context of a protein. The *trans* geometry of NMA was considered, again due to its similarity to the protein backbone. The potential energy surface of the NMA dimer is thoroughly probed so as to identify all minima, with no preconceived notions as to what these ought to be. The source of stability of each minimum is analyzed by various means including identification of any significant charge transfers, decomposition of the interaction energy into its various components, and interaction between electrostatic potentials of the two subunits. Most importantly, the application of high-level ab initio calculations facilitates a quantitative comparison of the relative energies of all minima on the surface in order to establish the fundamental preferences of peptide-peptide interactions.

9-2. Computational Methods

Calculations were carried out via the Gaussian 09 package.⁴² All geometries were optimized at the ab initio MP2/aug-cc-pVDZ level of theory which has been shown to be of high accuracy especially for those systems with intermolecular interactions of the type of interest here⁴³⁻⁴⁹ where the data are in close agreement with CCSD(T) with larger basis sets.⁵⁰⁻⁵² Optimizations were carried out both with and without inclusion of counterpoise⁵³ in the algorithm. The potential energy surface of the NMA dimer was examined thoroughly to identify all possible minima by optimizing from a range of possible starting points. Minima were verified as having all positive vibrational frequencies. Binding energies were evaluated as the difference between the energy of the dimer and twice that of the fully optimized NMA monomer, with counterpoise correction of basis set superposition error. Natural bond orbital (NBO)^{54,55} analyses were carried out via the procedure contained in Gaussian. The binding energy was decomposed by symmetry adapted perturbation theory⁵⁶ (SAPT) using the Molpro⁵⁷ set of codes.

9-3. Results

All minima obtained when counterpoise is included directly in the optimization algorithm are displayed in Figure 9-1. Structures **a**₁ and **a**₂ may be categorized as containing standard NH···O H-bonds. They are very similar to one another, differing primarily in a rotation of the righthand NMA molecule around its C=O axis. Consequently, the binding energies, both nearly 8 kcal/mol, are almost identical to one another, as indicated by the large blue numbers in Figure 9-1. The $\theta(\text{NH}\cdots\text{O})$ angle is within 9° of linearity in both, reported in Table 9-1, as expected for a H-bond, and the

R(H \cdots O) H-bond lengths are less than 2 Å. The $\theta(\text{CO}\cdots\text{H})$ angles differ a bit, 120° for structure **a**₁ and 142° for **a**₂. This deviation from linearity is consistent with the idea of a pair of roughly equivalent “rabbit ear” lone pairs on the carbonyl O. Also consistent with this notion, the bridging proton lies very close to the amide plane of the proton-acceptor molecule, with $\varphi(\text{H}\cdots\text{OCN})$ dihedral angles within 6-9° of a fully planar arrangement. The amide planes of the two molecules are close to perpendicular, with $\varphi(\text{CN}\cdots\text{OC})$ dihedral angles of nearly 80°. The last row of Table 9-1 shows a strong NBO second-order perturbation energy that corresponds to charge transfer from the O lone pairs to the NH σ^* antibonding orbital, a well understood aspect of a standard H-bond of this sort.

Structures **b** and **c** in Figure 9-1 are roughly similar to one another, in that both have the two amide planes stacked above one another. They differ primarily in their relative orientations: **b** can be described as antiparallel in that the NH of one amide lies above the C=O of the other. **c** represents a parallel structure with the two NH groups stacked above one another as are the pair of C=O groups. Note however that the two NH groups point in opposite directions, as do the two C=O groups. As another important point, the stacking is not perfect in the sense that the two amide planes are not fully parallel to one another in either **b** or **c**. The tilt allows a methyl group of the upper amide to engage in a CH \cdots O H-bond with the lower carbonyl in **b**; there are two such CH \cdots O H-bonds in **c**.

NBO analysis of these structures provides a mechanism to understand the individual elements of the binding. Both **b** and **c** include transfer from the π bond of one carbonyl to the π^* antibond of the partner C=O, and vice versa. This transfer is confirmed

by examination of the populations of the relevant NBOs. Formation of stacked complex **b**, for example, reduces the CO π -orbital population by 2-3 me relative to the monomer, whereas the π^* MOs gain between 2 and 7 me. The E(2) $\pi \rightarrow \pi^*$ energetic contribution is twice as large in **b** as in **c**, 1.36 vs 0.68 kcal/mol, as reported in Table 9-2. Both structures also include CH \cdots O H-bonding, but there is more of it in **c**. More precisely, the two CH \cdots O H-bonds in **c** add up to $O_{1p} \rightarrow \sigma^*(CH)$ E(2) of 2.26 kcal/mol, vs only 0.78 for the single CH \cdots O H-bond of **b**. And all three of these H-bonds are supplemented by a very significant element of charge transfer to the $\sigma^*(CH)$ from the CO π bonding orbital, 1.56 and 0.39 kcal/mol for **c** and **b**, respectively. The NBO data suggest then, that both stacked structures contain elements of both $\pi \rightarrow \pi^*$ transfer and CH \cdots O H-bonding. The former is more important in antiparallel structure **b** and the latter plays a larger role in **c**, partly because there are two such CH \cdots O H-bonds here. The interatomic distances support this distinction. The C \cdots C distance in **b** is some 0.05 Å shorter in **b** than in **c**, and the H-bonds in **c** shorter by 0.12 Å.

The decomposition of the total interaction energy into its constituent parts can aid in the analysis of the underlying differences between the minima. The components of SAPT deconstruction⁵⁶ are reported in Table 3 for the four structures of Figure 9-1. There are certain similarities amongst all four. For example, in all cases, the electrostatic term is the largest attractive component, followed by dispersion, and then by induction. But a closer examination reveals some substantive differences. In the first place, the electrostatic energy is considerably larger in the structures containing standard NH \cdots O H-bonds as compared to the stacked dimers. This pattern reverses in the case of

dispersion which is larger in the two latter geometries. In terms of patterns, the induction energy is almost as negative as dispersion in these NH··O structures, whereas the latter is two or three times larger than the former for the stacked geometries. In fact, the dispersion energy is very nearly as large as the electrostatic attraction in the stacked structures. In summary, the comparison of stacked to NH··O structures indicates a reduced electrostatic term and increased dispersion energy.

One may glean some insight into the origin of the electrostatic attraction by examination of the electrostatic potentials of each pair of monomers. These potentials are superimposed on the positions of the monomers within the context of each optimized dimer in Figure 9-2 where the blue contours represent positive regions, and negative is signified by red. The potential around the NMA monomer is largely positive in most areas, but contains a very prominent negative region that surrounds the carbonyl O atom. In all three cases, whether the NH··O H-bonded dimer **a**₁, or the stacked geometries, the negative red region of one molecule approaches a blue positive area of the partner molecule. In both **b** and **c**, the O atoms of both molecules participate in this electrostatic attraction. The more attractive electrostatic component for the H-bonded structure **a**₁ can be rationalized on the basis of the very direct interaction between positive and negative regions, as compared to the parallel arrangement in **b** and **c**. This comparison bears a certain resemblance to that between σ and π bonds.

Another window into the nature of the interaction can be opened via examination of electron density shifts that accompany dimerization. Figure 9-3 illustrates the difference in the density of each complex, with respect to the sum of the densities of the

two monomers, in the same internal geometries and positions which they adopt in the complex. Increases in density, indicated by purple regions, correspond to shifts of density into that area upon complexation; yellow areas denote decreases. The most substantial shift in complex **a**₁ occurs right along the NH··O H-bond, indicated by the broken red line. The pattern of charge shift away from the bridging proton, and into the purple regions on either side of it are characteristic of a H-bond. This same pattern is noted in the CH··O H-bonds of **b** and **c**, further bolstering the contention that these dimers are held together in part by such H-bonds.

As indicated above, the two stacked dimers are attracted to one another in part by transfer from the CO π orbital of one molecule to CO π^* of the partner, with a symmetric transfer occurring in the opposite direction. It is thus no surprise to note large shifts above and below each monomer, with very little taking place within each molecular plane of **b** and **c**. In other words, one can speak of large π shifts and very small σ shifts. There is a shift of density toward the O atoms, both above and below the molecular plane. But this increase is notably larger in the region between the two molecules. Likewise, there is a loss of density above and below the C atoms, albeit slightly smaller in magnitude than those associated with O; little change is observed near the N atoms. This pattern is what one might anticipate if the two monomers engage in $\pi(\text{CO}) \rightarrow \pi^*(\text{CO})$ charge transfers, as suggested by Table 9-2. Note also that the shifts above and below the carbonyl planes are more substantial in **b** than in **c**, again consistent with the more prominent role played by $\pi \rightarrow \pi^*$ transfers in **b**.

9-3.1. Sensitivity to Basis Set Superposition Error

In most cases in the literature, counterpoise corrections are added to a structure that has been optimized on an uncorrected surface.^{58,59} An alternate procedure, albeit a somewhat more time consuming one, performs the geometry optimization on a fully corrected potential energy surface. As such, it is normally found that the intermolecular distance is somewhat longer in the latter case, as the artificial attraction associated with basis set superposition error does not pull the two subunits too close together. But other than this small change in intermolecular separation, the minima optimized on the corrected and uncorrected surfaces are typically quite similar.

The NMA dimer represents a departure from this general observation. Significant differences in optimized geometry were noted first in the $\text{NH}\cdots\text{O}$ H-bonded complexes. The $\varphi(\text{H}\cdots\text{OCN})$ angles listed in Table 9-1 for \mathbf{a}_1 and \mathbf{a}_2 are -171° and -6° , respectively, both rather close to the placement of the bridging proton in the plane of the proton-accepting NMA molecule. In contrast, when the optimizations were performed without including counterpoise corrections at each step, the NH proton was positioned quite a bit out of this plane. Details of these structures are provided in Table 9-4, where it may be seen from the $\varphi(\text{H}\cdots\text{OCN})$ dihedral angles that the proton in question hovers between 50° and 65° above the plane of the partner amide. Because of this departure from the plane, the proton is further removed from the acceptor carbonyl O than in the planar cases of Table 9-1, despite the artificial attraction that arises from the basis set superposition error. And one might also note the greater disparity from H-bond linearity in these nonplanar structures, with $\theta(\text{NH}\cdots\text{O})$ between 137° and 155° , compared to 171° - 175° for the planar complexes. The four structures described in Table 9-4 are quite similar to one another,

differing primarily in the disposition of one molecule relative to another. Their geometries are displayed graphically in Figure 9-4 along with all other minima obtained on the uncorrected potential energy surface.

One consequence of the displacement of the NH from the carbonyl plane is a perturbation in the NBO E(2) quantity that reflects the transfer from the O lone pairs to the NH σ^* antibond. Compared to values between 12.6 and 13.8 kcal/mol in the planar geometries, this quantity drops down to between 4 and 8 kcal/mol when the H is situated above the plane of these O lone pairs. In partial compensation, a new charge transfer appears, one in which the density is removed from the CO π bonding orbital. E(2) for this $\pi(\text{CO}) \rightarrow \sigma^*\text{NH}$ transfer amounts to between 2.6 and 4.2 kcal/mol, as reported in the last column of Table 9-4.

One may conclude from the distinctions between the H-bonded structures obtained on the corrected and uncorrected potential energy surfaces that a displacement of the NH out of the amide plane of the partner molecule is not energetically costly. Indeed, it requires scrupulous correction of superposition error to place these proton donors very close to the carbonyl plane. While disturbing the charge transfer from the O lone pairs to the NH σ^* antibond, nonplanarity permits transfer from the CO π bond to take its place to a certain degree.

Failure to include counterpoise corrections in the potential energy surface also has certain consequences for the stacked structures **b** and **c**. The largest perturbation arises in the antiparallel dimer **b**, designated **b'** in Figure 9-4. Instead of the tilt between the two molecules in **b** that leads to a $\text{CH}\cdots\text{O}$ H-bond, the two molecules lie precisely parallel to one another, with both $\text{R}(\text{N}\cdots\text{C})$ distances equal to 3.710 Å. Without this tilt, the shortest

intermolecular CH \cdots O contact is 2.78 Å, beyond the range of a substantive H-bond. And indeed, there is no significant E(2) that would correspond to any such CH \cdots O H-bond. NBO analysis confirms the absence of this sort of H-bond with no significant O $\rightarrow\sigma^*$ (CH) transfer. On the other hand, the fully stacked arrangement of **b'**, as well as the closer approach of the two molecules, enhances the $\pi\rightarrow\pi^*$ charge transfer, with a combined E(2) of 2.48 kcal/mol, compared to the 1.36 kcal/mol in structure **b** where the molecules were tilted relative to one another. Structure **c'** is less distinct from **c**: The two molecules adopt essentially the same relative orientation in both. And in both cases, the R(C \cdots C) distance is shorter than R(N \cdots N) by about 0.5 Å, a tilt which facilitates formation of the two CH \cdots O H-bonds. The latter are both 2.372 Å in length in **c'**, slightly shorter than the 2.430 Å in **c**, an expected result of failure to correct the surface for basis set superposition error.

As a consequence of including the counterpoise corrections into the optimization procedure, the final structures in Figure 9-1 are significantly more stable than those in Figure 9-4. For example, dimer **a₁** is more stable by 0.63 kcal/mol than the most stable configuration in Figure 9-4 where counterpoise is corrected after the fact. **b** and **c** are both more stable than **b'** and **c'** by 0.35 kcal/mol. In these cases, then, including counterpoise correction into the optimization affects not only the geometrical dispositions, but also the energies to a significant degree.

9-3.2. Influence of C=O Dipole-Dipole Attractions

The literature contains a number of instances in which a pair of carbonyl C=O groups approach one another in what might appear to be an attractive interaction.³ Their

mutual orientation can be either parallel or perpendicular.^{1,2,17} Any such attraction has been attributed by some to simple dipole-dipole forces^{1,3,5,12} whereby the negatively charged O approaches the C of the other carbonyl which is of opposite charge. Another scenario considers $n \rightarrow \pi^*$ charge transfer from the O lone pairs to the carbonyl antibonding orbital of the other subunit.^{4,6,10,11,17} With specific regard to amide units, recent studies of di- and tripeptides in the gas phase have found occasions where a pair of peptide units are stacked above one another,¹³⁻¹⁵ as opposed to forming the normally expected $\text{NH} \cdots \text{O}$ H-bonds.

There are two minima, **b** and **c**, found by our calculations that can be described as stacked in some sense. They can be categorized as antiparallel and parallel, with binding energies of just over 6 kcal/mol, within about 2 kcal/mol of the preferred $\text{NH} \cdots \text{O}$ H-bonded structure. Although stacked, it cannot be said that the binding of either is attributable purely to $\pi \rightarrow \pi^*$ charge transfer, as both contain an essential element of $\text{CH} \cdots \text{O}$ H-bonding, more so for **c** than for **b**. At the same time, a fully parallel arrangement **b'**, with no significant H-bonding (see Figure 9-4), represents a stable minimum on the potential energy surface, albeit the surface without counterpoise corrections. And the binding energy of this dimer is only slightly less than that in **b** and **c**. So one might conclude that there is a strong theoretical basis for stacked arrangements of peptide units, whether fully parallel or tilted. Yet these structures do not show any evidence of the $n \rightarrow \pi^*$ charge transfers that have been hypothesized.

As there are no true minima in the NMA dimer surface that rely on the proposed $n \rightarrow \pi^*$ transfer as the basis of their stability, partial geometry optimizations were carried

out with some restriction to search for such a structure. The O atom of one NMA molecule was placed directly above the C of the other, and the $\theta(\text{O}\cdots\text{CO})$ angle held fixed at 90° . Such a prescription would allow the upper carbonyl to orient itself either perpendicular to the C=O below, or parallel to it. The optimization under this perpendicular sort of restriction led instead to an intermediate position, with $\theta(\text{C}\cdots\text{OC})=135^\circ$, and $R(\text{C}\cdots\text{O})=2.805 \text{ \AA}$. This orientation facilitates an interaction between a “rabbit ear” lone pair of the upper O and the C atom of the lower amide. And in fact, a NBO perturbation energy $E(2)$ of 1.64 kcal/mol was evaluated for this $\text{O}_{\text{lp}}\rightarrow\pi^*(\text{CO})$ charge transfer. This finding is consistent with the idea that such orientations can be stabilizing in peptide-peptide interactions, even if the geometry does not correspond to a true minimum on the NMA dimer surface. More quantitatively, the binding energy of this structure is only 1.71 kcal/mol, much smaller than those of the true minima, stabilized by $\text{NH}\cdots\text{O}$ or $\text{CH}\cdots\text{O}$ H-bonds and/or $\pi\rightarrow\pi^*$ charge transfer.

9-4. Conclusions and Discussion

The calculations have highlighted the minima on the potential energy surface of a pair of peptide units, each modeled by the NMA molecule. Two principal types of structure were found. The first class is stabilized by a classic $\text{NH}\cdots\text{O}$ H-bond, of the sort that is commonly considered to form between peptide units in such secondary structures as α -helices and β -sheets. The $\text{NH}\cdots\text{O}$ arrangement is very close to linear and the NH lies some 120 - 140° from the C=O axis, consonant with the idea of a pair of rabbit ear lone pairs on the O atom. The planes of the two amide groups are roughly perpendicular to one another.

There is a second type of dimer structure which is slightly less stable, with a binding energy only 23% smaller. The two amide units lie one above the other, in what may be termed a stacked configuration. The antiparallel structure places the CO of one molecule over the NH of the other, while the two CO groups lie directly above one another in the parallel arrangement, as do the two NH groups. There is only a very small energy difference between these two dimers. Part of the binding of these complexes arises from charge transfer from the CO π bonding orbital of one subunit to the antibonding $\pi^*(\text{CO})$ orbital of the other, and vice versa. A second stabilizing factor is one or more $\text{CH}\cdots\text{O}$ H-bonds. The former $\pi\rightarrow\pi^*$ transfer plays the dominant role in the antiparallel structure, while the $\text{CH}\cdots\text{O}$ H-bonds are more important in the parallel dimer. In contrast to an earlier work,¹³ there was no evidence found here of a significant transfer to the CO π^* antibonding orbital from a N lone pair, even in the antiparallel stacked structure.

For all stable dimers, there is a strong electrostatic component to the attraction, as the negative potential surrounding the carbonyl O is situated in proximity to the positive potential of the partner molecule. This electrostatic attraction is somewhat larger for the $\text{NH}\cdots\text{O}$ H-bonded dimers. Induction and dispersion forces are substantial as well, albeit smaller than Coulombic attraction. Dispersion is a bit larger than induction, especially in the stacked dimers where dispersion is nearly as large as the electrostatic component.

One of the more interesting issues that arose in this study is the surprising degree of sensitivity of the equilibrium geometries to basis set superposition error. Failure to include counterpoise corrections within the optimization algorithm distorted the $\text{NH}\cdots\text{O}$

H-bonded configurations, lifting the bridging proton and NH group well out of the plane of the proton-accepting amide unit. The reason that this distortion did not strongly affect the binding energy is that the loss of some of the $O_{ip} \rightarrow \sigma^*(NH)$ charge transfer is compensated by a new transfer into the NH σ^* antibonding orbital originating in the CO π bond. For example, the total $O_{ip} \rightarrow \sigma^*(NH)$ E(2) in dimer **a₁** is equal to 13.8 kcal/mol. This term is reduced to 8.0 kcal/mol in the distorted dimer where the NH is pulled out of the amide plane, but E(2) for the $\pi(CO) \rightarrow \sigma^*(NH)$ transfer of 3.0 kcal/mol makes up for some of this loss. One can thus conclude that the NH of one amide need not necessarily reside in the carbonyl plane, that even large displacements out of this plane incur only a small energetic cost. This idea is reinforced by IR/UV double resonance data of a capped tripeptide chain in the gas phase⁶⁰ wherein the NH was located above the peptide plane of the CO proton acceptor.

A second perturbation in structure that is associated with basis set superposition error is the tilt angle between the two amide units in the stacked structures. While the parallel dimer is not affected much, the antiparallel conformation loses its tilt when this error is uncorrected, and the two molecules become perfectly stacked. Again, this change is facilitated by compensation. The loss of the $CH \cdots O$ H-bond in the tilted true minimum is offset by an increase in the $\pi \rightarrow \pi^*$ transfer between the CO bonding and antibonding orbitals. In quantitative terms of E(2), the total in the true antiparallel, tilted minimum, arises from 1.4 kcal/mol for the $\pi \rightarrow \pi^*$ transfer plus 1.2 kcal from the $CH \cdots O$ H-bond. Although the latter is lost when the two molecules are fully stacked, the $\pi \rightarrow \pi^*$ E(2) rises to 2.5 kcal/mol. This perturbation can be taken as an indication that the notion of stacked

dimers need not be taken too literally: some tilting is enabled by formation of CH \cdots O H-bonds.

There is less evidence for the notion in the literature that there is a strong attraction between the carbonyl O of one group and the C atom of the other, in particular via a $O_{lp} \rightarrow \pi^*(CO)$ charge transfer. There is no minimum on the surface that corresponds to such an interaction. When the two groups are placed accordingly, the structures quickly shift to one of the true minima in the surface. When the O atom is forced to lie directly above the carbonyl group, which would maximize an interaction of this type, there is some attraction noted, but it is rather weak, with only 22% of the binding strength of the NH \cdots O structure which represents the global minimum on the surface. One may conclude then that there is some validity to the idea of $O_{lp} \rightarrow \pi^*(CO)$ stabilization, but this attraction is secondary to NH \cdots O H-bonding structures, as well as the stacked arrangements that are stabilized by some combination of $\pi \rightarrow \pi^*$ and CH \cdots O H-bonds.

NMA is of course only a model of the peptide unit in a full protein backbone. Nonetheless, it contains the essential elements of the peptide, which surrounds the amide group on both sides by a C atom, that corresponds to the C^α of a protein. And it is the $C^\alpha H$ of the protein backbone which could participate in the CH \cdots O H-bonds that represent a significant component in the stability of some of the stacked conformations. Yet it should be reiterated in this regard that such CH \cdots O H-bonds are not crucial to these stacked configurations, as the loss of the latter H-bond can be compensated to a large degree by a more parallel arrangement of the amides which adds to the $\pi \rightarrow \pi^*$ stabilization. And finally, there is little energetic distinction between the parallel and

antiparallel arrangements of the two amide units. Both are beneficiaries of the Coulombic attraction between the negative potential surrounding the carbonyl O of one amide and the positive regions of the other portions of the second amide unit.

It is tempting to speculate how these results might be altered if the NMA molecules were enlarged to di-, tri- or even larger oligopeptides. The first complicating issue would be the likely formation of internal H-bonds within each monomer. It is well known, for example, that dipeptides tend to form C5 and C7 conformations that contain as an essential element NH \cdots O H-bonds between adjacent peptide units.⁶¹⁻⁶³ The presence of any such internal H-bond could compete with NH \cdots O H-bonds between amide units involving a separate partner molecule. On the other hand, the formation of an internal H-bond that occupies a NH group on one amide may not interfere with the ability of the C=O on the same peptide unit to act as proton acceptor to the NH of a neighboring molecule. And indeed, such an arrangement might be anticipated to strengthen the latter intermolecular H-bond, according to the principles of H-bond cooperativity, wherein proton donation from one part of a molecule tends to strengthen proton acceptance on a neighboring segment.^{28,64,65} In fact, such positive cooperativity is a likely contributor to the stability of β -sheets containing three or more strands²³ or α -helices.^{66,67} Not only conventional NH \cdots O but also weaker CH \cdots O are subject to comparable cooperativity effects⁶⁸⁻⁷⁰ that might affect the stacked dimers in which they play some role. On the other hand, there is much less known about the positive or negative cooperativity that might arise in the stacking of multiple conjugated π systems, or concerning how the

involvement in a H-bond might affect $\pi \rightarrow \pi^*$ charge transfers. For these reasons, an exploration of larger systems represents a ripe area for future research.

References

- (1) Allen, F. H.; Baalham, C. A.; Lommerse, J. P. M.; Raithby, P. R. *Acta Cryst.* **1998**, *B54*, 320-329.
- (2) Santos-Contreras, R. J.; Martinez-Martinez, F. J.; Garcia-Baez, E. V.; Padilla-Martinez, I. I.; Peraza, A. L.; Hopfli, H. *Acta Cryst.* **2007**, *C63*, o239-o242.
- (3) Paulini, R.; Müller, K.; Diederich, F. *Angew. Chem., Int. Ed. Engl.* **2005**, *44*, 1788-1805.
- (4) DeRider, M. L.; Wilkens, S. J.; Waddell, M. J.; Bretscher, L. E.; Weinhold, F.; Raines, R. T.; Markley, J. L. *J. Am. Chem. Soc.* **2002**, *124*, 2497-2505.
- (5) Fischer, F. R.; Wood, P. A.; Allen, F. H.; Diederich, F. *Proc. Nat. Acad. Sci., USA* **2008**, *105*, 17290-17294.
- (6) Choudhary, A.; Gandla, D.; Krow, G. R.; Raines, R. T. *J. Am. Chem. Soc.* **2009**, *131*, 7244-7246.
- (7) Kotch, F. W.; Guzei, I. A.; Raines, R. T. *J. Am. Chem. Soc.* **2008**, *130*, 2952-2953.
- (8) Hodges, J. A.; Raines, R. T. *Org. Lett.* **2006**, *8*, 4695-4697.
- (9) Hinderaker, M. P.; Raines, R. T. *Protein Sci* **2003**, *12*, 1188-1194.
- (10) Bartlett, G. J.; Choudhary, A.; Raines, R. T.; Woolfson, D. N. *Nature Chem. Biol.* **2010**, *6*, 615-620.
- (11) Jakobsche, C. E.; Choudhary, A.; Miller, S. J.; Raines, R. T. *J. Am. Chem. Soc.* **2010**, *132*, 6651-6653.

- (12) Fäh, C.; Hardegger, L. A.; Ebert, M.-O.; Schweizer, W. B.; Diederich, F. *Chem. Commun.* **2010**, *46*, 67-69.
- (13) James, W. H.; Buchanan, E. G.; Muller, C. W.; Dean, J. C.; Kosenkov, D.; Slipchenko, L. V.; Guo, L.; Reidenbach, A. G.; Gellman, S. H.; Zwier, T. S. *J. Phys. Chem. A* **2011**, *115*, 13783-13798.
- (14) James, W. H.; Buchanan, E. G.; Guo, L.; Gellman, S. H.; Zwier, T. S. *J. Phys. Chem. A* **2011**, *115*, 11960-11970.
- (15) James, W. H.; Muller, C. W.; Buchanan, E. G.; Nix, M. G. D.; Guo, L.; Roskop, L.; Gordon, M. S.; Slipchenko, L. V.; Gellman, S. H.; Zwier, T. S. *J. Am. Chem. Soc.* **2009**, *131*, 14243-14245.
- (16) Buchanan, E. G.; James, W. H.; Choi, S. H.; Guo, L.; Gellman, S. H.; Müller, C. W.; Zwier, T. S. *J. Chem. Phys.* **2012**, *137*, 094301.
- (17) Pal, T. K.; Sankararamakrishnan, R. *J. Phys. Chem. B* **2010**, *114*, 1038-1049.
- (18) Scheiner, S.; Kern, C. W. *J. Am. Chem. Soc.* **1977**, *99*, 7042-7050.
- (19) Zhao, Y.-L.; Wu, Y.-D. *J. Am. Chem. Soc.* **2002**, *124*, 1570-1571.
- (20) Viswanathan, R.; Asensio, A.; Dannenberg, J. J. *J. Phys. Chem. A* **2004**, *108*, 9205-9212;.
- (21) Scheiner, S. *J. Phys. Chem. B* **2005**, *109*, 16132-16141.
- (22) Chin, W.; Piuzzi, F.; Dimicoli, I.; Mons, M. *Phys. Chem. Chem. Phys.* **2006**, *8*, 1033-1048.
- (23) Scheiner, S. *J. Phys. Chem. B* **2006**, *110*, 18670-18679.
- (24) Scheiner, S. *J. Phys. Chem. B* **2007**, *111*, 11312-11317.
- (25) Dixon, D. A.; Dobbs, K. D.; Valentini, J. J. *J. Phys. Chem.* **1994**, *98*, 13435-13439.

- (26) Mannfors, B.; Mirkin, N. G.; Palmo, K.; Krimm, S. *J. Comput. Chem.* **2001**, *22*, 1933-1943.
- (27) Frey, J. A.; Leutwyler, S. *J. Phys. Chem. A* **2006**, *110*, 12512-12518.
- (28) Esrafilii, M. D.; Behzadi, H.; Hadipour, N. L. *Theor. Chem. Acc.* **2008**, *121*, 135-146.
- (29) Sun, C.-L.; Jiang, X.-N.; Wang, C.-S. *J. Comput. Chem.* **2009**, *30*, 2567-2575.
- (30) Torii, H.; Tatsumi, T.; Kanazawa, T.; Tasumi, M. *J. Phys. Chem. B* **1998**, *102*, 309-314.
- (31) Watson, T. M.; Hirst, J. D. *J. Phys. Chem. A* **2002**, *106*, 4858-7867.
- (32) Langley, C. H.; Allinger, N. L. *J. Phys. Chem. A* **2003**, *107*, 5208-5216.
- (33) Mirzaei, M.; Hadipour, N. L. *Struct. Chem.* **2008**, *19*, 225-232.
- (34) Mathieu, S.; Trinquier, G. *Phys. Chem. Chem. Phys.* **2009**, *11*, 8183-8190.
- (35) Colominas, C.; Luque, F. J.; Orozco, M. *J. Phys. Chem. A* **1999**, *102*, 6200-6208.
- (36) Qian, W.; Mirkin, N. G.; Krimm, S. *Chem. Phys. Lett.* **1999**, *315*, 125-129.
- (37) Vargas, R.; Garza, J.; Friesner, R. A.; Stern, H.; Hay, B. P.; Dixon, D. A. *J. Phys. Chem. A* **2001**, *105*, 4963-4968.
- (38) Albrecht, M.; Rice, C. A.; Suhm, M. A. *J. Phys. Chem. A* **2008**, *112*, 7530-7542.
- (39) Deshmukh, M. M.; Gadre, S. R. *J. Phys. Chem. A* **2009**, *113*, 7927-7932.
- (40) Ham, S.; Cho, M. *J. Chem. Phys.* **2003**, *118*, 6915-6922.
- (41) Vargas, R.; Garza, J.; Dixon, D. A.; Hay, B. P. *J. Am. Chem. Soc.* **2000**, *122*, 4750-4755.
- (42) Frisch, M. J.; Trucks, G. W.; Schlegel, H. B.; Scuseria, G. E.; Robb, M. A.; Cheeseman, J. R.; Zakrzewski, V. G.; Montgomery, J., J. A.; Stratmann, R. E.;

Burant, J. C.; Dapprich, S.; Millam, J. M.; Daniels, A. D.; Kudin, K. N.; Strain, M. C.; Farkas, O.; Tomasi, J.; Barone, V.; Cossi, M.; Cammi, R.; Mennucci, B.; Pomelli, C.; Adamo, C.; Clifford, S.; Ochterski, J.; Petersson, G. A.; Ayala, P. Y.; Cui, Q.; Morokuma, K.; Malick, D. K.; Rabuck, A. D.; Raghavachari, K.; Foresman, J. B.; Cioslowski, J.; Ortiz, J. V.; Baboul, A. G.; Stefanov, B. B.; Liu, G.; Liashenko, A.; Piskorz, P.; Komaromi, I.; Gomperts, R.; Martin, R. L.; Fox, D. J.; Keith, T.; Al-Laham, M. A.; Peng, C. Y.; Nanayakkara, A.; Gonzalez, C.; Challacombe, M.; Gill, P. M. W.; Johnson, B.; Chen, W.; Wong, M. W.; Andres, J. L.; Gonzalez, C.; Head-Gordon, M.; Replogle, E. S.; Pople, J. A. Gaussian 09; Revision B.01 ed. Wallingford, CT, 2009.

- (43) Hyla-Kryspin, I.; Haufe, G.; Grimme, S. *Chem. Phys.* **2008**, *346*, 224-236.
- (44) Pedzisa, L.; Hay, B. P. *J. Org. Chem.* **2009**, *74*, 2554-2560.
- (45) Singh, P. C. *Chem. Phys. Lett.* **2011**, *515*, 206-209.
- (46) Li, H.; Lu, Y.; Liu, Y.; Zhu, X.; Liu, H.; Zhu, W. *Phys. Chem. Chem. Phys.* **2012**, *14*, 9948-9955.
- (47) Riley, K. E.; Murray, J. S.; Fanfrlík, J.; Rezáč, J.; Solá, R. J.; Concha, M. C.; Ramos, F. M.; Politzer, P. *J. Mol. Model.* **2011**, *17*, 3309-3318.
- (48) Hauchecorne, D.; Nagels, N.; Veken, B. J. v. d.; Herrebout, W. A. *Phys. Chem. Chem. Phys.* **2012**, *14*, 681-690.
- (49) Lu, Y.; Liu, Y.; Li, H.; Zhu, X.; Liu, H.; Zhu, W. *J. Phys. Chem. A* **2012**, *116*, 2591-2597.
- (50) Scheiner, S. *J. Phys. Chem. A* **2011**, *115*, 11202-11209.

- (51) Zhao, Q.; Feng, D.; Sun, Y.; Hao, J.; Cai, Z. *Int. J. Quantum Chem.* **2011**, *111*, 3881-3887.
- (52) Munusamy, E.; Sedlak, R.; Hobza, P. *ChemPhysChem.* **2011**, *12*, 3253-3261.
- (53) Boys, S. F.; Bernardi, F. *Mol. Phys.* **1970**, *19*, 553-566.
- (54) Reed, A. E.; Weinhold, F.; Curtiss, L. A.; Pochatko, D. J. *J. Chem. Phys.* **1986**, *84*, 5687-5705.
- (55) Reed, A. E.; Curtiss, L. A.; Weinhold, F. *Chem. Rev.* **1988**, *88*, 899-926.
- (56) Moszynski, R.; Wormer, P. E. S.; Jeziorski, B.; van der Avoird, A. *J. Chem. Phys.* **1995**, *103*, 8058-8074.
- (57) Werner, H.-J.; Knowles, P. J.; Manby, F. R.; Schütz, M.; P. Celani; Knizia, G.; Korona, T.; Lindh, R.; Mitrushenkov, A.; Rauhut, G.; Adler, T. B.; Amos, R. D.; Bernhardsson, A.; Berning, A.; Cooper, D. L.; Deegan, M. J. O.; Dobbyn, A. J.; Eckert, F.; Goll, E.; Hampel, C.; Hesselmann, A.; G. Hetzer; Hrenar, T.; Jansen, G.; Köppl, C.; Liu, Y.; Lloyd, A. W.; Mata, R. A.; May, A. J.; McNicholas, S. J.; Meyer, W.; Mura, M. E.; Nicklaß, A.; Palmieri, P.; Pflüger, K.; Pitzer, R.; Reiher, M.; Shiozaki, T.; Stoll, H.; Stone, A. J.; Tarroni, R.; Thorsteinsson, T.; Wang, M.; Wolf, A. MOLPRO; Version 2006 ed., 2010.
- (58) Gu, Y.; Kar, T.; Scheiner, S. *J. Mol. Struct.* **2000**, *552*, 17-31.
- (59) Kryachko, E.; Scheiner, S. *J. Phys. Chem. A* **2004**, *108*, 2527-2535.
- (60) Brenner, V.; Piuze, F.; Dimicoli, I.; Tardivel, B.; Mons, M. *J. Phys. Chem. A* **2007**, *111*, 7347-7354.
- (61) Scheiner, S. *Int. J. Quantum Chem.* **2010**, *110*, 2775-2783.
- (62) Scheiner, S. *J. Phys. Chem. B* **2009**, *113*, 10421-10427.

- (63) Scheiner, S.; Kar, T. *J. Mol. Struct.* **2007**, *844-845*, 166-172.
- (64) Tan, H.; Qu, W.; Chen, G.; Liu, R. *J. Phys. Chem. A* **2005**, *109*, 6303-6308.
- (65) Kobko, N.; Dannenberg, J. J. *J. Phys. Chem. A* **2003**, *107*, 10389-10395.
- (66) Wieczorek, R.; Dannenberg, J. J. *J. Am. Chem. Soc.* **2003**, *125*, 8124-8129.
- (67) Ireta, J.; Neugebauer, J.; Scheffler, M.; Rojo, A.; Galvan, M. *J. Phys. Chem. B* **2003**, *107*, 1432-1437.
- (68) Scheiner, S. *J. Mol. Struct.* **2010**, *976*, 49-55.
- (69) Kar, T.; Scheiner, S. *Int. J. Quantum Chem.* **2006**, *106*, 843-851.
- (70) Kar, T.; Scheiner, S. *J. Phys. Chem. A* **2004**, *108*, 9161-9168.

Table 9-1. Geometric and energetic (kcal/mol) aspects of NH••O H-bonded dimers.

ΔE	a₁ 7.91	a₂ 7.88
R(H•••O), Å	1.971	1.977
θ (NH•••O), degs	171	175
θ (CO•••H), degs	120	142
ϕ (H•••OCN), degs	-171	-6
ϕ (CN•••OC), degs	-76	-77
E(2) O _{1p} → σ^* NH	13.82	12.56

Table 9-2. Geometric and energetic (kcal/mol) aspects of stacked dimers.

ΔE	b 6.13	c 6.06
R(C•••C), Å	3.370	3.425
E(2) π (CO)→ π^* (CO)	1.36	0.68
R(H•••O), Å	2.552	2.430
E(2) O _{1p} → σ^* (CH)	0.78	2.26
R(H•••C), Å	3.298	3.122
E(2) π (CO)→ σ^* (CH)	0.39	1.56

Table 9-3. SAPT contributions (kcal/mol) to total interaction energies of NMA dimers.

	NH•••O		stacked	
	a₁	a₂	b	c
ES	-11.25	-10.46	-8.02	-7.41
EX	9.39	8.51	7.20	7.32
IND	-4.23	-3.69	-3.44	-2.87
IND+EXIND	-2.10	-1.97	-1.38	-1.34
DISP	-5.33	-5.38	-7.01	-6.82
DISP+EXDISP	-4.54	-4.66	-6.13	-6.00
total	-8.50	-8.58	-8.33	-7.44

Table 9-4. Geometric and energetic aspects of NH••O dimers obtained without inclusion of counterpoise corrections in optimization algorithm.

ΔE^a	$r(\text{H}\cdots\text{O})$	$\theta(\text{NH}\cdots\text{O})$	$\varphi(\text{H}\cdots\text{OCN})$	$\text{O}_{1p}\rightarrow\sigma^*\text{NH}$	$r(\text{H}\cdots\text{C})$	$\pi(\text{CO})\rightarrow\sigma^*\text{NH}$
Kcal/mol	Å	degs	degs	E(2), kcal/mol	Å	E(2), kcal/mol
7.28	1.985	155	-56	7.95	2.759	3.01
7.01	2.030	149	130	6.84	2.667	2.57
6.90	1.999	148	65	5.85	2.606	4.24
6.47	2.088	137	116	4.02	2.671	2.80

^a:including counterpoise correction after optimization

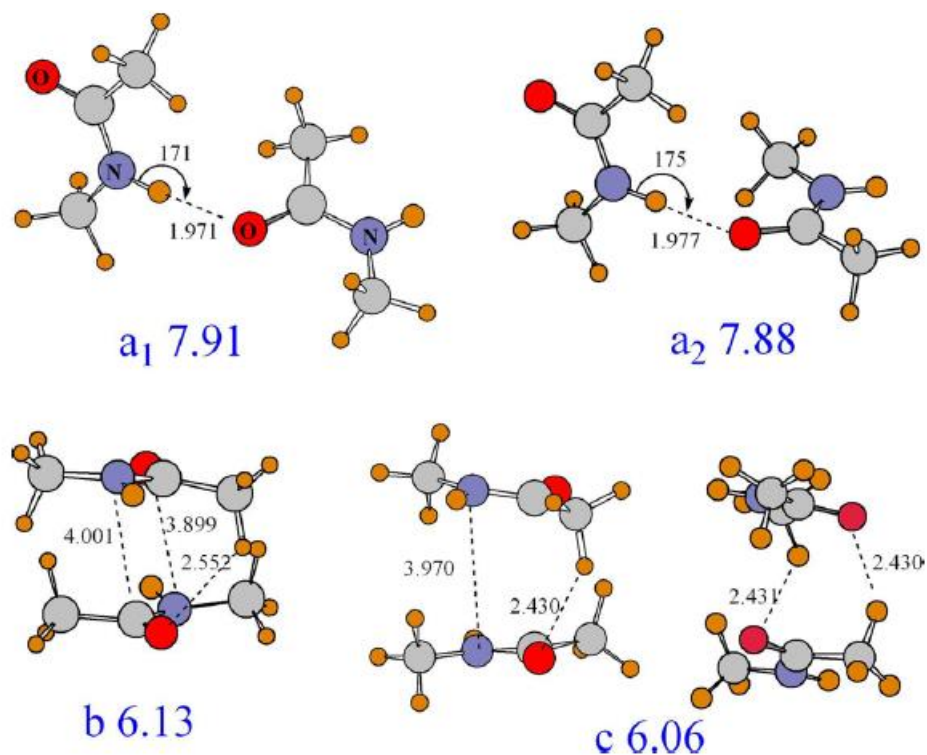


Figure 9-1. Geometrical dispositions of two NMA molecules in fully optimized dimers, with counterpoise corrections included in the optimization algorithm. Binding energies reported as large blue numbers; distances in Å and angles in degs. Two views are presented of dimer c so as to view both CH••O H-bonds.

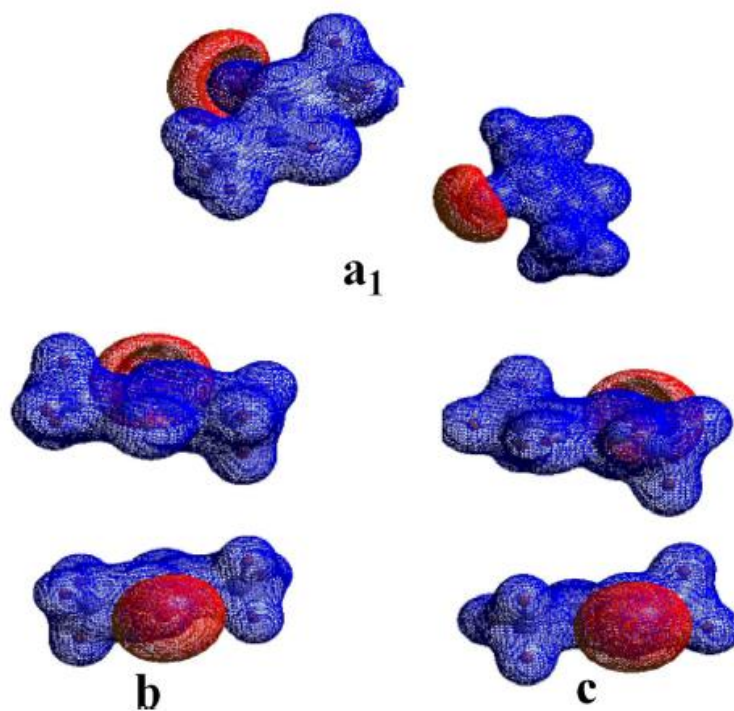


Figure 9-2. Electrostatic potentials of two NMA subunits in each of three different dimers. Blue regions correspond to positive potential, negative to red. Contour illustrated is 0.08 au.

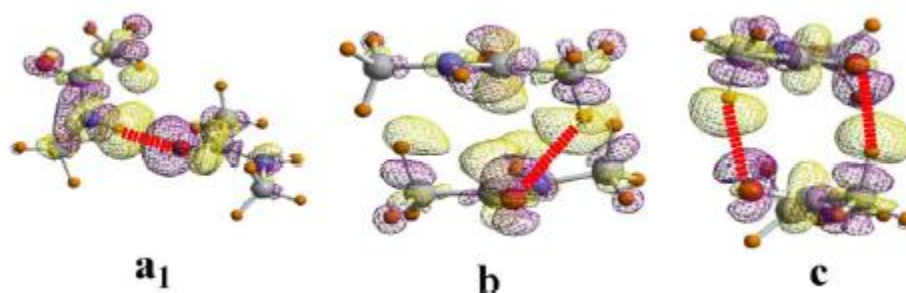


Figure 9-3. Shifts of electron density occurring in three NMA dimers. Purple regions denote added density, losses are shown in yellow. Contour illustrated is 0.0008 au. H-bonds are indicated by broken red line.

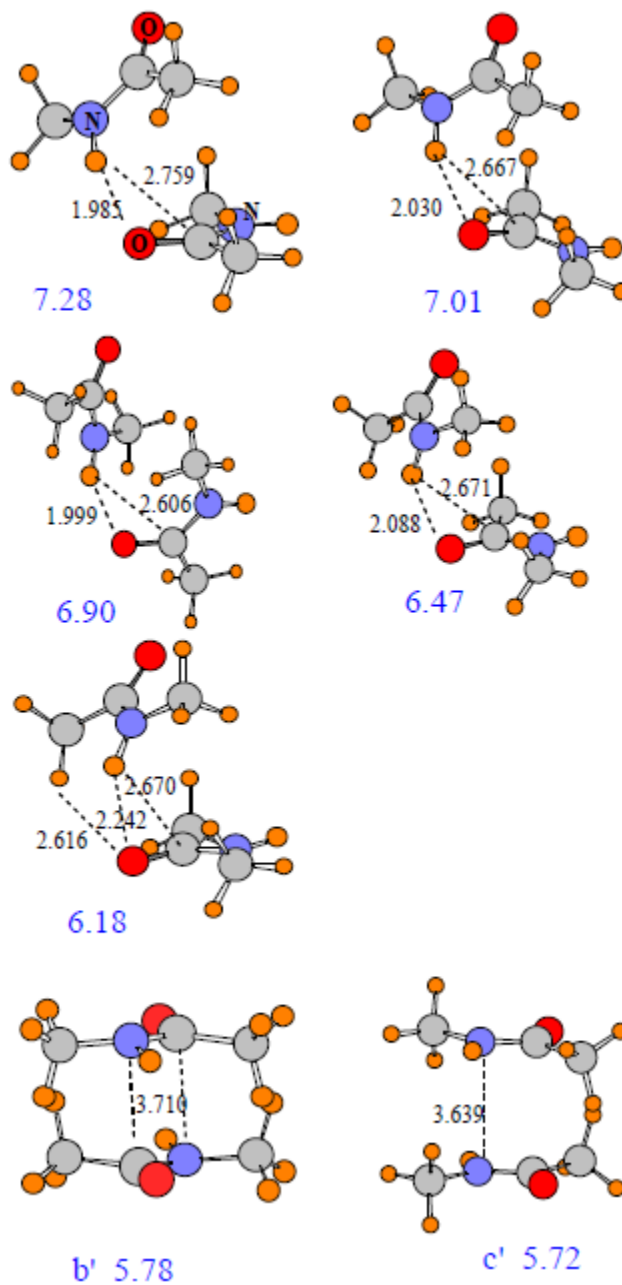


Figure 9-4. Geometrical dispositions of two NMA molecules in fully optimized dimers, with counterpoise corrections not included in the optimization algorithm. Binding energies, corrected for basis set superposition error, reported as large blue numbers; distances in Å and angles in degs.

CHAPTER 10
FIRST STEPS IN GROWTH OF A POLYPEPTIDE TOWARD β -SHEET
STRUCTURE¹

Abstract

The full conformational energy surface is examined for a molecule in which a dipeptide is attached to the same spacer group as another peptide chain, so as to model the seminal steps of β -sheet formation. This surface is compared with the geometrical preferences of the isolated dipeptide so as to extract the perturbations induced by interactions with the second peptide strand. These inter-peptide interactions remove any tendency of the dipeptide to form a C5 ring structure, one of its two normally stable geometries. A C7 structure, the preferred conformation of the isolated dipeptide, remains as the global minimum in the full molecule. However, the stability of this structure is highly dependent upon inter-peptide H-bonds with the second chain. The latter forces include not only the usual NH \cdots O interaction, but also a pair of CH \cdots O H-bonds. The secondary minimum is also of C7 type, and likewise depends in part upon CH \cdots O H-bonds for its stability. The latter interactions also play a part in the tertiary minimum. A two-strand β -sheet structure is not yet in evidence for this small model system, requiring additional peptide units to be added to each chain.

¹ Coauthored by Upendra Adhikari and Steve Scheiner. Reproduced with permission from *J. Phys. Chem. B* **2013**, *117*, 11575-11583. Copyright 2013, American Chemical Society.

10-1. Introduction

The three-dimensional structure adopted by proteins rests on a variety of different structural and energetic factors. In the first place, each residue has a different dependence upon internal rotations ϕ and ψ around the C^α atom, represented by its characteristic Ramachandran plot. There are also important interactions between non-adjacent residues that help the protein fold up into its native conformation. Probably the most well-known of the latter class are the inter-residue H-bonds. These H-bonds include not only peptide-peptide $NH\cdots O$ H-bonds, but also those that involve the polar sidechains of certain residues. A range of newer, and usually weaker, interactions have gained some attention in recent years, such as those involving the π systems of aromatic systems,¹⁻⁸ which also contribute to protein structure. Within the context of H-bonds, the ability of CH to act as proton donor has been clearly established,⁹⁻¹⁹ but there is lingering discussion concerning the ability of $CH\cdots O$ H-bonds to influence the structure of proteins.

Horowitz and Trievel have recently²⁰ summarized some of the strongest evidence to date concerning the ability of $CH\cdots O$ H-bonds to influence the structure and function of biological systems, which updates some of the earliest such compilations in this direction.²¹⁻²⁹ The combined work has catalogued such H-bonds that involve for example the $C^\alpha H$ of the backbone within the context of β -sheets.³⁰⁻³⁶ Certain residue sidechains³⁷⁻⁴⁰ are clearly involved as well, e.g. His.^{41,42} Much of the earlier work has since been verified by very high-resolution crystal structures, and NMR data, to the point where $CH\cdots O$ H-bonds can be considered “highly prevalent in protein structure.”²⁰ These interactions serve more than a simple structural role, at times participating in enzyme catalysis.^{41,43,44}

Given the complexity of proteins, and the multitude of forces that participate in their final three-dimensional structure, it is far from simple to elucidate the contribution of one specific interaction, and how the structure might differ in its absence. This problem has led to the synthesis and analysis of a number of organic systems that contain both apparent CH \cdots O bonds and some of the elements of a full protein, but which are more conducive to detailed study of individual interactions by virtue of their smaller size^{13,15,17,18,45-49} The Smith group in particular has constructed molecules⁵⁰⁻⁵³ that contain species by which the ability of a CH \cdots O H-bond to contribute to the beginnings of β -sheet structure in a protein may be tested.

A recent work in particular⁵⁴ applied a hybrid combination of computations, along with a variety of experimental measurements, to demonstrate that CH \cdots O H-bonds are potent enough to override the normal trans-planar conformational preferences of α -fluoroamide substituents, within the context of molecules that contain the seeds of interpeptide interactions within a protein β -sheet. First by direct calculation, and also by comparison with analogous molecules without such CH \cdots O H-bonds, the calculations estimated the strength of the interaction to lie in the neighborhood of 3-4 kcal/mol. Perhaps more to the point, both the computations and diffraction structures found geometries that would not occur were there no attractive CH \cdots O H-bond. This finding is quite consistent with prior direct calculations⁵⁵ of the β -sheet which found comparable energetics of interstrand NH \cdots O and CH \cdots O H-bonds, results which were confirmed by ensuing computations.⁵⁶⁻⁵⁹

At this point, then, there appears to be compelling evidence that CH \cdots O H-bonds can influence the preferred geometry of certain systems, in particular those that bear a

resemblance to β -sheet structure in proteins. There are also computational assessments of the energy of such bonds, in comparison to $\text{NH}\cdots\text{O}$. The question remains, however, as to just how these H-bonds might influence the structure during the process during which a β -sheet is being formed. In order to address this issue, the skeleton of a two-strand β -sheet is built by tethering both strands to a spacing unit that allows appropriate flexibility. This spacing unit is chosen not only to provide the proper positioning of the two strands, but also to maximize its similarity to molecules that have been examined experimentally, which will facilitate the checking of the results once the molecule is synthesized and exposed to diffraction and spectrometric analysis.

More specifically, the molecule to be examined here is illustrated in Figure 10-1 where it may be noted that it is composed of two strands. The upper chain contains a pair of peptide units bracketing a CH_2 group, as would occur for the Gly residue within a protein. The lower chain places a peptide unit between two C atoms, again simulating a very short protein chain. The two segments are connected via a phenyl ring and an ether linkage leading down to the lower chain, similar to molecules that have been previously synthesized and studied.⁵⁰⁻⁵³ This system can be considered as the very first stage of “zipping up” a β -sheet from one end to the other. Does this pair of peptide strands begin to form a β -sheet even at this very early stage, or are more peptide units required? How does the presence of the lower peptide chain influence the structure of the upper dipeptide? Analysis can also determine whether the interstrand interactions are dominated by conventional $\text{NH}\cdots\text{O}$ H-bonds, or if there is some influence by potential $\text{CH}\cdots\text{O}$ H-bonds or perhaps some other attractive forces.

10-2. Computational Methods

Calculations were carried out via the Gaussian 09 package⁶⁰ using the M06-2X variant of density functional theory⁶¹ with a 6-31+G** basis set. This approach was devised in part so as to better characterize intermolecular interactions of the sort being considered here, and has enjoyed good success in the past.^{14,62-71} The DFT calculations utilized the finegrid option, which is a pruned (75,302) one, specifically 75 radial shells and 302 angular points per shell, which amounts to about 7000 points for each atom. Natural bond orbital (NBO) calculations^{72,73} to assess intermolecular interactions were carried out using the analysis routines within the Gaussian program.

10-3. Results

The most important dihedral angles of the subject molecule I are illustrated in Figure 10-1a, where ϕ and ψ have their usual meanings in the context of proteins, dealing with rotations about the CH₂ group that lies between a pair of amide units. The orientation of the peptide unit in the lower chain is primarily controlled by the CCNC dihedral angle denoted χ_1 in Figure 10-1a. A rotation around this C-N bond can reorient the lower chain from a position where its O atom can form a NH \cdots O H-bond with the first upper peptide (1a, with χ_1 in the vicinity of -90°) to one in which the NH group of the lower peptide interacts with the C=O of the second upper peptide, as in Figure 10-1b, where χ_1 is in the $+75^\circ$ range.

The rotational profile of molecule I is presented as a function of dihedral angle ψ by the solid curve in Figure 10-2. This curve was generated by choosing a regular set of ψ angles, with 30° increments, between 0° and 360° . For each value of ψ , the remainder

of the molecular geometry was optimized. Since the various bond rotations can generate a number of local minima, optimizations were run for a variety of different starting values of φ and χ_1 , as well as certain other dihedral angles. The lowest-energy minimum was taken as the global minimum for a given ψ angle, and it is that energy which is plotted as the solid curve in Figure 10-2.

To be more specific, it was considered important to sample the full conformational space of the molecule, so as to be sure that all minima, local as well as global, were identified. Multiple minima are most likely associated with rotations around single bonds so this issue was of paramount concern. It was thus necessary to begin optimizations from a variety of starting points. First of all, peptide units were assumed to adopt their trans conformations, so geometry optimizations began with $\varphi(\text{OCNH})$ dihedral angles equal to 180° , although this angle was subject to change as a result of geometry optimization. As stated above, separate potential energy surfaces were generated for the CO-up and NH-up configurations of the lower peptide, which corresponded to geometry optimizations starting with $\chi_1 = -90^\circ$, and $\chi_1 = +75^\circ$, although this angle was of course allowed to freely change during the optimization. Multiple orientations of the terminal methyl groups were also adopted so as to ensure obtaining the lowest possible energy, as were multiple values of the $\varphi(\text{OCCN})$ and $\varphi(\text{COCC})$ dihedral angles in the lower chain. Four different starting points for the φ angle in Figure 10-1 were considered for each possible structure, again to be sure no minimum on the surface was overlooked. Altogether, geometry optimizations were carried out for nearly 200 different starting points, in each case holding fixed only the single parameter, ψ . The solid rotational profile for the model molecule I may be compared with the dashed line in

Figure 10-2, which represents the profile of the upper chain of I, the dipeptide $\text{NH}_2\text{COCH}_2\text{NHCOCH}_3$. The most stable structure of this simple dipeptide, illustrated in Fig 3a, occurs at $\psi=300^\circ$ (and its symmetrical equivalent at $\psi=60^\circ$) where its dominant feature is a C7 ring, encompassing a $\text{NH}\cdots\text{O}$ H-bond between H_{N1} and O_2 . A secondary minimum, about 1 kcal/mol higher in energy, is present at $\psi=180^\circ$, which is dominated by a C5 H-bond between H_{N2} and O_1 , as shown in Figure 10-3b. The energy barrier which the $\text{C5}\rightarrow\text{C7}$ pathway must traverse is roughly 1.3 kcal/mol, while a barrier of nearly 3 kcal/mol at $\psi=0^\circ$ impedes the interconversion between the two symmetric C7 structures at $\psi=60^\circ$ and 300° .

Comparison of the solid and dashed curves highlights some important perturbations caused by the presence of the lower peptide unit in full molecule I. The C7 minimum at $\psi=300^\circ$ remains intact, and retains its status as the global minimum. There is a secondary minimum at $\psi=60^\circ$, corresponding to the second C7 structure, but the absence of symmetry in I raises the energy of this configuration by nearly 1 kcal/mol relative to the global minimum. A more profound perturbation occurs at $\psi=180^\circ$ where the C5 minimum in the fragment is raised in energy, to the point where it becomes the highest-energy structure in the entire range. (In fact, as detailed below, the 180° geometry does not contain a C5 $\text{NH}\cdots\text{O}$ H-bond at all.) The other secondary minimum, only slightly higher than that at 60° , occurs at $\psi=150^\circ$. This displacement from $\psi=180^\circ$ in the fragment to 150° in the full I represents more than a slight rearrangement of the C5 fragment, encompassing an entirely new structure as described in greater detail below. Another strong perturbation is associated with $\psi=0^\circ$. The transition state for $\text{C7}\rightarrow\text{C7}'$ interconversion in the smaller fragment, represents a barrier no longer in the larger

molecule. This barrier is shifted over to $\psi=30^\circ$, and is significantly lowered, along with substantial changes in geometry.

The reader may have noticed that the solid curve in Figure 10-2 is blue for the $30^\circ < \psi < 270^\circ$ range, and is red elsewhere. The two colors indicate the orientation of the lower peptide of Figure 10-1. Red is used to indicate values of ψ for which the lowest energy geometry points the carbonyl O atom up toward the upper segment, as in Figure 10-1a, whereas conformations that orient the NH group toward the upper chain (10-1b) are indicated in blue. In other words, the participation in a H-bond by the lower peptide as proton acceptor is indicated by red, and as a donor by blue. It is fair to wonder why the molecule should reverse its preference partway through the ψ rotational profile. Why should it prefer CO up for some values of ψ and NH up for others?

10-3.1. Individual Rotational Profiles

In order to answer this question, rotational profiles were generated separately for structures 10-1a (CO up) and 10-1b (NH up). The solid red curve in Figure 10-4b presents the energy as a function of ψ for the entire molecule I, wherein the lower segment maintains its carbonyl O pointed up, even when that is not the lower energy structure. Again for reference, the rotational profile of the upper dipeptide segment by itself is illustrated by the broken curve in Figure 10-4a. Certain issues are particularly noticeable. For one thing, the C7 minimum at $\psi=300^\circ$ is intact in Figure 10-4b, but the other C7 minimum at $\psi=60^\circ$ is very shallow, almost entirely vanished. Indeed, the geometry of this structure does not have a C7 H-bond at all (see below). The C5 minimum at $\psi=180^\circ$ has in fact disappeared, shifted over by 30° to 210° . But both the

latter, and the $\psi=60^\circ$ minimum are much less stable than the $\psi=300^\circ$ conformation, by nearly 3 kcal/mol. The maximum at $\psi=240^\circ$ of the dipeptide remains, and is in fact doubled in height, as is the barrier at $\psi=120^\circ$ which is shifted over toward $\psi=90^\circ$.

There are a number of factors that must be considered in order to understand these perturbations. First and foremost is the interaction between the upper dipeptide chain and the lower peptide unit. This interaction is dominated, but not completely so, by the $\text{NH}\cdots\text{O}$ H-bond indicated in Figure 10-1a. The interaction energy between this pair of components was estimated by taking each geometry of the full molecule in Figure 10-4b, and removing the intervening groups. That is, the phenyl group was deleted, as was the connecting OCH_2CH_2 , leaving only the upper $\text{NH}_2\text{COCH}_2\text{NHCOCCH}_3$ and the lower $\text{CH}_3\text{NHCOCCH}_3$, in precisely the same geometries as they adopt in the full molecule I. The interaction energy between these two separate molecules was then computed as E_{int} .

A second factor relates to the internal geometries of the upper and lower segments. Taking the upper peptide segment as an illustration, the ϕ angle in the full molecule I is not necessarily equal to, or even close to, its value when the isolated upper segment is fully optimized. For example, when $\psi=180^\circ$, the lowest energy structure of the upper segment $\text{H}_2\text{COCH}_2\text{NHCOCCH}_3$ has $\phi=-179^\circ$, which enables the formation of the C5 $\text{NH}\cdots\text{O}$ H-bond. But in the full molecule I, when $\psi=180^\circ$, any advantage of a C5 intrapeptide H-bond is outweighed by the stability offered by interpeptide H-bonds with the lower segment, leading to an optimized ϕ of 78° . In order to adopt the latter conformation, the upper segment must overcome an internal "distortion energy," representing the energy difference of $\phi=78^\circ$, versus its natural minimum at $\phi=-179^\circ$ which would include the C5 minimum. This big difference in ϕ does not occur over the

entire range of ψ , but only at a few select angles, notably $150^\circ < \psi < 210^\circ$, as well as at $\psi = \pm 30^\circ$, so it is only here that this distortion energy must be accounted for. (There is also distortion energy within the lower segment of I, with a similar origin.)

The broken red curve of Figure 10-4c represents the total of the two aforementioned factors, the intersegment interaction energy plus the distortion energy, as a function of dihedral angle ψ . These two factors are most stabilizing (most negative values) in the vicinity of $\psi = 0$, where there is a particularly strong interpeptide $\text{NH}\cdots\text{O}$ H-bond, with $R(\text{H}\cdots\text{O}) = 2.08 \text{ \AA}$. Another value of ψ for which the interpeptide interactions are highly stabilizing occurs at 210° , containing a short 2.07 \AA $\text{NH}\cdots\text{O}$ H-bond, augmented by a pair of fairly strong $\text{CH}\cdots\text{O}$ H-bonds, with $R(\text{H}\cdots\text{O}) \sim 2.3 \text{ \AA}$. The interpeptide attractions that occur at the third minimum in Figure 10-4c, $\psi = 300^\circ$, represent a combination of $\text{NH}\cdots\text{O}$ and $\text{CH}\cdots\text{O}$ H-bonds, none of which are shorter than 2.3 \AA .

When these two factors are added to the rotational profile of the upper peptide fragment in Figure 10-4a, one obtains the profile illustrated in Figure 10-4d. It is readily apparent that the overall shape of this curve is quite similar to that of the (red) actual calculated energy of the full molecule I in Figure 10-4b. Both curves show a global minimum at $\psi = 300^\circ$, and a secondary minimum at $\psi = 210^\circ$, separated by a maximum at $\psi = 240^\circ$. In summary, then, one can account for some of the initially surprising aspects of the rotational profile of molecule I by simply adding the interpeptide interaction energy and the internal distortion energies to the intrinsic profile of the upper segment dipeptide molecule.

The same procedure was followed for the case where the NH group of the lower segment points up toward the upper dipeptide, and the comparable results displayed in Figure 10-5. The interaction energies (plus distortion energies) in Figure 10-5c are especially strong in the $120^\circ < \psi < 180^\circ$ region, which is attributed to a particularly short interpeptide NH \cdots O H-bond of 1.93-2.01 Å. The interpeptide interaction is quite weak in the vicinity of $\psi=330^\circ$. Although the sum of dipeptide molecule, interpeptide and distortion energies (Figure 10-5d) does not superimpose quite as readily on the actual profile of the full molecule I (Figure 10-5b), there are strong similarities nonetheless. The region around $\psi=150^\circ$ is of low energy in either case, and minima are present for $\psi=60^\circ$ and 300° (C7 regions). The peak in the energy at $\psi=330^\circ$ can be understood on the basis of the weak interpeptide interactions in this conformation (cf. Figure 10-5c).

10-3.2 Explanation

We are now in a position to understand the basis of the full rotational profile of I illustrated in Figure 10-2. The lowest energy structure is plotted for the full molecule I, regardless of whether the lower segment has the CO or NH group up. The red color in Figure 10-2 indicates that it is the CO-up structure that is the more stable of the two at a given value of ψ , while the lower energy of NH-up is designated by the blue color. In summary, the CO-up conformation is more stable for $270^\circ < \psi < 360^\circ$, while NH-up is preferred over the remainder of the ψ range.

Some of the more important structures are illustrated in Figure 10-6. The global minimum in Figure 10-6a contains first of all an internal C7 NH \cdots O H-bond of length 2.06 Å. One may obtain a rough estimate of the interaction energy of a H-bond such as

this via the NBO E(2) perturbation energy. This quantity is equal to 6.83 kcal/mol for the $O_{lp} \rightarrow \sigma^*(NH)$ charge transfer, and is supplemented by a $\pi(CO) \rightarrow \sigma^*(NH)$ contribution of 3.19 kcal/mol. Importantly, there is a very substantial *interpeptide* interaction energy for this structure of 10.47 kcal/mol. A chief contributor to this force is a pair of $CH \cdots O$ H-bonds, of lengths 2.42 and 2.48 Å, with respective NBO measures of attraction of E(2) 1.95 and 1.87 kcal/mol. The interpeptide $NH \cdots O$ H-bond would appear to be somewhat weaker. Even though $R(H \cdots O)$ is fairly short at 2.33 Å, the H-bond is far from linear, with $\theta(NH \cdots O) = 113^\circ$, and with E(2) of only 1.57 kcal/mol. It is worth comparing this global minimum with the other structure with $\psi = 300^\circ$ and a C7 internal H-bond, that with NH up instead of CO. Even though this conformation contains a strong interpeptide $NH \cdots O$ H-bond, with $R(H \cdots O)$ 2.01 Å, and E(2) = 12.52 kcal/mol, it lies 1.0 kcal/mol higher in energy than the global minimum in Figure 10-6a. One might thus attribute the greater stability of the CO-up structure to its $CH \cdots O$ H-bonds.

Another revealing point of comparison arises from the structure in Figure 10-6b with $\psi = 60^\circ$, also containing an intrapeptide C7 H-bond, and representing a second minimum in the full rotational profile. This conformation includes a single interpeptide $NH \cdots O$ H-bond, and a rather strong one at that, with $R(H \cdots O) = 1.97$ Å and E(2) = 13.74 kcal/mol. But again, this single $NH \cdots O$ H-bond results in a structure that is higher in energy than that in Figure 10-6a which contains two $CH \cdots O$ H-bonds, again by 1 kcal/mol. One may conclude that the pair of strong $CH \cdots O$ H-bonds in this molecule can compete effectively even with a strong $NH \cdots O$ H-bond.

The other minimum in the rotational profile of I occurs at $\psi = 150^\circ$. Like the 180° minimum in the small dipeptide profile, this structure in Figure 10-6c contains what

might appear at first sight to be an intrapeptide C5 NH··O H-bond. However, with $R(\text{H}\cdots\text{O})$ fairly long at 2.93 Å, such a bond would be quite weak, which is confirmed by an $E(2)$ of less than 0.5 kcal/mol. It might thus be misleading to characterize this minimum as a mere perturbation of the original C5 minimum in the dipeptide. Its stability is based instead on purely interpeptide interactions, primarily a NH··O H-bond of length 2.00 Å and with $E(2)=13.62$ kcal/mol. The next most important interaction would appear to be a H-bond connecting the NH donor of the upper dipeptide with the N atom of the lower. With $R(\text{NH}\cdots\text{N})=2.55$ Å and $E(2)=2.13$ kcal/mol, this bond represents a significant contribution. Finally, there is a CH··O H-bond, with $R(\text{H}\cdots\text{O})=2.49$ Å and $E(2)=0.92$ kcal/mol. It should be noted as well that, in order to adopt a configuration amenable to this interpeptide attraction, the ϕ angle of the upper dipeptide in 10-6c must change from the -170° in the small dipeptide molecule to -65° in the full molecule I, which encompasses an internal distortion energy of 0.8 kcal/mol. The strain energy in the lower segment is even larger, 1.4 kcal/mol. In other words, the interpeptide attraction is strong enough to force a total distortion energy of 2.2 kcal/mol, and yet remain a minimum in the rotational profile.

It might be noted that whereas $\psi=180^\circ$ represents a minimum in the profile of the small dipeptide segment, that same dihedral angle corresponds to the highest energy structure in the entire rotational profile of the full molecule I. It is immediately clear that this conformation in Figure 10-6d does not include anything resembling a C5 NH··O H-bond. Instead, the most significant contribution to its stability resides in an interpeptide NH··O H-bond, with length 2.01 Å and $E(2)=12.94$ kcal/mol. Part of the instability of this structure arises from the distortion energy imposed on its upper dipeptide segment of

2.3 kcal/mol in order to achieve a conformation amenable to this NH··O H-bond. In other words, in the small dipeptide molecule ϕ would be 180° when $\psi=180^\circ$. But ϕ readjusts to 68° in the full molecule, costing the system 2.3 kcal/mol. From a broader perspective, the C5 H-bond is the prime contributor to the minimum in the simple dipeptide. But this intrapeptide H-bond cannot be sustained in larger molecules where it is supplanted by interpeptide attractions, and the cost of breaking the intrapeptide H-bond raises the energy of the entire system.

10-4. Discussion

It is now possible to both summarize the overall effects of the presence of the lower peptide group upon the conformational profile of the upper dipeptide, and also account for these effects via fundamental principles. The preference of the dipeptide for a geometry that encompasses a C7 NH··O H-bond is left unaltered, with a global minimum occurring at $\psi=300^\circ$ in either case (and with $\phi=83^\circ$ in both systems). However, in order to retain this privileged status as structure of lowest energy, under competition from other geometries with a very substantial interpeptide NH··O H-bond, the global minimum relies upon a pair of CH··O H-bonds to supplement the weaker, highly angularly distorted NH··O interpeptide interaction. This geometry has a ψ angle quite close to that of the standard α -helix in the Ramachandran plot, that occurs at $(-58^\circ, -50^\circ)$. However, its ϕ angle of 83° is significantly distant from that of the α -helix at roughly -58° . So one might conclude that the presence of the lower peptide in I is insufficient to stimulate the adoption of an α -helical conformation in the dipeptide. This failure is not surprising since

the α -helical structure is stabilized by H-bonds between residues further separated along its chain than are possible in a dipeptide.

The second most stable minimum of the full molecule I is also of C7 type. In addition to the intrapeptide C7 H-bond, it contains a strong interpeptide NH \cdots O H-bond, with $R(\text{H}\cdots\text{O})=1.97 \text{ \AA}$, and with $\theta(\text{NH}\cdots\text{O})$ nearly linear at 163° . Nonetheless, the stability conferred by this latter interaction appears to be weaker than the $\psi=300^\circ$ minimum, relying upon CH \cdots O H-bonds to supplement a NH \cdots O H-bond of only moderate strength.

As mentioned above, the presence of the lower peptide eliminates the C5 minimum of the simple dipeptide which occurs at $(\phi,\psi)=(180^\circ,180^\circ)$. Instead, the tertiary minimum of the full molecule I shifts ψ down to 150° , and changes ϕ to -65° . While the ψ angle is beginning to approach its value of $112^\circ/135^\circ$ in the parallel/anti-parallel β -sheets, respectively, the ϕ angle of -65° is far removed from the corresponding values of -120° and -140° in the β -sheet. Molecule I is therefore too small a model to force the appearance of an incipient β -sheet, although the $\psi=150^\circ$ minimum does include the interpeptide NH \cdots O and CH \cdots O H-bonds that are a trademark of the β -sheet.

In summary, then, the presence of the lower peptide group leaves largely intact the preference of a dipeptide to adopt a C7-type geometry, even though its stability depends in large measure on interactions between the upper and lower peptide chains. The C5 structure of the dipeptide, on the other hand, is a fragile one, in that it vanishes upon placement of the lower peptide group in the vicinity of the upper dipeptide. The presence of the lower peptide group induces the formation of a tertiary minimum in the upper dipeptide, at $\psi=150^\circ$, whose stability rests upon both weak CH \cdots O and NH \cdots N H-bonds to supplement a much stronger NH \cdots O interaction.

Of course, a full β -sheet contains many more peptide units than does the model system considered here, which includes a pair of peptides on the upper strand and only a single peptide on the lower. And the structure of the connecting unit, with its phenyl ring and ether linkage, does not provide the full range of flexibility that would accrue to a protein molecule's longer, multistrand β -sheet. These factors might limit the ability of the model molecule to engage in a structure that is a truly accurate reproduction of a β -sheet.

Despite the small size, however, one can see abundantly clear evidence that the peptide units in the two strands do indeed have a strong influence upon the conformational preferences of one another. These effects are obvious first in the very different character of the rotational profiles of the fragment and full molecule, displayed by the broken and solid curves, respectively, in Figure 10-2. For example, it is this interstrand interaction that eliminates the C5 minimum present in the structure of a single strand, turning this sort of structure from a minimum to a maximum in the potential energy surface. And this mutual effect is unambiguously traced to the H-bonds that occur between the two strands, a necessary ingredient in the ultimate β -sheet formation in a protein. The evidence for this H-bond participation arises not only from NBO orbital interaction energies, but also from direct calculation of the interaction energies between the two segments. At this early stage of protein structure nucleation, the results further indicate that CH \cdots O H-bonds play a very important role, secondary only to the stronger NH \cdots O bonds that are normally considered to be completely dominant.

Lastly with respect to the accuracy that might be expected for the theoretical method applied here, the M06-2X approach was chosen in part for its design and superior performance in dealing with noncovalent interactions. Nonetheless, the data are not

perfect. A recent study⁷⁴ found that the M06 family of functionals handle H-bonded systems rather well, reproducing much of the dispersive attractions needed for long range interactions, but there is a lingering error in the range of perhaps 0.5-1.0 kcal in applications to H-bonded systems. DFT methods such as M06-2X also apply integration grid quadrature methods which can be subject to certain errors as well. However, a recent test⁷⁵ found the error to be expected from the grid applied here ought to be well under 0.1 kcal/mol.

In order to insure the validity of the M06-2X data, two other functionals were used to compare the energies of some of the most important structures. The geometries illustrated in Figure 10-6 for $\psi=300$, 60, and 150 all correspond to minima in the rotational profiles (see Figure 10-2). The energies of these structures were computed using two other functionals B97D⁷⁶ and ω B97XD,⁷⁷ both of which were designed in part to describe long-range dispersion effects. And indeed there is evidence⁷⁸ that the latter approach, as well as M06-2X, provide superior reproduction of the so-called gold standard for noncovalent forces, CCSD(T). Although there were of course some changes in the quantitative energy differences, both methods confirmed the energetic ordering obtained by M06-2X. As a further check on the M06-2X method, ab initio MP2 calculations were carried out on the same three important configurations, and again there was no change in their energetic ordering. This similarity is not surprising as MP2 and the M0n-2X series have been found⁷⁹ to correlate quite well with one another in complexes containing comparable sorts of interactions

References

- (1) Takahashi, O.; Kohno, Y.; Nishio, M. Relevance of Weak Hydrogen Bonds in the Conformation of Organic Compounds and Bioconjugates: Evidence from Recent Experimental Data and High-Level Ab Initio Mo Calculations. *Chem. Rev.*, **2010**, *110*, 6049-6076.
- (2) Wheeler, S. E.; McNeil, A. J.; Müller, P.; Swager, T. M.; Houk, K. N. Probing Substituent Effects in Aryl-Aryl Interactions Using Stereoselective Diels Alder Cycloadditions. *J. Am. Chem. Soc.*, **2010**, *132*, 3304-3311.
- (3) Nishio, M. The Ch/P Hydrogen Bond in Chemistry. Conformation, Supramolecules, Optical Resolution and Interactions Involving Carbohydrates. *Phys. Chem. Chem. Phys.*, **2011**, *13*, 13873-13900.
- (4) Kumar, S.; Pande, V.; Das, A. P-Hydrogen Bonding Wins over Conventional Hydrogen Bonding Interaction: A Jet-Cooled Study of Indole...Furan Heterodimer. *J. Phys. Chem. A*, **2012**, *116*, 1368-1374.
- (5) Gierszal, K. P.; Davis, J. G.; Hands, M. D.; Wilcox, D. S.; Slipchenko, L. V.; Ben-Amotz, D. P-Hydrogen Bonding in Liquid Water. *J. Phys. Chem. Lett.*, **2011**, *2*, 2930-2933.
- (6) Saggu, M.; Levinson, N. M.; Boxer, S. G. Experimental Quantification of Electrostatics in X-H...P Hydrogen Bonds. *J. Am. Chem. Soc.*, **2012**, *134*, 18986-18997.
- (7) Amicangelo, J. C.; Irwin, D. G.; Lee, C. J.; Romano, N. C.; Saxton, N. L. Experimental and Theoretical Characterization of a Lone Pair-P Complex: Water-Hexafluorobenzene. *J. Phys. Chem. A*, **2013**, *117*, 1336-1350.

- (8) Sherrill, C. D. Energy Component Analysis of P Interactions. *Acc. Chem. Res.*, **2013**, *46*, 1020-1028.
- (9) Sutor, D. J. Evidence for the Existence of C-H \cdots O Hydrogen Bonds in Crystals. *J. Chem. Soc.*, **1963**, 1105-1110.
- (10) Krimm, S.; Kuroiwa, K. Low Temperature Infrared Spectra of Polyglycines and C—H ... O=C Hydrogen Bonding in Polyglycine Ii. *Biopolymers*, **1968**, *6*, 401-407.
- (11) Taylor, R.; Kennard, O. Crystallographic Evidence for the Existence of C-H \cdots O, C-H \cdots N, and C-H \cdots Cl Hydrogen Bonds. *J. Am. Chem. Soc.*, **1982**, *104*, 5063-5070.
- (12) Schwalbe, C. H. June Sutor and the C—H...O Hydrogen Bonding Controversy. *Cryst. Rev.*, **2012**, *18*, 191-206.
- (13) You, L.-Y.; Chen, S.-G.; Zhao, X.; Liu, Y.; Lan, W.-X.; Zhang, Y.; Lu, H.-J.; Cao, C.-Y.; Li, Z.-T. C-H \cdots O Hydrogen Bonding Induced Triazole Foldamers: Efficient Halogen Bonding Receptors for Organohalogenes. *Angew. Chem. Int. Ed.*, **2012**, *51*, 1657-1661.
- (14) Lee, K.-M.; Chen, J. C. C.; Chen, H.-Y.; Lin, I. J. B. A Triple Helical Structure Supported Solely by C—H \cdots O Hydrogen Bonding. *Chem. Commun.*, **2012**, *48*, 1242-1244.
- (15) Vibhute, A. M.; Gonnade, R. G.; Swathi, R. S.; Sureshan, K. M. Strength from Weakness: Opportunistic CH \cdots O Hydrogen Bonds Differentially Dictate the Conformational Fate in Solid and Solution States. *Chem. Commun.*, **2012**, *48*, 717-719.

- (16) Sigalov, M. V.; Doronina, E. P.; Sidorkin, V. F. C_{ar}-H···O Hydrogen Bonds in Substituted Isobenzofuranone Derivatives: Geometric, Topological, and Nmr Characterization. *J. Phys. Chem. A*, **2012**, *116*, 7718-7725.
- (17) Lippert, K. M.; Hof, K.; Gerbig, D.; Ley, D.; Hausmann, H.; Guenther, S.; Schreiner, P. R. Hydrogen-Bonding Thiourea Organocatalysts: The Privileged 3,5-Bis(Trifluoromethyl)Phenyl Group. *Eur. J. Org. Chem.*, **2012**, *2012*, 5919-5927.
- (18) Huang, Z.; Chen, Z.; Lim, L. H.; Quang, G. C. P.; Hirao, H.; Zhou, J. S. Weak Arene C-H···O Hydrogen Bonding in Palladium-Catalyzed Arylation and Vinylation of Lactones. *Angew. Chem. Int. Ed.*, **2013**, *52*, 5807-5812.
- (19) Gao, X.; Liu, Y.; Li, H.; Bian, J.; Zhao, Y.; Cao, Y.; Mao, Y.; Li, X.; Xu, Y.; Ozaki, Y.; Wu, J. A Cooperative Hydrogen Bonding System with a C-H···O Hydrogen Bond in Ofloxacin. *J. Mol. Struct.*, **2013**, *1040*, 122-128.
- (20) Horowitz, S.; Trievel, R. C. Carbon-Oxygen Hydrogen Bonding in Biological Structure and Function. *J. Biol. Chem.*, **2012**, *287*, 41576-41582.
- (21) Huggins, M. L. The Structure of Fibrous Proteins. *Chem. Rev.*, **1943**, *32*, 195-218.
- (22) Krimm, S. Hydrogen Bonding of C-H···O=C in Proteins. *Science*, **1967**, *158*, 530-531.
- (23) Ramachandran, G. N.; Chandrasekharan, R. Interchain Hydrogen Bonds Via Bound Water Molecules in the Collagen Triple Helix. *Biopolymers*, **1968**, *6*, 1649-1658.
- (24) Derewenda, Z. S.; Lee, L.; Derewenda, U. The Occurrence of C-H···O Hydrogen Bonds in Proteins. *J. Mol. Biol.*, **1995**, *252*, 248-262.

- (25) Bella, J.; Berman, H. M. Crystallographic Evidence for C^a-H...O=C Hydrogen Bonds in a Collagen Triple Helix. *J. Mol. Biol.*, **1996**, *264*, 734-742.
- (26) Wahl, M. C.; Sundaralingam, M. C-H...O Hydrogen Bonding in Biology. *Trends Biochem. Sci.*, **1997**, *22*, 97-102.
- (27) Weiss, M. S.; Brandl, M.; Sühnel, J.; Pal, D.; Hilgenfeld, R. More Hydrogen Bonds for the (Structural) Biologist. *Trends Biochem. Sci.*, **2001**, *26*, 521-523.
- (28) Senes, A.; Ubarretxena-Belandia, I.; Engelman, D. M. The Ca-H O Hydrogen Bond: A Determinant of Stability and Specificity in Transmembrane Helix Interactions. *Proc. Nat. Acad. Sci., USA*, **2001**, *98*, 9056-9061.
- (29) Manikandan, K.; Ramakumar, S. The Occurrence of CH...O Hydrogen Bonds in α -Helices and Helix Termini in Globular Proteins. *Proteins Struct. Func. Genetics*, **2004**, *56*, 768-781.
- (30) Fabiola, G. F.; Krishnaswamy, S.; Nagarajan, V.; Pattabhi, V. C-H...O Hydrogen Bonds in B-Sheets. *Acta Cryst.*, **1997**, *D53*, 316-320.
- (31) Nagarajan, V.; Pattabhi, V.; Johnson, A.; Bobde, V.; Durani, S. Crystal Structures of Heterochiral Peptides. Part II. *Tert*-Boc-Valyl-D-Alanyl-Leucyl-Alanyl Methoxide. *J. Peptide Res.*, **1997**, *49*, 74-79.
- (32) Ridder, I. S.; Rozeboom, H. J.; Dijkstra, B. W. Haloalkane Dehalogenase from *Xanthobacter Autotrophicus* GJ10 Refined at 1.15 Å Resolution. *Acta Cryst.*, **1999**, *D55*, 1273-1290.
- (33) Sandalova, T.; Schneider, G.; Käck, H.; Lindqvist, Y. Structure of Dethiobiotin Synthetase at 0.97 Å Resolution. *Acta Cryst.*, **1999**, *D55*, 610-624.

- (34) Addlagatta, A.; Krzywda, S.; Czapinska, H.; Otlewski, J.; Jaskolski, M. Ultrahigh-Resolution Structure of a Bpti Mutant. *Acta Cryst.*, **2001**, *D57*, 649-663.
- (35) Cordier, F.; Barfield, M.; Grzesiek, S. Direct Observation of C^a-H^a...O=C Hydrogen Bonds in Proteins by Interresidue ^{h3}J_{CaC'} Scalar Couplings. *J. Am. Chem. Soc.*, **2003**, *125*, 15750-15751.
- (36) Kang, B. S.; Devedjiev, Y.; Derewenda, U.; Derewenda, Z. S. The Pd2 Domain of Syntenin at Ultra-High Resolution: Bridging the Gap between Macromolecular and Small Molecule Crystallography. *J. Mol. Biol.*, **2004**, *338*, 483-493.
- (37) Chakrabarti, P.; Chakrabarti, S. C-H...O Hydrogen Bond Involving Proline Residues in α -Helices. *J. Mol. Biol.*, **1998**, *284*, 867-873.
- (38) Babu, M. M.; Singh, S. K.; Balaram, P. A C-H...O Hydrogen Bond Stabilized Polypeptide Chain Reversal Motif at the C Terminus of Helices in Proteins. *J. Mol. Biol.*, **2002**, *322*, 871-880.
- (39) Shi, Z.; Olson, C. A.; Bell, A. J.; Kallenbach, N. R. Non-Classical Helix-Stabilizing Interactions: C-H...O H-Bonding between Phe and Glu Side Chains in α -Helical Peptides. *Biophys. Chem.*, **2002**, *101-102*, 267-279.
- (40) Singh, S. K.; Babu, M. M.; Balaram, P. Registering α -Helices and B-Strands Using Backbone C-H...O Interactions. *Proteins Struct. Func. Genetics*, **2003**, *51*, 167-171.
- (41) Ash, E. L.; Sudmeier, J. L.; Day, R. M.; Vincent, M.; Torchilin, E. V.; Haddad, K. C.; Bradshaw, E. M.; Sanford, D. G.; Bachovchin, W. W. Unusual ¹h Nmr Chemical Shifts Support (His) C^{ε1}-H...O=C H-Bond: Proposal for Reaction-Driven

- Ring Flip Mechanism in Serine Protease Catalysis. *Proc. Nat. Acad. Sci., USA*, **2000**, *97*, 10371-10376.
- (42) Nanda, V.; Schmiedekamp, A. Are Aromatic Carbon Donor Hydrogen Bonds Linear in Proteins? *Proteins Struct. Func. Genetics*, **2008**, *70*, 489-497.
- (43) Derewenda, Z. S.; Derewenda, U.; Kobos, P. M. (His) C^{ϵ} -H \cdots O=C< Hydrogen Bond in the Active Sites of Serine Hydrolases. *J. Mol. Biol.*, **1994**, *241*, 83-93.
- (44) Del Rizzo, P. A.; Couture, J.-F.; Dirk, L. M. A.; Strunk, B. S.; Roiko, M. S.; Brunzelle, J. S.; Houtz, R. L.; Trievel, R. C. Set7/9 Catalytic Mutants Reveal the Role of Active Site Water Molecules in Lysine Multiple Methylation. *J. Biol. Chem.*, **2010**, *285*, 31849-31858.
- (45) Seiler, P.; Weisman, G. R.; Glendening, E. D.; Weinhold, F.; Johnson, V. B.; Dunitz, J. D. Observation of an Eclipsed C_{sp^3} -CH₃ Bond in a Tricyclic Orthoamide; Experimental and Theoretical Evidence for C-H \cdots O Hydrogen Bonds. *Angew. Chem., Int. Ed. Engl.*, **1987**, *26*, 1175-1177.
- (46) Paton, R. S.; Goodman, J. M. Understanding the Origins of Remote Asymmetric Induction in the Boron Aldol Reactions of B-Alkoxy Methyl Ketones. *Org. Lett.*, **2006**, *8*, 4299-4302.
- (47) Samanta, A. K.; Pandey, P.; Bandyopadhyay, B.; Chakraborty, T. Cooperative Strengthening of an Intramolecular O—H \cdots O Hydrogen Bond by a Weak C—H \cdots O Counterpart: Matrix-Isolation Infrared Spectroscopy and Quantum Chemical Studies on 3-Methyl-1,2-Cyclohexanedione. *J. Phys. Chem. A*, **2010**, *114*, 1650-1656.

- (48) Sonoda, Y.; Goto, M.; Ikeda, T.; Shimoi, Y.; Hayashi, S.; Yamawaki, H.; Kanosato, M. Intermolecular CH \cdots O Hydrogen Bonds in Formyl-Substituted Diphenylhexatriene, a [2 + 2] Photoreactive Organic Solid: Crystal Structure and Ir, Nmr Spectroscopic Evidence. *J. Mol. Struct.*, **2011**, *1006*, 366-374.
- (49) Bandyopadhyay, B.; Pandey, P.; Banerjee, P.; Samanta, A. K.; Chakraborty, T. CH \cdots O Interaction Lowers Hydrogen Transfer Barrier to Keto-Enol Tautomerization of B-Cyclohexanedione: Combined Infrared Spectroscopic and Electronic Structure Calculation Study. *J. Phys. Chem. A*, **2012**, *116*, 3836-3845.
- (50) Kothari, A.; Qureshi, M. K. N.; Beck, E. M.; Smith, M. D. Bend-Ribbon Forming G-Peptides. *Chem. Commun.*, **2007**, 2814-2816.
- (51) Qureshi, M. K. N.; Smith, M. D. Parallel Sheet Structure in Cyclopropane G-Peptides Stabilized by C-H \cdots O Hydrogen Bonds. *Chem. Commun.*, **2006**, 5006-5008.
- (52) Jones, C. R.; Qureshi, M. K. N.; Truscott, F. R.; Hsu, S.-T. D.; Morrison, A. J.; Smith, M. D. A Nonpeptidic Reverse Turn That Promotes Parallel Sheet Structure Stabilized by C-H \cdots O Hydrogen Bonds in a Cyclopropane G-Peptide. *Angew. Chem. Int. Ed.*, **2008**, *47*, 7099-7102.
- (53) Jones, C. R.; Pantos, G. D.; Morrison, A. J.; Smith, M. D. Plagiarizing Proteins: Enhancing Efficiency in Asymmetric Hydrogen-Bonding Catalysis through Positive Cooperativity. *Angew. Chem. Int. Ed.*, **2009**, *48*, 7391-7394.
- (54) Jones, C. R.; Baruah, P. K.; Thompson, A. L.; Scheiner, S.; Smith, M. D. Can a C-H \cdots O Interaction Be a Determinant of Conformation. *J. Am. Chem. Soc.*, **2012**, *134*, 12064-12071.

- (55) Scheiner, S. Contributions of $\text{NH}\cdots\text{O}$ and $\text{CH}\cdots\text{O}$ H-Bonds to the Stability of B-Sheets in Proteins. *J. Phys. Chem. B*, **2006**, *110*, 18670-18679.
- (56) Vener, M. V.; Egorova, A. N.; Fomin, D. P.; Tsirelson, V. G. Q-taim Study of the Closed-Shell Interactions in Peptide Secondary Structures: A Cluster Treatment of Oligo- and Polyalanines. *Chem. Phys. Lett.*, **2007**, *440*, 279-285.
- (57) Parthasarathi, R.; Raman, S. S.; Subramanian, V.; Ramasami, T. Bader's Electron Density Analysis of Hydrogen Bonding in Secondary Structural Elements of Proteins. *J. Phys. Chem. A*, **2007**, *111*, 7141-7148.
- (58) Vener, M. V.; Egorova, A. N.; Fomin, D. P.; Tsirel'son, V. G. A Quantum-Topological Analysis of Noncovalent Interactions in Secondary Polyalanine Structures. *Russ. J. Phys. Chem. B.*, **2009**, *3*, 541-547.
- (59) Guo, H.; Gorin, A.; Guo, H. A Peptide-Linkage Deletion Procedure for Estimate of Energetic Contributions of Individual Peptide Groups in a Complex Environment: Application to Parallel B-Sheets. *Interdiscip. Sci. Comput. Life Sci.*, **2009**, *1*, 12-20.
- (60) Frisch, M. J.; Trucks, G. W.; Schlegel, H. B.; Scuseria, G. E.; Robb, M. A.; Cheeseman, J. R.; Scalmani, G.; Barone, V.; Mennucci, B.; Petersson, G. A.; et al. Gaussian 09. Revision B.01 ed. 2009
- (61) Zhao, Y.; Truhlar, D. G. Comparative Dft Study of Van Der Waals Complexes: Rare-Gas Dimers, Alkaline-Earth Dimers, Zinc Dimer, and Zinc-Rare-Gas Dimers. *J. Phys. Chem. A*, **2006**, *110*, 5121-5129.

- (62) Molnar, L. F.; He, X.; Wang, B.; Merz, K. M. Further Analysis and Comparative Study of Intermolecular Interactions Using Dimers from the S22 Database. *J. Chem. Phys.*, **2009**, *131*, 065102.
- (63) Vincent, M. A.; Hillier, I. H. The Structure and Interaction Energies of the Weak Complexes of CHClF_2 and CHF_3 with HCCH : A Test of Density Functional Theory Methods. *Phys. Chem. Chem. Phys.*, **2011**, *13*, 4388-4392.
- (64) Biller, M. J.; Mecozzi, S. A High Level Computational Study of the CH_4/CF_4 Dimer: How Does It Compare with the CH_4/CH_4 and CF_4/CF_4 Dimers? *Mol. Phys.*, **2012**, *110*, 377-387.
- (65) Podeszwa, R.; Szalewicz, K. Density Functional Theory Overcomes the Failure of Predicting Intermolecular Interaction Energies. *J. Chem. Phys.*, **2012**, *136*, 161102.
- (66) Forni, A.; Pieraccini, S.; Rendine, S.; Gabas, F.; Sironi, M. Halogen-Bonding Interactions with P Systems: CCSD(T), MP2, and DFT Calculations. *ChemPhysChem.*, **2012**, *13*, 4224-4234.
- (67) Kozuch, S.; Martin, J. M. L. Halogen Bonds: Benchmarks and Theoretical Analysis. *J. Chem. Theory Comput.*, **2013**, *9*, 1918-1931.
- (68) Kerdawy, A. E.; Murray, J. S.; Politzer, P.; Bleiziffer, P.; Heßelmann, A.; Görling, A.; Clark, T. Directional Noncovalent Interactions: Repulsion and Dispersion. *J. Chem. Theory Comput.*, **2013**, *9*, 2264-2275.
- (69) Remya, K.; Suresh, C. H. Which Density Functional Is Close to CCSD Accuracy to Describe Geometry and Interaction Energy of Small Non-Covalent Dimers? A Benchmark Study Using Gaussian09. *J. Comput. Chem.*, **2013**, *34*, 1341-1353.

- (70) Doemer, M.; Tavernelli, I.; Rothlisberger, U. Intricacies of Describing Weak Interactions Involving Halogen Atoms within Density Functional Theory. *J. Chem. Theory Comput.*, **2013**, *17*, 955-964.
- (71) Rosokha, S. V.; Stern, C. L.; Ritzert, J. T. Experimental and Computational Probes of the Nature of Halogen Bonding: Complexes of Bromine-Containing Molecules with Bromide Anions. *Chem. Eur. J.*, **2013**, *19*, 8774-8788.
- (72) Reed, A. E.; Weinhold, F.; Curtiss, L. A.; Pochatko, D. J. Natural Bond Orbital Analysis of Molecular Interactions: Theoretical Studies of Binary Complexes of HF, H₂O, NH₃, N₂, O₂, F₂, CO and CO₂ with HF, H₂O, and NH₃. *J. Chem. Phys.*, **1986**, *84*, 5687-5705.
- (73) Reed, A. E.; Curtiss, L. A.; Weinhold, F. Intermolecular Interactions from a Natural Bond Orbital, Donor-Acceptor Viewpoint. *Chem. Rev.*, **1988**, *88*, 899-926.
- (74) Marom, N.; Tkatchenko, A.; Rossi, M.; Gobre, V. V.; Hod, O.; Scheffler, M.; Kronik, L. Dispersion Interactions with Density-Functional Theory: Benchmarking Semiempirical and Interatomic Pairwise Corrected Density Functionals. *J. Chem. Theory Comput.*, **2011**, *7*, 3944-3951.
- (75) Wheeler, S. E.; Houk, K. N. Integration Grid Errors for Meta-Gga-Predicted Reaction Energies: Origin of Grid Errors for the M06 Suite of Functionals. *J. Chem. Theory Comput.*, **2010**, *6*, 395-404.
- (76) Grimme, S. Semiempirical Gga-Type Density Functional Constructed with a Long-Range Dispersion Correction. *J. Comput. Chem.*, **2007**, *27*, 1787-1799.
- (77) Chai, J.-D.; Head-Gordon, M. Systematic Optimization of Long-Range Corrected Hybrid Density Functionals. *J. Chem. Phys.*, **2008**, *128*, 084106.

- (78) Majumder, M.; Mishra, B. K.; Sathyamurthy, N. CH^{δ+}-P and P^{δ+}-P Interaction in Benzene-Acetylene Clusters. *Chem. Phys.*, **2013**, 557, 59-65.
- (79) Wu, W.; Lu, Y.; Liu, Y.; Li, H.; Peng, C.; Liu, H.; Zhu, W. Weak Energetic Effects between X-P and X-N Halogen Bonds: Csd Search and Theoretical Study. *Chem. Phys. Lett.*, **2013**, 582, 49-55.

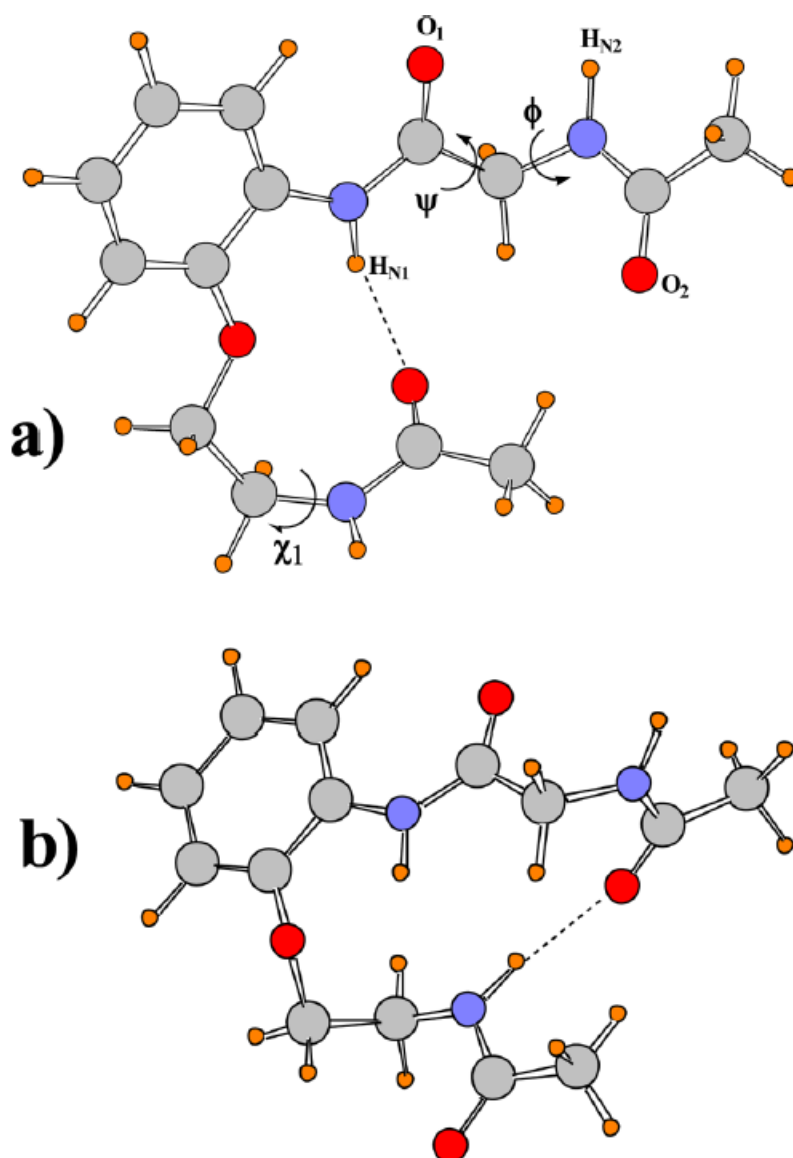


Figure 10-1. Structures of molecule I, with lower peptide group turned so as to present its CO group toward the upper in a, and its NH group turned in this direction in b. Important atoms are labeled, as are the dihedral angles discussed in the text.

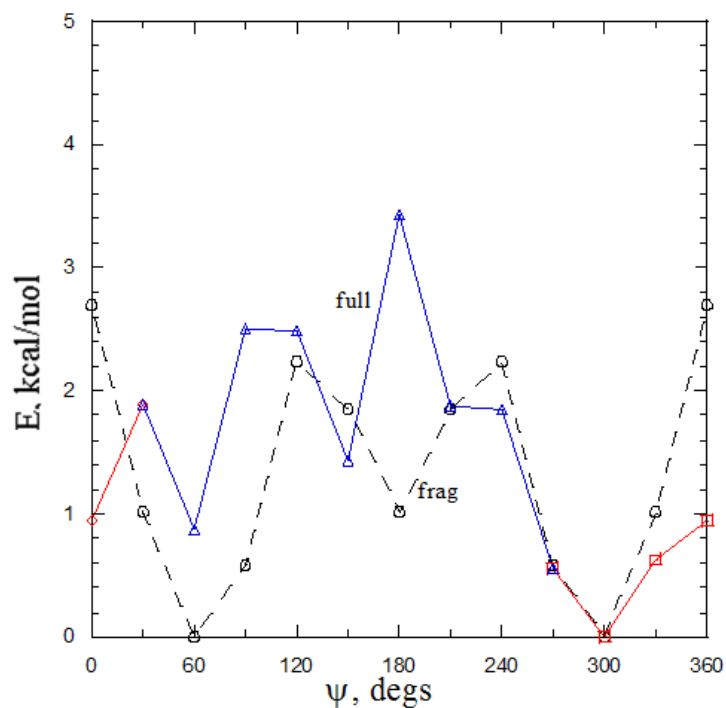


Figure 10-2. Energy as a function of dihedral angle ψ for the simple dipeptide (broken curve) and full molecule I (solid curve). Red and blue colors indicate respectively whether the lower peptide is oriented with CO or NH group pointing up toward the upper dipeptide. Zero of energy is taken as the lowest value in the profile of each.

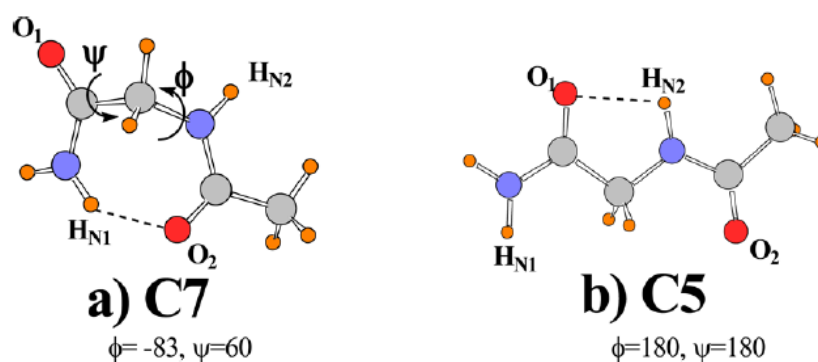


Figure 10-3. Structures of minima on the potential energy surface of the dipeptide segment $\text{NH}_2\text{COCH}_2\text{NHCOCH}_3$, indicating internal H-bond.

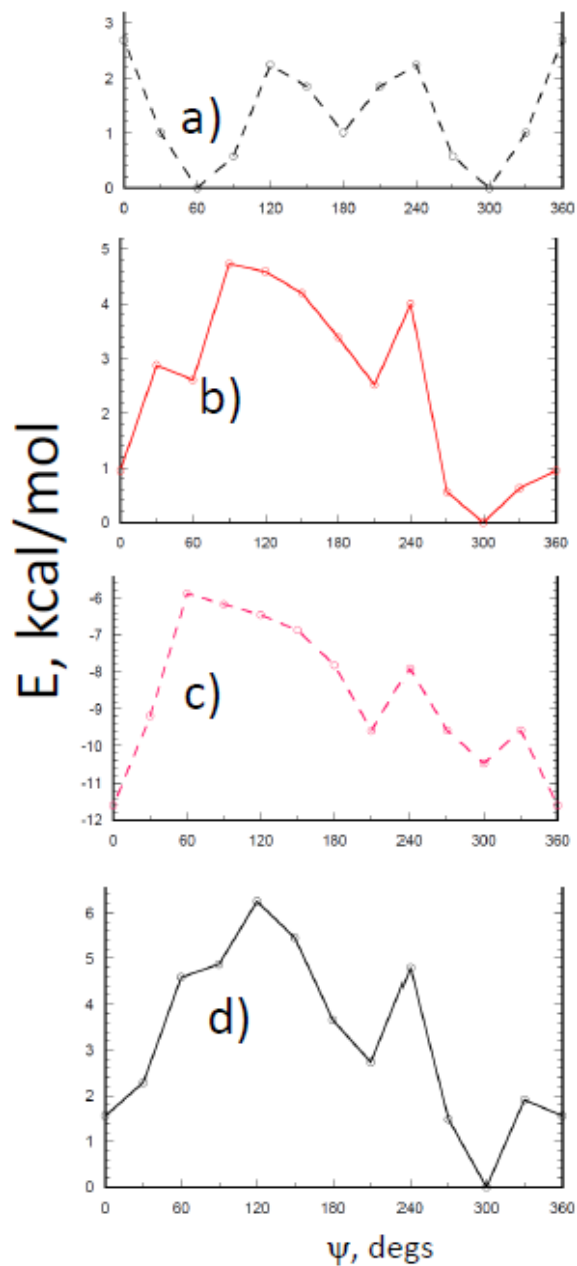


Figure 10-4. Energy as a function of dihedral angle ψ for a) simple dipeptide and b) full molecule I with lower peptide held with CO group up facing the dipeptide. The interaction energy computed for the upper and lower units, in the absence of intervening phenyl and other groups, is shown in c. The sum of the latter interaction energy in c and the intrinsic energy of the dipeptide in a is depicted in d. For a, b, and d, the value of zero is assigned to the lowest energy; quantities shown in c represent absolute values.

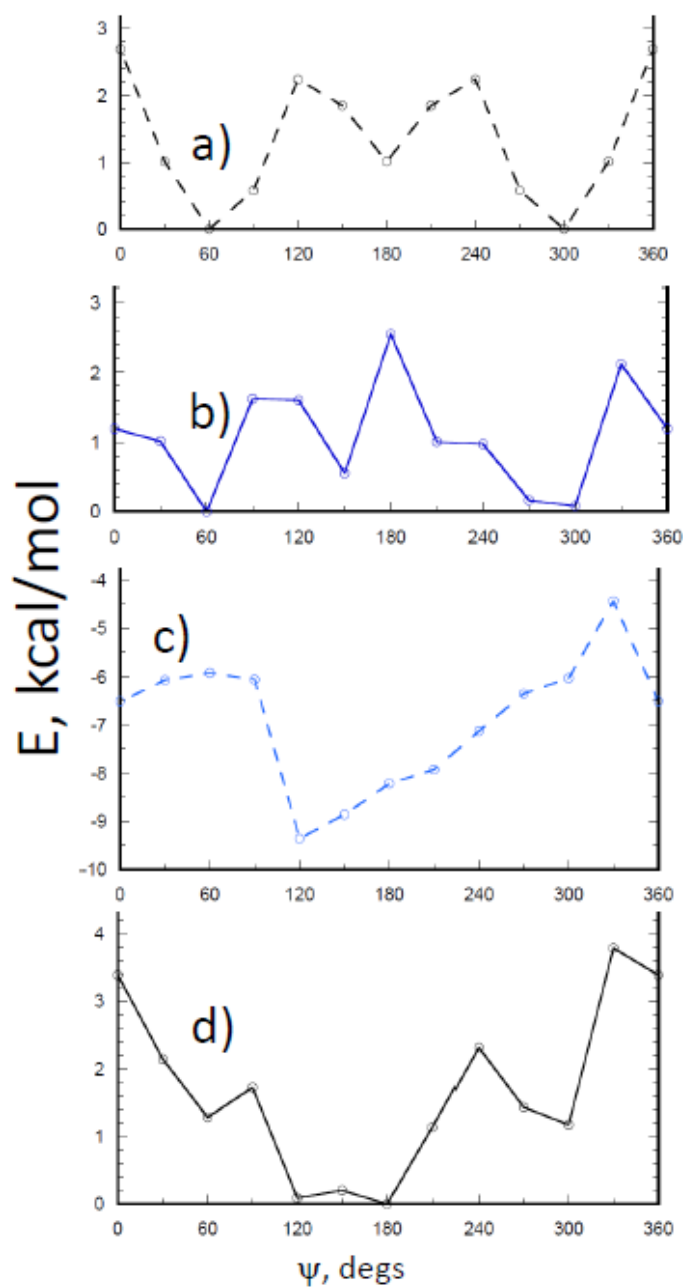


Figure 10-5. Energy as a function of dihedral angle ψ for a) simple dipeptide and b) full molecule I with lower peptide held with NH group up facing the dipeptide. c shows the interaction energy between the upper and lower units, in the absence of intervening phenyl and other groups, and d represents the sum of c and a.

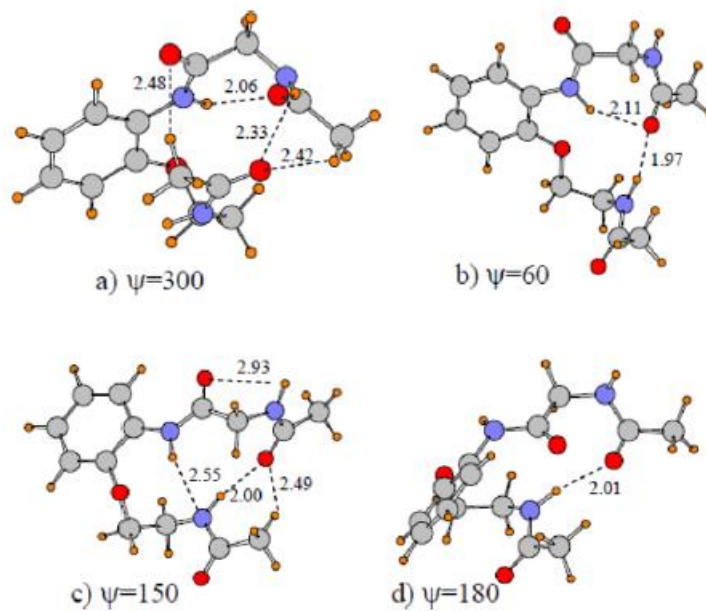


Figure 10-6. Structures of selected geometries of molecule I. Selected interatomic distances are in Å.

CHAPTER 11

MAGNITUDE AND MECHANISM OF CH \cdots O
HYDROGEN BONDS¹**Abstract**

Quantum calculations find that neutral methylamines and thioethers form complexes, with N-methylacetamide (NMA) as proton acceptor, with binding energies of 2-5 kcal/mol. This interaction is magnified by a factor of 4-9, bringing the binding energy up to as much as 20 kcal/mol, when a CH₃⁺ group is added to the proton donor. Complexes prefer trifurcated arrangements wherein three separate methyl groups donate a proton to the O acceptor. Binding energies lessen when the systems are immersed in solvents of increasing polarity, but the ionic complexes retain their favored status even in water. The binding energy is reduced when the methyl groups are replaced by longer alkyl chains. The proton acceptor prefers to associate with those CH groups which are as close as possible to the S/N center of formal positive charge. A single linear CH \cdots O H-bond is less favorable than is trifurcation with three separate methyl groups. A trifurcated arrangement with three H atoms of the *same* methyl group is even less favorable. Various means of analysis, including NBO, SAPT, NMR, and electron density shifts, all identify the ⁺CH \cdots O interaction as a true H-bond.

¹ Coauthored by Upendra Adhikari and Steve Scheiner. Reproduced with permission from *J. Phys. Chem. A* **2013**, *117*, 10551-10562. Copyright 2013, American Chemical Society.

11-1. Introduction

Of all the noncovalent forces that occur between separate molecules, or between various segments of the same molecule, H-bonding has arguably been the most intensively studied over the years. Decades of research have provided a wealth of information¹⁻⁴ about the underlying nature of the attraction, and of some of the accompanying phenomena. For example, the formation of a A-H \cdots D H-bond typically results in a small elongation of the A-H covalent bond, with an associated red shift of its stretching frequency.

Recent years have witnessed a broadening of the concept of H-bonding in a number of directions.^{5,6} For example, the electron donor D can be a H atom with a partial negative charge in what is usually called a dihydrogen bond.⁷⁻¹¹ Or the electrons can come not from a D lone pair, but rather from a π bond.^{7, 12-15} Another extension of the H-bond concept arises from the notion that the proton donor A atom can be less electronegative than the usual O, N, or F atoms. In addition to S or Cl,¹⁶⁻¹⁸ C has also been shown¹⁹⁻²⁸ to participate in H-bonds as the proton donor. In an interesting twist, certain CH \cdots O H-bonds violate the usual rule of a red shifted C-H stretching frequency, with this mode shifting instead to higher frequencies.²⁹⁻³⁶

Most of the extensions mentioned above are weaker than standard H-bonds, sometimes pushing the boundaries of the lower limit of strength. On the other end of the spectrum are very strong H-bonds, in which one of the two subunits carries an electric charge.³⁷⁻⁴⁰ The neutral water dimer, for example, is bound by some 5 kcal/mol, but if one of the two water molecules is replaced by either OH $^-$ or H $_3$ O $^+$, the interaction energy climbs⁴¹⁻⁴⁷ by a factor of 5-8. It is natural to wonder then whether such a charge-enhanced

interaction energy can transform a weak H-bond such as CH··O into a much stronger one. And indeed, there is some evidence in the literature that this might be the case. Placing a negative charge on the proton acceptor⁴⁸⁻⁵⁶ seems to cause a substantial strengthening of the attractive force within the dimer.

Likewise, adding a positive charge to the proton donor appears to have a comparable strengthening effect upon the H-bond. This phenomenon finds especial importance in the realm of biomolecular structure and function. As one example, the CH of a protonated Lys has been observed to attract a Trp sidechain.⁵⁷ Upon acquiring some charge from a nearby metal cation, the imidazole sidechain of a His residue forms CH··O H-bonds with heightened frequency of occurrence, as judged by analysis of the protein data bank.⁵⁸ The large number of CH··O H-bonds around the Cu coordination site of amicyanin⁵⁹ suggested that charge imparted by metal-coordination applies more generally to other CH donors as well.

One interesting case study arises in the activity of a particular class of enzymes. The Trievel group's delving into the mechanism of lysine methyltransferases and demethylases⁶⁰⁻⁶⁴ has revealed strong evidence that one or more CH··O H-bonds involving a cationic proton donor play an important role in their functioning. These donors involve either S (as in S-adenosyl-L-methionine, i.e. AdoMet) or N (lysine) as the center of positive charge (which partially motivates the model systems discussed below). However, the experimental data have not been capable of providing certain information that would aid in our understanding of how the enzymes function. For example, it is unclear whether one or more H atoms of each methyl group engage in H-bonding with a single acceptor atom. Nor has it been possible to extract the energetics of any individual

CH \cdots O interaction, an important consideration in terms of whether such bonds can hold the appropriate residues in position for enzymatic function and how they might compete with other potential H-bonds.

Quantum chemical methods offer the potential to address these issues with some clarity. One of the earliest related studies, limited to a very small basis set,⁶⁵ observed that the methyl group of a cationic system could form H-bonds as strong as 15 kcal/mol with a neutral proton acceptor. Kim et al.⁶⁶ later showed that protonated NH donors form H-bonds as strong as 20 kcal/mol with water, but that ^+CH donors are not far behind with a binding energy of 10 kcal/mol; H-bonds of these same donors with the π system of benzene were slightly weaker. The superiority of NH over CH, even in a charged situation, was verified by Cannizzaro and Houk⁶⁷ using esters as O proton acceptors. Nonetheless, a complex containing only $^+\text{CH}\cdots\text{O}$ type bonds still provided a very strong interaction of some 13 kcal/mol. When amplified by a positive charge, the C $^\alpha$ H of a lysine model was found⁶⁸ to engage in a CH \cdots O H-bond of some 4.9 kcal/mol, even though the center of positive charge was well removed from the bridging proton by several intervening methylene groups. With respect to aryl protons, benzene cation engages in a $^+\text{CH}\cdots\text{O}$ H-bond with water, with binding energy of 11.4 kcal/mol.⁶⁹ A single aryl CH of methylpyridinium forms a CH \cdots O bond with an ester⁷⁰ of 7.5 kcal/mol, raised to 10.0 kcal/mol when this bond is complemented by a second CH \cdots O involving a methyl H. The magnifying effect of charge was evident also⁷¹ in the CH \cdots O H-bond energies of imidazole with water, which jumped from 2.4 kcal/mol when imidazole was neutral up to 11.3 kcal/mol when protonated. This result was later confirmed by Schmiedekamp and Nanda⁵⁸ who extended the concept of positive charge to the proximate positioning of a

cationic metal. Along a similar vein, the effects of charge were manifest when the cationic imidazole donor $^+\text{CH}\cdots\text{O}$ H-bond supplanted a neutral $\text{NH}\cdots\text{O}$ bond as it led to triple helical structure⁷² of 1-acetamido-3-(2-pyrazinyl)-imidazolium.

While certainly providing some tantalizing glimpses into the magnification of $\text{CH}\cdots\text{O}$ H-bond strength, the body of past calculations of charge-activated $\text{CH}\cdots\text{O}$ H-bonds is not as thorough nor as robust as it might be. In particular, it leaves a number of questions only partially answered. Consider the general case where one or more alkyl groups R, each containing a number of potential CH donors, are bound to a central atom X, and the entire XR_n^+ system bears an overall positive charge. By just how much does the formal positive charge amplify the strength of the $\text{CH}\cdots\text{O}$ H-bonding to a proton acceptor, and how is the H-bond strength affected by the identity of the central atom X? Is the interaction weakened as the CH donor moves further along the alkyl group from the center of positive charge, and if so by how much? How sensitive is the H-bond to the linearity of the $\text{CH}\cdots\text{O}$ arrangement; are multiple bent $\text{CH}\cdots\text{O}$ bonds superior to a single linear bond? What is the effect of immersion of the system into a solvent of varying polarity? And as a particularly important question, can charge-magnified $\text{CH}\cdots\text{O}$ interactions compete effectively with neutral H-bonds of the conventional $\text{OH}\cdots\text{O}$ or $\text{NH}\cdots\text{O}$ sort?

The present work represents an attempt to answer these questions in a systematic manner. Quantum calculations are applied to systems that pair cationic XR_n^+ with the O atom of N-methylacetamide (NMA) as the common proton acceptor. The latter was chosen in part for its similarity to the peptide unit that is so pervasive in proteins. The central X atom was taken as first S and then N, so as to explore both chalcogen and

pnicogen types. And as noted above, both of these atoms are of particular relevance with regard to possible $^+\text{CH}\cdots\text{O}$ H-bonds within the transferase class of enzymes. Alkyl groups R were varied in length from methyl up to n-butyl which permit an exploration of the way in which distance from the central atom might affect the proton-donating potency of CH. The entire set of cationic systems are compared with their neutral analogues, to obtain direct estimates of the effects of charge. Finally, the systems are immersed in a variety of solvents, to assess how the results might be affected by the polarity of the surrounding medium. The results of this work will not only be of fundamental value in understanding ionic $\text{CH}\cdots\text{O}$ H-bonds in general, but of immediate use in better unraveling the mechanism of the methyl transferase enzymes as the model systems chosen bear a close resemblance to the actual enzymatic complexes.

11-2. Computational Methods

All calculations were performed via the Gaussian 09 package.⁷³ The MP2/aug-cc-pVDZ level of theory was chosen for its ability to handle H-bonding interactions at a high level of accuracy.^{55,74-79} The M06-2X density functional⁸⁰ was used for some of the larger systems. Not only was this method developed in order to handle intermolecular interactions, but it has shown good reliability in the past⁸¹⁻⁸⁴ when dealing specifically with CH H-bonds. In addition, as discussed below, the H-bond properties computed by M06-2X/6-31+G** were directly compared with MP2/aug-cc-pVDZ for the particular systems of interest here, and shown to be in close coincidence.

Binding energies were defined as the difference between the energy of the complex and the sum of energies of optimized monomers and were corrected for basis set

superposition error by the counterpoise procedure.⁸⁵ (Of all the possible conformers of each trialkylated monomer, the minimum chosen was that which most closely matched its structure in the complex, so as to avoid comparing unlike conformers.) All minima were verified as having no imaginary frequencies. Natural Bond Orbital (NBO) analyses^{86,87} were performed via the procedures contained within Gaussian. The binding energies of complexes were decomposed by symmetry adapted perturbation theory⁸⁸ (SAPT) via the Molpro⁸⁹ set of codes. The effects of solvation were estimated using the conductor polarized continuum model (CPCM).⁹⁰ NMR chemical shifts were calculated using the GIAO^{91,92} method, as coded in the Gaussian-09 program.

11-3. Results

N-methyl acetamide (NMA) as common proton acceptor was paired with the neutral $S(\text{Me})_2$ and $N(\text{Me})_3$ molecules, and then with the corresponding $S(\text{Me})_3^+$ and $N(\text{Me})_4^+$ cations. Full geometry optimizations were carried out at the MP2/aug-cc-pVDZ level of theory, and led to the structures illustrated in Figure 11-1. It may be noted first that these global minima all share one important characteristic: the NMA O atom interacts with as many methyl groups as possible. In other words, there are three $\text{CH}\cdots\text{O}$ bonds, each to a different methyl group for all complexes, with the exception of $S(\text{CH}_3)_2$ where there are only two such methyl groups present. The $\theta(\text{CH}\cdots\text{O})$ angles of these H-bonds all show a good deal of deviation from its ideal of 180° , with angles in the 137 - 150° range. Such nonlinearities are necessary in order to form multiple $\text{CH}\cdots\text{O}$ bonds with a single O atom. It might be emphasized that the three concurrent H-bonds formed

by the O atom in most of these complexes contradicts the notion that the presence of only two O lone pairs might similarly limit the number of potential H-bonds.

The counterpoise-corrected binding energies are displayed as the large blue numbers in Figure 11-1, and illustrate the magnification that is associated with the formal positive charge. The two neutral complexes are bound by 2-5 kcal/mol, with $\text{S}(\text{CH}_3)_2$ forming a stronger complex than does $\text{N}(\text{CH}_3)_3$. Along with its stronger binding, the CH \cdots O H-bonds are shorter in the former case. The $\text{N}(\text{CH}_3)_3$ complex is not symmetric, as one of the CH \cdots O bonds is some 0.3 Å longer than the other two. Note, however, the much shorter H-bonds in the two charged complexes in Figures 11-1b and 11-1d, with distances of about 2.2 Å. Along with this bond contraction comes a magnification of the binding energy to about 20 kcal/mol, with the S-containing complex again somewhat more strongly bound than its N analogue. The addition of the positive charge to the proton donor molecule enhances the binding energies by some 16 kcal/mol, representing a fourfold increase for S and ninefold for N.

11-3.1. Solvent Effects

It is generally thought that a polar solvent ought to weaken H-bonds, particularly those of ionic type. The effects of solvent were considered by applying the CPCM method which surrounds each system by a polarizable continuum of dielectric constant ϵ . The systems in Figure 11-1 were each subjected to a full geometry optimization in each solvent chosen, and again the identity as a minimum was verified by all positive vibrational frequencies. The binding energies of each complex are plotted against the Onsager function $F_o = (\epsilon - 1)/(\epsilon + 2)^{93}$ in Figure 11-2 where yellow and blue lines

indicate S and N complexes, respectively, with solid and broken curves designating cationic and neutral complexes. For purposes of comparison with a paradigmatic H-bond, the binding energy of the water dimer is included as the solid red curve. $F_o = 0$ for the gas phase, where $\epsilon = 1$, and this quantity rises asymptotically as the polarity increases, reaching its maximum of 0.963 for water where $\epsilon = 78$.

Examination of Figure 11-2 confirms that the interaction energy diminishes as the solvent becomes more polar. This relationship is largely a linear one, particularly for the neutral systems. It is evident that the charged complexes are more sensitive to solvent polarity, diminishing more quickly with F_o . Taking the cationic sulfonium S complex as an example, its binding energy decreases from 20.6 kcal/mol in the gas phase down to 12.8 kcal/mol when $\epsilon = 2.0$ and then further to a minimum of 4.6 kcal/mol in aqueous solvent. The decrease in the neutral complex of thioether $S(\text{Me})_2$ is more gradual, dropping from 4.9 kcal/mol at $\epsilon = 1$ to 2.3 kcal/mol at $\epsilon = 78$. Due to the higher sensitivity of the charged complexes to solvent polarity, as ϵ rises the energetic advantage of these ionic systems vs. the neutral complexes diminishes. Yet even for highly polar solvents, the cations form stronger H-bonds than do the neutral proton donors. In fact, even for aqueous solvation, the binding energies of the two charged complexes are twice that of their neutral parallels.

As the $\text{CH}\cdots\text{O}$ H bond weakens in more polar solvents, the two monomer units are drawn slightly further apart, in both neutral and charged complexes. The H-bond distance increases by $\sim 0.1 \text{ \AA}$ for S complexes and $\sim 0.2 \text{ \AA}$ for N complexes as ϵ climbs from 1 to 78. Surprisingly the change in H bond distance is approximately the same for neutral and cationic complexes, despite the higher sensitivity to ϵ of the binding energy of cationic

complexes compared to their neutral analogs. Along with this intermolecular stretching, the $\theta(\text{CH}\cdots\text{O})$ bonds become slightly more linear, increasing by 2-8°. It is perhaps worthy of note that the interoxygen distance of the water dimer behaves in an opposite fashion, shortening by $\sim 0.1 \text{ \AA}$ on going from gaseous to aqueous phase, despite its binding energy decrease. These trends are not entirely surprising as similar results were observed previously⁹³ for related systems.

One might expect that the solvation energy of each charged monomer should be greater than that of its complex with NMA, as the positive charge ought to be more dissipated in the larger system. And indeed, that is precisely what is found. The solvation energies reported for each system show that the computed solvation energy of sulfonium $\text{S}(\text{Me})_3^+$ is some 5-9 kcal greater than that of $\text{S}(\text{Me})_3^+\cdots\text{NMA}$ complex, while the difference between $\text{N}(\text{Me})_4^+\cdots\text{NMA}$ and $\text{N}(\text{Me})_4^+$ is roughly the same. The opposite trend is observed in the neutral systems where the solvation energy of the complex exceeds that of the isolated S or N-containing monomer. And of course, the solvation energies of all charged systems are many times greater than their neutral cousins.

11-3.2. Distance from Center of Charge

As noted above, adding a full positive charge to the proton donor molecule greatly enhances the strength of its $\text{CH}\cdots\text{O}$ H-bonds. It is logical to suppose that this change is at least partly the result of a more positive bridging proton which can better interact with the O on the proton acceptor. What then might be the effect of elongating the methyl group to ethyl, propyl, etc, and thereby moving the bridging proton further from the heteroatomic center of positive charge?

M06-2X/6-31+G** calculations were performed in order to address this question. The validity of this procedure for these calculations can first be tested by comparison of the binding energies of the methyl complexes. A comparison with MP2 values is displayed in Table 11-1 where it may be noted that the DFT values are fairly close to MP2/aug-cc-pVDZ quantities. There is a bit of an overestimate by the former, but this overestimate is fairly uniform, roughly 1 kcal/mol.

The geometries of the ethyl and propyl parallels of the ionic methyl complexes of Figure 11-1 are displayed in Figure 11-3, along with their counterpoise-corrected binding energies, all in the gas phase. These energies are plotted against the alkyl chain length in Figure 11-4, where yellow and blue curves again indicate S and N-containing complexes, respectively. The solid curves represent the structures in Figure 11-3 where the NMA proton acceptor binds to the terminal methyl groups in each case. Both S and N-type systems behave similarly, with the binding energy diminishing as the methyl group moves progressively further from the center of formal charge. Taking the cationic S complexes as an example, the binding energy of 22 kcal/mol for $S(\text{CH}_3)_3^+\cdots\text{NMA}$ is cut in half for the propyl analogue.

Along with a weakening of the interaction, there is a concomitant stretch of the distance between the two subunits. These distances are displayed in Table 11-2 for each of the three methyl groups involved in a given complex. The H-bond stretching that accompanies the lengthening of the alkyl groups is clear in this table. For example, the shortest such H-bond elongates from 2.162 to 2.254 and then to 2.420 Å as the alkyl is enlarged from methyl to ethyl to propyl in the charged S complexes; similar trends are observed in the N-containing structures.

It is not only the terminal methyl group which can engage in a $\text{CH}\cdots\text{O}$ H-bond, but the same is true for the methylene groups which lie closer to the heteroatom. The broken curves in Figure 11-4 show that when it is these CH_2 groups, those lying immediately adjacent to S or N, that form $\text{CH}\cdots\text{O}$ H-bonds with NMA, the drop in binding energy is much less precipitous. Put another way, if the alkyl groups are lengthened, but the O of NMA remains bonded to the CH nearest the heteroatom, there is only a small drop in binding energy. This decrease can be readily explained by the fact that the longer alkyl groups permit a greater dissipation of the overall positive charge of the cation, thereby reducing the charge on the bridging proton. Overall, then, the patterns in Figure 11-4 are consistent with a picture of positive charge on each cation that extends over the entire molecule, but becomes progressively smaller as one moves away from the heteroatom.

These ideas are confirmed by examination of the electrostatic potentials that surround each monomer. This potential is of course positive everywhere as the ion carries a positive charge. But there are gradations in this potential. The blue contours of Figure 11-5 indicate the most positive areas, and red the least positive, covering a range between 0.20 and 0.25 au. In both the S and N cases (upper and lower sections of Figure 11-5, respectively) as one progresses from methyl to ethyl to propyl, the terminal methyl groups become less positive, i.e. redder. Likewise, albeit more subtle, one can see a lessening of the positive potential around the H atoms that lie close to the N/S as each alkyl group grows. (The neutral molecules have a much weaker positive potential around the H atoms, peaking at around 0.08 au for $\text{S}(\text{CH}_3)_2$ and at 0.06 for $\text{N}(\text{CH}_3)_3$.) Not only the electrostatic potentials, but also the atomic charges, reflect these same patterns. The natural charges of the terminal methyl H atoms undergo a decrease as the alkyl chain

elongates. For example, the average natural charge of these three H atoms is 0.28 for $\text{N}(\text{Me})_4^+$ and drops to 0.26 in $\text{N}(\text{Pr})_4^+$. The H atoms that lie close to the N/S also undergo a drop in positive charge, but a lesser one.

11-3.3. Nature of Interaction

A question that arises concerns the nature of the interaction in these charged complexes. Is it primarily a simple electrostatic interaction between the two species or is there some degree of true H-bonding, as occurs in more classically H-bonded systems such as the water dimer? There are several vehicles to assess the nature of the interaction. For one thing, H-bonds typically involve a certain amount of charge transfer between the proton acceptor atom and the σ^* antibonding orbital of the donor, as measured by NBO parameters. Table 11-3 reports the second-order perturbation energy $E(2)$ for the putative $\text{CH}\cdots\text{O}$ H-bonds. $\text{O}_{\text{lp}}\rightarrow\sigma^*(\text{C-H})$ quantities are supplemented by transfers from the CO π bond (in parentheses). $\text{O}_{\text{lp}}\rightarrow\sigma^*(\text{C-H})$ $E(2)$ amounts to between 0.5 and 1.7 kcal/mol for the neutral complexes, supplemented by 0.4-0.8 kcal/mol from the $\pi(\text{CO})$ bond. These quantities lie in the range of what is expected for a H-bond. They are considerably enhanced when the proton donor is charged, rising to as much as 6.7 and 1.8 kcal/mol, respectively, for the methylated systems. The former quantities refer to each individual $\text{CH}\cdots\text{O}$ H-bond; when summed over all three such bonds, they amount to 14-18 kcal/mol (last column of Table 3), consistent with a strong charged H-bonded complex. Note that these $E(2)$ quantities drop as the CH donor is further removed from the heteroatom, fully consistent with the total binding energies reported above.

Decomposition of the binding energies also offers valuable clues about the nature of the interaction. Such a decomposition was carried out using the SAPT procedure, and the results are presented in Table 11-4. The electrostatic is the largest component for the ionic complexes in the last two columns, followed by induction and dispersion which make comparable contributions to one another. This pattern is consistent with what one would expect for H-bonds. The neutral complexes have a much reduced electrostatic component, although the dispersion energy is comparable to that of the ionic systems. The larger DISP as compared to ES is not a feature typically seen in H-bonds, although it does occur on occasion.

Yet another tool used to distinguish H-bonds concerns the electron density. More specifically, there is a characteristic pattern that occurs within the shifts of electron density when a H-bond is formed. These shifts are illustrated in Figure 11-6 where gains of density are indicated by blue contours and losses by red. In all complexes, there is a red region of density loss surrounding each bridging proton, as well as a blue region of gain in the vicinity of the proton-accepting O atom of NMA. This pattern reproduces a typical fingerprint of H-bond formation so supports its characterization as such. Further confirmation arises from the observation that these same patterns become more intense as the binding energy rises, as in the progression $S(\text{Me})_2 < S(\text{Pr})_3^+ < S(\text{Et})_3^+ < S(\text{Me})_3^+$. Whereas the formation of conventional H-bonds, e.g. $\text{OH}\cdots\text{O}$, induces a stretching of the O-H bond in the proton donor molecule, the situation with $\text{CH}\cdots\text{O}$ analogues has been found to be less predictable. While there is a trend for sp-hybridized CH bonds, as in HCCH, to stretch just like their OH counterparts, those that are engaged in sp³ hybridization tend³² to contract, although this is not a hard and fast rule. The geometric

changes occurring within the proton donor molecules here obey an interesting pattern. The bridging CH bond of the terminal methyl groups of the sulfonium SR_3^+ cation stretches when $\text{R}=\text{Me}$ or Et , but undergoes a contraction for $\text{R}=\text{Pr}$; the same is true for the N-containing molecules. On the other hand, when the bridging proton is associated with a methylene group that is immediately adjacent to the S/N heteroatom, the CH bond undergoes a small contraction, less than 3 mÅ.

A useful experimental tool for identifying H-bonds resides in NMR spectroscopy, as the bridging proton typically shifts downfield^{94,95} by several ppm. Prior work has shown that $\text{CH}\cdots\text{O}$ H-bonds conform to this trend,⁹⁶⁻⁹⁸ albeit generally exhibiting a smaller shift which comports with the weaker nature of this H-bond. In order therefore to add to our pallet of H-bond identification tools, the NMR chemical shieldings were computed for the various protons in each of the systems described above. The changes in the shielding, as compared to the isolated monomers, are reported in the first two columns of data in Table 11-5 where negative values correspond to a deshielding and downfield shift. As the geometries reflect a trifurcated arrangement, with very similar $\text{CH}\cdots\text{O}$ H-bond energies, it is not surprising to see very similar shifts for the three corresponding protons. Consequently, the values listed in Table 11-5 refer to the average changes of all three bridging protons. (Nonbridging protons exhibit much smaller changes, and in the upfield direction.)

Inspection of Table 11-5 quickly reveals that the downfield shifts are roughly proportional to the H-bond energies. Taking the S series as an example, the shift for neutral thioether $\text{S}(\text{Me})_2$ is less than 1 ppm, but this quantity enlarges to 2.23 ppm for the cationic $\text{S}(\text{Me})_3^+$. Following down the first column of Table 11-5, it is clear that as the

terminal methyl group moves further from the S atom, the shift lowers eventually down to 1.15 ppm for the tripropyl species. The next column of Table 11-5 refers to those complexes wherein the NMA acceptor binds not to the terminal methyl group, but rather to the methylene group adjacent to S. Just as in the case of the binding energy, the downfield shift is lowered much more slowly as the alkyl chain grows, remaining above 2 ppm. Very similar trends are observed for the N series. It may be concluded that the NMR chemical shifts fully support the characterization of these interactions as full bodied H-bonds.

Rapid rotations of methyl groups frequently make it difficult to experimentally separate the NMR signals of the bridging proton of a given methyl group from the H atoms that are not so involved. What is frequently observed instead is an average of all three of these signals. Therefore as a guide to experimentalists, the third column of Table 11-5 reports the average change in the chemical shielding of all protons of the terminal H-bonded methyl groups, both H-bonded and non-H-bonded. Due to the upfield shift of the latter, these averages are much smaller in magnitude than those in the first column, but are downfield nonetheless. As a rule of thumb, the downfield shift is less than -0.1 ppm for the neutral complexes, but lies in the range between -0.3 and -0.5 for the ionic H-bonds.

With specific respect to methyl rotations, each methyl group is staggered with respect to its neighbors in its optimal orientation. Rotation of a single methyl must cross a barrier which involves an eclipsed structure. These barriers are calculated in the methyl derivatives to vary from 2.2-2.6 kcal/mol for the thioethers and 4.8-5.0 kcal/mol for the

amines. When complexed with NMA, the barriers increase a small amount, between 0.1 and 0.9 kcal/mol, presumably due to the disruption of one of the CH \cdots O H-bonds.

11-3.4. Other Geometries of H-bonds

As indicated above, the most stable configuration of each dimer involves a trifurcated H-bond, in the sense that the NMA O atom engages in a H-bond simultaneously with three CH bonds, each on a different alkyl chain. The question that comes to mind is how much the energy might suffer if the trifurcation involves the three H atoms on a single methyl group. In order to answer this question, a set of restricted geometry optimizations were carried out wherein the $\theta(\text{XC}\cdots\text{O})$ angle ($X = \text{S}, \text{N}, \text{or C}$) was held equal to 180° . Counterpoise-corrected binding energies are plotted against the length of the alkyl chain in Figure 11-7 as broken curves where yellow and blue lines again represent S^+ and N^+ complexes, respectively. It is first clear that these binding energies diminish as the chain elongates and the terminal methyl group is drawn further from the heteroatomic center of positive charge, just as was noted earlier. The very near coincidence of the yellow and blue curves in Figure 11-7 indicates there is little difference imparted by the nature of this heteroatom. But perhaps most importantly, the binding energies in Figure 11-7 are considerably lower than those in Figure 11-4 so that one may conclude that trifurcation with three separate alkyl chains is preferable to trifurcation with a single methyl group. For example, the trifurcated complexes for the $\text{N}(\text{CH}_3)_4^+$ and $\text{S}(\text{CH}_3)_3^+$ cations in Figure 11-4 are bound by 20.3 and 22.2 kcal/mol respectively, considerably larger than the 14.5 kcal/mol when the O is allowed to interact with a single methyl group of either cation.

Part of the explanation of this weaker interaction is likely due to greater strain of the H-bonds. The $\theta(\text{CH}\cdots\text{O})$ angles lie in the $84\text{-}91^\circ$ range for the single methyl group, but this range extends to $125\text{-}151^\circ$ when three separate methyl groups interact with the proton acceptor. NBO analysis confirms that this angular factor is important. The small $\theta(\text{CH}\cdots\text{O})$ angles hinder the transfer of charge from the O lone pair to a CH σ^* antibond. Instead, what charge transfer there is goes from the O lone pair to the σ^* antibonding orbital of the X-C bond (X=S,N,C). And it should be emphasized the E(2) is rather small in any case, between 0.7 and 3.1 kcal/mol. Other evidence for the weakness of these H-bonds arises from the calculated NMR spectrum. As reported in the penultimate column of Table 11-5, the three bridging protons shift downfield by only 0.4 - 0.8 ppm, considerably less than the values listed in the preceding columns of Table 11-5 when three separate methyl groups are involved in the trifurcated arrangement. Finally, this trifurcated interaction with a single methyl group results in small contractions of the three C-H bonds, but only by about 1 mÅ, and this bond shortening is attenuated as the alkyl chain is elongated from methyl to butyl.

Another possibility which is worthy of examination involves a single, linear CH \cdots O H-bond. Since there is no minimum on the surface that corresponds to such a structure, a restriction of $\theta(\text{CH}\cdots\text{O}) = 180^\circ$ was introduced into the geometry optimization, after placing the NMA O atom proximate to a terminal methyl group. The counterpoise-corrected binding energies of these complexes are displayed as the solid curves in Figure 11-7, where again one sees a diminishing trend as the alkyl chain elongates. Note that these solid curves are slightly higher than the broken curves,

suggesting that a single linear CH··O H-bond is energetically superior to a trifurcated arrangement with one methyl group. In other words, a proton acceptor prefers to approach a methyl group along a C-H axis as compared to the tetrahedron face. But even these linear CH··O H-bonds are inferior to the trifurcated arrangements of Figure 11-4 which involve three different alkyl chains. As a secondary issue, the formation of the linear CH··O H-bonds results in a C-H stretch. In the case of the S cations, this elongation varies from a minimum of 0.4 mÅ for the terminal methyl of a butyl chain to 4.5 mÅ for a methyl group. The stretch is consonant with charge transfer into the CH σ^* antibond, which is largest for the methyl group where $E(2) = 13.7$ kcal/mol, and decreases monotonically as the alkyl chain elongates, to a minimum of 4.3 kcal/mol for the butyl chain. The strength of this single H-bond is further underscored by the NMR signal of the bridging proton, which the last column of Table 11-5 shows to shift downfield by 2.5 - 3.5 ppm, a somewhat greater amount than in the case of the three separate, bent H-bonds of the preceding columns of Table 11-5. As in the earlier bonding situations, the shift is roughly proportional to the binding energy, diminishing as the alkyl chain is elongated and the bridging proton is removed further from the S/N center of charge.

There were additional minima located in the potential energy surfaces that offer further refinements in terms of geometric preferences. For example, as one might expect two H-bonds are inferior to three, when all proton donors are terminal methyl groups. Similarly, a complex containing two H-bonds to methylene protons is of course more weakly bound than one which makes use of three such methylenes. On the other hand, these same two H-bonds that involve groups close to the S/N center of positive charge are superior to three CH··O bonds to terminal methyl groups, further from this center.

11-4. Summary and Discussion

The alkylated thioethers and amines engage in CH··O H-bonding to the NMA proton acceptor, with binding energies of 2-5 kcal/mol. The addition of a positive charge to the proton donor molecule magnifies the interaction by a factor of 4-9, such that sulfonium S(Me)₃⁺ is bound to NMA by more than 20 kcal/mol. In all cases, the proton acceptor atom prefers interacting with as many CH groups as possible, i.e. multiple bent CH··O H-bonds are more favorable than a single linear one. There is also an energetic preference for the O to interact with H atoms on separate alkyl groups, as compared to several H atoms on the same R. H atoms that lie closer to the central atom with its formal charge make the strongest H-bonds. The binding energy drops much more precipitously with alkyl chain length if the O is able to interact only with the terminal methyl H atoms, furthest from the central atom. This phenomenon may be explained on the basis of an attenuating positive electrostatic potential as one moves further from the S or N center of positive charge. The H-bonds formed by CH donors in species with a central S atom are slightly stronger than in the case of the amines. With regard to environment, the strengths of the CH··O H-bonds are reduced as the solvent in which the systems are immersed becomes more polarizable. Nonetheless, the ionic ⁺CH··O H-bonds remain stronger than neutral OH··O analogues, even in aqueous solution.

The CH··O interactions have all the hallmarks of true H-bonds. The shifts of electron density that accompany the formation of the dimers fit the usual fingerprint pattern of H-bonds. NBO analysis reveals a transfer of charge into the CH σ* antibonding orbital, and the magnitude of the corresponding second order energies are proportional to the overall binding energies. NMR chemical shifts of the bridging protons reflect the

deshielding that is another marker of H-bonds, and this shift is roughly proportional to binding energy. SAPT decomposition of the total interaction energy shows the dominant term to be electrostatic, but very substantial contributions are made by induction and dispersion as well. The change in the C-H bond length caused by H-bond formation is not uniform. Whereas this bond undergoes a stretch for the more strongly bound complexes, this trend reverses as the H-bond weakens. This pattern is not unlike what has been seen over the years for other CH \cdots O H-bonds, some of which lengthen while others contract.

The results described here agree well with earlier work in the recent literature on related systems. Our binding energy of N(CH₃)₄⁺ compares nicely with an earlier computation where this cation was paired with water for a binding energy of 9.7 kcal/mol at the MP2/6-311+G** level.⁶⁶ When other authors⁶⁷ interacted HN(CH₃)₃⁺ with an ester O, their optimized structure contained a trifurcated H-bond with three separate methyl groups like the ones found here, and with a binding energy of 12.9 kcal/mol with a 6-311++G** basis set. When this system was immersed in a dielectric medium, the binding energy suffered diminution, and became repulsive for $\epsilon > 8$. Other ⁺CH \cdots O H-bonds were also found to drop in binding energy as dielectric constant was raised,⁷⁰ in this case with methylpyridinium as proton donor. And a very recent work⁹⁹ agreed that a single linear ⁺CH \cdots O H-bond is energetically superior to a bifurcated arrangement when both H atoms are bonded to the same C.

There has been some question as to whether the interaction between an amine and proton acceptor such as NMA is strengthened by the charge or by the number of methyl groups bound to the central N atom. That is, what is the difference between adding a charge via a fourth methyl group to form N(CH₃)₄⁺ as was done here, as compared to

forming the cation via addition of a proton, as in $\text{HN}(\text{CH}_3)_3^+$ as might occur in low-pH solution? A full geometry optimization via the MP2/aug-cc-pVDZ of the complex between NMA and $\text{HN}(\text{CH}_3)_3^+$ was therefore performed. The counterpoise-corrected binding energy was computed to be 19.5 kcal/mol, 0.7 kcal/mol stronger than that of the tetramethylammonium complex of Figure 11-1d. The details of the two geometries are nearly identical, with $R(\text{CH}\cdots\text{O})=2.2 \text{ \AA}$ in either case, and with $\theta(\text{CH}\cdots\text{O})$ angles within 1° of one another. The very small energetic advantage of the $\text{HN}(\text{CH}_3)_3^+$ complex may be attributed to a slightly greater concentration of positive charge on the three remaining methyl groups.

It would appear then that $^+\text{CH}\cdots\text{O}$ H-bonds can be quite strong, with binding energies as high as 20 kcal/mol. These bonds exceed the strength of the typical $\text{NH}\cdots\text{O}=\text{C}$ H-bonds that provide the organizing force for such common protein structures as α -helix or β -sheet. While attenuated somewhat within the context of a polarizable medium, they nonetheless retain their greater strength when compared to neutral H-bonds. As such, these H-bonds can exert a strong influence on enzyme activity or in binding of substrates. The calculations reveal a greater depth about the specifics of the mode of binding. When a substrate of the type SR_3^+ is placed within a protein interior, there will be a strong tendency for its CH groups to engage in $\text{CH}\cdots\text{O}$ H-bonds with neighboring residues. If only a single proton acceptor is nearby, the overall preference will bring that acceptor as close as possible to the central S atom, and for three separate R chains to all participate in the trifurcated H-bonding. The interaction will weaken if the acceptor is forced by steric constraints to interact with CH groups that lie further from S, e.g. the terminal methyl groups. If other constraints permit H-bonding of the acceptor to only one methyl, a single

CH \cdots O is favored over three bent H-bonds to that same methyl group. But the latter issues notwithstanding, it is emphasized that even with some of these weakening factors in play, $^+\text{CH}\cdots\text{O}$ H-bonds are strong ones, surpassing neutral H-bonds, even those involving the electronegative O and N atoms as proton donors.

References

- (1) Gilli, G.; Gilli, P., *The Nature of the Hydrogen Bond*; Oxford University Press: Oxford, UK, 2009.
- (2) Scheiner, S., *Hydrogen Bonding: A Theoretical Perspective*; Oxford University Press: New York, 1997.
- (3) *Hydrogen Bonding - New Insights*; Grabowski, S. J., Ed.; Springer: Dordrecht, 2006.
- (4) *The Hydrogen Bond. Recent Developments in Theory and Experiments*; Schuster, P.; Zundel, G.; Sandorfy, C., Ed.; North-Holland Publishing Co.: Amsterdam, 1976.
- (5) Desiraju, G. R.; Steiner, T., *The Weak Hydrogen Bond in Structural Chemistry and Biology*; Oxford: New York, 1999.
- (6) Arunan, E.; Desiraju, G. R.; Klein, R. A.; Sadlej, J.; Scheiner, S.; Alkorta, I.; Clary, D. C.; Crabtree, R. H.; Dannenberg, J. J.; Hobza, P.; et al. Definition of the Hydrogen Bond. *Pure Appl. Chem.* **2011**, *83*, 1637-1641.
- (7) Oliveira, B. G. d. Structure, energy, vibrational spectrum, and Bader's analysis of $\pi\cdots\text{H}$ hydrogen bonds and $\text{H}^{-\delta}\cdots\text{H}^{+\delta}$ dihydrogen bonds. *Phys. Chem. Chem. Phys.* **2013**, *15*, 37-79.

- (8) Kar, T.; Scheiner, S. Comparison between hydrogen and dihydrogen bonds among H_3BNH_3 , H_2BNH_2 , and NH_3 . *J. Chem. Phys.* **2003**, *119*, 1473-1482.
- (9) Singh, P. C.; Patwari, G. N. The C–H \cdots H–B dihydrogen bonded borane-trimethylamine dimer: A computational study. *Chem. Phys. Lett.* **2006**, *419*, 265-268.
- (10) Belkova, N. V.; Shubina, E. S.; Epstein, L. M. Diverse world of unconventional hydrogen bonds. *Acc. Chem. Res.* **2005**, *38*, 624-631.
- (11) Solimannejad, M.; Scheiner, S. Theoretical Investigation of the dihydrogen bond linking MH_2 with HCCRgF (M=Zn,Cd; Rg=Ar,Kr). *J. Phys. Chem. A* **2005**, *109*, 11933-11935.
- (12) Saggu, M.; Levinson, N. M.; Boxer, S. G. Experimental quantification of electrostatics in X–H $\cdots\pi$ hydrogen bonds. *J. Am. Chem. Soc.* **2012**, *134*, 18986-18997.
- (13) Nishio, M. The CH/ π hydrogen bond in chemistry. Conformation, supramolecules, optical resolution and interactions involving carbohydrates. *Phys. Chem. Chem. Phys.* **2011**, *13*, 13873-13900.
- (14) Takahashi, O.; Kohno, Y.; Nishio, M. Relevance of weak hydrogen bonds in the conformation of organic compounds and bioconjugates: Evidence from recent experimental data and high-level ab initio MO calculations. *Chem. Rev.* **2010**, *110*, 6049-6076.
- (15) Nakanaga, T.; Buchhold, K.; Ito, F. Investigation of the NH- π hydrogen bond interaction in the aniline-alkene (C_2H_4 , C_3H_6 , C_4H_8) cluster cations by infrared depletion spectroscopy. *Chem. Phys.* **2003**, *288*, 69-76.

- (16) Bhattacharjee, A.; Matsuda, Y.; Fujii, A.; Wategaonkar, S. The intermolecular S-H \cdots Y (Y=S,O) hydrogen bond in the H₂S dimer and the H₂S–MeOH complex. *ChemPhysChem*. **2013**, *14*, 905-914.
- (17) Grzechnik, K.; Rutkowski, K.; Mielke, Z. The S–H \cdots N versus O–H \cdots N hydrogen bonding in the ammonia complexes with CH₃OH and CH₃SH. *J. Mol. Struct.* **2012**, *1009*, 96-102.
- (18) Biswal, H. S.; Wategaonkar, S. Sulfur, not too far behind O, N, and C: SH $\cdots\pi$ hydrogen bond. *J. Phys. Chem. A* **2009**, *113*, 12774-12782.
- (19) Allerhand, A.; Schleyer, P. v. R. A survey of C-H groups as proton donors in hydrogen bonding. *J. Am. Chem. Soc.* **1963**, *85*, 1715-1723.
- (20) Krimm, S.; Kuroiwa, K. Low temperature infrared spectra of polyglycines and C—H \cdots O=C hydrogen bonding in polyglycine II. *Biopolymers* **1968**, *6*, 401-407.
- (21) Gu, Y.; Kar, T.; Scheiner, S. Comparison of the CH \cdots N and CH \cdots O interactions involving substituted alkanes. *J. Mol. Struct.* **2000**, *552*, 17-31.
- (22) Howard, N. W.; Legon, A. C. Pulsed-nozzle, Fourier-transform microwave spectroscopy of the methyl cyanide-acetylene dimer. *J. Chem. Phys.* **1986**, *85*, 6898-6904.
- (23) Kryachko, E.; Scheiner, S. CH \cdots F hydrogen bonds. Dimers of fluoromethanes. *J. Phys. Chem. A* **2004**, *108*, 2527-2535.
- (24) Scheiner, S. Contributions of NH \cdots O and CH \cdots O H-bonds to the stability of β -sheets in proteins. *J. Phys. Chem. B* **2006**, *110*, 18670-18679.
- (25) van der Veken, B. J.; Delanoye, S. N.; Michielsens, B.; Herrebout, W. A. A cryospectroscopic study of the blue-shifting C–H \cdots O bonded complexes of

- pentafluoroethane with dimethyl ether-d₆, acetone-d₆ and oxirane-d₄. *J. Mol. Struct.* **2010**, *976*, 97-104.
- (26) You, L.-Y.; Chen, S.-G.; Zhao, X.; Liu, Y.; Lan, W.-X.; Zhang, Y.; Lu, H.-J.; Cao, C.-Y.; Li, Z.-T. C-H...O hydrogen bonding induced triazole foldamers: Efficient halogen bonding receptors for organohalogenes. *Angew. Chem. Int. Ed.* **2012**, *51*, 1657-1661.
- (27) Scheiner, S., The CH...O Hydrogen Bond. A Historical Account. In *Theory and Applications of Computational Chemistry: The First 40 Years*, ed.; Dykstra, C. E.; Frenking, G.; Kim, K. S.; Scuseria, G. E., Eds.; Elsevier: Amsterdam, 2005; pp 831-857.
- (28) Scheiner, S. Theoretical analysis of the contributions made by CH...O H-bonds to protein structure. *Curr. Org. Chem.* **2010**, *14*, 106-128.
- (29) Barnes, A. J.; Beech, T. R. The vibrational spectrum of the dimethyl ether-water complex. *Chem. Phys. Lett.* **1983**, *94*, 568-570.
- (30) Scheiner, S.; Kar, T. Spectroscopic and structural signature of the CH...O H-bond. *J. Phys. Chem. A* **2008**, *112*, 11854-11860.
- (31) Zierkiewicz, W.; Czarnik-Matusiewicz, B.; Michalska, D. Blue shifts and unusual intensity changes in the infrared spectra of the enflurane...acetone complexes: Spectroscopic and theoretical studies. *J. Phys. Chem. A* **2011**, *115*, 11362-11368.
- (32) Scheiner, S.; Grabowski, S. J.; Kar, T. Influence of hybridization and substitution upon the properties of the CH...O hydrogen bond. *J. Phys. Chem. A* **2001**, *105*, 10607-10612.

- (33) Ford, T. A.; Glasser, L. Ab initio calculations of the structural, energetic and vibrational properties of some hydrogen bonded and van der Waals dimers. Part 3. The formaldehyde dimer. *J. Mol. Struct. (Theochem)* **1997**, 398-399, 381-394.
- (34) Cubero, E.; Orozco, M.; Hobza, P.; Luque, F. J. Hydrogen bond versus anti-hydrogen bond: A comparative analysis based on the electron density topology. *J. Phys. Chem. A* **1999**, 103, 6394-6401.
- (35) Grabowski, S. J. Red- and blue-shifted hydrogen bonds: The Bent rule from quantum theory of atoms in molecules perspective. *J. Phys. Chem. A* **2011**, 115, 12789-12799.
- (36) Michielsen, B.; Dom, J. J. J.; van der Veken, B. J.; Hesse, S.; Xue, Z.; Suhm, M. A.; Herrebout, W. A. The complexes of halothane with benzene: The temperature dependent direction of the complexation shift of the aliphatic C–H stretching. *Phys. Chem. Chem. Phys.* **2010**, 12, 14034-14044.
- (37) Deakyne, C. A.; Meot-Ner, M. Ionic hydrogen bonds in bioenergetics. 4. Interaction energies of acetylcholine with aromatic and polar molecules. *J. Am. Chem. Soc.* **1999**, 121, 1546-1557.
- (38) Bojin, M. D.; Tantillo, D. J. Nonclassical carbocations as C-H hydrogen bond donors. *J. Phys. Chem. A* **2006**, 110, 4810-4816.
- (39) Cybulski, S. M.; Scheiner, S. Comparison of Morokuma and perturbation theory approaches to decomposition of interaction energy. $(\text{NH}_4)^+ \dots \text{NH}_3$. *Chem. Phys. Lett.* **1990**, 166, 57-64.

- (40) Shishkin, O. V.; Palamarchuk, G. V.; Gorb, L.; Leszczynski, J. Opposite charges assisted extra strong C–H \cdots O hydrogen bond in protonated 2'-deoxyadenosine monophosphate. *Chem. Phys. Lett.* **2008**, *452*, 198-205.
- (41) Meot-Ner, M. The ionic hydrogen bond and ion solvation. 1. NH $^+\cdots$ O, NH $^+\cdots$ N, and OH $^+\cdots$ O bonds. Correlations with proton affinity. Deviations due to structural effects. *J. Am. Chem. Soc.* **1984**, *106*, 1257-1264.
- (42) Scheiner, S.; Redfern, P.; Szczesniak, M. M. Effects of external ions on the energetics of proton transfers across hydrogen bonds. *J. Phys. Chem.* **1985**, *89*, 262-266.
- (43) Meot-Ner, M.; Sieck, L. W. The ionic hydrogen bond and ion solvation. 5. OH \cdots O $^-$ bonds. Gas phase solvation and clustering of alkoxide and carboxylate anions. *J. Am. Chem. Soc.* **1986**, *108*, 7525-7529.
- (44) Meot-Ner, M. Comparative stabilities of cationic and anionic hydrogen-bonded networks. Mixed clusters of water-methanol. *J. Am. Chem. Soc.* **1986**, *108*, 6189-6197.
- (45) Szczesniak, M. M.; Scheiner, S. Møller-Plesset treatment of electron correlation in (HOHOH) $^-$. *J. Chem. Phys.* **1982**, *77*, 4586-4593.
- (46) Paul, G. J. C.; Kebarle, P. Thermodynamics of the association reactions of OH $^-$ + H $_2$ O = HOHOH $^-$ and CH $_3$ O $^-$ + CH $_3$ OH = CH $_3$ OHOCH $_3^-$ in the gas phase. *J. Phys. Chem.* **1990**, *94*, 5184-5189.
- (47) Gronert, S. Theoretical studies of proton transfers. 1. The potential energy surfaces of the identity reactions of the first- and second-row non-metal hydrides with their conjugate bases. *J. Am. Chem. Soc.* **1993**, *115*, 10258-10266.

- (48) Berger, I.; Egli, M.; Rich, A. Inter-strand C-H \cdots O hydrogen bonds stabilizing four-stranded intercalated molecules: Stereoelectronic effects of O4' in cytosine-rich DNA. *Proc. Nat. Acad. Sci., USA* **1996**, *93*, 12116-12121.
- (49) Mallinson, P. R.; Wozniak, K.; Smith, G. T.; McCormack, K. L. A charge density analysis of cationic and anionic hydrogen bonds in a "proton sponge" complex. *J. Am. Chem. Soc.* **1997**, *119*, 11502-11509.
- (50) Chabynyc, M. L.; Brauman, J. I. Acidity, basicity, and the stability of hydrogen bonds: Complexes of RO $^-$ + HCF $_3$. *J. Am. Chem. Soc.* **1998**, *120*, 10863-10870.
- (51) Felemez, M.; Bernard, P.; Schlewer, G.; Spiess, B. Inframolecular protonation process of *myo*-inositol 1,4,5-tris(phosphate) and related compounds: Dynamics of the intramolecular interactions and evidence of C-H \cdots O hydrogen bonding. *J. Am. Chem. Soc.* **2000**, *122*, 3156-3165.
- (52) Kryachko, E. S.; Zeegers-Huyskens, T. Theoretical study of the CH \cdots X $^-$ interaction of fluoromethanes and chloromethanes with fluoride, chloride, and hydroxide anions. *J. Phys. Chem. A* **2002**, *106*, 6832-6838.
- (53) Wang, X.-B.; Woo, H.-K.; Kiran, B.; Wang, L.-S. Observation of weak C-H \cdots O hydrogen bonding to unactivated alkanes. *Angew. Chem., Int. Ed. Engl.* **2005**, *44*, 4968-4972.
- (54) Li, Y.; Flood, A. H. Pure C-H hydrogen bonding to chloride ions: A preorganized and rigid macrocyclic receptor. *Angew. Chem., Int. Ed. Engl.* **2008**, *47*, 2649-2652.
- (55) Pedzisa, L.; Hay, B. P. Aliphatic C-H \cdots anion hydrogen bonds: Weak contacts or strong interactions? *J. Org. Chem.* **2009**, *74*, 2554-2560.

- (56) Yang, H.; Wong, M. W. Oxyanion hole stabilization by C-H \cdots O interaction in a transition state-A three-point interaction model for cinchona alkaloid-catalyzed asymmetric methanolysis of meso-cyclic anhydrides. *J. Am. Chem. Soc.* **2013**, *135*, 5808-5818.
- (57) Tatko, C. D.; Waters, M. L. Comparison of C-H \cdots π and hydrophobic interactions in a β -hairpin peptide: Impact on stability and specificity. *J. Am. Chem. Soc.* **2004**, *126*, 2028 - 2034.
- (58) Schmiedekamp, A.; Nanda, V. Metal-activated histidine carbon donor hydrogen bonds contribute to metalloprotein folding and function. *J. Inorg. Biochem.* **2009**, *103*, 1054-1060.
- (59) Sukumar, N.; Mathews, F. S.; Langan, P.; Davidson, V. L. A joint x-ray and neutron study on amicyanin reveals the role of protein dynamics in electron transfer. *Proc. Nat. Acad. Sci., USA* **2010**, *107*, 6817-6822.
- (60) Couture, J.-F.; Hauk, G.; Thompson, M. J.; Blackburn, G. M.; Trievel, R. C. Catalytic roles for carbon-oxygen hydrogen bonding in SET domain lysine methyltransferases. *J. Biol. Chem.* **2006**, *281*, 19280-19287.
- (61) Couture, J.-F.; Collazo, E.; Ortiz-Tello, P. A.; Brunzelle, J. S.; Trievel, R. C. Specificity and mechanism of JMJD2A, a trimethyllysine-specific histone demethylase. *Nat. Struct. Mol. Biol.* **2007**, *14*, 689-695.
- (62) Couture, J.-F.; Dirk, L. M. A.; Brunzelle, J. S.; Houtz, R. L.; Trievel, R. C. Structural origins for the product specificity of SET domain protein methyltransferases. *Proc. Nat. Acad. Sci., USA* **2008**, *105*, 20659-20664.

- (63) Del Rizzo, P. A.; Couture, J.-F.; Dirk, L. M. A.; Strunk, B. S.; Roiko, M. S.; Brunzelle, J. S.; Houtz, R. L.; Trievel, R. C. SET7/9 catalytic mutants reveal the role of active site water molecules in lysine multiple methylation. *J. Biol. Chem.* **2010**, *285*, 31849-31858.
- (64) Horowitz, S.; Yessleman, J. D.; Al-Hashimi, H. M.; Trievel, R. C. Direct evidence for methyl group coordination by carbon-oxygen hydrogen bonds in the lysine methyltransferase SET7/9. *J. Biol. Chem.* **2011**, *286*, 18658-18663.
- (65) Sreerama, N.; Vishveshwara, S. An ab initio study of (C-H \cdots X)⁺ hydrogen bonds including biological systems. *J. Mol. Struct. (Theochem)* **1985**, *133*, 139-146.
- (66) Kim, K. S.; Lee, J. Y.; Lee, S. J.; Ha, T.-K.; Kim, D. H. On binding forces between aromatic ring and quaternary ammonium compound. *J. Am. Chem. Soc.* **1994**, *116*, 7399-7400.
- (67) Cannizzaro, C. E.; Houk, K. N. Magnitude and chemical consequences of R₃N⁺-C-H \cdots O=C hydrogen bonding. *J. Am. Chem. Soc.* **2002**, *124*, 7163-7169.
- (68) Scheiner, S.; Kar, T.; Gu, Y. Strength of the C ^{α} H \cdots O hydrogen bond of amino acid residues. *J. Biol. Chem.* **2001**, *276*, 9832-9837.
- (69) Kryachko, E. S.; Nguyen, M. T. Low energy barrier proton transfer in protonated benzene-water complex. *J. Phys. Chem. A* **2001**, *105*, 153-155.
- (70) Raymo, F. M.; Bartberger, M. D.; Houk, K. N.; Stoddart, J. F. The magnitude of [C-H \cdots O] hydrogen bonding in molecular and supramolecular assemblies. *J. Am. Chem. Soc.* **2001**, *123*, 9264-9267.
- (71) Scheiner, S.; Kar, T.; Pattanayak, J. Comparison of various types of hydrogen bonds involving aromatic amino acids. *J. Am. Chem. Soc.* **2002**, *124*, 13257-13264.

- (72) Chang, H.-C.; Lee, K. M.; Jiang, J.-C.; Lin, M.-S.; Chen, J.-S.; Lin, I. J. B.; Lin, S. H. Charge-enhanced C–H···O interactions of a self-assembled triple helical spine probed by high-pressure. *J. Chem. Phys.* **2002**, *117*, 1723-1728.
- (73) Frisch, M. J.; Trucks, G. W.; Schlegel, H. B.; Scuseria, G. E.; Robb, M. A.; Cheeseman, J. R.; Scalmani, G.; Barone, V.; Mennucci, B.; Petersson, G. A. et al. *Gaussian 09*, Revision B.01; Wallingford, CT, 2009.
- (74) Singh, P. C. C–H···O/N hydrogen bonded complexes of FKrCCH are stronger than FCCCH complexes: Effect of rare gas insertion. *Chem. Phys. Lett.* **2011**, *515*, 206-209.
- (75) Li, H.; Lu, Y.; Liu, Y.; Zhu, X.; Liu, H.; Zhu, W. Interplay between halogen bonds and π – π stacking interactions: CSD search and theoretical study. *Phys. Chem. Chem. Phys.* **2012**, *14*, 9948-9955.
- (76) Riley, K. E.; Murray, J. S.; Fanfrlík, J.; Rezáč, J.; Solá, R. J.; Concha, M. C.; Ramos, F. M.; Politzer, P. Halogen bond tunability I: The effects of aromatic fluorine substitution on the strengths of halogen-bonding interactions involving chlorine, bromine, and iodine. *J. Mol. Model.* **2011**, *17*, 3309-3318.
- (77) Hauchecorne, D.; Nagels, N.; van der Veken, B. J.; Herrebout, W. A. C–X··· π halogen and C–H··· π hydrogen bonding: Interactions of CF₃X (X = Cl, Br, I or H) with ethene and propene. *Phys. Chem. Chem. Phys.* **2012**, *14*, 681-690.
- (78) Scheiner, S. Effects of substituents upon the P···N noncovalent interaction: The limits of its strength. *J. Phys. Chem. A* **2011**, *115*, 11202-11209.

- (79) Munusamy, E.; Sedlak, R.; Hobza, P. On the nature of the stabilization of benzene–dihalogen and benzene–dinitrogen complexes: CCSD(T)/CBS and DFT-SAPT calculations. *ChemPhysChem*. **2011**, *12*, 3253-3261.
- (80) Zhao, Y.; Truhlar, D. G. The M06 suite of density functionals for main group thermochemistry, thermochemical kinetics, noncovalent interactions, excited states, and transition elements: Two new functionals and systematic testing of four M06-class functionals and 12 other functionals. *Theor. Chem. Acc.* **2008**, *120*, 215-241.
- (81) Vincent, M. A.; Hillier, I. H. The structure and interaction energies of the weak complexes of CHClF_2 and CHF_3 with HCCH : A test of density functional theory methods. *Phys. Chem. Chem. Phys.* **2011**, *13*, 4388-4392.
- (82) Biller, M. J.; Mecozzi, S. A high level computational study of the CH_4/CF_4 dimer: How does it compare with the CH_4/CH_4 and CF_4/CF_4 dimers? *Mol. Phys.* **2012**, *110*, 377-387.
- (83) Majumder, M.; Mishra, B. K.; Sathyamurthy, N. $\text{CH}\cdots\pi$ and $\pi\cdots\pi$ interaction in benzene-acetylene clusters. *Chem. Phys.* **2013**, *557*, 59-65.
- (84) Karthikeyan, S.; Ramanathan, V.; Mishra, B. K. Influence of the substituents on the $\text{CH}\cdots\pi$ interaction: Benzene–methane complex. *J. Phys. Chem. A* **2013**, *117*, 6687-6694.
- (85) Boys, S. F.; Bernardi, F. The calculation of small molecular interactions by the differences of separate total energies. Some procedures with reduced errors. *Mol. Phys.* **1970**, *19*, 553-566.
- (86) Reed, A. E.; Weinhold, F.; Curtiss, L. A.; Pochatko, D. J. Natural bond orbital analysis of molecular interactions: Theoretical studies of binary complexes of HF,

- H₂O, NH₃, N₂, O₂, F₂, CO and CO₂ with HF, H₂O, and NH₃. *J. Chem. Phys.* **1986**, *84*, 5687-5705.
- (87) Reed, A. E.; Curtiss, L. A.; Weinhold, F. Intermolecular interactions from a natural bond orbital, donor-acceptor viewpoint. *Chem. Rev.* **1988**, *88*, 899-926.
- (88) Moszynski, R.; Wormer, P. E. S.; Jeziorski, B.; van der Avoird, A. Symmetry-adapted perturbation theory of nonadditive three-body interactions in van der Waals molecules. I. General theory. *J. Chem. Phys.* **1995**, *103*, 8058-8074.
- (89) Werner, H.-J.; Knowles, P. J.; Manby, F. R.; Schütz, M.; P. Celani; Knizia, G.; Korona, T.; Lindh, R.; Mitrushenkov, A.; Rauhut, G. et al. *MOLPRO*, Version 2006; 2010.
- (90) Barone, V.; Cossi, M. Quantum calculation of molecular energies and energy gradients in solution by a conductor solvent model. *J. Phys. Chem. A* **1998**, *102*, (11), 1995-2001.
- (91) Ditchfield, R. Self-consistent perturbation theory of diamagnetism. I. A gauge-invariant LCAO method for N.M.R. chemical shifts. *Mol. Phys.* **1974**, *27*, 789-807.
- (92) Wolinski, K.; Hilton, J. F.; Pulay, P. Efficient implementation of the gauge-independent atomic orbital method for NMR chemical shift calculations. *J. Am. Chem. Soc.* **1990**, *112*, 8251-8260.
- (93) Scheiner, S.; Kar, T. Effect of solvent upon CH··O hydrogen bonds with implications for protein folding. *J. Phys. Chem. B* **2005**, *109*, 3681-3689.
- (94) Ando, S.; Ando, I.; Shoji, A.; Ozaki, T. Intermolecular hydrogen-bonding effect on carbon-13 NMR chemical shifts of glycine residue carbonyl carbons of peptides in the solid state. *J. Am. Chem. Soc.* **1988**, *110*, (11), 3380-3386.

- (95) Hibbert, F.; Emsley, J. Hydrogen bonding and chemical reactivity. *Adv. Phys. Org. Chem.* **1990**, *26*, 255-379.
- (96) Mizuno, K.; Ochi, T.; Shindo, Y. Hydrophobic hydration of acetone probed by nuclear magnetic resonance and infrared: Evidence for the interaction C-H \cdots OH₂. *J. Chem. Phys.* **1998**, *109*, 9502-9507.
- (97) Afonin, A. V.; Vashchenko, A. V.; Takagi, T.; Kimura, A.; Fujiwara, H. Specific intramolecular interactions C-H \cdots N in heteroaryl vinyl ethers and heteroaryl vinyl sulfides studied by ¹H, ¹³C, and ¹⁵N NMR spectroscopies and by ab initio calculations on molecular structures as well as on nuclear shieldings. *Can. J. Chem.* **1999**, *77*, 416-424.
- (98) Scheiner, S.; Gu, Y.; Kar, T. Evaluation of the H-bonding properties of CH \cdots O interactions based upon NMR spectra. *J. Mol. Struct. (Theochem)* **2000**, *500*, 441-452.
- (99) Isaev, A. N. C-H \cdots O, OH \cdots C, and C-H \cdots C interactions in complexes of carbocations and carboanions. *Russ. J. Inorg. Chem.* **2013**, *58*, 817-823.

Table 11-1. Binding energies (kcal/mol) of complexes with NMA computed at two levels of theory.

proton donor	MP2/aug-cc-pVDZ	M06-2X/6-31+G**
S(Me) ₂	4.88	6.26
S(Me) ₃ ⁺	20.55	22.17
N(Me) ₃	2.05	2.83
N(Me) ₄ ⁺	18.79	20.29

Table 11-2. R(H••O) distances (Å) in complexes of NMA with terminal methyl groups, at M06-2X/6-31+G** level.

proton donor	binding E, kcal/mol	R(H••O), Å		
		Me-1	Me-2	Me-3
S(Me) ₂	6.26	2.385	2.457	
S(Me) ₃ ⁺	22.17	2.162	2.188	2.192
S(Et) ₃ ⁺	15.00	2.254	2.258	2.279
S(Pr) ₃ ⁺	10.71	2.420	2.442	2.473
N(Me) ₃	2.83	2.605	2.633	2.941
N(Me) ₄ ⁺	20.29	2.205	2.214	2.23
N(Et) ₄ ⁺	14.10	2.265	2.268	2.273
N(Pr) ₄ ⁺	10.47	2.385	2.385	2.402

Table 11-3. NBO values of E(2) (kcal/mol) for complexes involving terminal methyl groups, at M06-2X/6-31+G** level.

proton donor	O _{lp} →σ*(C-H) (πCO→σ*(C-H))			Total
	Me-1	Me-2	Me-3	
S(Me) ₂	1.29(0.59)	1.72(0.84)		4.44
S(Me) ₃ ⁺	4.82(1.03)	3.72(1.81)	6.65(0.18)	18.21
S(Et) ₃ ⁺	3.25(1.00)	3.59(0.52)	4.54(0.06)	12.96
S(Pr) ₃ ⁺	1.51	1.20(0.26)	1.09(0.10)	4.16
N(Me) ₃	0.54(0.56)	0.86(0.41)		2.50
N(Me) ₄ ⁺	3.81(0.92)	3.11(1.18)	5.27(0.06)	14.35
N(Et) ₄ ⁺	4.30(0.06)	3.00(1.04)	3.75(0.39)	12.54
N(Pr) ₄ ⁺	2.21	1.60(0.34)	1.77(0.20)	6.12

Table 11-4. SAPT decomposition of total binding energies (kcal/mol) of S and N complexes with NMA as H-bond acceptor.

	S(Me) ₂	N(Me) ₃	S(Me) ₃ ⁺	N(Me) ₄ ⁺
ES	-7.39	-3.32	-25.23	-22.60
EX	10.47	7.25	14.50	12.44
IND	-4.57	-3.26	-8.38	-7.01
IND+EXIND	-1.26	-0.66	-5.50	-4.73
DISP	-8.56	-6.53	-7.29	-6.48
DISP+EXDISP	-7.31	-5.60	-6.20	-5.55

Table 11-5. Changes in NMR chemical shielding (σ , ppm) of protons caused by complexation with NMA at M06-2X/6-31+G** level.

	terminal CH ₃ ^a	CH adjacent to S/N ^b	average of all H ^c	single CH ₃ ··O ^d	single CH··O ^e
S(Me) ₂	-0.74	-0.74	-0.09	-0.46	-1.91
S(Me) ₃ ⁺	-2.23	-2.23	-0.44	-0.79	-3.50
S(Et) ₃ ⁺	-1.73	-2.12	-0.41	-0.52	-2.98
S(Pr) ₃ ⁺	-1.15	-2.11	-0.33	-0.51	-2.49
N(Me) ₃	-0.82	-0.82	-0.07	-0.46	-1.36
N(Me) ₄ ⁺	-2.01	-2.01	-0.45	-0.70	-3.22
N(Et) ₄ ⁺	-1.76	-1.78	-0.46	-0.52	-2.99
N(Pr) ₄ ⁺	-1.46	-1.92	-0.44	-0.56	-2.50

^aaverage of only bridging H atoms, with NMA H-bonded to multiple terminal methyl groups

^baverage of only bridging H atoms, with NMA H-bonded to methylene groups adjacent to central atom

^caverage change of *all* H atoms, bridging and non-bridging, of terminal methyl groups H-bonded to NMA

^daverage of bridging H atoms, with NMA H-bonded to 3 H atoms of a single methyl group

^eNMA H-bonded to a single H atom in a linear CH··O arrangement

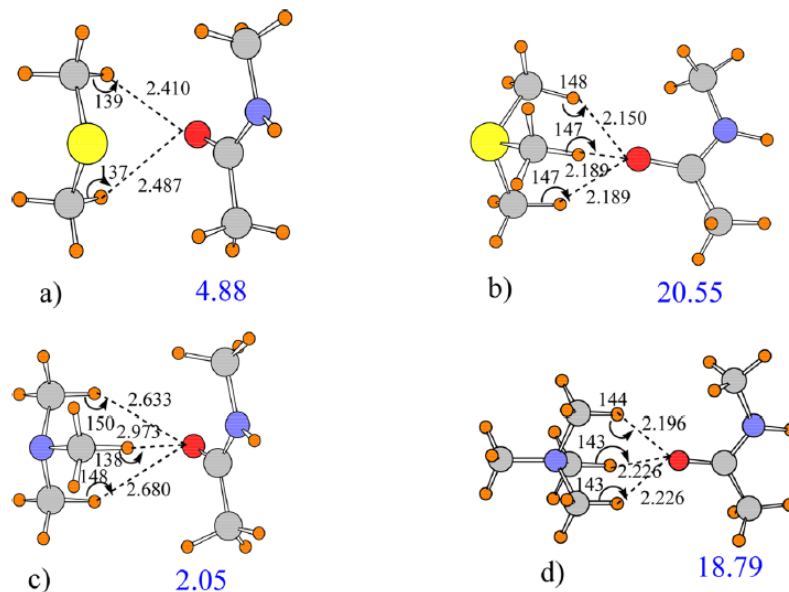


Figure 11-1. Optimized geometries (MP2/aug-cc-pVDZ) of a) S(Me)₂, b) S(Me)₃⁺, c) N(Me)₃, and d) N(Me)₄⁺ complexes with NMA as H bond acceptor. Blue numbers represent counterpoise-corrected binding energies in kcal/mol. Distances in Å and angles in degrees.

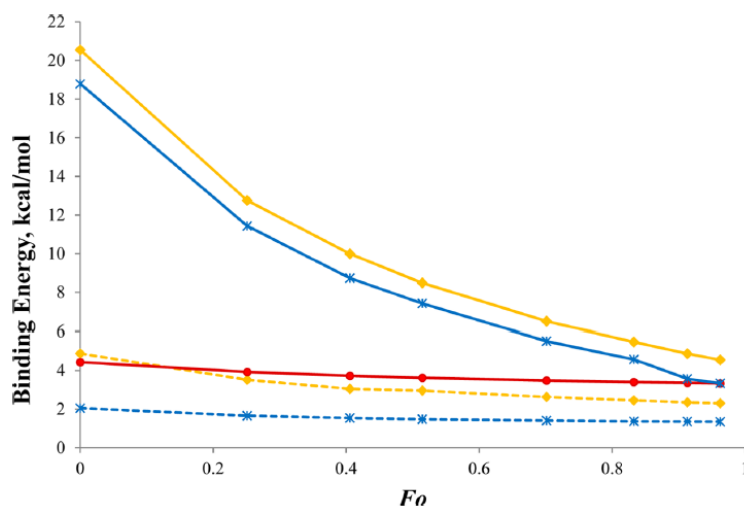


Figure 11-2. Binding energies plotted against Onsager function (Fo) for S(Me)₂, S(Me)₃⁺, N(Me)₃ and N(Me)₄⁺ complexes with NMA as proton acceptor, as MP2/aug-cc-pVDZ level. Yellow and blue colors indicate S and N donors, respectively, solid curves for cationic and dotted for neutral complexes. Red line represents neutral water dimer.

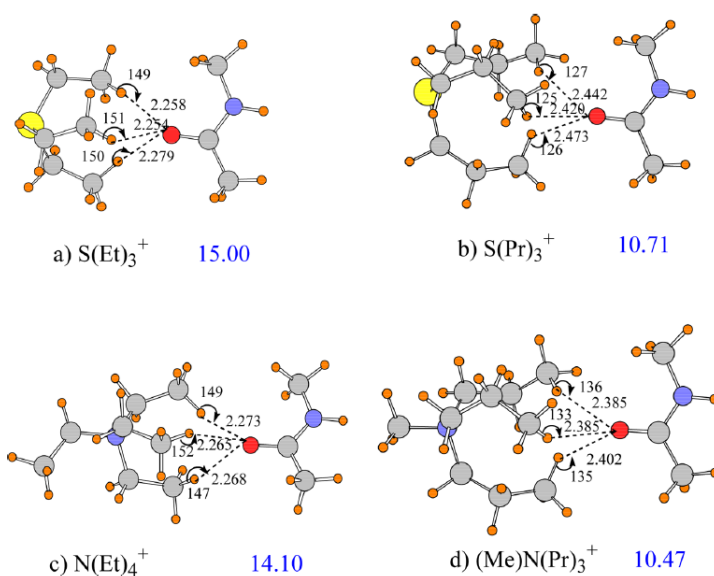


Figure 11-3. Optimized geometries (M06-2X/6-31+G**) for S^+ and N^+ complexes with elongated alkyl groups; NMA as proton acceptor. Blue numbers indicate counterpoise-corrected binding energies in kcal/mol. Distances in Å and angles in degrees.

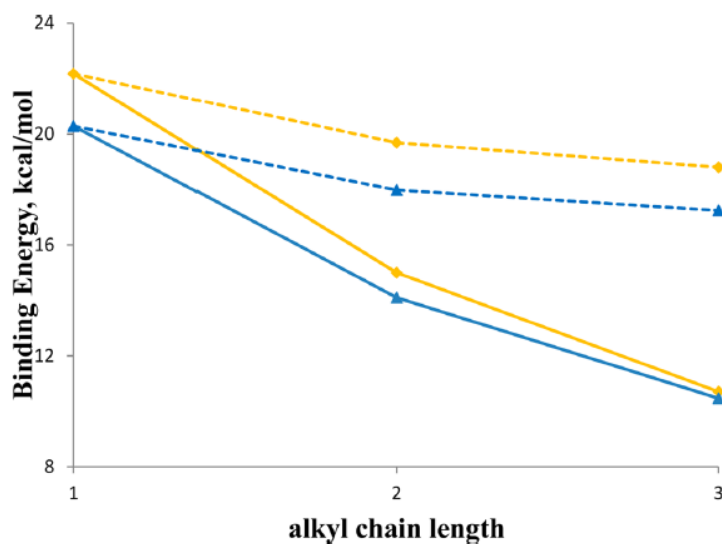


Figure 11-4. Variation of binding energy with increase in alkyl chain length of R_3S^+ (yellow) and R_4N^+ (blue) complexes with NMA. Solid lines represent trifurcated $\text{CH}\cdots\text{O}$ H bonding with one CH of each of three terminal CH_3 groups; dotted lines indicate O interacting with the three CH_2 groups closest to central S or N atom.

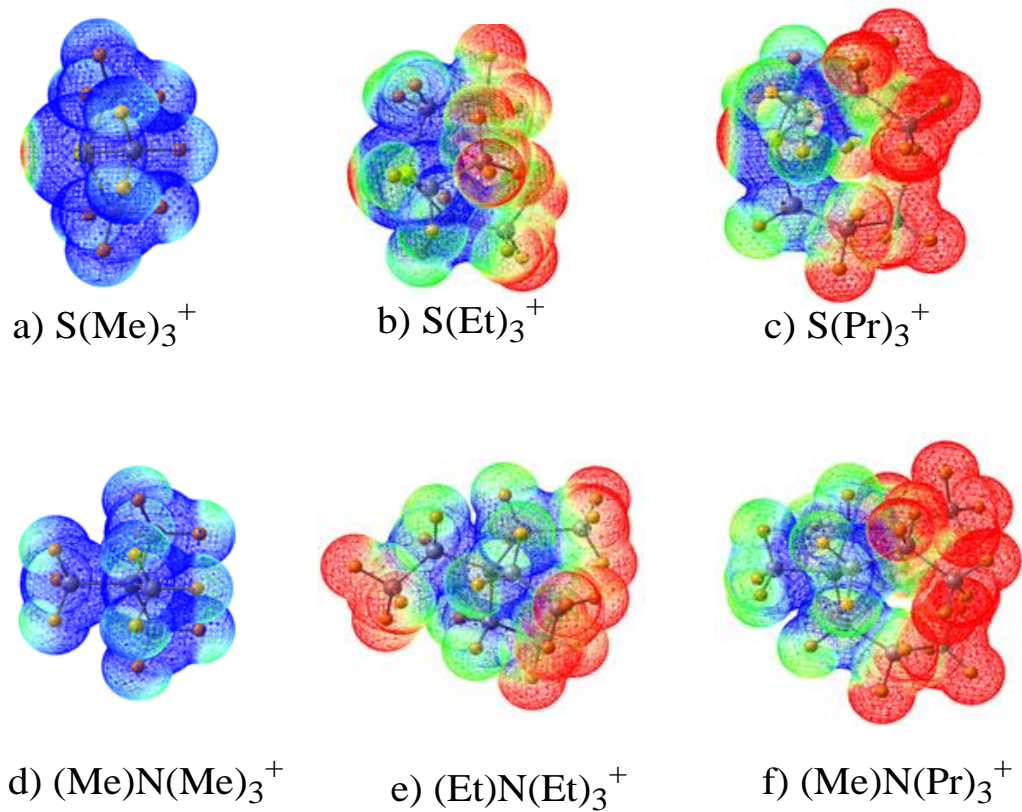


Figure 11-5. Electrostatic potential maps for alkyl-substituted S^+ and N^+ monomers. Contours range from 0.20 - 0.25 au. Blue and red colors indicate most and least positive regions, respectively, on the van der Waals atomic surface.

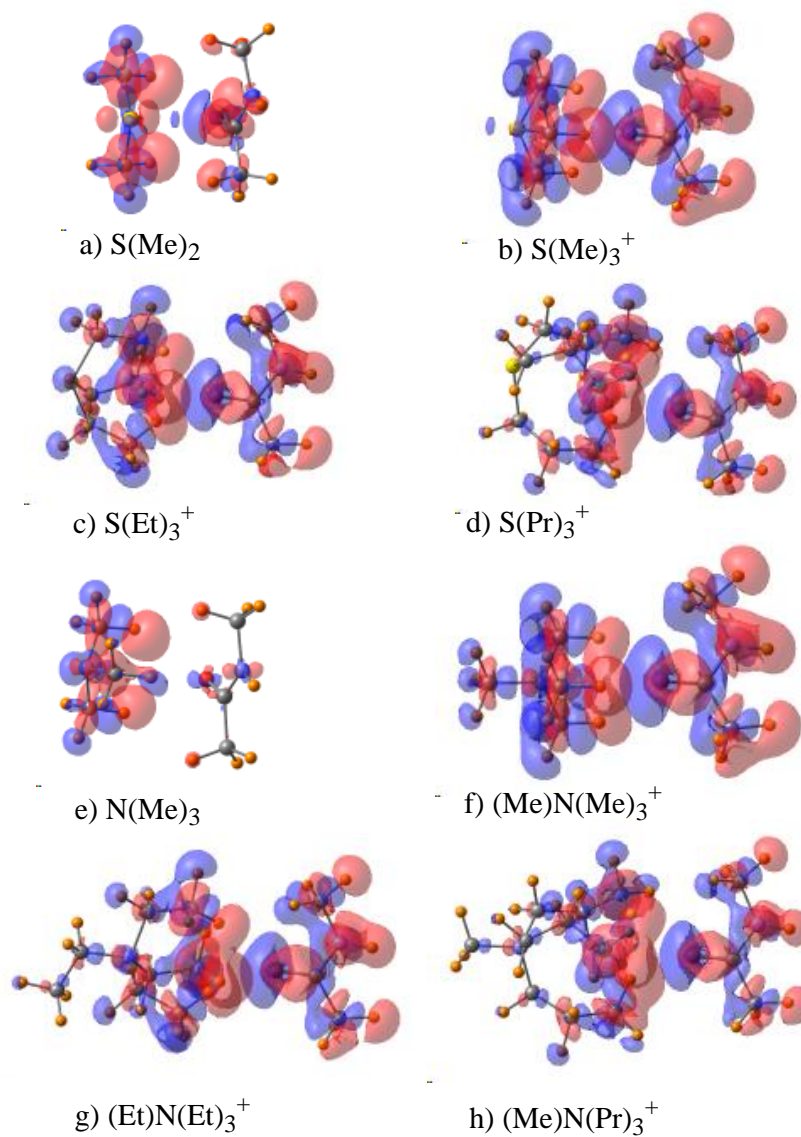


Figure 11-6. Electron density shifts arising from formation of each complex: proton donor is listed, and NMA is proton acceptor in all cases. Blue regions indicate density increase, and red a density loss. Contours are shown at the 0.0005 au level.

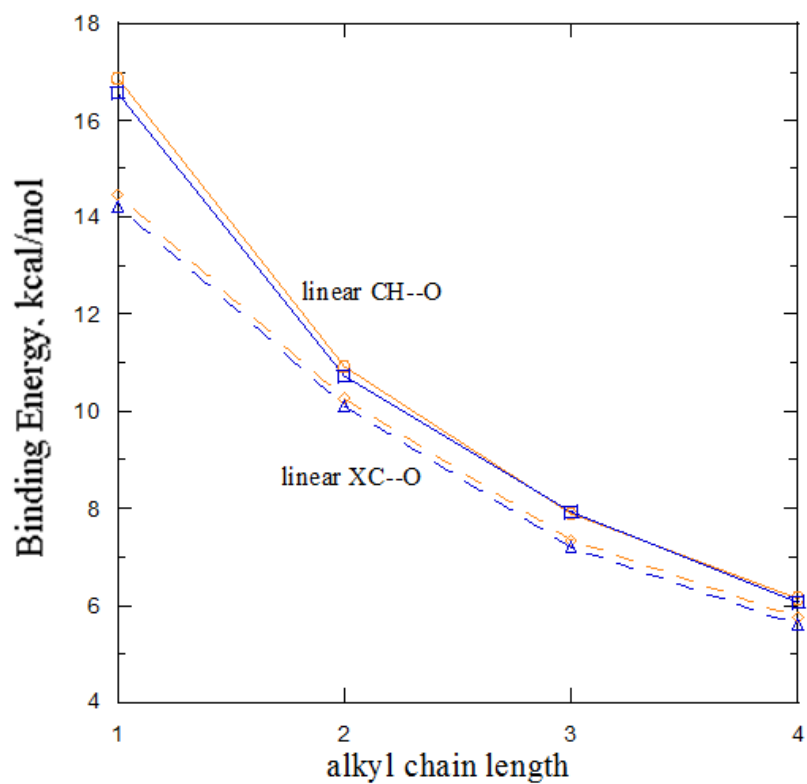


Figure 11-7. Variation of binding energy for cationic complexes with increase in alkyl chain length. Broken curves were generated when all three CH donors arise from the same terminal methyl group; a single CH...O H-bond is characterized by solid curves. N donors are indicated by blue, and S by yellow.

CHAPTER 12

DO PHENOLIC AND CARBOXYLIC GROUPS COEXIST AT THE TIPS OF
OXIDIZED SINGLE-WALL CARBON NANOTUBES (O-SWNTs)?¹**Abstract**

Vibrational frequency analyses using density functional theory (DFT) resolves some structural features of purified oxidized single-wall carbon nanotubes (o-SWNTs). Both –COOH and phenolic –OH (OH_{ph}) groups, predicted in several experimental studies to be present in o-SWNTs, were considered at the tips of armchair and zigzag tubes with varying diameters. Hydrogen bonding, where carbonyl oxygen acts as proton acceptor while phenolic OH donates the proton, leads to the most stable isomers, with a H-bond energy of 9-12 kcal/mol, almost double that of simpler systems. Vibrational frequencies of participating bonds are significantly red-shifted, which is not reflected in experimental spectra, and which leads to the conclusion that phenolic OH is likely not present at the tips of o-SWNTs.

12-1. Introduction

Raw single-wall carbon nanotube (SWNTs) samples are typically purified [1-5] by mild to strong acid treatments, followed by repeated wash and dry techniques to remove metal catalysts and carbonaceous particles. Such oxidation processes introduce several oxygen-containing functional groups preferentially at the tips of SWNTs as well as at the surface or wall [6-9]. IR spectroscopy has served as a workhorse to determine

¹ Coauthored by Upendra Adhikari, Steve Scheiner, Ajit K. Roy and Tapas Kar. Reproduced with permission from *Carbon* **2014**, 73, 194-205. Copyright 2014, Elsevier.

the presence of functional groups on the oxidized-SWNT (o-SWNTs) structures. The presence of these functional groups, especially COOH, elevated the importance of o-SWNTs since further functionalization [8, 10-17] can create a wide range of application-driven nanomaterials. Thus, understanding the structure of o-SWNTs, the number and location of these functional groups, and how they interact with one another is crucial in making advances in this arena. Although significant progress has been made on oxidized and functionalized single-wall carbon nanotubes (f-SWNTs), their structures have not been fully understood due to several problems, such as inhomogeneity in raw as well as in oxidized SWNTs samples, oxidation processes, and conditions.

Unambiguous assignment of different functional groups has been complicated by several intermingling factors, such as hydrogen bonding among groups, and coupling and conjugation with other vibrational modes. Moreover, complexity arises in analyzing spectral data, as several C=O vibrational bands appear in the same region. Assignment of different peaks of complicated IR spectra of o-SWNTs to particular functional groups is based on the standard IR data of simple organic molecules. For example, a strong IR band around $1720 - 1760 \text{ cm}^{-1}$ (characteristic of a C=O mode), in addition to a broad peak in the $3000-3600 \text{ cm}^{-1}$ range (O-H mode) [18] is taken as indicative of the presence of a COOH group.

However, some of the reference frequencies of standalone functional groups may change when part of o-SWNT for several reasons. The most common factor is the formation of OH--O hydrogen bonding, where the participating C=O or O-H mode undergoes a red-shift [19]. Another key factor, that either up-shifts or down-shifts the

relevant frequencies, is the conjugation or coupling of close energy bands, as well as the concentration of functional groups.

Recent theoretical studies [20, 21] revealed a new structural factor that has significant influence on vibrational spectra of carboxylated SWNTs, one which was not envisioned earlier from fundamental concepts. Some of the carboxylic acid groups located at the tips of zigzag tubes exhibit a low-frequency peak around 1650 cm^{-1} with significantly higher intensity than the standard C=O stretching frequency of this acid group. (It is worth mentioning that absorption in this region is in fact observed in several experimental spectra of o-SWNTs [3, 22-28]. Due to its similarity with standard quinone C=O frequency [29] this peak was assigned as a quinone C=O mode.) This lower frequency C=O band, that distinguishes between zigzag and armchair tubes, is not a result of H-bonding among acid groups, nor can it be reproduced by small models such as benzoic acid. Its origin was attributed instead to the curvature of zigzag tubes in addition to their structural arrangement, where the C=O distance is longer, by about 0.01 \AA , than standard C=O bonds. In fact, carboxylated graphene also exhibits such a low-frequency mode when a COOH group is located at the zigzag edge which distinguishes them from corner or armchair sites [30].

It seems clear then that well-established reference IR data may not be used blindly in characterizing functional groups located at SWNTs. Moreover, the character of the hydrogen bond linking different O-containing groups may differ from what is observed in simple organic molecules. The magnitude of red or blue shift may vary significantly depending on the interaction strengths and structural factors. Since acid groups at the tips of zigzag (m,0) tubes differ in character from those of armchair (n,n) tubes, the behavior

of these groups when participating in H-bonds with other groups is subject to question. For example, do their strengths differ, and if so, by how much? What are the magnitudes of red -shift of participating modes when located on either (m,0) or (n,n) tubes? Resolving these issues would not only improve our understanding of the structure of o-SWNTs, but may reveal some new principles, as noted in our previous studies [20, 21], that are unusual and that might not fit into the current concept scheme of organic chemistry or H-bonding.

According to experimental studies, carboxylic -COOH and phenolic -OH groups, among several other oxygen containing functional groups (such as quinone, ester, carbonyl, etc.) are most commonly observed. (It may be noted that zigzag tubes may not contain quinone C=O as their presence would disrupt the conjugation, like *meta*-benzoquinone, of the entire system). We considered both -COOH and OH groups at the tips of armchair and zigzag tubes in the present computational study. Different possible structural arrangements, H-bonded as well as non-bonded, were considered, and results were compared with SWNT-COOH and SWNT-OH to assess the effects of H-bonding. Emphasis is placed on calculating vibrational spectra of all possible structures and theoretical vibrational data are used to disentangle experimental spectra. There have been prior theoretical studies of SWNT-COOH [31, 32], SWNT-OH [32-34] and SWNT-COOH-OH [35] but these were focused on structures and energetics of a limited variety of SWNTs with varying number of functional groups.

12-2. Models and Method of Calculations

Investigations on large systems like nanotubes, including calculation of vibrational frequencies, are computationally highly demanding and so require a protocol that is both accurate and feasible. Kar and coworkers have [36-39] shown the advantages of using the *same level different basis* (SLDB) prescription over other procedures, such as the widely used ONIOM [40, 41] method for studying SWNTs and their chemical modifications. In fact, several other studies also indicated ONIOM is not a reliable method for studying functionalized nanotubes due to disruption of the π -network [42-45]. In the SLDB approach, atoms in defined active sites are provided with large sets of basis functions, while smaller sets are applied to the remaining atoms. Previous studies [37, 38] demonstrated that the use of a larger basis set for a small number of atoms at active sites is sufficient to reproduce structure, energetics, and vibrational spectra for sidewall and end-functionalized nanotubes.

This DFT-SLDB technique was used throughout in the present study. In this protocol, $4n$ ($2m$) carbons at the functionalized site of armchair (zigzag) tubes and functional groups were treated with 6-31G*(O+) basis (where C and H atoms are treated with double-zeta quality 6-31G* basis functions and diffuse functions are included for better description of electronegative oxygen atoms) and 3-21G basis was used for the remaining carbons. A larger basis set was used for terminal hydrogens at the functionalized end and 3-21G for hydrogens at the other end of SWNTs. Thus, 6-31G*(O+) is used for 16 carbons of (4,4) or (8,0), 20 carbons of (5,5) or (10,0), 18 carbons for (9,0) and 24 carbons of (6,6). Use of such a combined basis set reduces computational time by more than 50% for SCF steps and by more than 60% for

vibrational steps, while reproducing properties quite accurately [20]. The B3LYP variant of density functional theory (DFT) [46, 47] was employed in order to include correlation effects. The accuracy of normal mode calculations using the B3LYP functional is sufficiently high and includes an optimal cost-to-benefit ratio [48-51].

Relative energies (E_{rel}) and enthalpies (H_{rel}) were obtained by considering energy and enthalpy of the most stable structure, respectively, as reference. Since trends in H_{rel} are similar to E_{rel} , the latter quantity is primarily used in discussing the stability of different structures. Introduction of functional groups, by replacing hydrogens of the pristine tube, causes slight deformation of the tube structure, mainly in the vicinity of functionalized sites. Such deformation costs some energy, and this energy term was estimated as the difference between the energy of the non-functionalized tube with the functionalized tube geometry from the energy of the fully optimized pristine tube.

Because computed harmonic vibrational frequencies are typically slightly overestimated (even for more accurate methods, such as MP2, CCSD(T) etc, as well as for larger basis sets) a scale factor is commonly used to improve agreement with experimental spectra. For example, a value of 0.960 is recommended for B3LYP/6-31G* method [52]. Since we are primarily interested in the spectra of attached functional groups, application of a scale factor of 0.96 was deemed a reasonable choice.

All calculations were performed using the Gaussian-09 [53] code. Theoretical vibrational modes were analyzed using Molden [54] and Chemcraft [55]. Pristine nanotube models were obtained using TubeVBS software [56], and in the o-SWNTs models COOH and OH groups and terminal hydrogen atoms were positioned using

Chemcraft [55], which was also used to generate o-SWNTs figures for geometry analyses.

12-3. Results and Discussion

The specific models of o-SWNTs considered in the present study are armchair (n,n), n=4, 5 and 6, and zigzag (m,0), m=8, 9 and 10. Each armchair (n,n) tube contains 4n carbon atoms compared to 2m for zigzag (m,0) in each layer. Our SWNT models are composed of four layers of carbons for both kinds of tube. The smallest (4,4) and (8,0) tubes thus contain 64 C atoms whereas there are 96 and 80 atoms in the largest (6,6) and (10,0) tubes, respectively. Thus the length of the tube in all models is just less than 1.0 nm. As the present study is focused on the intrinsic properties of COOH and OH groups present at the tips of SWNTs, their vibrational modes are not likely to be sensitive to small differences in tube length. In fact, in the case of the single acid group of SWNT-COOH, the length of the nanotube had practically no effect on C=O vibrational modes [38].

12-3.1. SWNT-COOH

Single and multiple COOH groups at the tips of a wide range of SWNTs were reported in our previous studies [20, 21, 37, 38, 57] and results relevant to the context of present study are briefly summarized here. Fully optimized geometries of (4,4)-COOH and (8,0)-COOH, representing (n,n)-COOH and (m,0)-COOH respectively, are depicted in Figure 12-1. Relevant geometric parameters and vibrational frequencies along with their intensities are summarized in the first section of Table 12-1. Side views of SWNT-

COOH (Figure 12-1) clearly indicate the tube surface is not distorted by the introduction of a single acid group at the tip, except right in the vicinity of the functionalized site.

The second column of Table 12-1 indicates a difference between C=O stretching modes in armchair (n,n) and zigzag (m,0) tubes. The former category of SWNT exhibits $\nu(\text{C=O})$ frequencies greater than 1700 cm^{-1} which is typical of most carboxylic groups [18]. The C=O modes of zigzag-COOH, irrespective of their diameter, exhibit a much lower frequency (below 1650 cm^{-1}), which is very unusual and uncommon for carboxylic acids in organic molecules.

Successive increase in the diameter of the armchair (n,n) tube by about 0.13 nm causes the C=O mode to red-shift by 1 cm^{-1} and intensity decreases by about 20 km/mol. In contrast, as the diameter of the semiconducting (m,0, m = 8 and 10) tube increases from 0.63 to 0.78 nm a 2 cm^{-1} blue-shift was found with almost the same intensity. However, the metallic zigzag (9,0)-COOH tube exhibits lower C=O frequency with slightly higher intensity compared to the smaller or larger semiconducting (m,0) tubes. These vibrational data clearly suggest the C=O mode is a good candidate to distinguish SWNTs based on chirality, but seems to have less potential to determine the diameter of tubes.

No definite trends, based on diameter of tubes, are observed in the O-H stretching vibrational modes of the COOH group. However, $\nu(\text{O-H})$ values for zigzag-COOH are slightly higher (by about 16 cm^{-1}) than those of armchair-COOH tubes. In addition, the intensities of O-H bands are slightly higher in the former tubes. Such differences in the O-H band of COOH, combined with C=O modes, may be a signature in identifying tubes based on their chirality.

Key geometric parameters, summarized in Table 12-1, are insensitive to the diameter of (n,n)-COOH tubes. For example, the C=O, C-O and O-H bond length of COOH in all three tubes are 1.220 Å, 1.360 Å and 0.976 Å, respectively. The C=O bonds of (m,0)-COOH tubes are slightly longer (by about 12 mÅ) than that of armchair tubes, which is reflected also in their lower vibrational frequencies discussed above. The C-O bond lengths of zigzag-COOH also follow the same trend, but the difference is slightly higher than in the C=O bonds. In comparison with semiconducting (8,0)-COOH and (10,0)-COOH, the metallic (9,0)-COOH tube exhibits a slightly longer C-O bond. The C-COOH bonds of all zigzag tubes are shorter by about 40 mÅ than their counterparts for armchair tubes. The O-H bonds of COOH shrink by only 1 mÅ as the chirality of the tube changes from (n,n) to (m,0). In summary, the major and most noticeable difference in structural parameters of both kinds of tubes resides in the C=O bond length, as well as its stretching frequency.

12-3.2. SWNT-OH

A single -OH (phenolic OH) group at the tip of various SWNTs was considered and the results are reported in the lower section of Table 12-1, with optimized structure of (4,4)-OH and (8,0)-OH depicted in Figure 12-2. Similar to -COOH, a single -OH has practically no effect on the surface of the tubes and the orientation of the -OH is apparently the same for all tubes, irrespective of their diameter and chirality. The O-H bonds of both kinds of tube, displayed in the last column of Table 12-1, are insensitive to tube diameter. Differences in this bond length between armchair and zigzag tubes are only 1 mÅ, the former being longer. In comparison to OH bond lengths of COOH groups,

phenolic OH bonds are slightly (by about 5 mÅ) shorter. Similar to C-COOH linking bonds of SWNT-COOH, C-OH bonds of SWNTs-OH are also insensitive to diameter. However, this bond is slightly longer in zigzag tubes (by about 10 mÅ) than armchair tubes.

The O-H frequencies of (n,n)-OH tubes are slightly lower than those of (m,0)-OH, with close to half the intensity. With the increase in diameter of (n,n) tube, $\nu(\text{O-H})$ increases by 4 cm^{-1} without any change in intensity. In the case of semiconducting (m,0)-OH, this frequency increases by only 1 cm^{-1} , and $\nu(\text{OH})$ of metallic (9,0)-OH is lowest among (m,0)-OH tubes considered herein. These small changes in O-H frequency do not serve as a useful signature for distinguishing among tubes.

12-3.3. SWNT-COOH-OH

Different possible arrangements of carboxylic acid and phenolic -OH have been considered for both (n,n) and (m,0) tubes. Since both groups can be involved in O--HO H-bonding, emphases were given to all such possible structures. (It may be worth mentioning that multiple COOH groups do not [20, 21, 57] H-bond among themselves in carboxylated SWNTs, even at very high content of -COOH groups.) Fully optimized structures and key geometric parameters of (4,4)-COOH-OH and (8,0)-COOH-OH are displayed in Figures 12-3 and 12-4, and relative energies along with vibrational frequencies of characteristic bands are summarized in Tables 12-2 and 12-3, respectively.

12-3.3.1. (n,n)-COOH-OH

The most stable structure of (4,4)-COOH-OH is one where both groups are located on the same arm of the (4,4) tube and carbonyl (C=O) oxygen is H-bonded to

phenolic-OH group (3A in Figure 12-3). Rotation of COOH group of 12-3A by $\sim 180^\circ$ also yielded O--HO H-bonded structure (12-3B) where oxygen of acidic O-H is the proton acceptor. Since the carbonyl oxygen is a stronger proton acceptor than oxygen of C-O, the former structure is more stable by 4.7 kcal/mol. All relevant structural parameters are in accord with the characteristics of O--HO H-bonding [19]. For example, a stronger H-bond is associated with shorter O--H distance and elongation of the proton donor and acceptor bonds compared with isolated species. In the present cases, the O--H distance of 3A is 0.07 \AA shorter than the weaker H-bond in 12-3B. H-bonding causes elongation of the C=O distance of 3A by 23 m\AA from (4,4)-COOH and the phenolic O-H of 3A stretches by 27 m\AA compared to (4,4)-OH. The magnitude of elongation of the proton donor O-H bond of 12-3B is 1/3 that of 12-3A, an indication of a weaker H-bond in the former.

Next two structures (12-3C and 12-3D), where COOH and OH are attached to carbons of adjacent arms of (4,4), also form O--HO H-bonds, similar to 12-3A and 12-3B, respectively. Such structures are less stable by 8-10 kcal/mol indicating weakening of H-bond strength. H-bond lengths in 12-3C and 12-3D are longer by the same amount (0.072 \AA) than those of 12-3A and 12-3B, respectively. In addition, the C=O bond of 12-3C is less stretched by 13 m\AA than the C=O bond of 12-3A and changes in the proton donor -OH bond length follows the same trend but with about half the magnitude. The longest O--HO distance (1.833 \AA) among the hydrogen bonded (4,4)-COOH-OH is found in 12-3D, which is 9.6 kcal/mol less stable than 12-3A.

In structure 12-3E, functional groups are placed far from each other so as to avoid any possible H-bond interaction. Comparison of energies of this non-hydrogen bonded

structure with bonded structures provides a reasonable hint of H-bond strength in SWNT-COOH-OH. The energy difference between most stable 12-3A and 12-3E is 10.4 kcal/mol. Functionalization caused slight deformation of the tube at the active sites and such deformation energies are close to each other: i.e., 1.1 kcal/mol in 12-3A and 1.0 kcal/mol in 12-3E. Since deformation energies are the same for both structures, 10.4 kcal/mol may be considered as mainly due to O--HO interaction in the most stable 12-3A, assuming other effects are negligible. This value indicates a strong H-bond in 12-3A, compared to H-bond strength of simple organic molecules. For example, hydrogen bonds in salicylic acid (Figure 12-8), representing (n,n)-COOH-OH, are much weaker (by about 5.0 kcal/mol) than extended (4,4)-COOH-OH (3A). Similarly, structure 12-3B exhibits about 4.0 kcal/mol higher bond energy than 12-8B. The O--HO distances of 12-8A and 12-8B are longer than that of 12-3A and 12-3B, respectively. This result indicates stronger H-bonds in the latter structures and also that the tubular network of carbons in oxidized-SWNT has significant influence on O--HO H-bond strength. Hydrogen-bond energies of (n,n)-COOH-OH at M06-2X level [58] which is believed to accurately describe such weaker interactions, are 9.9, 9.1 and 9.2 kcal/mol for $n = 4, 5$ and 6 , respectively. At the same level, the H-bond energy of salicylic acid is 5.2 kcal/mol. These values clearly validate B3LYP results.

Similar structural arrangements were also considered for larger (n,n) tubes where $n = 5$ and 6 , i.e., an increase in diameter from 0.54 (4,4) to 0.68 (5,5) to 0.81 nm (6,6). Optimized structures are shown in Figures 12-9 and 12-10, and relative energies are summarized in Table 12-2. The stability order of different isomers of larger armchair tubes is close to that of the (4,4)-COOH-OH, indicating diameter has negligible effect on

the stability. H-bond energy decreases from 10.4 to 9.1 kcal/mol as the diameter increases from 0.54 to 0.81 nm. Interestingly, the O--H distance behaves differently than the standard criteria of H-bonding; a decrease in this distance from 1.688 to 1.662 Å is found. Other key parameters (C=O, O-H distances and O--H-O angle) involved in hydrogen bonding are insensitive to the diameter of the (n,n) tubes.

12-3.3.2. *(m,0)-COOH-OH*

Three different zigzag tubes with COOH and OH groups at one end of the tubes were considered and results are reported in Figure 12-4 and Table 12-3. Similar to their armchair counterparts, the most stable structures of (m,0)-COOH-OH are the ones where carbonyl oxygen acts as proton acceptor (iso1) in O--HO hydrogen bond, followed by structures (iso2) where oxygen of acidic-OH is the proton acceptor. Relative energy differences of about 5.0 kcal/mol between these two structures are close to those of oxidized armchair tubes. This energy difference is slightly higher for metallic (9,0) tubes than for semiconducting (8,0) and (10,0) tubes. Comparison of energies between structures having separated groups (as in iso3) and H-bonded structure (iso1) show the strongest interaction (about 12.0 kcal/mol) in the most stable (9,0)-COOH-OH (iso1) tube. Corresponding energies for (8,0) and (10,0) tube are 10.6 and 9.2 kcal/mol, respectively. M06-2X values are about 1.0 kcal/mol higher than the B3LYP quantities. The H-bond distance of 1.472 Å is the shortest among all SWNTs studied herein, and as a consequence C=O and phenolic-OH distances are longest. Another noticeable difference between oxidized zigzag and armchair tubes is the $\theta(\text{O--H-O})$ angle: this angle which is about 20° higher (166° vs. 146°) in the zigzag tubes.

12-3.4. Charge distribution:

Hydrogen bonding causes some charge redistribution [19] where the bridging hydrogen loses some electron density, that is, becomes more positively charged. Besides this change, there is also transfer of electron density from the proton acceptor (PA) to the proton donor (PD) upon H-bond formation. To verify such characteristic of H-bonding, we have calculated natural charges (NPA) [59, 60] for H-bonded and non-bonded isomers. Indeed, bridging protons lose about 34 me in (n,n) tubes and the corresponding value is about 24 me for (m,0) tubes. Changes in the proton charge in SWNTs-COOH-OH are more than that of salicylic acid, where the proton loses 15 me at the same level of theory.

Group NPA charge analyses indicate transfer of electron density from SWNTs to functional groups and the magnitude of electron density shift depends on the location of the acid and phenolic-OH groups. When groups are not forming H-bond, about 0.23e and 0.30e are transferred from (n,n) and (m,0) tubes, respectively, to functional groups. Hydrogen bond formation, as in iso1 structures, makes tubes more positively charged, that is, losing more electron density in oxidized forms. The NPA charges of (n,n) tubes in most stable iso1 structures are independent of the diameter of tubes and close to +0.24, whereas corresponding charge of (m,0) tube, also independent on the diameter, is +0.37. Thus charge exchange is more prominent in oxidized-zigzag tubes than oxidized-armchair tubes.

Exact determination of electron transfer from PA to PD, another characteristic of H-bonding, is only possible when two isolated molecules are forming H-bond. Since in the present scenario, both groups are linked to a conjugated system which is also

exchanging electron density with attached functional groups, makes complication in assigning charge exchange only between PA and PD. Also, exchange of electron density among three zones (-COOH, -OH and SWNT), may apparently cause reversal of charge transfer between PA and PD. The NPA group charges of three sections of (4,4)-COOH-OH in iso1 (H-bonded) are -0.074 (-COOH), -0.163 (-OH) and +0.237 (SWNT); and corresponding values in iso5 are -0.011, -0.196 and +0.207. Comparison among these values indicates a gain of electron density at -COOH (PA) by 0.063e, and loss of density at -OH (PD) by 0.033e and at SWNT by 0.030e. Corresponding values in (8,0)-COOH-OH iso1 are 0.073e (gain), 0.012e (loss) and 0.061e (loss) in comparison to structure where groups are not H-bonded (iso3). Other (n,n) and (m,0) tubes exhibit similar charge redistribution. Thus it may happen that electron transfer from -COOH to -OH (due to characteristics of H-bonding) and concurrently from -OH to SWNT (due to resonance effect between -OH and conjugated system) and from SWNT to -COOH (due to inductive effect of acid group), where latter charge transfer outweighs the first transfer process, resulting an overall gain at -COOH.

12-4. COOH and OH at the surface

Since hydrogen bonding among acid and -OH groups at the tips showed some unusual properties compared to standard O--H-O bonds, a preliminary investigation has been carried out by placing those groups at the surface of (4,4) and (8,0) SWNTs to check if those properties are really unique at the former location. Fully optimized geometries of (8,0)-COOH-OH and (4,4)-COOH-OH, where groups are located at the adjacent carbons of a hexagonal ring at the surface, are given in Figure 12-5. Most relevant geometric

parameters obtained at M06-2X and B3LYP (not shown) are close to each other. The O--H bonds in the range of 2.3 to 2.5 Å are bit longer for such H-bonds (standard distance would be less than 2.0 Å [19]) and the O--H-O angles of 104 to 116 degrees are also not supportive of considering such interaction as H-bonding. It can be seen from Figure 12-5 that bridging hydrogen, in both cases, point away from the proton acceptor oxygen of carbonyl group.

To estimate such interaction energies both groups need to be placed far from each other and compare energies between such structures with the one where they are close, as used in tip functionalized cases. Unlike tip-functionalized cases, attaching one group on top of a carbon atom of any hexagon at the surface will change hybridization from sp^2 to sp^3 on that center. As a consequence, a dangling bond is created at the adjacent carbon centers. Unless such dangling bond is saturated, an odd electron on the adjacent center is created (a doublet state) and an open-shell treatment is required to properly describe such structure. That odd-electron may be localized to one of the adjacent carbons or may be delocalized to three adjacent carbons of the attached site. Thus, placing acid and -OH groups far from each other will create two odd-electrons. An open-shell treatment or saturating such dangling bond might be appropriate to properly describe such systems, which is beyond the scope of the present study. More detailed investigation are in progress and results will be published elsewhere.

12-5. Vibrational spectra of SWNT-COOH-OH

Frequencies of the most characteristic stretching vibrational mode C=O along with those of O-H of COOH and phenolic-OH, are summarized in Tables 12-2 and 12-3,

and variations of frequencies and intensities with diameter are depicted in Figures 12-6 and 12-7, respectively. It may be noted first that both O-H groups exhibit a broad peak close to one another and that the O-H bond in an alcohol absorbs at a slightly higher wavenumber than it does in an acid. In general, both –OH modes are pure for all cases and hydrogen bonded C=O modes of most stable structures (iso1) are coupled with both C-OH bending modes. However, for second-most stable isomers (iso2), where the other oxygen of COOH is H-bonded to phenolic-OH, the C=O mode is coupled only with C-OH bend of acid group. Similar mixing of modes was found for iso3 and iso4 of all (n,n)-COOH-OH and iso2 of (m,0)-COOH-OH.

A well-characterized feature of H-bonds in organic and biological systems is the red-shift [19] in relevant stretching modes with increased intensity of participating bonds; nanotubes do not behave otherwise. For example, the C=O mode is red shifted by about 70 cm^{-1} for most stable isomers of (n,n)-COOH-OH (iso1) tubes with slight enhancement in intensity. Although the most stable isomers of zigzag-COOH-OH (iso1) exhibit red-shifted C=O modes, close in magnitude to those observed in armchair tubes, the intensity follows a reverse trend, especially for metallic (9,0)-COOH-OH. The most striking difference is the H-bonded C=O band of the most stable structure of armchair tubes which appears around 1630 cm^{-1} , whereas the same band of zigzag tubes shows a peak around 1565 cm^{-1} (see Figure 12-6). Such differences in C=O bands originate from the difference between (n,n)-COOH ($\sim 1704\text{ cm}^{-1}$) and (m,0)-COOH ($\sim 1640\text{ cm}^{-1}$); H-bonding down-shifts both modes by almost the same amount. Since the $\nu(\text{C=O})$ of zigzag-COOH-OH coincides with $\nu(\text{C=C})$ of tubes in the same region, and a peak around

1630 cm^{-1} may be due to a quinone group of armchair tubes, characterization of H-bonded acid group, solely based on C=O modes, is fraught with complications. It may be noted that $\nu(\text{C}=\text{C})$ values in the present o-SWNTs fall in the 1509-1536 cm^{-1} range with low intensity.

Changes in vibrational modes of phenolic-OH might provide additional features that could help identifying both groups whether H-bonded or not. In comparison to SWNT-OH, $\nu(\text{O-H})_{\text{ph}}$ of most stable isomers of (n,n)-COOH-OH is lowered by about 500 cm^{-1} with an approximate five-fold increase in intensity. Thus, phenolic O-H of armchair tubes, involved in H-bonding with COOH, exhibits a peak around 3100 cm^{-1} , which is also the region where C-H stretching vibration appears. This red-shift of phenolic-OH is almost double (about 1000 cm^{-1}) for semiconducting (8,0) and (10,0), and close to 2.5 times in metallic (9,0) tube. This band's intensity increases slightly in the former tubes, but an enhancement of about seven times is found in the (9,0) tube (Figure 12-7). This down-shifting places the $\nu(\text{O-H})_{\text{ph}}$ band close to 2680 cm^{-1} in semiconducting (m,0) tubes and 2322 cm^{-1} in (9,0) tube. Red-shift of the same band in salicylic acid (representing armchair tubes) is about 300 cm^{-1} with an intensity enhancement of about six-fold. (It may be noted that present theoretical frequency values of salicylic acid are in excellent agreement with experimental frequencies [61]: 1662 cm^{-1} ($\nu_{\text{C}=\text{O}}$) and 3238 cm^{-1} ($\nu_{\text{O-H}}$)). Similarly, the red shift in the phenolic-OH mode of 8-hydroxy-1-naphthoic acid (representing zigzag structure) is about 350 cm^{-1} . Thus, the magnitude of red-shift in phenolic O-H is quite large, especially for zigzag tubes, in comparison to simple organic molecular models.

Non-participating O-H bands of COOH are also red-shifted by about 45 cm^{-1} in armchair tubes with 2.3 times more intensity. However, this O-H mode is blue-shifted by about 8 cm^{-1} in all zigzag tubes. Interestingly, when the oxygen of that O-H participates in H-bonding, as in iso2 in Figures 12-2 – 12-6, changes in O-H vibrational mode follow the same trend, but by a lesser magnitude.

In summary, if both COOH and –OH groups are present in oxidized SWNT samples, H-bonding among those groups causes significant changes in the IR spectra. In the most stable arrangements, where carbonyl oxygen is proton acceptor and phenolic–OH is the donor, key vibrational modes are: $\sim 1630\text{ cm}^{-1}$ (C=O), $\sim 3100\text{ cm}^{-1}$ (phenolic –OH), $\sim 3540\text{ cm}^{-1}$ (acidic –OH) in (n,n)-COOH-OH; the corresponding frequencies for (m,0)-COOH-OH tubes are ~ 1565 , ~ 2680 , $\sim 3560\text{ cm}^{-1}$, respectively. Although, C=O and acidic OH modes are similar in semiconducting and metallic zigzag tubes, the phenolic –OH band differs significantly, 2684 cm^{-1} in (8,0) or 2688 cm^{-1} in (10,0) vs., 2322 cm^{-1} in (9,0). Thus, all three bands should be taken into account for identification of any O--HO hydrogen-bonded structures between COOH and –OH groups of o-SWNTs.

On the other hand, these characteristic vibrational modes will differ significantly when acid and phenolic–OH groups are not participating in H-bonding, when those groups are located far from each other (as shown in iso5 for (n,n) and iso3 for (m,0) in Figures 12-3 – 12-6) at the end of tubes. In those arrangements, the $\nu(\text{C=O})$, $\nu(\text{O-H})_{\text{acid}}$ and $\nu(\text{O-H})_{\text{ph}}$ are ~ 1710 , ~ 3540 and $\sim 3600\text{ cm}^{-1}$ in o-armchair tubes, respectively. These modes in o-zigzag tubes are close to that of o-(n,n), except the C=O mode that appears around 1640 cm^{-1} .

12-5.1. Interpretation of Experimental IR spectra

Most experimental studies [3, 4, 8, 24-26, 62-68] reported IR spectra of oxidized samples and a few [3, 4, 24] critically analyzed spectral data to assign different modes. Those spectra were obtained for different oxidized tube samples synthesized by CVD, arc-discharge, and laser ablation methods, and also used different oxidation processes, conditions and starting materials. These synthetic procedures generate a wide range of tubes with varying diameters [69] from 0.7 – 1.4 nm. Although our theoretical models represent smaller diameter (0.54 – 0.81 nm) tubes, results may change slightly for larger tubes but not to the extent that would alter the conclusions obtained for smaller tubes. In fact, our previous study [21] on IR spectra of a wide range of carboxylated armchair and zigzag tubes (diameters of 0.54 – 1.36 nm) clearly showed insignificant changes in spectra due to increasing diameter, and there is no H-bonding among acid groups even at higher concentration, that has been envisioned in several experimental studies due to small red-shift in C=O modes.

In general, reported experimental IR spectra of the oxidized SWNTs exhibit a strong peak in the 1700-1760 cm^{-1} range, and a broad peak around 3000 – 3600 cm^{-1} , which is an indication of COOH groups. Had those acid groups been involved in any H-bonding, their C=O or O-H modes would have been significantly red-shifted, which is not reflected in those experimental IR spectra. Since stretching frequency of phenolic-OH and OH of acid group occur in the same region of IR absorption spectra and exhibit a broad band, it is difficult to distinguish [3] those two modes, unless a C=O mode appears in the spectrum. A peak at 3000-3600 cm^{-1} without a peak in 1700-1760 cm^{-1} is, in

general, indicative of the presence of solely phenolic-OH, which is not the case in any experimental studies.

However, some studies show peaks below 1700 cm^{-1} : 1651 and 1685 cm^{-1} [70], 1630 and 1680 cm^{-1} [28] and 1689 cm^{-1} [71]. The former two studies used raw samples from the same source (Carbolex, Inc.) and the latter study used samples from Sino-Nano Co. Kim et al. [3] reported peaks around 1623 and 1650 cm^{-1} in addition to $\sim 1720\text{ cm}^{-1}$ using a sample from the former source. Those peaks were assigned as H-bonded $-\text{COOH}$ (higher frequencies) and $\sim 1650\text{ cm}^{-1}$ peak as quinone $\text{C}=\text{O}$. Present theoretical results indicate a $\text{C}=\text{O}$ mode around 1630 cm^{-1} may be due to H-bonded (n,n)- COOH-OH or non-hydrogen bonded (m,0)- COOH-OH , or even from (m,0)- COOH . Had there been a H-bonded structure, the OH mode of phenolic-OH should have significantly red-shifted but not OH of acid. That was not reflected in those experimental IR spectra.

From energetic point of view, if both COOH and OH are present at the tips of o-SWNT samples then they ought to be H-bonded as their interaction energy is sufficient (about 9-12 kcal/mol) to stabilize the structure. However, vibrational data do not indicate formation of such bonds. This leads one to presume either phenolic $-\text{OH}$ are not present, or such groups are located at sites other than the tips. During oxidation processes, oxidized samples are normally washed and dried at different temperature, and more volatile alcohol groups, in addition to some COOH , may have been removed in purified samples, leaving few carboxylic groups at the tips. This presumption is strengthened by the fact that extensive second functionalizations of o-SWNTs have been reported in the literature where COOH groups were the only target and not the phenolic-OH.

12-6. Conclusions

Intrinsic properties of o-SWNTs, where both –COOH and phenolic –OH groups are present at the tips of tubes, were studied using DFT-SLDB approach, which has been proven to be reliable and computationally highly efficient for studying any extended carbon network base systems, such as nanotubes and graphene. Hydrogen bonding among these groups leads to significant effects on the structure and IR spectra. Characteristics of standard H-bonds appear in o-SWNTs, however, the magnitudes are significantly enhanced in the extended carbon tubular networks. For example, the estimated O–HO hydrogen bond energy of 9-12 kcal/mol is almost double that found in simpler systems. Also, red-shifts of C=O modes and especially phenolic –OH stretching modes are amplified in nanotubes.

If these two functional groups are present at the tips of o-SWNTs, they ought to form such H-bonds by placing them in adjacent sites. In the most stable structures, the O-atom of the carbonyl unit of COOH acts as proton acceptor while phenolic –OH donates the proton. Accordingly, red-shift occurs in both C=O and O-H modes, and all three bands are equally important to identify such bonding. Key vibrational modes in H-bonded structures are: $\sim 1630\text{ cm}^{-1}$ (C=O), $\sim 3100\text{ cm}^{-1}$ (phenolic –OH), $\sim 3540\text{ cm}^{-1}$ (acidic –OH) in (n,n)-COOH-OH, and corresponding frequency values for (m,0)-COOH-OH tubes are ~ 1565 , ~ 2680 , $\sim 3560\text{ cm}^{-1}$. These data may be helpful in assigning vibrational modes of complicated experimental spectra.

Since experimental spectra reported so far do not show peaks in those regions, one may raise question about such hydrogen bonding between acid and phenolic –OH groups at the tips of o-SWNTs. The latter group may be present at different sites, such as

at the wall but not at the tips. Other conclusions from analyses of theoretical and experimental spectra may be drawn that during processing of acid-treating samples by wash and dry technique, alcohol groups may have evaporated out leaving some acid groups for second functionalization.

References

- [1] Zhang J, Zou H, Qing Q, Yang Y, Li Q, Liu Z, et al. Effect of chemical oxidation on the structure of single-walled carbon nanotubes. *J Phys Chem B* 2003;107:3712–8.
- [2] Haddon RC, Sippel J, Rinzler AG, Papadimitrakopoulos F. Purification and separation of carbon nanotubes. *MRS Bull* 2004;29:252–9.
- [3] Kim UJ, Furtado CA, Liu X, Chen G, Eklund PC. Raman and IR spectroscopy of chemically processed single-wall carbon nanotubes. *J Am Chem Soc* 2005;127:15437–45.
- [4] Andersson C-H, Grennberg H. Reproducibility and efficiency of carbon nanotube end-group generation and functionalization. *Eur J Org Chem* 2009;2009:4421–8.
- [5] Park T-J, Banerjee S, Hemraj-Benny T, Wong SS. Purification strategies and purity visualization techniques for single-walled carbon nanotubes. *J Mater Chem* 2006;16:141–54.
- [6] Hu H, Bhowmick P, Zhao B, Hamon MA, Itkis ME, Haddon RC. Determination of the acidic sites of purified single-walled carbon nanotubes by acid–base titration. *Chem Phys Lett* 2001;345:25–8.
- [7] Marshall MW, Popa-Nita S, Shapter JG. Measurement of functionalized carbon

- nanotube carboxylic acid groups using a simple chemical process. *Carbon* 2006;44:1137–41.
- [8] Basiuk VA, Basiuk (Golovataya-Dzhymbeeva) EV. *Chemical derivatization of carbon nanotube tips*. California: American Scientific Publishers; 2004.
- [9] Gerber I, Oubenali M, Bacsa R, Durand J, Goncalves A, Pereira MFR, et al. Theoretical and experimental studies on the carbon-nanotube surface oxidation by nitric acid: interplay between functionalization and vacancy enlargement. *Chem Eur J* 2011;17:11467–77.
- [10] Niyogi S, Hamon MA, Hu H, Zhao B, Bhowmick P, Sen R, et al. Chemistry of single-walled carbon nanotubes. *Acc Chem Res* 2002;35:1105–13.
- [11] Lin T, Bajpai V, Ji T, Dai L. Chemistry of carbon nanotubes. *Aust J Chem* 2003;56:635–51.
- [12] Banerjee S, Benny-Hemraj T, Wong SS. Routes towards separating metallic and semiconducting nanotubes. *J Nanosci Nanotechnol* 2005;5:841–55.
- [13] Nakashima N. Soluble carbon nanotubes: fundamentals and applications. *Int J Nanosci* 2005;4:119–37.
- [14] Murakami H, Nakashima N. Soluble carbon nanotubes and their applications. *J Nanosci Nanotechnol* 2006;6:16–27.
- [15] Britz DA, Khlobystov AN. Noncovalent interactions of molecules with single walled carbon nanotubes. *Chem Soc Rev* 2006;35:637–59.
- [16] Tasis D, Tagmatarchis N, Bianco A, Prato M. Chemistry of carbon nanotubes. *Chem Rev* 2006;106:1105–36.
- [17] Hodge SA, Bayazit MK, Coleman KS, Shaffer MSP. Unweaving the rainbow: a

- review of the relationship between single - walled carbon nanotube molecular structures and their chemical reactivity. *Chem Soc Rev* 2012;41:4409–29.
- [18] Segneanu AE, Gozescu I, Dabici A, Sfirloaga P, Szabadai Z. In: Uddin J, editor. *Macro to nano spectroscopy*. InTech; 2012. <http://dx.doi.org/10.5772/50183>.
- [19] Scheiner S. *Hydrogen bonding. A theoretical perspective*. Oxford: Oxford University Press; 1997.
- [20] Kar T, Scheiner S, Roy AK. Reliability of approximate methods to study tip-functionalized single-wall carbon nanotubes. *J Phys Chem C* 2012;116:25401–6.
- [21] Kar T, Scheiner S, Roy AK, Bettinger HF. Unusual low- frequency C@O mode of COOH group can distinguish between carboxylated zigzag and armchair nanotubes. *J Phys Chem C* 2012;116:26072–83.
- [22] Mawhinney DB, Naumenko V, Kuznetsova A, Yates Jr JT, Liu J, Smalley RE. Infrared spectral evidence for the etching of carbon nanotubes: ozone oxidation at 298 K. *J Am Chem Soc* 2000;122:2383–4.
- [23] Kuznetsova A, Mawhinney DB, Naumenko V, Yates Jr JT, Liu J, Smalley RE. Enhancement of adsorption inside of single- walled nanotubes: Opening of the entry ports. *Chem Phys Lett* 2000;321:292–6.
- [24] Zhang J, Zou H, Qing Q, Yang Y, Li Q, Liu Z, et al. Effect of chemical oxidation of the structure of single-walled carbon nanotubes. *J Phys Chem B* 2003;107:3712–8.
- [25] Wang Y, Iqbal Z, Mitra S. Rapidly functionalized, water - dispersed carbon nanotubes at high concentration. *J Am Chem Soc* 2005;128:95–9.
- [26] Shieh Y-T, Liu G-L, Wu H-H, Lee C-C. Effect of polarity and pH on the solubility

- of acid-treated carbon nanotubes in different media. *Carbon* 2007;45:1880–90.
- [27] Ramanathan T, Fisher FT, Ruoff RS, Brinson LC. Apparent enhanced solubility of single-wall carbon nanotubes in deuterated acid mixture. *Res Lett Nanotechnol* 2008;2008:296928.
- [28] Cortes P, Deng S, Camacho L, Smith GB. The adsorption properties of bacillus atrophaeus spore on functionalized nanotubes. *J Sens* 2010;2010:691585.
- [29] Berger S, Hertl P, Rieker A. In: Patai S, Rappoport Z, editors. *The chemistry of quinonoid compounds*, vol. II. John Wiley & Sons Ltd.; 1988. pp 29–86.
- [30] Kar T, Scheiner S, Adhikari U, Roy AK. Site preferences of carboxyl groups on the periphery of graphene and their characteristic IR spectra. *J Phys Chem C* 2013;117:18206–15.
- [31] Chelmecka E, Pasterny K, Kupka T, Stobinski L. DFT studies of COOH tip-functionalized zigzag and armchair single wall carbon nanotubes. *J Mol Model* 2012;18:2241–6.
- [32] Wongchoosuk C, Udomvech A, Kerdcharoen T. The geometrical and electronic structures of open-end fully functionalized single-walled carbon nanotubes. *Curr Appl Phys* 2009;9:352–8.
- [33] Chelmecka E, Pasterny K, Kupka T, Stobinski L. OH- functionalized open-ended armchair single-wall carbon nanotubes (SWCNT) studied by density functional theory. *J Mol Model* 2012;18:1463–72.
- [34] Dinadayalane TC, Leszczynski J. Comparative theoretical study on the positional preference for functionalization of two OH and SH groups with (5,5) armchair SWCNT. *J Phys Chem C* 2013;117:14441–50.

- [35] Milowski KZ, Majewski JA. Functionalization of carbon nanotubes with ACHn, ANH2 fragments, ACOOH and AOH groups. *J Chem Phys* 2013;138:194704–14.
- [36] Kar T, Akdim B, Duan X, Pachter R. A theoretical study of functionalized single-wall carbon nanotubes: ONIOM calculations. *Chem Phys Lett* 2004;392:176–80.
- [37] Kar T, Akdim B, Duan X, Pachter R. Open-ended modified single-wall carbon nanotubes: a theoretical study of the effects of purification. *Chem Phys Lett* 2006;423:126–30.
- [38] Kar T, Scheiner S, Roy AK. The effect on acidity of size and shape of carboxylated single-wall carbon nanotubes. A DFT – SLDB study. *Chem Phys Lett* 2008;460:225–9.
- [39] Kar T, Bettinger HF, Scheiner S, Roy AK. Noncovalent p–p stacking and CH–p interactions of aromatics on the surface of single-wall carbon nanotubes (SWNTs) – an MP2 study. *J Phys Chem C* 2009;112:20070–5.
- [40] Maseras F, Morokuma K. IMOMM: a new integrated ab initio + molecular mechanics geometry optimization scheme of equilibrium structures and transition states. *J Comput Chem* 1995;16:1170.
- [41] Morokuma K. ONIOM and its applications to material chemistry and catalyses. *Bull Korean Chem Soc* 2003;24:797–801.
- [42] Montoya A, Mondragon F, Truong TN. Adsorption on carbonaceous surfaces: cost-effective computational strategies for quantum chemistry studies of aromatic systems. *Carbon* 2002;40:1863–72.
- [43] Yim WL, Lou ZF. A reexamination of the chemisorption and desorption of ozone on the exterior of a (5,5) single-wall carbon nanotube. *Chem Phys Lett*

2004;398:297–303.

- [44] Chen Z, Nagase S, Hirsch A, Haddon R, Thiel C, Schleyer W. Side-wall opening of single-walled carbon nanotubes (SWCNTs) by chemical modification: a critical theoretical study. *Angew Chem Int Ed* 2004;43:1552–4.
- [45] Vreven T, Thompson LM, Larkin SM, Kirker I, Bearpark MJ. Deconstructing the ONIOM hessian: investigating method combinations for transition structures. *J Chem Theory Comput* 2012;8:4907–14.
- [46] Becke AD. Density-functional thermochemistry. III. The role of exact exchange. *J Chem Phys* 1993;98:5648–52.
- [47] Lee C, Yang W, Parr RG. Development of the Colle-Salvetti correlation-energy formula into a functional of the electron density. *Phys Rev B* 1988;37:785–9.
- [48] Stephens PJ, Devlin FJ, Chabalowski CF, Frisch MJ. Ab initio calculation of vibrational absorption and circular dichroism spectra using density functional force fields. *J Phys Chem* 1994;98:11623–7.
- [49] Scott AP, Radom L. Harmonic vibrational frequencies: an evaluation of Hartree–Fock, Møller–Plesset, quadratic configuration interaction, density functional theory, and semiempirical scale factors. *J Phys Chem* 1996;100:16502–13.
- [50] Cheeseman JR, Frisch MJ, Devlin FJ, Stephens PJ. Ab initio calculation of atomic axial tensors and vibrational rotational strengths using density functional theory. *Chem Phys Lett* 1996;252:211–20.
- [51] Devlin FJ, Finley JW, Stephens PJ, Frisch MJ. Ab initio calculation of vibrational absorption and circular dichroism spectra using density functional force fields: a comparison of local, nonlocal, and hybrid density functionals. *J Phys Chem*

1995;99:16883–902.

- [52] Johnson III RD. in: Johnson III RD, editor. NIST computational chemistry comparison and benchmark database. (eds.), Russell D. Johnson III. 2006. <http://cccbdb.nist.gov/>
- [53] Frisch MJ, Trucks GW, Schlegel HB, Scuseria GE, Robb MA, Cheeseman JR, et al. Gaussian 09. Wallingford CT, USA: Gaussian Inc.; 2009.
- [54] Schaftenaar G, Noordik JH. Molden: a pre and post-processing program for molecular and electronic structures. *J Comput Aided Mol Des* 2000;14:123–34.
- [55] Zhurko GA. <<http://www.chemcraftprog.com>>.
- [56] Veiga RGA, Tomanek D, Tube VBS, <<http://k.1asphost.com/tubeasp/tubevbs.html>>, 2007.
- [57] Kar T, Scheiner S, Patnaik SS, Bettinger HF, Roy AK. IR characterization of tip-functionalized single-wall carbon nanotubes. *J Phys Chem C* 2010;114:20955–61.
- [58] Zhao Y, Truhlar DG. The M06 suite of density functionals for main group thermochemistry, thermochemical kinetics, noncovalent interactions, excited states, and transition elements: two new functionals and systematic testing of four M06-class functionals and 12 other functionals. *Theor Chem Acc* 2008;120:215–41.
- [59] Reed AE, Weinhold F, Curtiss LA, Pochatko DJ. Natural bond orbital analysis of molecular interactions: theoretical studies of binary complexes of HF, H₂O, NH₃, N₂, O₂, F₂, CO, and CO₂ with HF, H₂O, and NH₃. *J Chem Phys* 1986;84:5687–705.
- [60] Reed AE, Curtiss LA, Weinhold F. Intermolecular interactions from a natural bond orbital, donor–acceptor viewpoint. *Chem Rev* 1988;88:899–926.

- [61] Jadrijevic-Mladar Takac M, Topic DV. FT-IR and NMR spectroscopic studies of salicylic acid derivatives. II. Comparison of 2-hydroxy- and 2,4- and 2,5-dihydroxy derivatives. *Acta Pharm* 2004;54:177–91.
- [62] Chen Z, Kobashi K, Rauwald U, Booker R, Fan H, Hwang W-F, et al. Soluble ultra-short single-wall carbon nanotubes. *J Am Chem Soc* 2006;128:10568–71.
- [63] Hu C, Chen Z, Shen A, Shen X, Li J, Hu S. Water-soluble single-walled carbon nanotubes via noncovalent functionalization by a rigid, planar and conjugated diazo dye. *Carbon* 2006;44:428–34.
- [64] Park MJ, Lee JK, Lee BS, Lee Y-W, Choi IS, Lee S-G. Covalent modification of multiwalled carbon nanotubes with imidazolium-based ionic liquids: effect of anions on solubility. *Chem Mater* 2006;18:1546–51.
- [65] Martinez-Rubi Y, Guan J, Lin S, Scriver C, Sturgeon RE, Simard B. Rapid and controllable covalent functionalization of single-walled carbon nanotubes at room temperature. *Chem Commun* 2007:5146–8.
- [66] Umeyama T, Tezuka N, Fujita M, Matano Y, Takeda N, Murakoshi K, et al. Retention of intrinsic electronic properties of soluble single-wall carbon nanotubes after significant degree of sidewall functionalization by the Bingel reaction. *J Phys Chem C* 2007;111:9734–41.
- [67] Imasaka K, Kato Y, Suehiro J. Enhancement of microplasma-based water-solubilization of single-walled carbon nanotube using gas bubbling in water. *Nanotechnology* 2007;18:335602–9.
- [68] Naseh MV, Khodadadi AA, Mortazavi Y, Sahraei OA, Pourfayaz F, Sedghi SM. Functionalization of carbon nanotubes using nitric acid oxidation and DBD plasma.

- World Acad Sci Eng Technol 2009;49:177–9.
- [69] Hamon MA, Itkis ME, Niyogi S, Alvaraez T, Kuper C, Menon M, et al. Effect of rehybridizations on the electronic structure of single-walled carbon nanotubes. *J Am Chem Soc* 2001;123:11292–3.
- [70] Nogueira AF, Lomba BS, Soto-Oviedo MA, Corio P, Furtado CA, Hummelgen IA. Polymer solar cells using single-wall carbon nanotubes modified with thiophene pedant groups. *J Phys Chem C* 2007;111:18431–8.
- [71] Li R, Wu R, Zhao L, Wu M, Yang L, Zou H. P-glycoprotein antibody functionalized carbon nanotube overcomes the multidrug resistance of human leukemia cells. *ACS Nano* 2010;4:1399–408.

Table 12-1. Vibrational frequencies (ν , in cm^{-1}), intensity (I , in km/mol , in parenthesis), bond distances (R , in \AA) of SWNT-COOH^a and SWNT-OH^b.

SWNT-COOH (diameter of pristine SWNT in nm)	$\nu_{\text{C=O}}$ (I)	$\nu_{\text{O-H}}$ (I)	$R(\text{C=O})$	$R(\text{C-O})^c$	$R(\text{C-COOH})$	$R(\text{O-H})$
(4,4)-COOH (0.54)	1704 (627)	3541 (145)	1.220	1.361	1.481	0.976
(5,5)-COOH (0.68)	1703 (605)	3541 (150)	1.220	1.360	1.483	0.976
(6,6)-COOH (0.81)	1702 (585)	3538 (154)	1.220	1.360	1.484	0.976
(8,0)-COOH (0.63)	1639 (1378)	3554 (212)	1.232	1.376	1.447	0.975
(9,0)-COOH (0.70)	1627 (1448)	3556 (194)	1.235	1.382	1.438	0.974
(10,0)-COOH (0.78)	1641 (1341)	3552 (222)	1.231	1.376	1.452	0.975
SWNT-OH		$\nu_{\text{O-H}}$ (I)			$R(\text{C-OH})$	$R(\text{O-H})$
(4,4)-OH		3585 (76)			1.370	0.971
(5,5)-OH		3589 (80)			1.371	0.971
(6,6)-OH		3593 (82)			1.372	0.971
(8,0)-OH		3612 (153)			1.362	0.970
(9,0)-OH		3609 (156)			1.360	0.970
(10,0)-OH		3613 (141)			1.362	0.969

^a See Figure 12-1 for structures of SWNT-COOH. ^b See Figure 12-2 for structures of SWNT-OH. ^cFor SWNT-COOH, $R(\text{C-O})$ refers to C-O(H) distances of COOH group and for SWNT-OH distance between carbon of SWNT and OH group.

Table 12-2. Relative energies (E_{rel} , in kcal/mol), relative enthalpy (H_{rel} , in kcal/mol), vibrational frequencies (ν , in cm^{-1}), intensity (I , in km/mol ; in parenthesis) of (n,n)-COOH-OH^a.

(n,n)-COOH-OH	E_{rel}	H_{rel}	$\nu(\text{C}=\text{O})$	$\nu(\text{O}-\text{H})$	$\nu(\text{O}-\text{H})$ (COOH)
(4,4)-COOH-OH-iso1 3A	0.00	0.00	1632(733)	3100(453)	3543(175)
(4,4)-COOH-OH-iso2 3B	4.71	4.65	1708(548)	3423(425)	3554(155)
(4,4)-COOH-OH-iso3 3C	7.81	7.49	1662(570)	3366(383)	3552(191)
(4,4)-COOH-OH-iso4 3D	9.56	9.29	1720(732)	3486(404)	3536(130)
(4,4)-COOH-OH-iso5 3E	10.37	10.02	1706(628)	3604(93)	3541(146)
(5,5)-COOH-OH-iso1 4A	0.00	0.00	1629(752)	3089(490)	3543(186)
(5,5)-COOH-OH-iso2 4B	4.61	4.62	1708(567)	3421(463)	3552(159)
(5,5)-COOH-OH-iso3 4C	7.60	7.48	1656(610)	3345(436)	3552(205)
(5,5)-COOH-OH-iso4 4D	9.71	9.51	1719(748)	3476(477)	3535(135)
(5,5)-COOH-OH-iso5 4E	9.70	9.54	1703(609)	3604(94)	3539(151)
(6,6)-COOH-OH-iso1 5A	0.00	0.00	1628(773)	3086(511)	3542(196)
(6,6)-COOH-OH-iso2 5B	5.45	5.21	1709(585)	3419(495)	3549(162)
(6,6)-COOH-OH-iso3 5C	8.70	8.22	1654(642)	3337(477)	3552(217)
(6,6)-COOH-OH-iso4 5D	10.97	10.40	1719(764)	3472(540)	3534(138)
(6,6)-COOH-OH-iso5 5E	9.07	8.56	1703(589)	3592(85)	3538(154)

^a See Figures 12-3, 12-9, and 12-10 for different isomers of (n,n)-COOH-OH. Key geometric parameters are shown in figures.

Table 12-3. Relative energies (E^{rel} , in kcal/mol), relative enthalpy (H^{rel} , in kcal/mol), vibrational frequencies (ν , in cm^{-1}), intensity (I , in km/mol , in parenthesis) of (m,0)-COOH-OH^a.

(m,0)-COOH-OH	E_{rel}	H_{rel}	$\nu(\text{C}=\text{O})$	$\nu(\text{O}-\text{H})$	$\nu(\text{O}-\text{H})$ COOH
(8,0)-COOH-OH-iso1	0.00	0.00	1563(1364)	2684(267)	3561(296)
(8,0)-COOH-OH-iso2	5.02	4.93	1641(2220)	3244(397)	3558(254)
(8,0)-COOH-OH-iso3	10.62	9.91	1639(1393)	3609(147)	3554(210)
(9,0)-COOH-OH-iso1	0.00	0.00	1563(683)	2322(1323)	3564(229)
(9,0)-COOH-OH-iso2	5.65	6.19	1643(1802)	3159(995)	3560(195)
(9,0)-COOH-OH-iso3	11.95	12.29	1628(1515)	3600(175)	3556(192)
(10,0)-COOH-OH-iso1	0.00	0.00	1567(1141)	2688(208)	3560(322)
(10,0)-COOH-OH-iso2	4.59	5.04	1641(2234)	3261(425)	3556(272)
(10,0)-COOH-OH-iso3	9.22	9.54	1641(1418)	3613(137)	3552(229)

^a See Figure 12-4 for different isomers of (m,0)-COOH-OH. Key geometric parameters are shown in figures.

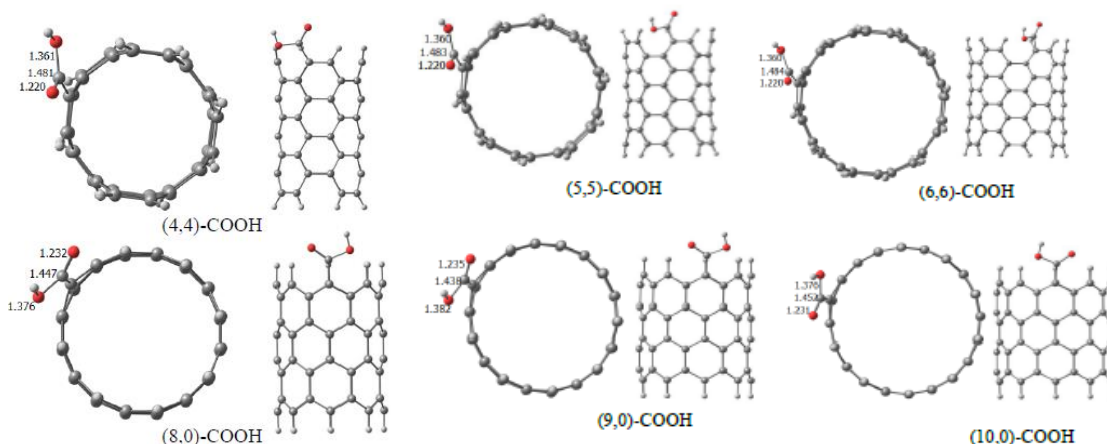


Figure 12-1. Optimized structures (top and side-view) of (n,n)-COOH and (m,0)-COOH. Distances in Å and angles in degree.

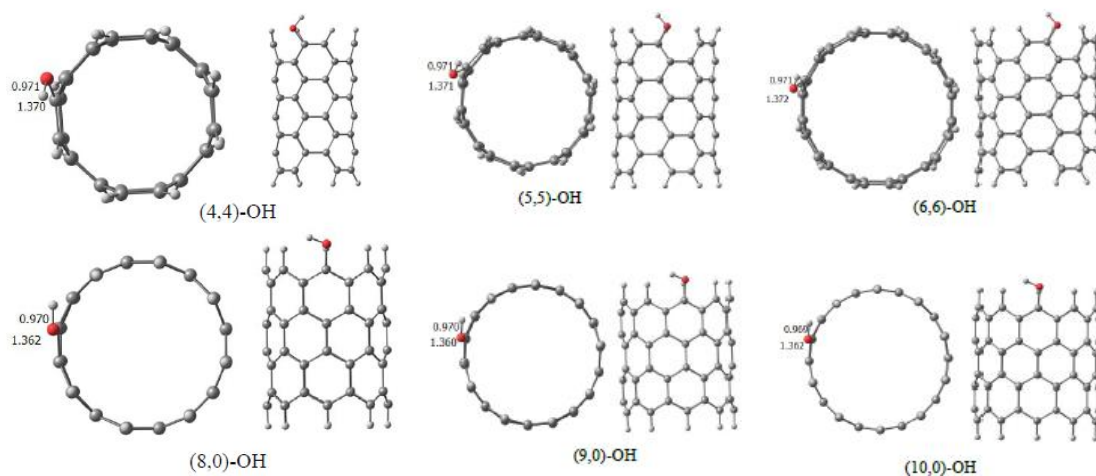


Figure 12-2. Optimized structures of (n,n)-COOH and (m,0)-OH. Distances in Å and angles in degree.

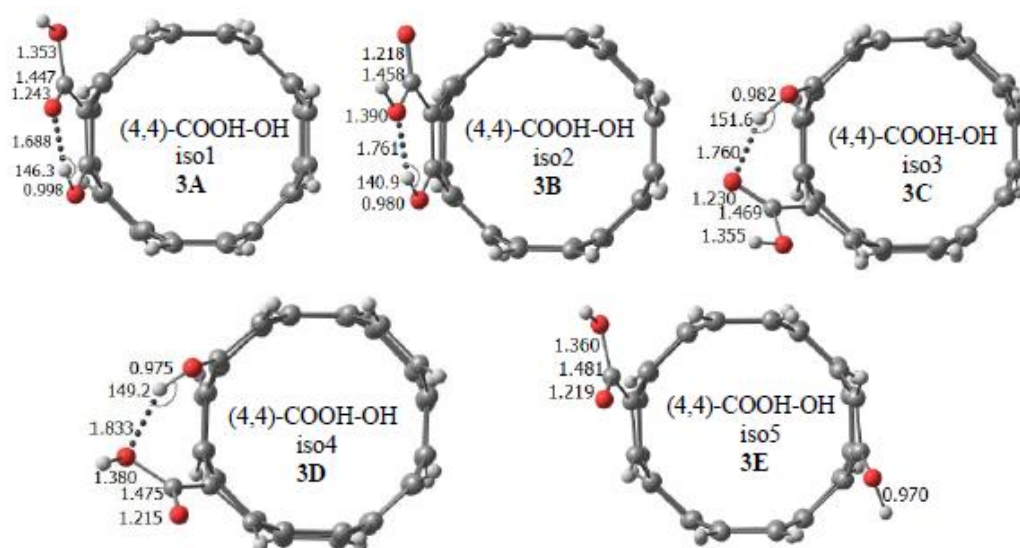


Figure 12-3. Optimized structures of (4,4)-COOH-OH. Distances in Å and angles in degree.

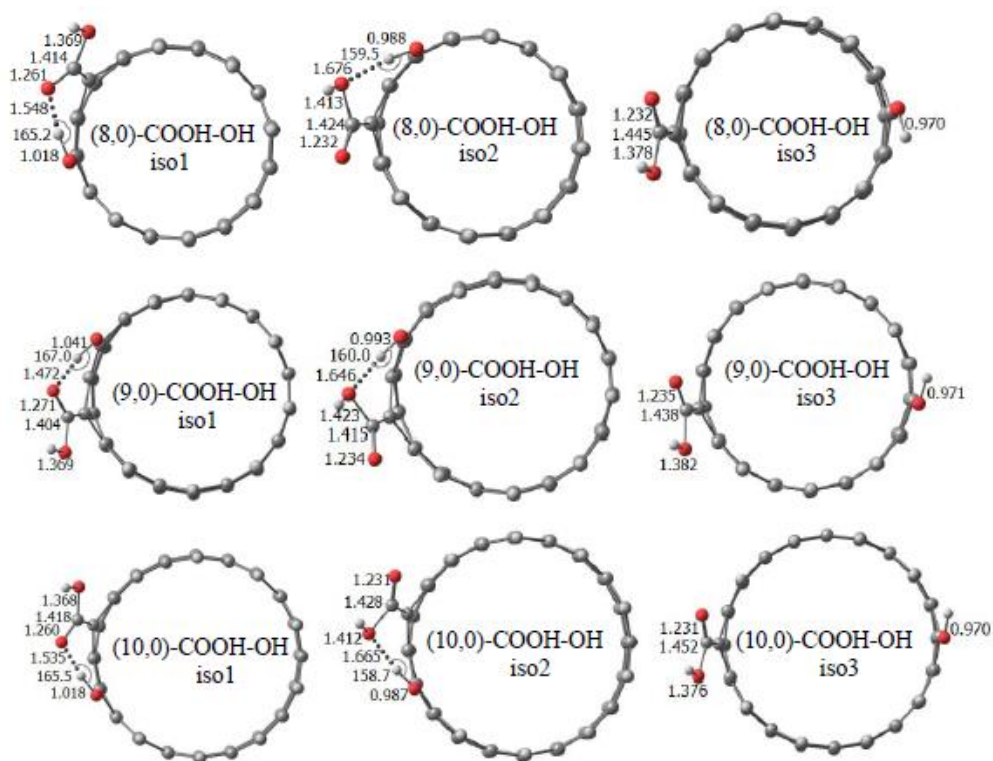


Figure 12-4. Optimized structures of (m,0)-COOH-OH, $m = 8, 9, 10$. Distances in Å and angles in degree.

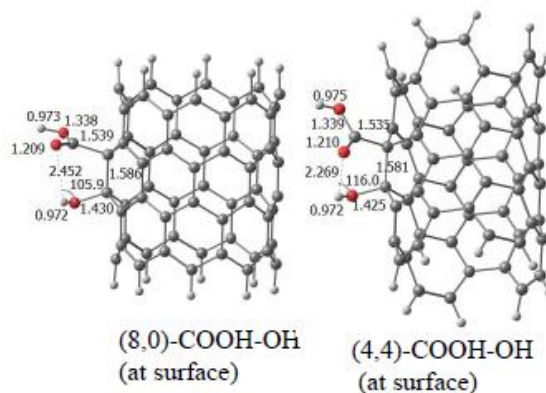


Figure 12-5. M06-2X optimized structures of (8,0)-COOH-OH and (4,4)-COOH-OH where both functional groups are at the surface. Distances in Å and angles in degree. 6-31G* basis functions are used for all C and H atoms, and 6-31+G* is used for all oxygen atoms.

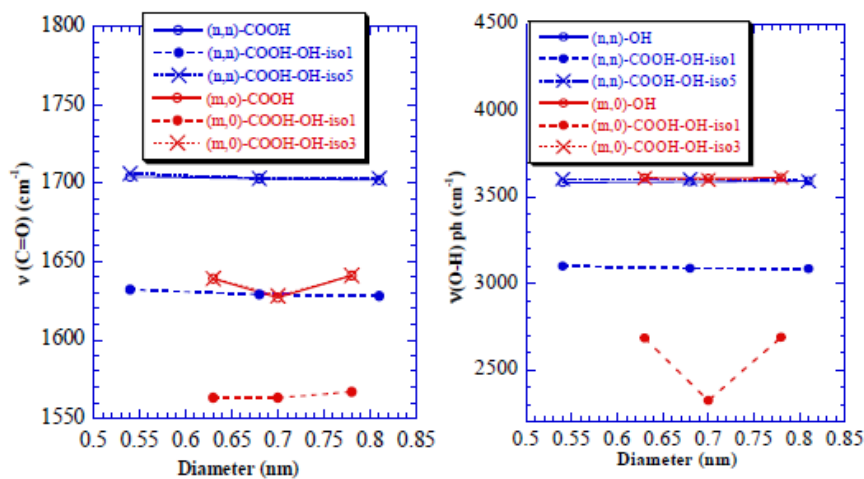


Figure 12-6. Variation of C=O (left) and ph-OH (right) frequencies of SWNTs-COOH-OH with diameter of SWNTs.

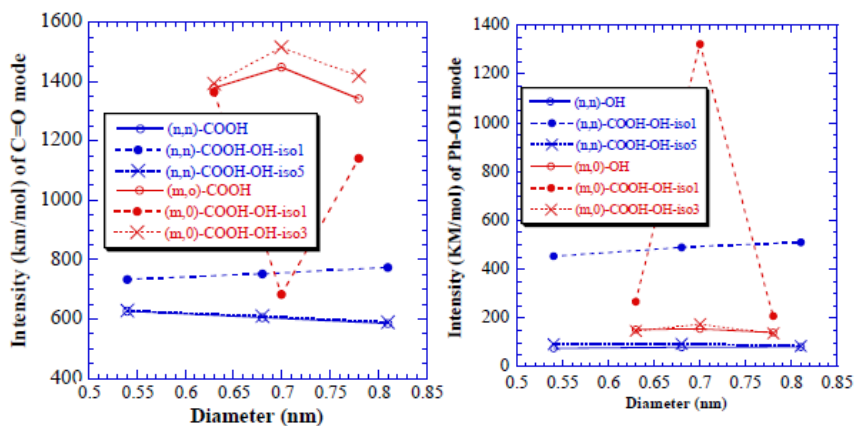


Figure 12-7. Variation of intensity of C=O mode (left) and Ph-OH (right) of SWNTs-COOH-OH with diameter of tubes.

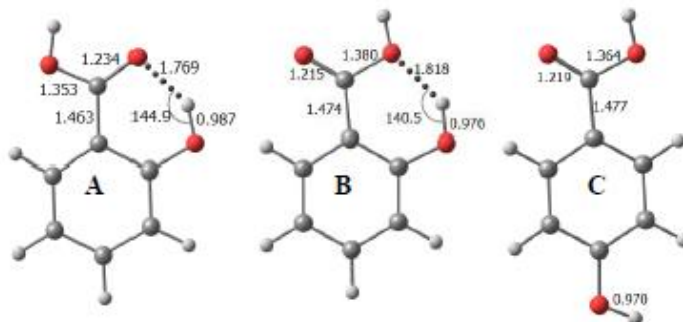


Figure 12-8. Structure of salicylic acid and different isomers obtained from B3LYP/6-31G*(O+). Bond distances are in Å, and angles are in degree.

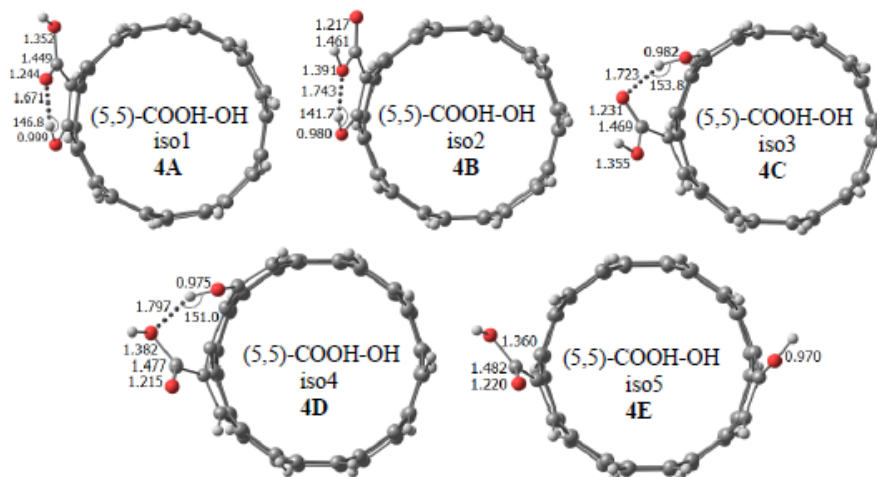


Figure 12-9. Optimized structures of (5,5)-COOH-OH. Distances in Å and angles in degree.

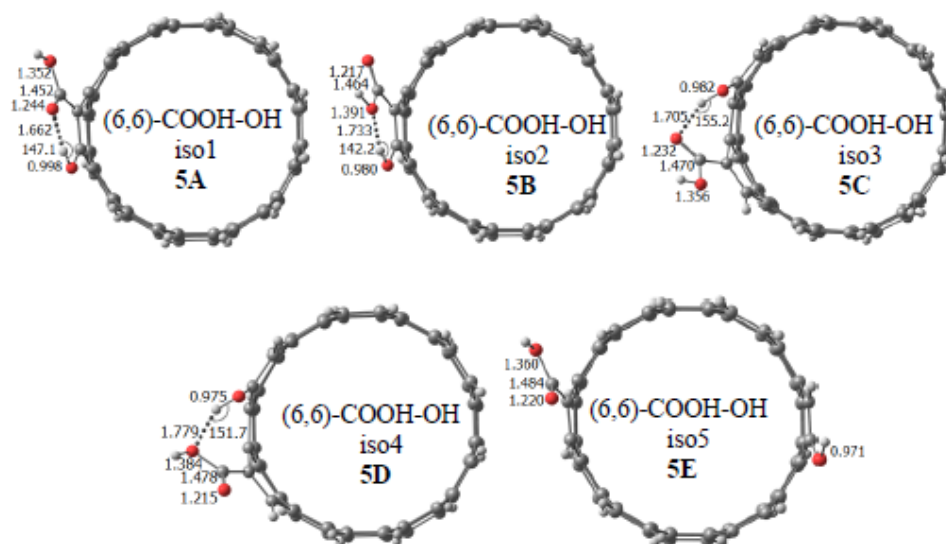


Figure 12-10. Optimized structures of (6,6)-COOH-OH. Distances in Å and angles in degree.

CHAPTER 13

SUMMARY

The importance of noncovalent interactions cannot be overestimated. From weak van der Waal's forces to stronger charge containing H-bonds, all of them have some potential to bring different molecules or molecular fragments together. Albeit much weaker than covalent bonds, the collective strength of noncovalent interactions is capable of holding various biomolecules like base pairs of nucleic acids and different peptide units together, and are the basic building blocks of all the biological systems.

This dissertation has demonstrated the strength and consequences of various noncovalent interactions. First and foremost, a new sort of noncovalent interaction $BA\cdots D$ is explored, and its competition with other noncovalent interactions is thoroughly studied. Similarly, different approach of peptide-peptide and peptide-amino acid side chain interactions is investigated. The strength and role of neutral and cationic $CH\cdots O$ interactions are studied. The possibility of hydrogen bonding at the tips of oxidized carbon nanotubes is also studied.

A fundamentally new sort of interaction ($BA\cdots D$) is identified where two electronegative atoms A and D interact directly with each other with no bridging hydrogen or halogen atoms.¹⁻⁴ These interactions are stabilized by charge transfer from electron donor D to A-B σ^* antibond, in addition to electrostatics and dispersion. When one of the H atoms of H_2S is substituted by a halogen atom (X) and is allowed to interact with N atom of NH_3 , a strong $S\cdots N$ interaction is resulted. All $S\cdots N$ interacted complexes are true minimum on their potential energy surface regardless of nature of X.⁵

The S...N interaction energy ranges from 7.9 kcal/mol for X = F to 4.7 kcal/mol for X = Br. The F and Cl substituted S...N interacted complexes represent the global minima and are much stronger than NH...F and SH...N H-bonds. For X = Br, S...N interaction is energetically comparable to other H-bonds. These quantum mechanical calculations are supported by the close contacts between S and donor (D) atoms in several crystal structures as found in the literatures.⁶⁻⁷

Similar to P and S atoms, Cl is also capable of formation of direct Cl...N interaction.^{1,8} The strength of the interactions depends on nature of substituent B present on the electron acceptor. The climbing of interaction energy for P...N, S...N and Cl...N interactions is in the order of B = CH₃ < NH₂ < CF₃ < OH < Cl < NO₂ < F with some variability by the NO₂ group.⁹ The interaction energy is as strong as 10 kcal/mol for FCl...N interaction. In most of the cases, there is stretching of B-A bond length due to the increased occupancy of the B-A σ^* antibonding orbital. However, NO₂ shows an unusual shortening of B-A bond length. This shortening of B-A bond length is due to the fact that the charge transferred from the electron donor does not remain in the B-A σ^* antibond, instead it is transferred to two O atoms as shown by the increase in occupancy of lone pairs of O atoms of NO₂. Induction component of these interactions is slightly dominant over electrostatics and dispersion for stronger complexes whereas opposite is true for weaker complexes. A characteristic electron density shift pattern is observed for the BA...D interactions and is independent of the nature of the substituent B. There is an increase in density at the D lone pair whereas a substantial loss is observed at the opposite side of D lone pair. There is some charge loss on the electron acceptor A around

the A...D axis, but increase in density is observed in the B-A bond and on the far side of the substituents.

Various carbon chain substituents show different effects on the P...N noncovalent interactions.¹⁰ Saturated carbon chains show mild weakening of P...N interaction whereas unsaturated carbon chains tend to strengthen the interaction. Conjugated double bond shows slightly bigger strengthening effect than aromatic phenyl system, and triple bond shows the largest effect. Making any carbon chains longer weakens the interaction. Adding F atoms in the carbon chains slightly enhances the P...N interaction but the effect vanishes as F atom is gradually shifted away from the P...N center.

A direct P...N and P...P interactions, as observed previously³ in the dimers, also exist in the molecular aggregates.¹¹ In fact, the global minimum obtained for the PH₃ trimer and tetramer consists of cyclic structure stabilized by P...P interactions. Similarly, hetero PH₃ trimers with one of the PH₃ substituted by FPH₂ and NH₃ also show the presence of P...N and P...P interactions as the dominant force. Several minima are obtained on the potential energy surface but the most stable minimum contains one or more P...N or P...P interaction. Other weak interactions like PH...P, NH...P, and PH...F H-bonds are also present in the secondary minima.

The BA...D angles in such interactions are almost linear.^{3-5,12-14} Other noncovalent interactions like hydrogen bonds have shown some sensitivity towards linearity, and any deviation from linearity is energetically costly. Similar scenario is found for P...N, S...N and Cl...N interactions.¹⁵ A study constituting various substituents B at different BA...D angles show the propensity of these interactions

towards BA...D angular distortion. *Ab initio* calculations show that these interactions are strongly anisotropic and are more sensitive toward angular distortion than H- bonds.

O and S atoms, and even π -systems participate in BA...D interaction as electron donors.¹⁶ FPH₂ forms a direct P...D interaction with single bonded OH₂, CH₃OH and SH₂, double bonded O=CH₂ and S=CH₂, and various π -systems like -C=C-, -C≡C-, -C=C-C=C- and C₆H₆. The P...D binding energy varies in the order of NH₃ > H₂CO > H₂CS > H₂O > H₂S. Although the binding energy ranges only within 4-5 kcal/mol, this energetic ordering is different than hydrogen and halogen bonds. And, these FP...D interactions are almost as strong as OH...O H-bond between two water dimer. Within the context of π -donors, the binding energy diminishes in the order of benzene > butadiene > H₂C=CH₂ > HC≡CH. These P... π interactions are stronger than corresponding OH... π interactions for all π -systems and are even comparable with FH... π interactions. In fact it is found that P... π binding energies are augmented by the reverse charge transfer from P lone pair to π^* antibond in addition to usual π →P-F σ^* charge transfer. Electron density shift shows similar characteristic pattern as that of other BA...D interactions.

The BA...D interactions are significantly different in many ways as described earlier including energy components, electron density shifts, sensitivity towards electron acceptors and donors, and sensitivity towards angular distortions. These interactions are quite strong and are competitive with regular hydrogen and halogen bonds, and might play very important role in biological systems. Indeed, another set of calculations revealed that these sorts of interaction are part of the stabilizing factor in the peptide interaction with S containing amino acid side chain molecules. Allowing N-methylacetamide as a peptide unit to interact with CH₃SH, CH₃SCH₃ and CH₃SSCH₃

separately as a representation of Lys side chain, model Met and disulfide bond connecting Cys side chains respectively, shows that several sorts of noncovalent interactions are responsible for holding them together.¹⁷ A full potential energy surface analysis shows charge transfer interactions like $\text{CO}\cdots\text{S}$, $\text{CS}\cdots\text{N}$, $\text{SS}\cdots\text{N}$ and $\text{SS}\cdots\text{O}=\text{C}$ are prevalent forces, in addition to $\text{SH}\cdots\text{O}$, $\text{CH}\cdots\text{O}$, $\text{NH}\cdots\text{S}$, $\text{CH}\cdots\text{S}$, $\text{SH}\cdots\pi$, and $\text{CH}\cdots\pi$ H-bonds.

Within the context of proteins, peptides are found to be linked by interpeptide $\text{NH}\cdots\text{O}$ H-bonds.¹⁸⁻²¹ Recent studies have also shown the involvement of $\text{CH}\cdots\text{O}$ H-bonds in the interpeptide bond formation.²²⁻²⁴ Another type of interaction between the two peptide units is found in which two $\text{C}=\text{O}$ groups are stacked upon each other.²⁵ Just like $\text{NH}\cdots\text{O}$ H-bonds between two peptide units, carbonyl stacking geometry occurs in both parallel and antiparallel fashion. These interactions are stabilized by charge transfer from one CO π -bond to another CO π^* antibond, and a $\text{CH}\cdots\text{O}$ H-bond. These carbonyl stacking geometries are slightly less stable than $\text{NH}\cdots\text{O}$ H-bonds. So, these carbonyl stacking interactions are more than just a dipole-dipole interaction and constitute a significant $\pi\rightarrow\pi^*$ charge transfer as shown by the NBO analysis.

The role of $\text{CH}\cdots\text{O}$ H-bond is observed at the beginning stages of interpeptide interaction. A full conformational analysis of a molecule with a dipeptide and a peptide groups connected to a common spacer group, shows the initial stages of a β -sheet formation.²⁶ Out of two common orientation of a dipeptide $\text{C}5$ and $\text{C}7$, $\text{C}7$ geometry exists in the most stable geometry of the full molecule and consists of a usual $\text{NH}\cdots\text{O}$ H-bond and a couple of $\text{CH}\cdots\text{O}$ H-bonds. β -sheet formation needs the peptide conformation

favorable to C5, which suggests that this phenomenon requires few more peptide units and is not visible at this early stages of peptide interactions.

The charge assisted $\text{CH}\cdots\text{O}$ H-bond plays very important role in the methyl transfer reactions in certain biochemical processes.²⁷ Quantum mechanical calculations proved this fact as methylated sulfonium and ammonium ion forms trifurcated $^+\text{CH}\cdots\text{O}$ hydrogen bonds with N-methylacetamide, a prototype peptide unit, with 4-9 times enhancement in binding energy.²⁸ $^+\text{CH}\cdots\text{O}$ H-bonds in those cases become as strong as 20 kcal/mol. Multiple $^+\text{CH}\cdots\text{O}$ H-bonds with multiple CH_3 groups are favorable over single H-bond which in turn is more favorable than multiple H-bonds formed with single methyl group. Substitution of methyl groups of sulfonium and ammonium cations by alkyl groups of increasing chain length diminishes the binding energy of terminal $^+\text{CH}\cdots\text{O}$ H-bonds. This decrease of H-bond energy with increasing distance from heteroatom is due to the decreasing positive potential of the terminal CH_3 groups in longer alkyl chains. The $^+\text{CH}\cdots\text{O}$ H-bonds have all the characteristics of true H-bonds, proved by the presence of characteristic density shift pattern, deshielding of H-bonded proton, NBO charge transfer and presence of all the components of binding energy like electrostatic, induction, exchange and dispersion in a similar proportion as that of true H-bonds. The presence of solvent attenuates the binding energy in all the systems but is particularly visible in charge assisted H-bonding. Even in the solvent of high polarity $^+\text{CH}\cdots\text{O}$ hydrogen bonds are much stronger than their neutral analogs and other regular $\text{OH}\cdots\text{O}$ and $\text{NH}\cdots\text{O}$ H-bonds.

Hydrogen bonds also play very important role in the characterization of various materials. Quantum calculations show that OH and COOH groups when present at the tip

of single walled carbon nanotubes (o-SWNTs) together, form strong OH...O H-bonds.²⁹ The strongly H-bonded structures are the global minimum structures regardless of the diameter and length of the tubes. These H-bonds are twice as strong as regular OH...O H-bonds. The presence of H-bonding causes the C=O and OH stretching IR frequency to be red shifted by more than 50 cm⁻¹ and a few hundred cm⁻¹, respectively. But the experimental IR spectra does not show so much red shifted stretching frequencies, ruling out the possibility of OH and COOH groups staying together at the tip of o-SWNTs.

In conclusion, this dissertation presents a rigorous theoretical analysis of various noncovalent interactions, starting from the exploration of a new sort of BA...D type interaction for various electron acceptors and donors, to expansion of the applications of already existing NH...O and CH...O hydrogen bonding. These various noncovalent interactions, although of different nature, have a common function which is binding the various molecules or different fragments together. These interactions not only hold the essential biomolecules like nucleic acids and proteins together, but also play catalytic roles in several enzymatic and biomolecular reactions, organic and inorganic reactions, crystal packing, protein folding and formation of different materials. The strength and stability of various noncovalent interactions show that they can be wisely applied in various chemical and biological phenomena, and design of various materials.

References

- (1) Scheiner, S. *Phys. Chem. Chem. Phys.* **2011**, *13*, 13860-13872.
- (2) Solimannejad, M.; Gharabaghi, M.; Scheiner, S. *J. Chem. Phys.* **2011**, *134*, 024312.

- (3) Scheiner, S. *J. Chem. Phys.* **2011**, *134*, 094315.
- (4) Scheiner, S. *J. Phys. Chem. A* **2011**, *115*, 11202-11209.
- (5) Adhikari, U.; Scheiner, S. *Chem. Phys. Lett.* **2011**, *514*, 36-39.
- (6) Rosenfield, R. E.; Parthasarathy, R.; Dunitz, J. D. *J. Am. Chem. Soc.* **1977**, *99*, 4860-4862.
- (7) Iwaoka, M.; Takemoto, S.; Tomoda, S. *J. Am. Chem. Soc.* **2002**, *124*, 10613-10620.
- (8) Scheiner, S. *J. Chem. Phys.* **2011**, *134*, 164313.
- (9) Adhikari, U.; Scheiner, S. *J. Phys. Chem. A* **2012**, *116*, 3487-3497.
- (10) Adhikari, U.; Scheiner, S. *Chem. Phys. Lett.* **2012**, *536*, 30-33.
- (11) Adhikari, U.; Scheiner, S. *J. Chem. Phys.* **2011**, *135*, 184306.
- (12) Del Bene, J. E.; Alkorta, I.; Sanchez-Sanz, G.; Elguero, J. *J. Phys. Chem. A* **2011**, *115*, 13724-13731.
- (13) Del Bene, J. E.; Sanchez-Sanz, G.; Alkorta, I.; Elguero, J. *Chem. Phys. Lett.* **2012**, *538*, 14-18.
- (14) Del Bene, J. E.; Alkorta, I.; Sanchez-Sanz, G.; Elguero, J. *J. Phys. Chem. A* **2012**, *116*, 3056-3060.
- (15) Adhikari, U.; Scheiner, S. *Chem. Phys. Lett.* **2012**, *532*, 31-35.
- (16) Scheiner, S.; Adhikari, U. *J. Phys. Chem. A* **2011**, *115*, 11101-11110.
- (17) Adhikari, U.; Scheiner, S. *ChemPhysChem* **2012**, *13*, 3535-3541.
- (18) Deshmukh, M. M.; Gadre, S. R. *J. Phys. Chem. A* **2009**, *113*, 7927-7932.
- (19) Esrafil, M. H.; Behzadi, H.; Hadipour, N. L. *Theor. Chem. Account* **2008**, *121*, 135-146.

- (20) Grabowski, S. J.; Sokalski, W. A.; Leszczynski, J. *J. Phys. Chem. A* **2006**, *110*, 4772-4779.
- (21) Vargas, R.; Garza, J.; Friesner, R. A.; Stern, H.; Hay, B. P.; Dixon, D. A. *J. Phys. Chem. A* **2001**, *105*, 4963-4968.
- (22) Derewenda, Z. S.; Lee, L.; Derewenda, U. *J. Mol. Biol.* **1995**, *252*, 248-262.
- (23) Scheiner, S.; Kar, T. *J. Phys. Chem. B* **2005**, *109*, 3681-3689.
- (24) Taylor, R.; Kennard, O. *J. Am. Chem. Soc.* **1982**, *104*, 5063-5070.
- (25) Adhikari, U.; Scheiner, S. *J. Phys. Chem. A* **2013**, *117*, 489-496.
- (26) Adhikari, U.; Scheiner, S. *J. Phys. Chem. B* **2013**, *117*, 11575-11583.
- (27) Horowitz, S.; Yessleman, J. D.; Al-Hashimi, H. M.; Trievel, R. C. *J. Biol. Chem.* **2011**, *286*, 18658-18663.
- (28) Adhikari, U.; Scheiner, S. *J. Phys. Chem. A* **2013**, *117*, 10551-10562.
- (29) Adhikari, U.; Scheiner, S.; Roy, A. K.; Kar, T. *Carbon* **2014**, *73*, 194-205.

APPENDIX

PERMISSIONS

ELSEVIER LICENSE
TERMS AND CONDITIONS

Feb 19, 2014

This is a License Agreement between Utah State University ("You") and Elsevier ("Elsevier") provided by Copyright Clearance Center ("CCC"). The license consists of your order details, the terms and conditions provided by Elsevier, and the payment terms and conditions.

All payments must be made in full to CCC. For payment instructions, please see information listed at the bottom of this form.

Supplier	Elsevier Limited The Boulevard, Langford Lane Kidlington, Oxford, OX5 1GB, UK
Registered Company Number	1982084
Customer name	Utah State University
Customer address	Old Main Hill Logan, UT 84322
License number	3332160433682
License date	Feb 18, 2014
Licensed content publisher	Elsevier
Licensed content publication	Chemical Physics Letters
Licensed content title	The S···N noncovalent interaction: Comparison with hydrogen and halogen bonds
Licensed content author	Upendra Adhikari, Steve Scheiner
Licensed content date	27 September 2011
Licensed content volume number	514
Licensed content issue number	1–3
Number of pages	4
Start Page	36
End Page	39
Type of Use	reuse in a thesis/dissertation
Intended publisher of new work	other
Portion	full article
Format	both print and electronic
Are you the author of this Elsevier article?	Yes
Will you be translating?	No

Title of your thesis/dissertation	QUANTUM MECHANICAL STUDY OF WEAK MOLECULAR INTERACTIONS
Expected completion date	Apr 2014
Estimated size (number of pages)	400
Elsevier VAT number	GB 494 6272 12
Permissions price	0.00 USD
VAT/Local Sales Tax	0.00 USD / 0.00 GBP
Total	0.00 USD
Terms and Conditions	

INTRODUCTION

1. The publisher for this copyrighted material is Elsevier. By clicking "accept" in connection with completing this licensing transaction, you agree that the following terms and conditions apply to this transaction (along with the Billing and Payment terms and conditions established by Copyright Clearance Center, Inc. ("CCC"), at the time that you opened your Rights link account and that are available at any time at <http://myaccount.copyright.com>).

Licensing material from an Elsevier book: A hyper-text link must be included to the Elsevier homepage at <http://www.elsevier.com>. All content posted to the web site must maintain the copyright information line on the bottom of each image.

Posting licensed content on Electronic reserve: In addition to the above the following clauses are applicable: The web site must be password-protected and made available only to bona fide students registered on a relevant course. This permission is granted for 1 year only. You may obtain a new license for future website posting.

For journal authors: the following clauses are applicable in addition to the above: Permission granted is limited to the author accepted manuscript version* of your paper.

***Accepted Author Manuscript (AAM) Definition:** An accepted author manuscript (AAM) is the author's version of the manuscript of an article that has been accepted for publication and which may include any author-incorporated changes suggested through the processes of submission processing, peer review, and editor-author communications. AAMs do not include other publisher value-added contributions such as copy-editing, formatting, technical enhancements and (if relevant) pagination.

21. **Other Conditions:**

v1.7

If you would like to pay for this license now, please remit this license along with your payment made payable to "COPYRIGHT CLEARANCE CENTER" otherwise you will be invoiced within 48 hours of the license date. Payment should be in the form of a check or money order referencing your account number and this invoice number RLNK501229821.

Once you receive your invoice for this order, you may pay your invoice by credit card. Please follow instructions provided at that time.

**Make Payment To:
Copyright Clearance Center
Dept 001
P.O. Box 843006
Boston, MA 02284-3006**

For suggestions or comments regarding this order, contact RightsLink Customer Support: customercare@copyright.com or +1-877-622-5543 (toll free in the US) or +1-978-646-2777.

Gratis licenses (referencing \$0 in the Total field) are free. Please retain this printable license for your reference. No payment is required.



RightsLink[®]

[Home](#)
[Account Info](#)
[Help](#)


ACS Publications
High quality. High impact.

Title: Abilities of Different Electron Donors (D) to Engage in a P...D Noncovalent Interaction

Author: Steve Scheiner and Upendra Adhikari

Publication: The Journal of Physical Chemistry A

Publisher: American Chemical Society

Date: Oct 1, 2011

Copyright © 2011, American Chemical Society

Logged in as:
Upendra Adhikari
Utah State University
Account #:
3000750440

[LOGOUT](#)

Quick Price Estimate

Permission for this particular request is granted for print and electronic formats, and translations, at no charge. Figures and tables may be modified. Appropriate credit should be given. Please print this page for your records and provide a copy to your publisher. Requests for up to 4 figures require only this record. Five or more figures will generate a printout of additional terms and conditions. Appropriate credit should read: "Reprinted with permission from {COMPLETE REFERENCE CITATION}. Copyright {YEAR} American Chemical Society." Insert appropriate information in place of the capitalized words.

I would like to... ? reuse in a Thesis/Dissertation ▼

Requestor Type ? Author (original work) ▼

Portion ? Full article ▼

Format ? Print and Electronic ▼

Will you be translating? ? No ▼

Select your currency USD - \$ ▼

Quick Price [Click Quick Price](#)

This service provides permission for reuse only. If you do not have a copy of the article you are using, you may copy and paste the content and reuse according to the terms of your agreement. Please be advised that obtaining the content you license is a separate transaction not involving Rightslink.

[QUICK PRICE](#)
[CONTINUE](#)

To request permission for a type of use not listed, please contact [the publisher](#) directly.

Copyright © 2014 [Copyright Clearance Center, Inc.](#) All Rights Reserved. [Privacy statement.](#)
Comments? We would like to hear from you. E-mail us at customercare@copyright.com

**RightsLink**[®][Home](#)[Account Info](#)[Help](#)**ACS Publications**
High quality. High impact.

Title: Abilities of Different Electron Donors (D) to Engage in a P...D Noncovalent Interaction
Author: Steve Scheiner and Upendra Adhikari
Publication: The Journal of Physical Chemistry A
Publisher: American Chemical Society
Date: Oct 1, 2011
Copyright © 2011, American Chemical Society

Logged in as:
Upendra Adhikari
Utah State University
Account #:
3000750440

[LOGOUT](#)**PERMISSION/LICENSE IS GRANTED FOR YOUR ORDER AT NO CHARGE**

This type of permission/license, instead of the standard Terms & Conditions, is sent to you because no fee is being charged for your order. Please note the following:

- Permission is granted for your request in both print and electronic formats, and translations.
- If figures and/or tables were requested, they may be adapted or used in part.
- Please print this page for your records and send a copy of it to your publisher/graduate school.
- Appropriate credit for the requested material should be given as follows: "Reprinted (adapted) with permission from (COMPLETE REFERENCE CITATION). Copyright (YEAR) American Chemical Society." Insert appropriate information in place of the capitalized words.
- One-time permission is granted only for the use specified in your request. No additional uses are granted (such as derivative works or other editions). For any other uses, please submit a new request.

[BACK](#)[CLOSE WINDOW](#)

Copyright © 2014 [Copyright Clearance Center, Inc.](#) All Rights Reserved. [Privacy statement.](#)
Comments? We would like to hear from you. E-mail us at customer@copyright.com

AIP PUBLISHING LLC LICENSE
TERMS AND CONDITIONS

Feb 19, 2014

All payments must be made in full to CCC. For payment instructions, please see information listed at the bottom of this form.

License Number	3332600401384
Order Date	Feb 19, 2014
Publisher	AIP Publishing LLC
Publication	Journal of Chemical Physics
Article Title	Comparison of P···D (D = P,N) with other noncovalent bonds in molecular aggregates
Author	Upendra Adhikari, Steve Scheiner
Online Publication Date	Nov 14, 2011
Volume number	135
Issue number	18
Type of Use	Thesis/Dissertation
Requestor type	Author (original article)
Format	Print and electronic
Portion	Excerpt (> 800 words)
Will you be translating?	No
Title of your thesis / dissertation	QUANTUM MECHANICAL STUDY OF WEAK MOLECULAR INTERACTIONS
Expected completion date	Apr 2014
Estimated size (number of pages)	400
Total	0.00 USD

Terms and Conditions

AIP Publishing LLC -- Terms and Conditions: Permissions Uses

AIP Publishing LLC ("AIPP") hereby grants to you the non-exclusive right and license to use and/or distribute the Material according to the use specified in your order, on a one-time basis, for the specified term, with a maximum distribution equal to the number that you have ordered. Any links or other content accompanying the Material are not the subject of this license.

1. You agree to include the following copyright and permission notice with the reproduction of the Material: "Reprinted with permission from [FULL CITATION]. Copyright [PUBLICATION YEAR], AIP Publishing LLC." For an article, the copyright and permission notice must be printed on the first page of the article or book chapter. For photographs, covers, or tables, the copyright and permission

- notice may appear with the Material, in a footnote, or in the reference list.
2. If you have licensed reuse of a figure, photograph, cover, or table, it is your responsibility to ensure that the material is original to AIPP and does not contain the copyright of another entity, and that the copyright notice of the figure, photograph, cover, or table does not indicate that it was reprinted by AIPP, with permission, from another source. Under no circumstances does AIPP, purport or intend to grant permission to reuse material to which it does not hold copyright.
 3. You may not alter or modify the Material in any manner. You may translate the Material into another language only if you have licensed translation rights. You may not use the Material for promotional purposes. AIPP reserves all rights not specifically granted herein.
 4. The foregoing license shall not take effect unless and until AIPP or its agent, Copyright Clearance Center, receives the Payment in accordance with Copyright Clearance Center Billing and Payment Terms and Conditions, which are incorporated herein by reference.
 5. AIPP or the Copyright Clearance Center may, within two business days of granting this license, revoke the license for any reason whatsoever, with a full refund payable to you. Should you violate the terms of this license at any time, AIPP, AIP Publishing LLC, or Copyright Clearance Center may revoke the license with no refund to you. Notice of such revocation will be made using the contact information provided by you. Failure to receive such notice will not nullify the revocation.
 6. AIPP makes no representations or warranties with respect to the Material. You agree to indemnify and hold harmless AIPP, AIP Publishing LLC, and their officers, directors, employees or agents from and against any and all claims arising out of your use of the Material other than as specifically authorized herein.
 7. The permission granted herein is personal to you and is not transferable or assignable without the prior written permission of AIPP. This license may not be amended except in a writing signed by the party to be charged.
 8. If purchase orders, acknowledgments or check endorsements are issued on any forms containing terms and conditions which are inconsistent with these provisions, such inconsistent terms and conditions shall be of no force and effect. This document, including the CCC Billing and Payment Terms and Conditions, shall be the entire agreement between the parties relating to the subject matter hereof.

This Agreement shall be governed by and construed in accordance with the laws of the State of New York. Both parties hereby submit to the jurisdiction of the courts of New York County for purposes of resolving any disputes that may arise hereunder.

If you would like to pay for this license now, please remit this license along with your payment made payable to "COPYRIGHT CLEARANCE CENTER" otherwise you will be invoiced within 48 hours of the license date. Payment should be in the form of a check or money order referencing your account number and this invoice number RLNK501230767.

Once you receive your invoice for this order, you may pay your invoice by credit card. Please follow instructions provided at that time.

Make Payment To:
Copyright Clearance Center
Dept 001
P.O. Box 843006
Boston, MA 02284-3006

For suggestions or comments regarding this order, contact RightsLink Customer Support: customercare@copyright.com or +1-877-622-5543 (toll free in the US) or +1-978-646-2777.

Gratis licenses (referencing \$0 in the Total field) are free. Please retain this printable license for your reference. No payment is required.

ELSEVIER LICENSE
TERMS AND CONDITIONS

Feb 19, 2014

This is a License Agreement between Utah State University ("You") and Elsevier ("Elsevier") provided by Copyright Clearance Center ("CCC"). The license consists of your order details, the terms and conditions provided by Elsevier, and the payment terms and conditions.

All payments must be made in full to CCC. For payment instructions, please see information listed at the bottom of this form.

Supplier	Elsevier Limited The Boulevard, Langford Lane Kidlington, Oxford, OX5 1GB, UK
Registered Company Number	1982084
Customer name	Utah State University
Customer address	Old Main Hill Logan, UT 84322
License number	3332600717219
License date	Feb 19, 2014
Licensed content publisher	Elsevier
Licensed content publication	Chemical Physics Letters
Licensed content title	Sensitivity of pnictogen, chalcogen, halogen and H-bonds to angular distortions
Licensed content author	Upendra Adhikari, Steve Scheiner
Licensed content date	12 April 2012
Licensed content volume number	532
Licensed content issue number	
Number of pages	5
Start Page	31
End Page	35
Type of Use	reuse in a thesis/dissertation
Intended publisher of new work	other
Portion	full article
Format	both print and electronic
Are you the author of this Elsevier article?	Yes
Will you be translating?	No

Title of your thesis/dissertation	QUANTUM MECHANICAL STUDY OF WEAK MOLECULAR INTERACTIONS
Expected completion date	Apr 2014
Estimated size (number of pages)	400
Elsevier VAT number	GB 494 6272 12
Permissions price	0.00 USD
VAT/Local Sales Tax	0.00 USD / 0.00 GBP
Total	0.00 USD
Terms and Conditions	

INTRODUCTION

1. The publisher for this copyrighted material is Elsevier. By clicking "accept" in connection with completing this licensing transaction, you agree that the following terms and conditions apply to this transaction (along with the Billing and Payment terms and conditions established by Copyright Clearance Center, Inc. ("CCC"), at the time that you opened your Rightslink account and that are available at any time at <http://myaccount.copyright.com>).

Licensing material from an Elsevier book: A hyper-text link must be included to the Elsevier homepage at <http://www.elsevier.com>. All content posted to the web site must maintain the copyright information line on the bottom of each image.

Posting licensed content on Electronic reserve: In addition to the above the following clauses are applicable: The web site must be password-protected and made available only to bona fide students registered on a relevant course. This permission is granted for 1 year only. You may obtain a new license for future website posting.

For journal authors: the following clauses are applicable in addition to the above: Permission granted is limited to the author accepted manuscript version* of your paper.

***Accepted Author Manuscript (AAM) Definition:** An accepted author manuscript (AAM) is the author's version of the manuscript of an article that has been accepted for publication and which may include any author-incorporated changes suggested through the processes of submission processing, peer review, and editor-author communications. AAMs do not include other publisher value-added contributions such as copy-editing, formatting, technical enhancements and (if relevant) pagination.

21. **Other Conditions:**

v1.7

If you would like to pay for this license now, please remit this license along with your payment made payable to "COPYRIGHT CLEARANCE CENTER" otherwise you will be invoiced within 48 hours of the license date. Payment should be in the form of a check or money order referencing your account number and this invoice number RLNK501230773.

Once you receive your invoice for this order, you may pay your invoice by credit card. Please follow instructions provided at that time.

**Make Payment To:
Copyright Clearance Center
Dept 001
P.O. Box 843006
Boston, MA 02284-3006**

For suggestions or comments regarding this order, contact RightsLink Customer Support: customercare@copyright.com or +1-877-622-5543 (toll free in the US) or +1-978-646-2777.

Gratis licenses (referencing \$0 in the Total field) are free. Please retain this printable license for your reference. No payment is required.



RightsLink[®]

[Home](#)
[Account Info](#)
[Help](#)


ACS Publications
High quality. High impact.

Title: Substituent Effects on C···N, S···N, and P···N Noncovalent Bonds
Author: Upendra Adhikari and Steve Scheiner
Publication: The Journal of Physical Chemistry A
Publisher: American Chemical Society
Date: Apr 1, 2012
 Copyright © 2012, American Chemical Society

Logged in as:
 Upendra Adhikari
 Utah State University
 Account #:
 3000750440

[LOGOUT](#)

Quick Price Estimate

Permission for this particular request is granted for print and electronic formats, and translations, at no charge. Figures and tables may be modified. Appropriate credit should be given. Please print this page for your records and provide a copy to your publisher. Requests for up to 4 figures require only this record. Five or more figures will generate a printout of additional terms and conditions. Appropriate credit should read: "Reprinted with permission from {COMPLETE REFERENCE CITATION}. Copyright {YEAR} American Chemical Society." Insert appropriate information in place of the capitalized words.

I would like to... [?](#) reuse in a Thesis/Dissertation ▼

Requestor Type [?](#) Author (original work) ▼

Portion [?](#) Full article ▼

Format [?](#) Print and Electronic ▼

Will you be translating? [?](#) No ▼

Select your currency USD - \$ ▼

Quick Price Click Quick Price

This service provides permission for reuse only. If you do not have a copy of the article you are using, you may copy and paste the content and reuse according to the terms of your agreement. Please be advised that obtaining the content you license is a separate transaction not involving Rightslink.

[QUICK PRICE](#)
[CONTINUE](#)

To request permission for a type of use not listed, please contact [the publisher](#) directly.

Copyright © 2014 [Copyright Clearance Center, Inc.](#) All Rights Reserved. [Privacy statement.](#)
 Comments? We would like to hear from you. E-mail us at customer@copyright.com



RightsLink®

Home

Account Info

Help



ACS Publications
High quality. High impact.

Title: Substituent Effects on C···N, S···N, and P···N Noncovalent Bonds
Author: Upendra Adhikari and Steve Scheiner
Publication: The Journal of Physical Chemistry A
Publisher: American Chemical Society
Date: Apr 1, 2012
 Copyright © 2012, American Chemical Society

Logged in as:
 Upendra Adhikari
 Utah State University
 Account #:
 3000750440

LOGOUT

PERMISSION/LICENSE IS GRANTED FOR YOUR ORDER AT NO CHARGE

This type of permission/license, instead of the standard Terms & Conditions, is sent to you because no fee is being charged for your order. Please note the following:

- Permission is granted for your request in both print and electronic formats, and translations.
- If figures and/or tables were requested, they may be adapted or used in part.
- Please print this page for your records and send a copy of it to your publisher/graduate school.
- Appropriate credit for the requested material should be given as follows: "Reprinted (adapted) with permission from (COMPLETE REFERENCE CITATION). Copyright (YEAR) American Chemical Society." Insert appropriate information in place of the capitalized words.
- One-time permission is granted only for the use specified in your request. No additional uses are granted (such as derivative works or other editions). For any other uses, please submit a new request.

BACK

CLOSE WINDOW

Copyright © 2014 [Copyright Clearance Center, Inc.](#) All Rights Reserved. [Privacy statement.](#)
 Comments? We would like to hear from you. E-mail us at customercare@copyright.com

ELSEVIER LICENSE
TERMS AND CONDITIONS

Feb 19, 2014

This is a License Agreement between Utah State University ("You") and Elsevier ("Elsevier") provided by Copyright Clearance Center ("CCC"). The license consists of your order details, the terms and conditions provided by Elsevier, and the payment terms and conditions.

All payments must be made in full to CCC. For payment instructions, please see information listed at the bottom of this form.

Supplier	Elsevier Limited The Boulevard, Langford Lane Kidlington, Oxford, OX5 1GB, UK
Registered Company Number	1982084
Customer name	Utah State University
Customer address	Old Main Hill Logan, UT 84322
License number	3332601089549
License date	Feb 19, 2014
Licensed content publisher	Elsevier
Licensed content publication	Chemical Physics Letters
Licensed content title	Effects of carbon chain substituents on the P···N noncovalent bond
Licensed content author	Upendra Adhikari, Steve Scheiner
Licensed content date	21 May 2012
Licensed content volume number	536
Licensed content issue number	
Number of pages	4
Start Page	30
End Page	33
Type of Use	reuse in a thesis/dissertation
Intended publisher of new work	other
Portion	full article
Format	both print and electronic
Are you the author of this Elsevier article?	Yes
Will you be translating?	No

Title of your thesis/dissertation	QUANTUM MECHANICAL STUDY OF WEAK MOLECULAR INTERACTIONS
Expected completion date	Apr 2014
Estimated size (number of pages)	400
Elsevier VAT number	GB 494 6272 12
Permissions price	0.00 USD
VAT/Local Sales Tax	0.00 USD / 0.00 GBP
Total	0.00 USD
Terms and Conditions	

INTRODUCTION

1. The publisher for this copyrighted material is Elsevier. By clicking "accept" in connection with completing this licensing transaction, you agree that the following terms and conditions apply to this transaction (along with the Billing and Payment terms and conditions established by Copyright Clearance Center, Inc. ("CCC"), at the time that you opened your Rightslink account and that are available at any time at <http://myaccount.copyright.com>).

Licensing material from an Elsevier book: A hyper-text link must be included to the Elsevier homepage at <http://www.elsevier.com>. All content posted to the web site must maintain the copyright information line on the bottom of each image.

Posting licensed content on Electronic reserve: In addition to the above the following clauses are applicable: The web site must be password-protected and made available only to bona fide students registered on a relevant course. This permission is granted for 1 year only. You may obtain a new license for future website posting.

For journal authors: the following clauses are applicable in addition to the above: Permission granted is limited to the author accepted manuscript version* of your paper.

***Accepted Author Manuscript (AAM) Definition:** An accepted author manuscript (AAM) is the author's version of the manuscript of an article that has been accepted for publication and which may include any author-incorporated changes suggested through the processes of submission processing, peer review, and editor-author communications. AAMs do not include other publisher value-added contributions such as copy-editing, formatting, technical enhancements and (if relevant) pagination.

21. Other Conditions:

v1.7

If you would like to pay for this license now, please remit this license along with your payment made payable to "COPYRIGHT CLEARANCE CENTER" otherwise you will be invoiced within 48 hours of the license date. Payment should be in the form of a check or money order referencing your account number and this invoice number RLNK501230781.

Once you receive your invoice for this order, you may pay your invoice by credit card. Please follow instructions provided at that time.

**Make Payment To:
Copyright Clearance Center
Dept 001
P.O. Box 843006
Boston, MA 02284-3006**

For suggestions or comments regarding this order, contact RightsLink Customer Support: customercare@copyright.com or +1-877-622-5543 (toll free in the US) or +1-978-646-2777.

Gratis licenses (referencing \$0 in the Total field) are free. Please retain this printable license for your reference. No payment is required.

JOHN WILEY AND SONS LICENSE
TERMS AND CONDITIONS

Feb 19, 2014

This is a License Agreement between Utah State University ("You") and John Wiley and Sons ("John Wiley and Sons") provided by Copyright Clearance Center ("CCC"). The license consists of your order details, the terms and conditions provided by John Wiley and Sons, and the payment terms and conditions.

All payments must be made in full to CCC. For payment instructions, please see information listed at the bottom of this form.

License Number	3332601351046
License date	Feb 19, 2014
Licensed content publisher	John Wiley and Sons
Licensed content publication	ChemPhysChem
Licensed content title	Contributions of Various Noncovalent Bonds to the Interaction between an Amide and S-Containing Molecules
Licensed copyright line	Copyright © 2012 WILEY-VCH Verlag GmbH & Co. KGaA, Weinheim
Licensed content author	Upendra Adhikari, Steve Scheiner
Licensed content date	Jul 31, 2012
Start page	3535
End page	3541
Type of use	Dissertation/Thesis
Requestor type	Author of this Wiley article
Format	Print and electronic
Portion	Full article
Will you be translating?	No
Title of your thesis / dissertation	QUANTUM MECHANICAL STUDY OF WEAK MOLECULAR INTERACTIONS
Expected completion date	Apr 2014
Expected size (number of pages)	400
Total	0.00 USD
Terms and Conditions	

TERMS AND CONDITIONS

This copyrighted material is owned by or exclusively licensed to John Wiley & Sons, Inc. or one of its group companies (each a "Wiley Company") or a society for whom a Wiley Company has exclusive publishing rights in relation to a particular journal (collectively "WILEY"). By clicking "accept" in connection with completing this licensing transaction, you agree that the following terms and conditions apply to this transaction (along with the billing and payment terms and conditions established by the Copyright Clearance Center Inc., ("CCC's Billing and Payment terms and conditions"), at the time that you opened your RightsLink account (these are available at any time at <http://myaccount.copyright.com>).

Terms and Conditions

1. The materials you have requested permission to reproduce (the "Materials") are protected by copyright.
2. You are hereby granted a personal, non-exclusive, non-sublicensable, non-transferable, worldwide, limited license to reproduce the Materials for the purpose specified in the licensing process. This license is for a one-time use only with a maximum distribution equal to the number that you identified in the licensing process. Any form of republication granted by this license must be completed within two years of the date of the grant of this license (although copies prepared before may be distributed thereafter). The Materials shall not be used in any other manner or for any other purpose. Permission is granted subject to an appropriate acknowledgement given to the author, title of the material/book/journal and the publisher. You shall also duplicate the copyright notice that appears in the Wiley publication in your use of the Material. Permission is also granted on the understanding that nowhere in the text is a previously published source acknowledged for all or part of this Material. Any third party material is expressly excluded from this permission.
3. With respect to the Materials, all rights are reserved. Except as expressly granted by the terms of the license, no part of the Materials may be copied, modified, adapted (except for minor reformatting required by the new Publication), translated, reproduced, transferred or distributed, in any form or by any means, and no derivative works may be made based on the Materials without the prior permission of the respective copyright owner. You may not alter, remove or suppress in any manner any copyright, trademark or other notices displayed by the Materials. You may not license, rent, sell, loan, lease, pledge, offer as security, transfer or assign the Materials, or any of the rights granted to you hereunder to any other person.
4. The Materials and all of the intellectual property rights therein shall at all times remain the exclusive property of John Wiley & Sons Inc or one of its related companies (WILEY) or their respective licensors, and your interest therein is only that of having possession of

and the right to reproduce the Materials pursuant to Section 2 herein during the continuance of this Agreement. You agree that you own no right, title or interest in or to the Materials or any of the intellectual property rights therein. You shall have no rights hereunder other than the license as provided for above in Section 2. No right, license or interest to any trademark, trade name, service mark or other branding ("Marks") of WILEY or its licensors is granted hereunder, and you agree that you shall not assert any such right, license or interest with respect thereto.

5. NEITHER WILEY NOR ITS LICENSORS MAKES ANY WARRANTY OR REPRESENTATION OF ANY KIND TO YOU OR ANY THIRD PARTY, EXPRESS, IMPLIED OR STATUTORY, WITH RESPECT TO THE MATERIALS OR THE ACCURACY OF ANY INFORMATION CONTAINED IN THE MATERIALS, INCLUDING, WITHOUT LIMITATION, ANY IMPLIED WARRANTY OF MERCHANTABILITY, ACCURACY, SATISFACTORY QUALITY, FITNESS FOR A PARTICULAR PURPOSE, USABILITY, INTEGRATION OR NON-INFRINGEMENT AND ALL SUCH WARRANTIES ARE HEREBY EXCLUDED BY WILEY AND ITS LICENSORS AND WAIVED BY YOU.

6. WILEY shall have the right to terminate this Agreement immediately upon breach of this Agreement by you.

7. You shall indemnify, defend and hold harmless WILEY, its Licensors and their respective directors, officers, agents and employees, from and against any actual or threatened claims, demands, causes of action or proceedings arising from any breach of this Agreement by you.

8. IN NO EVENT SHALL WILEY OR ITS LICENSORS BE LIABLE TO YOU OR ANY OTHER PARTY OR ANY OTHER PERSON OR ENTITY FOR ANY SPECIAL, CONSEQUENTIAL, INCIDENTAL, INDIRECT, EXEMPLARY OR PUNITIVE DAMAGES, HOWEVER CAUSED, ARISING OUT OF OR IN CONNECTION WITH THE DOWNLOADING, PROVISIONING, VIEWING OR USE OF THE MATERIALS REGARDLESS OF THE FORM OF ACTION, WHETHER FOR BREACH OF CONTRACT, BREACH OF WARRANTY, TORT, NEGLIGENCE, INFRINGEMENT OR OTHERWISE (INCLUDING, WITHOUT LIMITATION, DAMAGES BASED ON LOSS OF PROFITS, DATA, FILES, USE, BUSINESS OPPORTUNITY OR CLAIMS OF THIRD PARTIES), AND WHETHER OR NOT THE PARTY HAS BEEN ADVISED OF THE POSSIBILITY OF SUCH DAMAGES. THIS LIMITATION SHALL APPLY NOTWITHSTANDING ANY FAILURE OF ESSENTIAL PURPOSE OF ANY LIMITED REMEDY PROVIDED HEREIN.

9. Should any provision of this Agreement be held by a court of competent jurisdiction to be illegal, invalid, or unenforceable, that provision shall be deemed amended to achieve as nearly as possible the same economic effect as the original provision, and the legality, validity and enforceability of the remaining provisions of this Agreement shall not be

affected or impaired thereby.

10. The failure of either party to enforce any term or condition of this Agreement shall not constitute a waiver of either party's right to enforce each and every term and condition of this Agreement. No breach under this agreement shall be deemed waived or excused by either party unless such waiver or consent is in writing signed by the party granting such waiver or consent. The waiver by or consent of a party to a breach of any provision of this Agreement shall not operate or be construed as a waiver of or consent to any other or subsequent breach by such other party.

11. This Agreement may not be assigned (including by operation of law or otherwise) by you without WILEY's prior written consent.

12. Any fee required for this permission shall be non-refundable after thirty (30) days from receipt

13. These terms and conditions together with CCC's Billing and Payment terms and conditions (which are incorporated herein) form the entire agreement between you and WILEY concerning this licensing transaction and (in the absence of fraud) supersedes all prior agreements and representations of the parties, oral or written. This Agreement may not be amended except in writing signed by both parties. This Agreement shall be binding upon and inure to the benefit of the parties' successors, legal representatives, and authorized assigns.

14. In the event of any conflict between your obligations established by these terms and conditions and those established by CCC's Billing and Payment terms and conditions, these terms and conditions shall prevail.

15. WILEY expressly reserves all rights not specifically granted in the combination of (i) the license details provided by you and accepted in the course of this licensing transaction, (ii) these terms and conditions and (iii) CCC's Billing and Payment terms and conditions.

16. This Agreement will be void if the Type of Use, Format, Circulation, or Requestor Type was misrepresented during the licensing process.

17. This Agreement shall be governed by and construed in accordance with the laws of the State of New York, USA, without regards to such state's conflict of law rules. Any legal action, suit or proceeding arising out of or relating to these Terms and Conditions or the breach thereof shall be instituted in a court of competent jurisdiction in New York County in the State of New York in the United States of America and each party hereby consents and submits to the personal jurisdiction of such court, waives any objection to venue in such court and consents to service of process by registered or certified mail, return receipt requested, at the last known address of such party.

Wiley Open Access Terms and Conditions

Wiley publishes Open Access articles in both its Wiley Open Access Journals program [<http://www.wileyopenaccess.com/view/index.html>] and as Online Open articles in its subscription journals. The majority of Wiley Open Access Journals have adopted the [Creative Commons Attribution License](#) (CC BY) which permits the unrestricted use, distribution, reproduction, adaptation and commercial exploitation of the article in any medium. No permission is required to use the article in this way provided that the article is properly cited and other license terms are observed. A small number of Wiley Open Access journals have retained the [Creative Commons Attribution Non Commercial License](#) (CC BY-NC), which permits use, distribution and reproduction in any medium, provided the original work is properly cited and is not used for commercial purposes.

Online Open articles - Authors selecting Online Open are, unless particular exceptions apply, offered a choice of Creative Commons licenses. They may therefore select from the CC BY, the CC BY-NC and the [Attribution-NoDerivatives](#) (CC BY-NC-ND). The CC BY-NC-ND is more restrictive than the CC BY-NC as it does not permit adaptations or modifications without rights holder consent.

Wiley Open Access articles are protected by copyright and are posted to repositories and websites in accordance with the terms of the applicable Creative Commons license referenced on the article. At the time of deposit, Wiley Open Access articles include all changes made during peer review, copyediting, and publishing. Repositories and websites that host the article are responsible for incorporating any publisher-supplied amendments or retractions issued subsequently.

Wiley Open Access articles are also available without charge on Wiley's publishing platform, **Wiley Online Library** or any successor sites.

Conditions applicable to all Wiley Open Access articles:

- The authors' moral rights must not be compromised. These rights include the right of "paternity" (also known as "attribution" - the right for the author to be identified as such) and "integrity" (the right for the author not to have the work altered in such a way that the author's reputation or integrity may be damaged).
- Where content in the article is identified as belonging to a third party, it is the obligation of the user to ensure that any reuse complies with the copyright policies of the owner of that content.
- If article content is copied, downloaded or otherwise reused for research and other purposes as permitted, a link to the appropriate bibliographic citation (authors, journal, article title, volume, issue, page numbers, DOI and the link to the definitive published version on Wiley Online Library) should be maintained. Copyright notices and disclaimers must not be deleted.
 - Creative Commons licenses are copyright licenses and do not confer any

other rights, including but not limited to trademark or patent rights.

- Any translations, for which a prior translation agreement with Wiley has not been agreed, must prominently display the statement: "This is an unofficial translation of an article that appeared in a Wiley publication. The publisher has not endorsed this translation."

Conditions applicable to non-commercial licenses (CC BY-NC and CC BY-NC-ND)

For non-commercial and non-promotional purposes individual non-commercial users may access, download, copy, display and redistribute to colleagues Wiley Open Access articles. In addition, articles adopting the CC BY-NC may be adapted, translated, and text- and data-mined subject to the conditions above.

Use by commercial "for-profit" organizations

Use of non-commercial Wiley Open Access articles for commercial, promotional, or marketing purposes requires further explicit permission from Wiley and will be subject to a fee. Commercial purposes include:

- Copying or downloading of articles, or linking to such articles for further redistribution, sale or licensing;
- Copying, downloading or posting by a site or service that incorporates advertising with such content;
- The inclusion or incorporation of article content in other works or services (other than normal quotations with an appropriate citation) that is then available for sale or licensing, for a fee (for example, a compilation produced for marketing purposes, inclusion in a sales pack)
- Use of article content (other than normal quotations with appropriate citation) by for-profit organizations for promotional purposes
- Linking to article content in e-mails redistributed for promotional, marketing or educational purposes;
- Use for the purposes of monetary reward by means of sale, resale, license, loan, transfer or other form of commercial exploitation such as marketing products
- Print reprints of Wiley Open Access articles can be purchased from:

corporatesales@wiley.com

The modification or adaptation for any purpose of an article referencing the CC BY-NC-ND License requires consent which can be requested from RightsLink@wiley.com .

Other Terms and Conditions:

BY CLICKING ON THE "I AGREE..." BOX, YOU ACKNOWLEDGE THAT YOU HAVE READ AND FULLY UNDERSTAND EACH OF THE SECTIONS OF AND PROVISIONS SET FORTH IN THIS AGREEMENT AND THAT YOU ARE IN AGREEMENT WITH AND ARE WILLING TO ACCEPT ALL OF YOUR OBLIGATIONS AS SET FORTH IN THIS AGREEMENT.

v1.8

If you would like to pay for this license now, please remit this license along with your payment made payable to "COPYRIGHT CLEARANCE CENTER" otherwise you will be invoiced within 48 hours of the license date. Payment should be in the form of a check or money order referencing your account number and this invoice number RLNK501230786.

Once you receive your invoice for this order, you may pay your invoice by credit card. Please follow instructions provided at that time.

**Make Payment To:
Copyright Clearance Center
Dept 001
P.O. Box 843006
Boston, MA 02284-3006**

For suggestions or comments regarding this order, contact RightsLink Customer Support: customercare@copyright.com or +1-877-622-5543 (toll free in the US) or +1-978-646-2777.

Gratis licenses (referencing \$0 in the Total field) are free. Please retain this printable license for your reference. No payment is required.



RightsLink®

[Home](#)
[Account Info](#)
[Help](#)


ACS Publications
High quality. High impact.

Title: Preferred Configurations of Peptide–Peptide Interactions
Author: Upendra Adhikari and Steve Scheiner
Publication: The Journal of Physical Chemistry A
Publisher: American Chemical Society
Date: Jan 1, 2013
 Copyright © 2013, American Chemical Society

Logged in as:
 Upendra Adhikari
 Utah State University
 Account #:
 3000750440

[LOGOUT](#)

Quick Price Estimate

Permission for this particular request is granted for print and electronic formats, and translations, at no charge. Figures and tables may be modified. Appropriate credit should be given. Please print this page for your records and provide a copy to your publisher. Requests for up to 4 figures require only this record. Five or more figures will generate a printout of additional terms and conditions. Appropriate credit should read: "Reprinted with permission from {COMPLETE REFERENCE CITATION}. Copyright {YEAR} American Chemical Society." Insert appropriate information in place of the capitalized words.

I would like to... ?

Requestor Type ?

Portion ?

Format ?

Will you be translating? ?

Select your currency

Quick Price

Click Quick Price

[QUICK PRICE](#)
[CONTINUE](#)

This service provides permission for reuse only. If you do not have a copy of the article you are using, you may copy and paste the content and reuse according to the terms of your agreement. Please be advised that obtaining the content you license is a separate transaction not involving Rightslink.

To request permission for a type of use not listed, please contact [the publisher](#) directly.

Copyright © 2014 [Copyright Clearance Center, Inc.](#) All Rights Reserved. [Privacy statement.](#)
 Comments? We would like to hear from you. E-mail us at customer@copyright.com



RightsLink®

[Home](#)[Account Info](#)[Help](#)ACS Publications
High quality. High impact.

Title: Preferred Configurations of Peptide–Peptide Interactions
Author: Upendra Adhikari and Steve Scheiner
Publication: The Journal of Physical Chemistry A
Publisher: American Chemical Society
Date: Jan 1, 2013

Copyright © 2013, American Chemical Society

Logged in as:
Upendra Adhikari
Utah State University
Account #:
3000750440

[LOGOUT](#)**PERMISSION/LICENSE IS GRANTED FOR YOUR ORDER AT NO CHARGE**

This type of permission/license, instead of the standard Terms & Conditions, is sent to you because no fee is being charged for your order. Please note the following:

- Permission is granted for your request in both print and electronic formats, and translations.
- If figures and/or tables were requested, they may be adapted or used in part.
- Please print this page for your records and send a copy of it to your publisher/graduate school.
- Appropriate credit for the requested material should be given as follows: "Reprinted (adapted) with permission from (COMPLETE REFERENCE CITATION). Copyright (YEAR) American Chemical Society." Insert appropriate information in place of the capitalized words.
- One-time permission is granted only for the use specified in your request. No additional uses are granted (such as derivative works or other editions). For any other uses, please submit a new request.

[BACK](#)[CLOSE WINDOW](#)

Copyright © 2014 [Copyright Clearance Center, Inc.](#) All Rights Reserved. [Privacy statement.](#)
Comments? We would like to hear from you. E-mail us at customer care@copyright.com



RightsLink®

[Home](#)
[Account Info](#)
[Help](#)


ACS Publications
High quality. High impact.

Title: First Steps in Growth of a Polypeptide toward β -Sheet Structure
Author: Upendra Adhikari and Steve Scheiner
Publication: The Journal of Physical Chemistry B
Publisher: American Chemical Society
Date: Oct 1, 2013
 Copyright © 2013, American Chemical Society

Logged in as:
 Upendra Adhikari
 Utah State University
 Account #:
 3000750440

[LOGOUT](#)

Quick Price Estimate

Permission for this particular request is granted for print and electronic formats, and translations, at no charge. Figures and tables may be modified. Appropriate credit should be given. Please print this page for your records and provide a copy to your publisher. Requests for up to 4 figures require only this record. Five or more figures will generate a printout of additional terms and conditions. Appropriate credit should read: "Reprinted with permission from {COMPLETE REFERENCE CITATION}. Copyright {YEAR} American Chemical Society." Insert appropriate information in place of the capitalized words.

I would like to... [?](#) reuse in a Thesis/Dissertation ▾

Requestor Type [?](#) Author (original work) ▾

Portion [?](#) Full article ▾

Format [?](#) Print and Electronic ▾

Will you be translating? [?](#) No ▾

Select your currency USD - \$ ▾

Quick Price Click Quick Price

This service provides permission for reuse only. If you do not have a copy of the article you are using, you may copy and paste the content and reuse according to the terms of your agreement. Please be advised that obtaining the content you license is a separate transaction not involving Rightslink.

[QUICK PRICE](#)
[CONTINUE](#)

To request permission for a type of use not listed, please contact [the publisher](#) directly.

Copyright © 2014 [Copyright Clearance Center, Inc.](#) All Rights Reserved. [Privacy statement.](#)
 Comments? We would like to hear from you. E-mail us at customercare@copyright.com



RightsLink®

Home

Account
Info

Help



ACS Publications
High quality. High impact.

Title: First Steps in Growth of a Polypeptide toward β -Sheet Structure
Author: Upendra Adhikari and Steve Scheiner
Publication: The Journal of Physical Chemistry B
Publisher: American Chemical Society
Date: Oct 1, 2013
 Copyright © 2013, American Chemical Society

Logged in as:
 Upendra Adhikari
 Utah State University
 Account #:
 3000750440

LOGOUT

PERMISSION/LICENSE IS GRANTED FOR YOUR ORDER AT NO CHARGE

This type of permission/license, instead of the standard Terms & Conditions, is sent to you because no fee is being charged for your order. Please note the following:

- Permission is granted for your request in both print and electronic formats, and translations.
- If figures and/or tables were requested, they may be adapted or used in part.
- Please print this page for your records and send a copy of it to your publisher/graduate school.
- Appropriate credit for the requested material should be given as follows: "Reprinted (adapted) with permission from (COMPLETE REFERENCE CITATION). Copyright (YEAR) American Chemical Society." Insert appropriate information in place of the capitalized words.
- One-time permission is granted only for the use specified in your request. No additional uses are granted (such as derivative works or other editions). For any other uses, please submit a new request.

BACK

CLOSE WINDOW

Copyright © 2014 [Copyright Clearance Center, Inc.](#) All Rights Reserved. [Privacy statement.](#)
 Comments? We would like to hear from you. E-mail us at customercare@copyright.com



RightsLink®

[Home](#)
[Account Info](#)
[Help](#)


ACS Publications
High quality. High impact.

Title: Magnitude and Mechanism of Charge Enhancement of CH₃-O Hydrogen Bonds

Author: Upendra Adhikari and Steve Scheiner

Publication: The Journal of Physical Chemistry A

Publisher: American Chemical Society

Date: Oct 1, 2013

Copyright © 2013, American Chemical Society

Logged in as:

Upendra Adhikari
Utah State University

Account #:
3000750440

[LOGOUT](#)

Quick Price Estimate

Permission for this particular request is granted for print and electronic formats, and translations, at no charge. Figures and tables may be modified. Appropriate credit should be given. Please print this page for your records and provide a copy to your publisher. Requests for up to 4 figures require only this record. Five or more figures will generate a printout of additional terms and conditions. Appropriate credit should read: "Reprinted with permission from {COMPLETE REFERENCE CITATION}. Copyright {YEAR} American Chemical Society." Insert appropriate information in place of the capitalized words.

I would like to... [?](#)

reuse in a Thesis/Dissertation ▼

Requestor Type [?](#)

Author (original work) ▼

Portion [?](#)

Full article ▼

Format [?](#)

Print and Electronic ▼

Will you be translating? [?](#)

No ▼

Select your currency

USD - \$ ▼

Quick Price

Click Quick Price

This service provides permission for reuse only. If you do not have a copy of the article you are using, you may copy and paste the content and reuse according to the terms of your agreement. Please be advised that obtaining the content you license is a separate transaction not involving Rightslink.

[QUICK PRICE](#)

[CONTINUE](#)

To request permission for a type of use not listed, please contact [the publisher](#) directly.

Copyright © 2014 [Copyright Clearance Center, Inc.](#) All Rights Reserved. [Privacy statement.](#)
Comments? We would like to hear from you. E-mail us at customer@copyright.com

RightsLink[®][Home](#)[Account Info](#)[Help](#)ACS Publications
High quality. High impact.

Title: Magnitude and Mechanism of Charge Enhancement of CH₂O Hydrogen Bonds

Author: Upendra Adhikari and Steve Scheiner

Publication: The Journal of Physical Chemistry A

Publisher: American Chemical Society

Date: Oct 1, 2013

Copyright © 2013, American Chemical Society

Logged in as:
Upendra Adhikari
Utah State University
Account #:
3000750440

[LOGOUT](#)

PERMISSION/LICENSE IS GRANTED FOR YOUR ORDER AT NO CHARGE

This type of permission/license, instead of the standard Terms & Conditions, is sent to you because no fee is being charged for your order. Please note the following:

- Permission is granted for your request in both print and electronic formats, and translations.
- If figures and/or tables were requested, they may be adapted or used in part.
- Please print this page for your records and send a copy of it to your publisher/graduate school.
- Appropriate credit for the requested material should be given as follows: "Reprinted (adapted) with permission from (COMPLETE REFERENCE CITATION). Copyright (YEAR) American Chemical Society." Insert appropriate information in place of the capitalized words.
- One-time permission is granted only for the use specified in your request. No additional uses are granted (such as derivative works or other editions). For any other uses, please submit a new request.

[BACK](#)[CLOSE WINDOW](#)

Copyright © 2014 [Copyright Clearance Center, Inc.](#) All Rights Reserved. [Privacy statement.](#)
Comments? We would like to hear from you. E-mail us at customercare@copyright.com

ELSEVIER LICENSE TERMS AND CONDITIONS

Mar 30, 2014

This is a License Agreement between Utah State University ("You") and Elsevier ("Elsevier") provided by Copyright Clearance Center ("CCC"). The license consists of your order details, the terms and conditions provided by Elsevier, and the payment terms and conditions.

All payments must be made in full to CCC. For payment instructions, please see information listed at the bottom of this form.

Supplier	Elsevier Limited The Boulevard, Langford Lane Kidlington, Oxford, OX5 1GB, UK
Registered Company Number	1982084
Customer name	Utah State University
Customer address	Old Main Hill Logan, UT 84322
License number	3358901406514
License date	Mar 30, 2014
Licensed content publisher	Elsevier
Licensed content publication	Carbon
Licensed content title	Do phenolic and carboxylic groups coexist at the tips of oxidized single-wall carbon nanotubes (o-SWNTs)?
Licensed content author	Upendra Adhikari, Steve Scheiner, Ajit K. Roy, Tapas Kar
Licensed content date	July 2014
Licensed content volume number	73
Licensed content issue number	
Number of pages	12
Start Page	194
End Page	205
Type of Use	reuse in a thesis/dissertation
Portion	full article
Format	both print and electronic

Are you the author of this Elsevier article?	Yes
Will you be translating?	No
Title of your thesis/dissertation	QUANTUM MECHANICAL STUDY OF WEAK MOLECULAR INTERACTIONS
Expected completion date	Apr 2014
Estimated size (number of pages)	400
Elsevier VAT number	GB 494 6272 12
Permissions price	0.00 USD
VAT/Local Sales Tax	0.00 USD / 0.00 GBP
Total	0.00 USD
Terms and Conditions	

INTRODUCTION

1. The publisher for this copyrighted material is Elsevier. By clicking "accept" in connection with completing this licensing transaction, you agree that the following terms and conditions apply to this transaction (along with the Billing and Payment terms and conditions established by Copyright Clearance Center, Inc. ("CCC"), at the time that you opened your Rightslink account and that are available at any time at <http://myaccount.copyright.com>).

Licensing material from an Elsevier book: A hyper-text link must be included to the Elsevier homepage at <http://www.elsevier.com>. All content posted to the web site must maintain the copyright information line on the bottom of each image.

Posting licensed content on Electronic reserve: In addition to the above the following clauses are applicable: The web site must be password-protected and made available only to bona fide students registered on a relevant course. This permission is granted for 1 year only. You may obtain a new license for future website posting.

For journal authors: the following clauses are applicable in addition to the above: Permission granted is limited to the author accepted manuscript version* of your paper.

***Accepted Author Manuscript (AAM) Definition:** An accepted author manuscript (AAM) is the author's version of the manuscript of an article that has been accepted for publication and which may include

any author-incorporated changes suggested through the processes of submission processing, peer review, and editor-author communications. AAMs do not include other publisher value-added contributions such as copy-editing, formatting, technical enhancements and (if relevant) pagination.

21. Other Conditions:

v1.7

If you would like to pay for this license now, please remit this license along with your payment made payable to "COPYRIGHT CLEARANCE CENTER" otherwise you will be invoiced within 48 hours of the license date. Payment should be in the form of a check or money order referencing your account number and this invoice number RLNK501264506.

Once you receive your invoice for this order, you may pay your invoice by credit card. Please follow instructions provided at that time.

**Make Payment To:
Copyright Clearance Center
Dept 001
P.O. Box 843006
Boston, MA 02284-3006**

For suggestions or comments regarding this order, contact RightsLink Customer Support: customercare@copyright.com or +1-877-622-5543 (toll free in the US) or +1-978-646-2777.

Gratis licenses (referencing \$0 in the Total field) are free. Please retain this printable license for your reference. No payment is required.



DEPARTMENT OF THE AIR FORCE
AIR FORCE RESEARCH LABORATORY
WRIGHT-PATTERSON AIR FORCE BASE OHIO 45433

17 February 2014

FROM: AFRL/RXAN
2941 Hobson Way, Rm 136
Wright-Patterson AFB OH 45433-7750

Graduate Program Committee
Department of Chemistry and Biochemistry
Utah State University
Logan, UT 84322

SUBJECT: PhD Dissertation of Mr. Upendra Adhikari

This is to inform you that I co-authored the paper entitled "Do phenolic and carboxylic groups coexist at the tips of oxidized single-wall carbon nanotubes (o-SWNTs)?" with Mr. Upendra Adhikari, which is recently accepted for publication. Mr. Adhikari has my full permission to use the technical content of the paper in his dissertation.

Should you have any questions, please do not hesitate to contact me at (937) 255-9034, ajit.roy@us.af.mil.

Sincerely,

A handwritten signature in black ink that reads "Ajit K. Roy".

Ajit K. Roy
Principal Materials Research Engineer
Nanoelectronic Materials Branch

CURRICULUM VITAE

Upendra Adhikari

Department of Chemistry and Biochemistry

Utah State University

0300 Old Main Hill, Logan, UT, 84322-0300

Email: upendra.adhikari@aggiemail.usu.edu

EDUCATION**PhD in Chemistry** (GPA = 4.0) 2014

Department of Chemistry and Biochemistry, Utah State University, Logan, UT, USA

Advisor: Prof. Steve Scheiner

Co-advisor: Dr. Tapas Kar

M. S. in Chemistry (GPA≈4.0) 2008

Central Department of Chemistry, Tribhuvan University, Kathmandu, Nepal

Advisor: Prof. Raja Ram Pradhananga

HONORS AND AWARDS**School of Graduate Studies Dissertation Fellowship**, Utah State University, 2013-2014**Marjorie H. Gardner Teaching Award**, Department of Chemistry and Biochemistry,
Utah State University, 2013**Claude E. Zobell Scholarship**, College of Science, Utah State University, 2013-2014**Award for Early Research Progress in Chemistry**, Department of Chemistry and
Biochemistry, Utah State University, 2012

P. M. Singh Gold medal, Tribhuvan University, 2009

Amrit medal, Tribhuvan University, 2009

Kirti-Sanu Gold Medal, Sesh-Hira Organization, 2009

Best Student Award of Chemistry-2007, Nepal Academy of Science and Technology (NAST), 2007

Collegiate Ambassador for Peace, UPF, W-CARP, 2007

PUBLICATIONS

- 1.** The S \cdots N Noncovalent Interaction: Comparison with Hydrogen and Halogen Bonds
U. Adhikari, S. Scheiner. *Chem. Phys. Lett.* **2011**, *514*, 36-39.
- 2.** Abilities of Different Electron Donors (D) to Engage in a P \cdots D Noncovalent Interactions
S. Scheiner, U. Adhikari. *J. Phys. Chem. A* **2011**, *115*, 11101-11110.
- 3.** Comparison of P \cdots D (D=P, N) with other Noncovalent Bonds in Molecular Aggregates
U. Adhikari, S. Scheiner. *J. Chem. Phys.* **2011**, *135*, 184306.
- 4.** Sensitivity of Pnicogen, Chalcogen, Halogen and Hydrogen Bonds to Angular Distortions
U. Adhikari, S. Scheiner. *Chem. Phys. Lett.* **2012**, *532*, 31-35.
- 5.** Substituent Effects on Cl \cdots N, S \cdots N and P \cdots N Noncovalent Bonds
U. Adhikari, S. Scheiner. *J. Phys. Chem. A* **2012**, *116*, 3487-3497.
- 6.** Effects of Carbon Chain Substituents on the P \cdots N Noncovalent Bond
U. Adhikari, S. Scheiner. *Chem. Phys. Lett.* **2012**, *536*, 30-33.

7. Theoretical Study on Relationship Between Structure of Mercapto-Triazole Derivatives and Inhibition Performance
S. Chen, S. Scheiner, T. Kar, U. Adhikari. *Int. J. Electrochem. Sci.* **2012**, 7, 7128-7139.
8. Contributions of Various Noncovalent Bonds to the Interaction between an Amide and S-Containing Molecules
U. Adhikari, S. Scheiner. *ChemPhysChem* **2012**, 13, 3535-3541.
9. Preferred Configurations of Peptide-Peptide Interactions
U. Adhikari, S. Scheiner. *J. Phys. Chem. A* **2013**, 117, 489-496.
10. Site Preferences of Carboxyl Groups on the Periphery of Graphene and their Characteristic IR Spectra
T. Kar, S. Scheiner, U. Adhikari, A. Roy. *J. Phys. Chem. C* **2013**, 117, 18206-18215.
11. First Steps in the Growth of a Polypeptide Towards a β -Sheet Structure
U. Adhikari, S. Scheiner. *J. Phys. Chem. B* **2013**, 117, 11575-11583.
12. The Magnitude and Mechanism of Charge Enhancement of CH \cdots O H-bonds
U. Adhikari, S. Scheiner. *J. Phys. Chem. A* **2013**, 117, 10551-10562.
13. Conservation and Functional Importance of Carbon-Oxygen Hydrogen Bonding in AdoMet-Dependent Methyltransferases
S. Horowitz, L. M. A. Dirk, J. D. Yesselman, J. S. Nimtz, U. Adhikari, R. A. Mehl, S. Scheiner, R. L. Houtz, H. M. Al-Hashimi, R. C. Trievel. *J. Am. Chem. Soc.* **2013**, 135, 15536-15548.
14. Do Phenolic and Carboxylic Groups Coexist at the Tip of Oxidized Single-wall Carbon Nanotubes (o-SWNTs)?

U. Adhikari, S. Scheiner, A. Roy, T. Kar. *Carbon* **2014**, 73, 194-205.

15. Thermodynamic Measures of Binding Strength in Pnicogen, Chalcogen, Halogen and Hydrogen Bonds

Jared Moss, U. Adhikari, S. Scheiner. *Int. J. Chem. Mod. (In Press)*.

TEACHING EXPERIENCE

2010-Present: Teaching Assistant, Department of Chemistry and Biochemistry, Utah State University, Logan, UT, USA.

Computational Chemistry: CHEM 7030

Recitation: CHEM 1210 and CHEM 1220

Laboratory: CHEM 1125, CHEM 1215 and CHEM 1225

2010: Teaching Assistant Workshop, Utah State University, Logan, UT, USA.

2009-2010: Lecturer of Chemistry, Trinity International College, Kathmandu, Nepal.